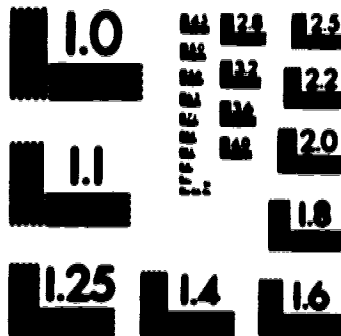


1

PM-1 3 1/2"x4" PHOTOGRAPHIC MICROCOPY TARGET
NBS 1910a ANSI/ISO #2 EQUIVALENT





National Library
of Canada

Acquisitions and
Bibliographic Services Branch

385 Wellington Street
Ottawa, Ontario
K1A 0N4

Bibliothèque nationale
du Canada

Direction des acquisitions et
des services bibliographiques

385, rue Wellington
Ottawa (Ontario)
K1A 0N4

Your library's address

Your library's address

NOTICE

The quality of this microform is heavily dependent upon the quality of the original thesis submitted for microfilming. Every effort has been made to ensure the highest quality of reproduction possible.

If pages are missing, contact the university which granted the degree.

Some pages may have indistinct print especially if the original pages were typed with a poor typewriter ribbon or if the university sent us an inferior photocopy.

Reproduction in full or in part of this microform is governed by the Canadian Copyright Act, R.S.C. 1970, c. C-30, and subsequent amendments.

AVIS

La qualité de cette microforme dépend grandement de la qualité de la thèse soumise au microfilmage. Nous avons tout fait pour assurer une qualité supérieure de reproduction.

S'il manque des pages, veuillez communiquer avec l'université qui a conféré le grade.

La qualité d'impression de certaines pages peut laisser à désirer, surtout si les pages originales ont été dactylographiées à l'aide d'un ruban usé ou si l'université nous a fait parvenir une photocopie de qualité inférieure.

La reproduction, même partielle, de cette microforme est soumise à la Loi canadienne sur le droit d'auteur, SRC 1970, c. C-30, et ses amendements subséquents.

Canada

UNIVERSITY OF ALBERTA

WELL TEST ANALYSIS FOR MULTI-LAYERED COMPOSITE SYSTEMS

BY



EDMOND GOMES

**A thesis submitted to the Faculty of Graduate Studies and Research in partial fulfillment of
the requirements for the degree of DOCTOR OF PHILOSOPHY**

IN

PETROLEUM ENGINEERING

**DEPARTMENT OF MINING, METALLURGICAL AND PETROLEUM
ENGINEERING**

EDMONTON, ALBERTA

SPRING 1994



National Library
of Canada

Acquisitions and
Bibliographic Services Branch

395 Wellington Street
Ottawa, Ontario
K1A 0N4

Bibliothèque nationale
du Canada

Direction des acquisitions et
des services bibliographiques

395, rue Wellington
Ottawa (Ontario)
K1A 0N4

Votre copie - Votre référence

Votre copie - Votre référence

The author has granted an irrevocable non-exclusive licence allowing the National Library of Canada to reproduce, loan, distribute or sell copies of his/her thesis by any means and in any form or format, making this thesis available to interested persons.

L'auteur a accordé une licence irrévocable et non exclusive permettant à la Bibliothèque nationale du Canada de reproduire, prêter, distribuer ou vendre des copies de sa thèse de quelque manière et sous quelque forme que ce soit pour mettre des exemplaires de cette thèse à la disposition des personnes intéressées.

The author retains ownership of the copyright in his/her thesis. Neither the thesis nor substantial extracts from it may be printed or otherwise reproduced without his/her permission.

L'auteur conserve la propriété du droit d'auteur qui protège sa thèse. Ni la thèse ni des extraits substantiels de celle-ci ne doivent être imprimés ou autrement reproduits sans son autorisation.

ISBN 0-612-11221-7

Canada

**UNIVERSITY OF ALBERTA
RELEASE FORM**

NAME OF AUTHOR: Edmond Gomes

TITLE OF THESIS: Well Test Analysis for Multi-Layered Composite Systems

DEGREE: Doctor of Philosophy

YEAR THIS DEGREE GRANTED: Spring, 1994

Permission is hereby granted to the University of Alberta Library to reproduce single copies of this thesis and to lend or sell such copies for private, scholarly or scientific research purposes only.

The author reserves all other publication and other rights in association with the copyright in the thesis, and except as hereinbefore provided neither the thesis nor any substantial portion thereof may be printed or otherwise reproduced in any material form whatever without the author's prior written permission.



**Lucus House
Village: Borogolla
P.O.: Gobindapur
District: Dhaka
Bangladesh**

Dated: April 8, 1994

THE UNIVERSITY OF ALBERTA

FACULTY OF GRADUATE STUDIES AND RESEARCH

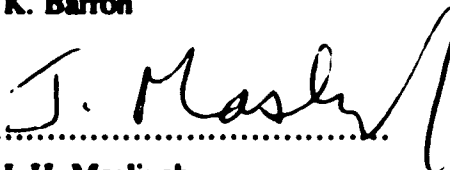
The undersigned certify that they have read, and recommend to the Faculty of Graduate Studies and Research for acceptance, a thesis entitled **WELL TEST ANALYSIS FOR MULTI-LAYERED COMPOSITE SYSTEMS** submitted by **EDMOND GOMES** in partial fulfillment of the requirements for the degree of **DOCTOR OF PHILOSOPHY** in **PETROLEUM ENGINEERING**.

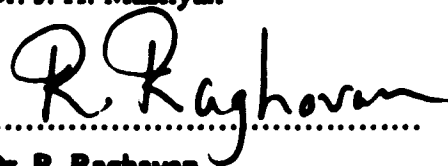
..........
Dr. A. K. Ambastha (Supervisor)

..........
Dr. R. G. Bettsen

..........
Dr. W. S. Tortike

..........
Dr. K. Barron

..........
Dr. J. H. Masliyah

..........
Dr. R. Raghavan

Dated: March 25, 1994

DEDICATION

To my parents

ABSTRACT

Reservoir deposition occurs over geological time and, thus, most reservoirs are heterogeneous in nature. Some common forms of heterogeneity are the presence of layers and the presence of different zones of fluids and/or rocks in the formation. When an enhanced recovery method, such as steam-flooding, is implemented for a heavy-oil reservoir, the reservoir resembles a composite reservoir. Because of the gravity override effect, the fluid front of the swept region is not vertical, but tilted or inclined. Sometimes, reservoirs are accompanied by a bottom-water or a gas-cap zone of various sizes. In the presence of a bottom-water or a gas-cap zone, the well is partially-penetrated to avoid or delay the water or gas coning problem.

In this study, a new analytical solution for multi-layer, composite reservoirs with pseudosteady state interlayer crossflow has been developed. Fluid flow in the reservoir has been treated as a generalized eigenvalue problem. The developed analytical solution for an n-layer composite reservoir is applicable for a tilted or irregularly-shaped discontinuity boundary, and for closed, constant-pressure, and infinite outer-boundary conditions. For tilted front cases, a pseudosteady-state (pss) flow period exists in some average sense and pss analysis will result in considerable underestimation of the swept volume for tilted front reservoirs. A correction factor has been developed to correct the estimated swept volume from pss analysis. Well-test analysis under infinite and finite bottom-water conditions has been considered and the effect of aquifer size on well-test analysis has been investigated.

For partially-penetrating wells in multi-layer reservoirs, new analytical expressions for the pseudoskin factor have been developed for both closed top and bottom boundaries, and with bottom-water zones and/or gas caps. Evaluation of the pseudoskin factor using these expressions requires a knowledge of two parameters when the top and the bottom boundaries are closed, and three parameters in the presence of a bottom-water zone or a gas cap, regardless of the number of layers. The estimated pseudoskin factor is very close to the actual pseudoskin obtained from the complete analytical solution.

ACKNOWLEDGEMENTS

I would like to thank Dr. A. K. Ambastha for his supervision, guidance, and encouragement throughout this work.

I would like to thank Dr. G. Ford and Dr. F. D. Otto for their support and encouragement. I would also like to thank Mr. R. Schmidt and Ms. Lori Constantine of Alberta International for their support during my study at the University of Alberta.

I would like to thank my wife, Shema, for her understanding, support, and help during this work.

Finally, I would like to thank the University of Alberta-BUET (Bangladesh University of Engineering and Technology)-CIDA (Canadian International Development Agency) Linkage Project officials for offering me a full scholarship for my study at the University of Alberta and for making every effort to make my stay in Canada pleasant.

TABLE OF CONTENTS

Chapter	Page
1.0 INTRODUCTION	1
2.0 MODEL DEVELOPMENT	6
2.1 Introduction	6
2.2 Model Development	8
2.3 Solution Methodology	18
2.4 Model Validation	19
2.5 Future Possibilities	21
2.6 Conclusions	22
References	22
3.0 WELL-TEST ANALYSIS FOR THERMAL RECOVERY SYSTEMS	37
3.1 Introduction	37
3.2 Effect of Front Angle	40
3.3 Layer Refinement Effect	42
3.4 Effect of Mobility and Storativity Ratio	43
3.5 Pseudosteady-State Analysis Method	45
3.6 Pseudosteady-State Analysis	46
3.7 Conclusions	50
References	51
4.0 PARTIALLY-PENETRATING WELLS	72
4.1 Introduction	72
4.2 Pseudoskin Factor Expression For Closed Top and Bottom Boundaries	75
4.3 Pseudoskin Factor Expression For a Gas-Cap or a Bottom- Water Drive	77
4.4 Accuracy of Pseudoskin Factor Expressions	78

4.5	Comparison with Reference 3	79
4.6	Comparison with References 12 and 14.....	80
4.7	Development of New Time Criteria and Comparison with Reference 4	80
4.8	Effect of Gas-Cap (or Bottom-Water) Drive on Pseudoskin and Comparison with Reference 5	84
4.9	Comparison with Reference 10.....	85
4.10	Effect of Layer Refinement on Pseudoskin Factor	86
4.11	Conclusions	86
	References	87
5.0	THERMAL, WELL-TEST ANALYSIS UNDER BOTTOM-WATER CONDITIONS	101
5.1	Introduction	101
5.2	Modelling of Infinite and Finite Bottom-water Zones	103
5.3	Infinitely-Large Bottom-Water Zone and No Bottom-Water Zone Cases	104
5.4	Finite Aquifers	109
5.5	Conclusions	112
	References	113
6.0	AN ANALYTICAL PRESSURE-TRANSIENT MODEL FOR COMPLEX RESERVOIR SCENARIOS	127
6.1	Introduction	127
6.2	Model Description	127
6.3	Solution Description	128
6.4	Solution Algorithm	129
6.5	Model Validation	131

6.6	Reservoir with Complex Front Shapes	131
6.7	Summary	132
	References	133
7.0	DISCUSSION, CONCLUSIONS, AND RECOMMENDATIONS	138
7.1	Discussion	138
7.2	Conclusions	140
7.3	Recommendations	142
	APPENDICES	144
	Appendix A: Calculation of Layer Front Radii for Inclined Front Reservoirs	144
	Appendix B: Defining an Average Front Radius for a Multi-Layer, Composite Reservoir with an Inclined Front.....	146
	Appendix C: Pseudoskin Factor for Closed Top and Bottom Boundaries	148
	Appendix D: Pseudoskin Factor for Gas-Cap Condition.....	155
	Appendix E: Late-Time Approximation of σ_2^2	160
	Appendix F: Computer Program	162
	Appendix G: Published Paper From Chapter 2	182
	Appendix H: Presented Paper From Chapter 4	198

LIST OF TABLES

Table		Page
Table 2.1:	Published Results on Layered Reservoirs.....	31
Table 3.1	Effect of front angle on $(t_{DR})_{end}$ and $(t_{DR})_{max}$ for various mobility and storativity ratios.....	54
Table 3.2:	Equivalence between the ratios of R_{Davg}/R_{Dmin} and m_w/m_{cal} for inclined front reservoirs(for $M=1000$ and $F_r=1$).....	55
Table 4.1:	Summary of studies on partially-penetrating wells.....	90
Table 4.2:	Comparison of pseudoskin factors estimated from the simplified expression and that from the actual analytical solution.....	91
Table 4.3:	Reservoir configurations considered in Tables 4.2 and 4.6.....	91
Table 4.4:	Comparison of pseudoskin factors estimated from this study with those estimated from other studies for a three-layer reservoir with closed top and bottom boundaries and with layer 3 open to flow ($h=200$ m and $k_1=4.9346 \times 10^{-14}$ m ²).....	92
Table 4.5:	Data for the development of Equations (4.6) and (4.7)	93
Table 4.6:	Effect of gas cap (bottom-water) on pseudoskin factor (three-layered reservoir, $h=200$ m, $k_1=k_2=k_3=4.9346 \times 10^{-14}$ m ²).....	93
Table 4.7:	Effect of layer refinement on pseudoskin factor ($k=22.9477 \times 10^{-14}$ m ² , $k_v=2.9477 \times 10^{-15}$ m ²)	94

LIST OF FIGURES

Figure		Page
Figure 1.1	Layered composite reservoir with a tilted front under a bottom-water condition	5
Figure 2.1a:	Layered reservoir with interlayer crossflow	32
Figure 2.1b:	Radial, layered composite reservoir with a tilted front	32
Figure 2.2:	Schematic of an n-layer composite reservoir in radial geometry with two different rock and/ or fluid types in each layer.....	33
Figure 2.3:	Comparison of this study with Agarwal <i>et al.</i> solution for a homogeneous reservoir	33
Figure 2.4:	Comparison of this study with Tariq and Ramey's solution for a two-layer reservoir with a closed outer boundary.	34
Figure 2.5:	Comparison of this study with Eggenschwiler <i>et al.</i> solution for a two-region composite reservoir.....	34
Figure 2.6:	Comparison of this study with Ambastha and Ramey's study for a two-region, composite reservoir.....	35
Figure 2.7:	Comparison of this study with Ambastha and Ramey's study for an infinitely large, three-region, composite reservoir.....	35
Figure 2.8:	Effect of crossflow on wellbore pressure for a two-layer reservoir.....	36
Figure 2.9:	Pressure drawdown responses of a partially-penetrating well in a two-layer reservoir subject to bottom-water drive.....	36
Figure 3.1a:	Layered reservoir with interlayer crossflow.....	56

Figure 3.1b:	Radial, layered composite reservoir with a tilted front.....	56
Figure 3.2:	Schematic of the swept section of a two-layer, composite reservoir.....	57
Figure 3.3:	Effect of front angle on pressure derivative responses for $h_{1D}=1000$	58
Figure 3.4:	Effect of front angle on pressure derivative responses for $h_{1D}=150$	58
Figure 3.5:	Effect of front angle on pressure derivative responses for $h_{1D}=30$.	59
Figure 3.6:	Effect of front angle on pressure derivative responses for $h_{1D}=1000$.	59
Figure 3.7:	Effect of front angle on pressure derivative responses for $h_{1D}=150$.	60
Figure 3.8:	Effect of crossflow on pressure derivative responses of a fully-penetrating well	60
Figure 3.9:	Effect of crossflow on pressure derivative responses of a partially-penetrating well.	61
Figure 3.10:	Effect of layer refinement on pressure derivative responses for a front angle=30°.....	61
Figure 3.11:	Effect of layer refinement on pressure derivative responses for a front angle=60°.....	62
Figure 3.12:	Effect of mobility ratio on pressure derivative responses for a front angle=30°.....	62
Figure 3.13:	Effect of mobility ratio on pressure derivative responses for a front angle=60°.....	63

Figure 3.14:	Effect of mobility ratio on the pressure derivative responses for a sharp front reservoir.....	63
Figure 3.15:	Effect of front angle on pressure derivative responses.....	64
Figure 3.16:	Effect of storativity ratio on pressure derivative responses for a front angle=30°.....	64
Figure 3.17:	Effect of storativity ratio on pressure derivative responses for a front angle=60°.....	65
Figure 3.18:	Effect of storativity ratio on pressure derivative responses for a sharp front reservoir.....	65
Figure 3.19:	Effect of front angle on pseudosteady-state analysis for $h_D=400$.	66
Figure 3.20:	Effect of front angle on pseudosteady-state analysis for $h_D=300$.	66
Figure 3.21:	Effect of front angle on pseudosteady-state analysis for $h_D=100$.	67
Figure 3.22:	Effect of reservoir thickness on pseudosteady-state analysis for a front angle=30°.....	67
Figure 3.23:	Effect of reservoir thickness on pseudosteady-state analysis for a front angle=45°.....	68
Figure 3.24:	Effect of reservoir thickness on pseudosteady-state analysis for a front angle=60°.....	68
Figure 3.25:	Effect of front angle on pseudosteady-state analysis for $R_{Dmin}=300$.....	69
Figure 3.26:	Effect of front angle on pseudosteady-state analysis for $R_{Dmin}=1000$.....	69

Figure 3.27:	Effect of mobility ratio on pseudosteady-state analysis for a front angle=45°.....	70
Figure 3.28:	Effect of mobility ratio on pseudosteady-state analysis for a front angle=60°.....	70
Figure 3.29	Effect of storativity ratio on pseudosteady-state analysis for a front angle=45°.....	71
Figure 3.30:	Effect of storativity ratio on pseudosteady-state analysis for a front angle=60°.....	71
Figure 4.1:	Schematic of a two-layer, partially-penetrated reservoir with closed top and bottom boundaries.....	95
Figure 4.2:	Schematic of a two-layer, partially-penetrated reservoir with a gas cap.....	95
Figure 4.3:	Comparison of the pseudoskin factor from this study with that from Brons and Marting.....	96
Figure 4.4	Ratio of pseudoskin factor from Brons and Marting study to that of this study	96
Figure 4.5:	Effect of the crossflow parameter and the mobility-thickness ratio on pressure derivative responses.....	97
Figure 4.6	Verification of the accuracy of Equation (4.6).....	97
Figure 4.7	Verification of the accuracy of Equation (4.7).....	98
Figure 4.8:	Comparison of the correlation for the time to the beginning of the second radial flow from this study and from Reference 4	98
Figure 4.9:	Comparison of pseudoskin and dimensionless pressure from this study with those from the Bilhartz and Ramsey study.....	99

Figure 4.10:	Comparison of the pseudoskin factor from this study with that from the Streltsova-Adams study for a reservoir with a gas cap.....	99
Figure 4.11	Ratio of the pseudoskin factor from the Streltsova-Adams study to that of this study	100
Figure 4.12:	Comparison of the pseudoskin factor from this study with that from the Olarewaju and Lee study.....	100
Figure 5.1:	Steam-flooded heavy oil reservoir with an infinitely-large bottom-water region.....	115
Figure 5.2:	Steam-flooded heavy oil reservoir with a finite bottom-water zone.....	115
Figure 5.3:	Effect of mobility-thickness ratio on pressure responses of a partially-penetrating well in a composite reservoir for $M=10$.....	116
Figure 5.4:	Effect of mobility-thickness ratio on pressure derivative responses of a partially-penetrating well for $M=10$.....	116
Figure 5.5:	Effect of mobility-thickness ratio on pressure derivative responses of a partially-penetrating well for $M=100$.	117
Figure 5.6:	Effect of mobility-thickness ratio on pressure derivative responses of a partially-penetrating well for $M=1000$.....	117
Figure 5.7:	Effect of mobility-thickness ratio on pressure derivative responses of a composite reservoir with no bottom-water zone.....	118
Figure 5.8:	Effect of mobility-thickness ratio on the Cartesian pressure derivative of a partially-penetrating well for $M=10$.....	118
Figure 5.9:	Effect of mobility-thickness ratio on the Cartesian pressure derivative of a partially-penetrating well for $M=100$.	119

Figure 5.10:	Effect of mobility-thickness ratio on the Cartesian pressure derivative of a partially-penetrating well for $M=1000$.....	119
Figure 5.11:	Effect of mobility-thickness ratio on the Cartesian pressure derivative of a partially-penetrating well with no bottom-water zone.....	120
Figure 5.12:	Effect of mobility-thickness ratio on pressure derivative responses when mobility-thickness ratio has been varied by changing the permeability of the penetrated layer.....	120
Figure 5.13:	Effect of the storativity ratio on pressure derivative responses of a partially-penetrating well for $M=100$.....	121
Figure 5.14:	Effect of the dimensionless discontinuity radius in Layer 1 on pressure derivative responses of a partially-penetrating well.....	121
Figure 5.15:	Effect of the crossflow parameters on the semi-log pressure derivative responses for $M = 100$.....	122
Figure 5.16:	Effect of the crossflow parameters on the semi-log pressure derivative responses for $M = 1000$.....	122
Figure 5.17:	Effect of the crossflow parameters on the Cartesian pressure derivative for $M=100$.....	123
Figure 5.18:	Effect of the crossflow parameters on the Cartesian pressure derivative for $M=1000$.....	123
Figure 5.19:	Effect of the aquifer mobility-thickness ratio on the semi-log pressure derivative responses for $M=100$.....	124
Figure 5.20:	Effect of the aquifer mobility-thickness ratio on the semi-log pressure derivative responses for $M=1000$.....	124
Figure 5.21:	Effect of the aquifer mobility-thickness ratio on the semi-log pressure derivative responses when layer 1 is penetrated	125

Figure 5.22:	Effect of layering in the aquifer on semi-log pressure derivative responses for $M=100$.....	125
Figure 5.23:	Effect of the dimensionless outer boundary radius on the wellbore pressure of a reservoir with finite aquifer.....	126
Figure 5.24:	Effect of the dimensionless outer boundary radius on the semi-log pressure derivative of a reservoir with a finite aquifer.....	126
Figure 6.1:	Schematic of an n-layer composite reservoir in radial geometry with two different rock and/or fluid types in each layer.....	135
Figure 6.2:	Complex swept zones resulting from very high permeability in Layer 2.....	136
Figure 6.3:	Complex swept zones resulting from very high permeability in Layer 3 and very low permeability in Layer 2.....	136
Figure 6.4:	Effect of a complex front shape on the transient wellbore pressure	137
Figure 6.5:	Effect of a complex front shape on the semi-log pressure derivative responses.....	137

NOMENCLATURE

A'	=	Constant in Equation (C.25)
A_1	=	Constant in Equation (C.36)
A_2	=	Constant in Equation (C.37)
A_i^k	=	Constant in Equation (2.46)
a_1, a_2	=	Constants in Equations (C.36) and (C.37)
a_{1L}, a_{2L}	=	Limiting values of a_1 and a_2 as $t_D \rightarrow \infty$
B	=	Formation volume factor, res m^3 / S m^3
B'	=	Constant in Equation (C.26)
B_1	=	Constant in Equation (C.36)
B_2	=	Constant in Equation (C.37)
B_i^k	=	Constant in Equation (2.47)
b	=	Penetration ratio = h_w/h
b_L	=	Constant defined by Equation (D.30)
C	=	Wellbore storage coefficient, m^3/Pa
C_A	=	Shape factor
C_D	=	Dimensionless wellbore storage, $\frac{C}{2\pi(\phi c_r h) r_w^2}$
c_t	=	Total system compressibility, Pa^{-1}
E_i^k	=	Eigenvector for the region i
F_0	=	Storativity ratio, $(\phi c_r h)_1/(\phi c_r h)_2$

- F_{12} = Storativity ratio between regions 1 and 2 for a 3-region reservoir, $(\phi c_i h)_1 / (\phi c_i h)_2$
- F_{13} = Storativity ratio between regions 1 and 3 for a 3-region reservoir, $(\phi c_i h)_1 / (\phi c_i h)_3$
- f_c = Correction factor for estimating the swept volume
- h, h_i = Formation thickness, m
- h_j = Thickness of the layer j, m
- h_w = Open interval thickness, m
- h_D = Dimensionless wellbore thickness, see Equation (4.4)
- h_D = Dimensionless total reservoir thickness, h/r_w
- k = Horizontal permeability, m²
- k_v = Vertical permeability, m²
- $(k/\phi\mu c_i)_1$ = Diffusivity for the swept region
- l = Laplace variable
- M = Mobility ratio, $(k/\mu)_{\text{swept}} / (k/\mu)_{\text{unswept}}$
- M_{12} = Mobility ratio between Regions 1 and 2 for a 3-region reservoir, $(k/\mu)_1 / (k/\mu)_2$
- M_{13} = Mobility ratio between Regions 1 and 3 for a 3-region reservoir, $(k/\mu)_1 / (k/\mu)_3$
- M_{ij} = Mobility ratio between Zone (i,j) and (i+1,j)
- m_s = Dimensionless Cartesian pressure derivative for any reservoir
- m'_s = Cartesian pressure derivative for any reservoir, Pa/sec
- m_{srf} = Dimensionless Cartesian pressure derivative for a sharp-front reservoir
- n = Number of layers

P	=	Pressure, Pa
P_{in}	=	Initial pressure, Pa
P_D	=	Dimensionless pressure
P_{wD}	=	Dimensionless wellbore pressure
P_{wDPL}	=	Late time dimensionless pressure presented in Equation (D.28)
p_{wDPL}	=	Late time dimensionless pressure presented in Equation (D.29)
r	=	Radial distance, m
r_D	=	Dimensionless radial distance, r/r_w
r_o	=	Radial front distance, m
r_{oD}	=	Dimensionless outer boundary radius for the reservoir and the aquifer, r_o/r_w
r_{oj}	=	Outer boundary distance of layer j, m
R_{avg}	=	Average front radius, m
R_j	=	Radial front distance in layer j, m
R_1	=	Radial front distance in layer 1, m
R_2	=	Radial front distance in layer 2, m
R_{min}	=	Minimum front radius, m
R_{Di}	=	Dimensionless front radius between regions i and i+1
R_{D1}	=	Dimensionless front radius in layer 1, R_1/r_w
R_{D2}	=	Dimensionless front radius in layer 2, R_2/r_w
R_{Dmin}	=	Dimensionless minimum front radius, R_{min}/r_w
R_{Davg}	=	Dimensionless average front radius, R_{avg}/r_w

q	= Flow rate, m ³ /s
s	= Wellbore skin effect
s_j	= Wellbore skin effect for layer j
s_b	= Pseudoskin factor because of partial penetration
s_{bc}	= Pseudoskin factor from the analytical solution
s_{bGA}	= Pseudoskin factor from the simplified expressions
s_{bDR}	= Pseudoskin factor from the Ding and Reynolds study
s_{bYR}	= Pseudoskin factor from the Yeh and Reynolds study
t	= Time, sec
t_{end}	= Time to the end of first radial flow period, sec
t_{max}	= Time for the maximum pressure derivative, sec
t_D	= Dimensionless time
t_{D1}	= Dimensionless time for the end of the first radial flow period
t_{D2}	= Dimensionless time for the beginning of the second radial flow period
t_{DR}	= Dimensionless time based on radial front distance, R , $tk_p/[R^2 (\mu\phi c_1)_1]$
t_{DR1}	= Dimensionless time based on radial front distance, R_1 , $tk_p/[R_1^2 (\mu\phi c_1)_1]$
t_{DR2}	= Dimensionless time based on R_2 , $(k/\mu c_1)_{end}/R_2^2$
t_{DA}	= Dimensionless time based on the swept area
t_{Dmin}	= Dimensionless time based on R_{min} , $(k/\mu c_1)_1/R_{min}^2$
$t_{(DR)end}$	= Dimensionless time to the end of the first radial flow period, $(k/\mu c_1)_1 t_{end}/R_{min}^2$
$t_{(DR)end,cf}$	= Dimensionless time to the end of the first radial flow period for a sharp front

$$\text{case, } (k/\phi\mu c_i)_1 t_{\text{end}}/R_{\text{min}}^2 = 0.18$$

$$t_{(DR)_{\text{max}}} = \text{Dimensionless time for the maximum pressure derivative, } (k/\phi\mu c_i)_1 t_{\text{max}}/R_{\text{min}}^2$$

$$t_{(DR)_{\text{max},f}} = \text{Dimensionless time for the maximum pressure derivative for a sharp front}$$

$$\text{case, } (k/\phi\mu c_i)_1 t_{\text{max}}/R_{\text{min}}^2 = (1.8 + 0.4 \log F_s)M$$

$$X_A = \text{Semi-permeability between layers 1 and 2} = 2/[(h\mu/k_r)_1 + (h\mu/k_r)_2]$$

$$X_{A,j} = \text{Semi-permeability of the zone (i,j) between layers j and j+1}$$

$$X_{B,j} = \text{Semi-permeability of the zone (i,j) between layers j and j-1}$$

$$X_C = \text{Semi-permeability between layer 2 and the gas cap region} = 2/(h\mu/k_r)_2$$

$$V_d = \text{Volume of the half cone frustum in Figure 3.2, m}^3$$

$$V_s = \text{Swept volume, m}^3$$

Greek Symbols

$$\sigma_1, \sigma_2 = \text{Eigenvalues}$$

$$\sigma_i^k = \text{Eigenvalues for region i}$$

$$\kappa = \text{Mobility-thickness ratio} = (kh/\mu)_{\text{aquifer}} / (\overline{kh/\mu})$$

$$\kappa_a = \text{Mobility-thickness ratio of the aquifer, defined by Equation (6.3)}$$

$$\bar{\kappa} = \text{Total mobility-thickness ratio for a multi-layer reservoir}$$

$$\kappa_j = \text{Defined by Equation (2.22)}$$

$$\theta = \text{Front angle, degrees}$$

$$\partial = \text{Partial}$$

- λ, λ_A = Crossflow parameter for a two-layer reservoir, $\frac{2r_w^2}{\left(\frac{h\mu}{k_v}\right)_1 + \left(\frac{h\mu}{k_v}\right)_2} \left(\frac{kh}{\mu}\right)$
- $\overline{\lambda_A}$ = Crossflow parameter for a multi-layer reservoir
- λ_{Aij} = Defined by Equation (2.24)
- λ_{Bij} = Defined by Equation (2.25)
- λ_c = Crossflow parameter between the reservoir and the gas cap = $r_w^2 X_o (kh/\mu)$
- μ = Viscosity, Pa-sec
- ω_{ij} = Defined by Equation (2.23)
- ϕ = Porosity
- ∇ = Differential operator
- Δ = Expression defined by Equation (C.35)

Subscripts

- $1, 2$ = Layer number
- D = Dimensionless
- j = Any layer j
- L = Limiting value as $t_D \rightarrow \infty$
- Open = Layers representing perforated interval
- w = Wellbore

1.0 INTRODUCTION

Most reservoirs are heterogeneous in nature. The presence of layers and zones of different fluid and/or rocks is a common cause for reservoir heterogeneity. The layers may be communicating or non-communicating. Formation crossflow is present when the layers are communicating. When the layers do not communicate with each other, except through the wellbore, then the reservoir is termed a "commingled reservoir". A layered, composite reservoir situation occurs when all or some of the layers have two or more regions of different rock and/or fluid properties.

Because of thermal recovery processes such as steam-flooding, a layered reservoir may resemble a layered, composite reservoir. As a result of steam-flooding, a swept region is created in the reservoir. Usually, the fluid front in such a reservoir is not vertical, but tilted or inclined, because of the gravity override effect. Tilted fronts can also occur in a thick, homogeneous reservoir owing to gravity override effects. Figure 1.1 schematically shows a steam-flooded reservoir under a bottom-water condition. The inclined line shows the fluid front and θ is the angle of inclination. Vertical arrows show the crossflow between layers and between the reservoir and the aquifer. The size of the aquifer may be finite or infinite. When the aquifer is very large compared to the reservoir, the aquifer is called an infinite aquifer and the boundary between the reservoir and the aquifer is considered as a constant pressure boundary¹.

Under a bottom-water condition, wells are partially perforated to avoid or delay the production of water. Figure 1.1 shows a partially penetrating well. Because of partial penetration, an additional pressure drop occurs near the wellbore which is known as a "pseudoskin factor". Several analytical expressions are available in the literature² to estimate the pseudoskin factor due to partial penetration, but are only applicable for closed top and bottom boundaries.

Numerous studies have been reported in the literature on layered and composite reservoirs, and Gomes and Ambastha¹ have presented an extensive literature review on these studies. Most of these studies are limited to layered systems without composite zones in the radial direction or to single-layer, composite reservoirs.

A limited number of studies have been conducted on multi-layer, composite reservoirs. Satman³ presented injectivity and falloff responses for a commingled, multi-layer composite reservoir and introduced the concept of a tilted front. Satman and Oskay⁴ considered the discontinuity boundary as a tilted front (inclined front) to account for the gravity override effect and modelled the reservoir as a multi-layer, composite reservoir without formation crossflow.

The objective of this study is to develop an analytical solution for a multi-layer, composite reservoir with pseudosteady-state formation crossflow and conduct transient pressure analysis for thermal recovery processes, such as steam-flooding, in which the gravity override effect is important. Because of layering or the gravity override effects, the fluid boundary is tilted or irregularly-shaped. The objective of this study is to investigate the effect of the tilted or irregularly-shaped front on transient pressure analysis. The objective includes an investigation of the pseudoskin factors for partially-penetrating wells in multi-layer reservoirs with or without a bottom-water condition. The objective also includes a study of the transient pressure behaviour for wells in multi-layer, composite reservoirs under finite or infinite bottom-water conditions.

Chapter 2 presents the development and the verification of the analytical solution for multi-layer composite reservoirs with pseudosteady-state (pps) formation crossflow. Using the eigenvalues and eigenvectors of the system, this method computes transient pressure behaviour more efficiently than the method described by Anbarci et al.⁵ The developed model can handle tilted or irregularly-shaped fluid fronts, multiple, composite regions,

bottom-water condition, partially-penetrating wells, and all commonly-used outer-boundary conditions. Chapter 3 presents well test analysis for multi-layer composite reservoirs with tilted fronts. The effects of the front angle and layer refinement on transient pressure analysis have been discussed. The applicability of the pseudosteady-state analytical method to estimate the swept volume has been investigated and a correction factor has been developed to correct the swept volume from *pas* analysis.

Chapter 4 presents new analytical expressions for pseudoskin factors for partially-penetrating wells in multi-layer reservoirs with both closed top and bottom boundaries and with bottom-water zones or gas caps. These new pseudoskin expressions are very easy to use and require a knowledge of two parameters when the top and bottom boundaries are closed, and three parameters in the presence of a bottom-water zone or a gas cap. Chapter 5 presents transient pressure responses of a well in a multi-layer, composite reservoir under bottom-water. Both finite and infinite, bottom-water conditions have been considered and the effect of aquifer size on transient pressure analysis has been investigated.

Chapter 6 presents the algorithm and the computer program of the model. The computer program has been written in FORTRAN 77. Eigenvalues and eigenvectors have been calculated using the IMSL Math Library. The system of simultaneous equations resulting from the boundary conditions has also been solved using the IMSL Math Library. Chapter 7 presents a general discussion and the conclusions of the entire study and recommends some studies to extend this work.

Appendices A, B, C, D, and E show the derivations of some expressions in detail. Appendix F shows the computer program for the model developed. Appendices G and H show published or presented papers from this study.

References

1. Gomes, E. and Ambastha, A.K.: "An Analytical Pressure-Transient Model for Multilayered, Composite Reservoirs with Pseudosteady-State Formation Crossflow," paper SPE 26049 presented at the 1993 Western Regional Meeting, Anchorage, AK (May 26-28); see also *AOSTRA Journal of Research*, Vol. 8, No.2 (Spring 1992) 63-77.
2. Gomes, E. and Ambastha, A.K.: "Analytical Expressions For Pseudoskin for Partially-Penetrating Wells Under Various Reservoir Conditions," paper SPE 26484 presented at the 1993 Annual Meeting, Houston, TX, Oct. 3-6.
3. Satman, A.: "An Analytical Study of Transient Flow in Stratified Systems with Fluid Banks," paper SPE 10264 presented at the 1981 Annual Meeting, San Antonio, TX, Oct. 5-7).
4. Satman, A. and Oskay, M.M.: "Effect of a Tilted Front on Well Test Analysis," paper SPE 14701 available from SPE (1985).
5. Anbarci, K., Grader, A.S. and Ertekin, T.: "Determination of Front Locations in Multilayer Composite Reservoir," paper SPE 19799 presented at the 1989 Annual Meeting, San Antonio, TX, Oct. 8-11.

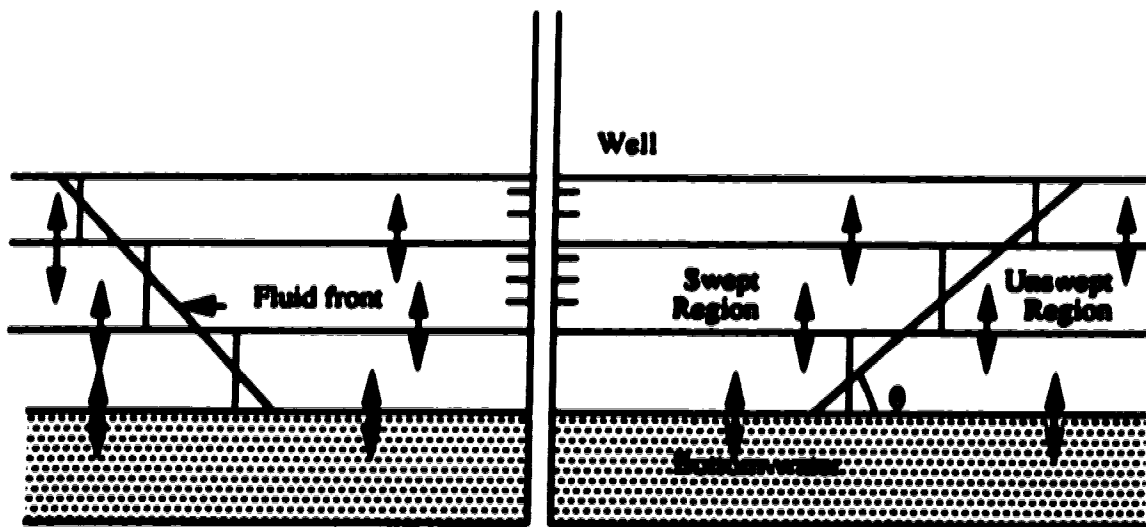


Figure 1.1 : Layered composite reservoir with a tilted front under a bottom-water condition.

2.0 MODEL DEVELOPMENT

2.1 Introduction

Most reservoirs are heterogeneous in nature. The presence of layers and zones of different fluid and/or rocks is a common cause for reservoir heterogeneity. Figures 2.1a and 2.1b show a layered reservoir and a layered, composite reservoir, respectively. The horizontal lines show the layering and the arrows show the presence of crossflow. The layers may be communicating or non-communicating. Formation crossflow is present when the layers are communicating. When the layers do not communicate with each other, except through the wellbore, then the reservoir is termed a "commingled reservoir". A layered, composite reservoir may result because of artificial processes. Enhanced oil recovery processes, such as steam flooding, CO₂ flooding, and in-situ combustion, tectonic movements, phase changes, acidizing, and temperature differences may cause a reservoir to behave as a composite reservoir. The tilted line in Figure 2.1b shows the discontinuity boundary or the fluid front. A layered, composite reservoir situation occurs when all or some of the layers have two or more regions of different rock and/or fluid properties.

Numerous studies¹⁻⁹⁹ have been reported in the literature on layered reservoirs and Table 2.1 lists the relevant papers on layered reservoirs. One aspect in which the studies differ is the way they model crossflow between the layers. Formation crossflow has been modelled mainly by two methods: pseudosteady-state crossflow and transient crossflow. Pseudosteady-state crossflow assumes that the resistance to crossflow is confined to the interlayer boundary and the flow is horizontal within each layer. This assumption reduces a two-dimensional problem to a one-dimensional problem. Transient crossflow utilizes the two-dimensional diffusivity equation for each layer. Table 2.1 also shows that, although numerous studies have appeared on layered reservoirs with formation crossflow, very little work has been reported for layered, composite reservoirs with formation crossflow.

Responses of layered reservoirs may be summarized as follows: for commingled reservoirs, the time needed to reach pseudosteady state is an order of magnitude higher than that for homogeneous reservoirs; semi-log analysis can be used to estimate the average permeability-thickness product and the skin effect; initially, a crossflow system and a commingled system have the same responses; then there is a transition period and, finally, the crossflow system behaves like an equivalent homogeneous system.

Satman²¹ presented drawdown and buildup responses for a commingled, multi-layered composite reservoir. In his model, he considered different discontinuity boundary radii for different layers. He used the concept of a tilted front for layered composite reservoirs, because the fluid front would propagate at different rates in different layers. For enhanced recovery processes, such as steam flooding, Satman and Oskay³⁴ considered the discontinuity boundary as a tilted front to account for the gravity-override effects and modelled the reservoir as a multi-layer, composite reservoir without crossflow. They concluded that the tilted front model is a better representation of the actual reservoir than the sharp-front model when the gravity override effect is present. Hatzignatiou et al.⁴⁵ presented a solution for interference pressure transient behaviour in a two-layer reservoir having pseudosteady state formation crossflow and described a type-curve matching technique to estimate the reservoir properties. Anbarci et al.³⁵ presented an analytical solution for a two-layer, composite reservoir. They included wellbore storage and skin, and considered pseudosteady state crossflow between the layers. They conducted a limited sensitivity study and used a type-curve matching technique to locate the front in a particular layer. The preceding discussion shows that a general solution for an n-layer composite reservoir with crossflow is yet to be developed. In this study, an analytical solution and its validation for multi-layered, composite reservoirs with formation crossflow have been presented. The usefulness of this solution for future studies has also been discussed.

2.2 Model Development

This study considers an n -layer, radial, composite reservoir as shown in Figure 2.2. A symmetrically located well fully penetrates the reservoir. The well produces at a constant flow rate and pseudosteady-state formation crossflow is present between the layers. The problem is solved by starting with the approach of Anbarci et al.³⁵. In Figure 2.2, the discontinuity boundary in each layer is represented by a vertical solid line. These discontinuity boundaries have been vertically extended across all the layers. As a result, depending on the total number of discontinuity boundaries and their locations, an n -layer reservoir may have m number of regions in each layer. Therefore, the reservoir is divided into $n \times m$ zones and each zone may be identified by (i,j) , in which i and j denote the region and the layer, respectively. Each zone may have different rock and/or fluid properties, and can have variable length in the radial direction depending on the discontinuity boundary locations. In an actual reservoir, we may not need $n \times m$ zones of different rock and/or fluid properties. In Figure 2.2, the shaded and non-shaded areas represent two different fluid and/or rock types. Each layer has only two different rock and/or fluid types separated by a discontinuity boundary. In each layer, the discontinuity boundary is placed at a different location to simulate a tilted-front discontinuity boundary for the reservoir and for this particular situation, $m=n+1$. Layers are assumed to be of constant thicknesses throughout the reservoir.

The crossflow between layers within the reservoir is modelled as in the semi-permeable wall model proposed by Gao²⁸. Thus, crossflow resistance is assumed to be confined to the interlayer boundary and flow in each layer is horizontal. It is also assumed that the upper boundary of the top layer and the lower boundary of the bottom layer are closed. Other assumptions for the development of the mathematical model are as follows:

1. Reservoir fluids are slightly compressible and have constant compressibility.

2. The effects of gravity and capillary forces are negligible.
3. The flow in the formation is described by Darcy's law.
4. When a fluid crosses the boundary of its zone, it behaves as the fluid on the downstream side.

The flow equation for zone i,j can be written as:

$$\left(\frac{kh}{\mu} \right)_{ij} \left(\frac{\partial^2 p_{ij}}{\partial r^2} + \frac{1}{r} \frac{\partial p_{ij}}{\partial r} \right) = (\phi c_i h)_{ij} \frac{\partial p_{ij}}{\partial t} + X_{Aij}(p_{ij} - p_{ij+1}) + X_{Bij}(p_{ij} - p_{ij-1}) \quad (2.1)$$

where X_{Aij} and X_{Bij} are defined as follows:

$$X_{Aij} = \frac{2}{\left(\frac{h\mu}{k_v} \right)_{ij} + \left(\frac{h\mu}{k_v} \right)_{ij+1}} \quad (2.2)$$

$$X_{Bij} = \frac{2}{\left(\frac{h\mu}{k_v} \right)_{ij} + \left(\frac{h\mu}{k_v} \right)_{ij-1}} \quad (2.3)$$

$$X_{Bij} = 0 \quad \text{for } i = 1, \dots, m \quad (2.4)$$

$$X_{Aij} = 0 \quad \text{for } i = 1, \dots, m \quad (2.5)$$

Initial condition: Initially all zones are at initial pressure and thus,

$$p_{ij}(r,0) = p_m \quad \text{for all } i \text{ and } j \quad (2.6)$$

Inner boundary condition:

$$p_{wf} = p_{1,j}(r_w, t) - s_j \left(r_w \frac{\partial p_{1,j}}{\partial r} \right)_{r=r_w} \text{ for } j = 1, \dots, n \quad (2.7)$$

$$q = -C \frac{\partial p_{wf}}{\partial t} + 2\pi r_w \sum_{j=1}^n \left(\frac{kh}{\mu} \right)_{1,j} \left(\frac{\partial p_{1,j}}{\partial r} \right)_{r=r_w} \text{ for } j = 1, \dots, n \quad (2.8)$$

Outer boundary conditions:

Infinitely large system:

$$p_{m,j} = p_{in} \text{ for } r \rightarrow \infty \text{ and } j = 1, n \quad (2.9)$$

Finite system with a constant pressure equal to the initial pressure at the outer boundary:

$$p_{m,j} = p_{in} \text{ for } r=r_{ej} \text{ and } j = 1, \dots, n \quad (2.10)$$

Finite system with a closed outer boundary:

$$\frac{\partial p_{m,j}}{\partial r} = 0 \text{ for } r=r_{ej} \text{ and } j = 1, \dots, n \quad (2.11)$$

The flow equations for different zones in the same layer are coupled using the following interface conditions defining pressure and flow rate continuity between these zones:

$$p_{i,j} = p_{i+1,j} \text{ for } r=R_i \text{ and } i = 1, \dots, m-1 \text{ and } j = 1, \dots, n \quad (2.12)$$

$$\frac{\partial p_{i,j}}{\partial r} = M_{i,j} \frac{\partial p_{i+1,j}}{\partial r} \text{ for } r=R_i \text{ and } i = 1, \dots, m-1 \text{ and } j = 1, \dots, n \quad (2.13)$$

where,

$$M_{i,j} = \frac{\left(\frac{kh}{\mu} \right)_{i+1,j}}{\left(\frac{kh}{\mu} \right)_{i,j}} \quad (2.14)$$

Dimensionless variables are defined as follows:

$$r_D = \frac{r}{r_w} \quad \dots\dots\dots (2.15)$$

$$p_{Dij} = \frac{2\pi}{q} \left(\frac{kh}{\mu} \right) (p_{in} - p_{ij}) \quad \dots\dots\dots (2.16)$$

$$p_{wD} = \frac{2\pi}{q} \left(\frac{kh}{\mu} \right) (p_{in} - p_{wf}) \quad \dots\dots\dots (2.17)$$

$$t_D = \frac{1}{r_w^2} \frac{\left(\frac{kh}{\mu} \right)}{\left(\phi_{ci} h \right)}, \quad \dots\dots\dots (2.18)$$

where,

$$\left(\frac{kh}{\mu} \right) = \sum_{j=1}^n \left(\frac{kh}{\mu} \right)_{1,j} \quad \dots\dots\dots (2.19)$$

$$\left(\phi_{ci} h \right) = \sum_{j=1}^n \left(\phi_{ci} h \right)_{1,j}, \quad \dots\dots\dots (2.20)$$

Expressing the flow equation and the boundary conditions in terms of dimensionless variables yields:

$$\begin{aligned} \alpha_{ij} \left(\frac{\partial^2 p_{Dij}}{\partial r_D^2} + \frac{1}{r_D} \frac{\partial p_{Dij}}{\partial r_D} \right) &= \alpha_{ij} \frac{\partial p_{Dij}}{\partial t_D} + \lambda_{1ij} (p_{Dij} - p_{Dij+1}) \\ &+ \lambda_{2ij} (p_{Dij} - p_{Dij-1}), \quad \dots\dots\dots (2.21) \end{aligned}$$

where,

$$\alpha_{ij} = \frac{\left(\frac{kh}{\mu} \right)_{1,j}}{\left(\frac{kh}{\mu} \right)} \quad \dots\dots\dots (2.22)$$

$$\omega_{ij} = \frac{(\phi c_i h)_{ij}}{(\phi c_i h)} \dots\dots\dots (2.23)$$

$$\lambda_{Aij} = \frac{r_{ij}^2}{\left(\frac{kh}{\mu}\right)} X_{Aij} \dots\dots\dots (2.24)$$

$$\lambda_{Bij} = \frac{r_{ij}^2}{\left(\frac{kh}{\mu}\right)} X_{Bij} \dots\dots\dots (2.25)$$

Initial condition:

$$p_{Di,j}(r_D, 0) = 0, \quad \text{for all } i \text{ and } j \dots\dots\dots (2.26)$$

Inner boundary condition:

$$p_w = p_{Di,j}(1, t_D) - s_j \left(\frac{\partial p_{Di,j}}{\partial r_D} \right), \quad \text{for } j = 1, \dots, n \dots\dots\dots (2.27)$$

$$1 = C_D \frac{\partial p_w}{\partial t_D} - \sum_{j=1}^n \kappa_{1j} \left(\frac{\partial p_{Di,j}}{\partial r_D} \right), \dots\dots\dots (2.28)$$

Outer boundary conditions:

Infinitely large system:

$$p_{Dm,j} = 0, \quad \text{for } r_D \rightarrow \infty \text{ and } j = 1, \dots, n \dots\dots\dots (2.29)$$

Finite system with a constant pressure at the outer boundary:

$$p_{Dm,j} = 0, \quad \text{for } r_D = r_{oD,j} \text{ and } j = 1, \dots, n \dots\dots\dots (2.30)$$

Finite system with a closed outer boundary:

$$\frac{\partial p_{Dm,j}}{\partial r_D} = 0, \quad \text{for } r_D = r_{eD,j} \text{ and } j = 1, \dots, n \quad \dots\dots\dots (2.31)$$

Interface conditions defining pressure and flow rate continuity between the zones of a layer:

$$p_{Di,j} = p_{Di+1,j} \quad \text{for } r_D = R_{Di} \text{ and } i = 1, \dots, m-1 \text{ and } j = 1, \dots, n \quad \dots\dots\dots (2.32)$$

$$\frac{\partial p_{Di,j}}{\partial r_D} = M_{i,j} \frac{\partial p_{Di+1,j}}{\partial r_D} \quad \text{for } r_D = R_{Di} \text{ and } i = 1, \dots, m-1 \text{ and } j = 1, \dots, n \quad \dots\dots\dots (2.33)$$

The Laplace transformation of Equations (2.21), and (2.27) through (2.33), yields:

$$\kappa_{i,j} \left(\frac{d^2 \bar{p}_{Di,j}}{dr_D^2} + \frac{1}{r_D} \frac{d\bar{p}_{Di,j}}{dr_D} \right) = \omega_{i,j} \bar{p}_{Di,j} + \lambda_{i,j} (\bar{p}_{Di,j} - \bar{p}_{Di,j+1}) \\ + \lambda_{i,j} (\bar{p}_{Di,j} - \bar{p}_{Di,j-1}), \quad \dots\dots\dots (2.34)$$

Inner boundary condition:

$$\bar{p}_{wD} = \bar{p}_{Di,j}(1) - s_j \left(\frac{d\bar{p}_{Di,j}}{dr_D} \right), \quad \text{for } j = 1, \dots, n \quad \dots\dots\dots (2.35)$$

$$\frac{1}{f} = C_D \bar{p}_{wD} - \sum_{j=1}^n \kappa_{i,j} \left(\frac{d\bar{p}_{Di,j}}{dr_D} \right), \quad \dots\dots\dots (2.36)$$

Outer boundary conditions:

Infinitely large system:

$$\bar{p}_{Dm,j} = 0, \quad \text{for } r_D \rightarrow \infty \text{ and } j = 1, \dots, n \quad \dots\dots\dots (2.37)$$

Finite system with a constant pressure at the outer boundary:

$$\bar{p}_{Dm,j} = 0, \quad \text{for } r_D = r_{eD,j} \text{ and } j = 1, \dots, n \quad \dots\dots\dots (2.38)$$

Finite system with a closed outer boundary:

$$\frac{d\bar{p}_{Dm,j}}{dr_D} = 0, \quad \text{for } r_D = r_{eD,j} \text{ and } j = 1, \dots, n \quad (2.39)$$

Interface conditions defining pressure and flow rate continuity between the zones of a layer:

$$\bar{p}_{Di,j} = \bar{p}_{Di+1,j} \quad \text{for } r_D = R_{Di} \text{ and } i = 1, \dots, m-1 \text{ and } j = 1, \dots, n \quad (2.40)$$

$$\frac{d\bar{p}_{Di,j}}{dr_D} = M_{i,j} \frac{d\bar{p}_{Di+1,j}}{dr_D}, \quad \text{for } r_D = R_{Di} \text{ and } i = 1, \dots, m-1 \text{ and } j = 1, \dots, n \quad (2.41)$$

Equation (2.34) has the form of a modified Bessel's equation and thus, assume a solution of the following form for Equation (2.34):

$$\bar{p}_{Di,j} = A_{i,j} K_0(\sigma r_D) + B_{i,j} I_0(\sigma r_D), \quad (2.42)$$

Introducing Equation (2.42) into the left-hand side of Equation (2.34), we get:

$$\kappa_{i,j} \left(\frac{d^2 \bar{p}_{Di,j}}{dr_D^2} + \frac{1}{r_D} \frac{d\bar{p}_{Di,j}}{dr_D} \right) = \kappa_{i,j} \sigma^2 \bar{p}_{Di,j} \quad (2.43)$$

Substituting Equation (2.43) into Equation (2.34) results in the following general equation:

$$\lambda_{i,j} \bar{p}_{Di,j+1} + (\sigma^2 \kappa_{i,j} - \kappa_{i,j} - \lambda_{i,j} - \lambda_{i,j}) \bar{p}_{Di,j} + \lambda_{i,j} \bar{p}_{Di,j-1} = 0 \quad (2.44)$$

Equation (2.44) has the form of a generalized eigenvalue system. As pointed out by Ehlig-Economides and Joseph⁴³, Equation (2.44) has a non-trivial solution (i.e., $\bar{p}_{Di,j} \neq 0$) if and only if its coefficient matrix is singular. Thus, the determinant of the coefficient matrix has to be zero. The coefficient matrix is an $n \times m$ by $n \times m$ tridiagonal matrix. The coefficient matrix can be divided into m smaller real-symmetric, positive-definitive tridiagonal matrices, where the σ^2 terms act as the eigenvalues, and these eigenvalues are always positive. The determinant of each of these sub-matrices is an n th order polynomial in σ^2 ,

and, from each determinant, n eigenvalues can be obtained. Now, a general solution for each zone can be written as:

$$P_{DU} = \sum_{k=1}^n [A_{ij}^k K_0(\sigma_1^k r_D) + B_{ij}^k I_0(\sigma_1^k r_D)], \quad \dots\dots\dots (2.45)$$

Constants A_{ij}^k and B_{ij}^k can be split into two parts as follows:

$$A_{ij}^k = E_{ij}^k A_i^k, \quad \dots\dots\dots (2.46)$$

and

$$B_{ij}^k = E_{ij}^k B_i^k, \quad \dots\dots\dots (2.47)$$

where E_{ij}^k is the eigenvector for region i, and this eigenvector can be calculated from Equation (2.44). Constants A_i^k and B_i^k are to be determined from the boundary conditions. Now, a general solution for region i and layer j becomes:

$$P_{DU} = \sum_{k=1}^n [A_i^k E_{ij}^k K_0(\sigma_1^k r_D) + B_i^k E_{ij}^k I_0(\sigma_1^k r_D)], \quad \dots\dots\dots (2.48)$$

Equation (2.48) contains $2n \times m$ constants to be evaluated from the boundary conditions.

For the inner boundary condition, without considering wellbore storage, we can write:

$$P_{wD} = \sum_{k=1}^n \left[\begin{aligned} & (A_i^k E_{ij}^k K_0(\sigma_1^k) + B_i^k E_{ij}^k I_0(\sigma_1^k)) \\ & + z_j \sigma_1^k (A_i^k E_{ij}^k K_1(\sigma_1^k) - B_i^k E_{ij}^k I_1(\sigma_1^k)) \end{aligned} \right] \quad \text{for } j=1, \dots n \quad \dots\dots\dots (2.49)$$

$$\frac{1}{r} = \sum_{j=1}^n \kappa_{ij} \sum_{k=1}^n \sigma_1^k [A_i^k E_{ij}^k K_1(\sigma_1^k) - B_i^k E_{ij}^k I_1(\sigma_1^k)] \quad \text{for } j=1, \dots n \quad \dots\dots\dots (2.50)$$

For an infinite outer boundary condition, we can write:

$$\sum_{k=1}^n [A_i^k E_{mj}^k K_0(\sigma_m^k r_D) + B_i^k E_{mj}^k I_0(\sigma_m^k r_D)] = 0$$

for $r_D \rightarrow \infty$ and $j = 1, \dots n \quad \dots\dots\dots (2.51)$

The condition that the pressure is bounded yields:

$$\sum_{k=1}^n B_m^k = 0 \quad \text{for } j = 1, \dots, n \quad \dots\dots\dots (2.52)$$

A constant-pressure, outer boundary condition yields:

$$\sum_{k=1}^n \left[A_m^k E_{mj}^k K_0(\sigma_m^k r_{oD}) + B_m^k E_{mj}^k I_0(\sigma_m^k r_{oD}) \right] = 0 \quad \text{for } j = 1, \dots, n \quad \dots\dots\dots (2.53)$$

A no-flow, outer boundary condition yields:

$$\sum_{k=1}^n \left[A_m^k E_{mj}^k K_1(\sigma_m^k r_{oD}) + B_m^k E_{mj}^k I_1(\sigma_m^k r_{oD}) \right] = 0 \quad \text{for } j = 1, \dots, n \quad \dots\dots\dots (2.54)$$

The interface conditions defining continuity in pressure and flow rate yield, respectively:

$$\begin{aligned} \sum_{k=1}^n \left[A_i^k E_{ij}^k K_0(\sigma_i^k R_{Di}) + B_i^k E_{ij}^k I_0(\sigma_i^k R_{Di}) \right] = \\ \sum_{k=1}^n \left[A_{i+1}^k E_{i+1,j}^k K_0(\sigma_{i+1}^k R_{Di}) + B_{i+1}^k E_{i+1,j}^k I_0(\sigma_{i+1}^k R_{Di}) \right] \\ \text{for } j = 1, \dots, n \text{ and } i = 1, \dots, m-1 \quad \dots\dots\dots (2.55) \end{aligned}$$

$$\begin{aligned} \sum_{k=1}^n \left[A_i^k E_{ij}^k K_1(\sigma_i^k R_{Di}) - B_i^k E_{ij}^k I_1(\sigma_i^k R_{Di}) \right] = \\ \sum_{k=1}^n \left[A_{i+1}^k E_{i+1,j}^k K_1(\sigma_{i+1}^k R_{Di}) - B_{i+1}^k E_{i+1,j}^k I_1(\sigma_{i+1}^k R_{Di}) \right] \\ \text{for } j = 1, \dots, n \text{ and } i = 1, \dots, m-1 \quad \dots\dots\dots (2.56) \end{aligned}$$

Equations (2.49) through (2.56) give a total of $2n \times m$ simultaneous equations which can be solved to find $2n \times m$ values of the coefficients A_j^k and B_j^k .

Thus, the preceding solution models transient fluid flow in an n-layer, composite reservoir with pseudosteady-state crossflow. This new solution uses the eigenvalues and eigenvectors of the system and is computationally more efficient than other methods proposed in the literature. For example, for a 5-layer, composite reservoir ($m=6$), this new solution requires the solution of only 60 simultaneous equations, whereas the method proposed by Anbarci et al.³⁵ requires the solution of 300 simultaneous equations to solve the same problem. By assigning a constant-pressure boundary at the top or at the bottom, this new solution can include a gas cap or a bottom-water drive, respectively. This new solution is also capable of treating any irregularly-shaped fluid-front by dividing the reservoir into a number of mathematical layers.

To include bottom-water drive, the lower boundary of the bottom layer is considered as a constant-pressure boundary. Mathematically, the vertical permeability of the bottom-water zone is considered infinite and Equation (2.4) is modified as follows:

$$X_{B,i,1} = \frac{2}{\left(\frac{h\mu}{k_v}\right)_{i,1}} \quad \text{for } i = 1, \dots, m \quad \dots\dots\dots (2.4a)$$

Also, in the diffusivity equation for layer $j=1$, $p_{i,j,1}$ is replaced by the initial pressure, p_{in} . Similarly, to include a gas-cap drive, the upper boundary of the top layer is considered as a constant-pressure boundary, and the vertical permeability of the gas-cap zone is considered to be infinite. Therefore, Equation (2.5) is modified as follows:

$$X_{A,i,n} = \frac{2}{\left(\frac{h\mu}{k_v}\right)_{i,n}} \quad \text{for } i = 1, \dots, m \quad \dots\dots\dots (2.5a)$$

Also, in the diffusivity equation for layer $j=n$, $p_{i,j,1}$ is replaced by the initial pressure, p_{in} . For a partially-penetrating well, the inner boundary condition needs some modification. Both Equations (2.7) and (2.8) are considered to apply only for layers penetrated by the

well. For layers that are not open to flow to the wellbore, the inner boundary condition can be written as:

$$\frac{\partial p_{1,j}}{\partial r} = 0, \quad \text{for } r = r_w \text{ and } j = \text{layers not open to flow to the wellbore} \quad \dots\dots\dots (2.8a)$$

For a partially-penetrating well, Equations (2.7), (2.8) and (2.8a) together describe the inner boundary condition.

2.3 Solution Methodology

The following steps were involved to solve Equation (2.48) at any region i and layer j :

1. From Equation (2.44), eigenvalues and eigenvectors were calculated using an appropriate subroutine from the IMSL Math/Library⁴⁰.
2. From the boundary conditions, $2n \times m$ simultaneous equations were set up and then solved using Gauss' elimination routine from the IMSL Math/Library⁴⁰ for the constants A_i^k and B_i^k .
3. Dimensionless pressure in Laplace space is calculated using Equation (2.48) and then numerically inverted using the Stehfest algorithm⁴¹.
4. The wellbore storage effect is included using the following well-known relationship:

$$\bar{p}_{wD} = \frac{1}{C_D s^2 + \frac{1}{(\bar{p}_{wD})_{C_D=0}}} \quad \dots\dots\dots (2.57)$$

The computation process involves repeated calculation of Bessel's functions. Very small and large arguments of Bessel's functions create an overflow problem during the computational process. This problem is overcome by using a dimensionless radius, r_D .

based on the minimum front radius, R_1 , instead of the wellbore radius, and by calculating Bessel's functions in exponentiated form.

2.4 Model Validation

The analytical solution was validated by generating some well-known pressure transient responses for various cases of homogeneous, composite, and layered reservoirs, which are subsets of the general solution developed. Figure 2.3 shows a comparison of results generated by the new analytical solution with an Agarwal *et al.*⁶² type-curve for homogeneous reservoirs. Homogeneous reservoir responses were generated by setting identical reservoir properties for each of the layers of a two-layer reservoir and by setting very high crossflow (of the order of 10^3) parameters. The responses were generated for different wellbore-storage and skin effects. Figure 2.3 shows a successful match between the two solutions. Figure 2.4 shows a comparison of the responses of this study with Tariq and Ramey's solution¹⁸ for a two-layer, commingled reservoir with a closed outer boundary. Commingled layered reservoir responses were generated by setting different layer properties for each layer and by assigning very small (of the order of 10^{-13}) crossflow parameters. Figure 2.4 shows a very good match between the two results for different wellbore-storage effects. Figure 2.5 shows a comparison of responses of this study with the Eggenschwiler *et al.*⁶³ solution for a single-layer, two-region composite reservoir. In the model, a single-layer, composite reservoir is obtained by dividing a two-layer reservoir into two regions and setting different properties for them. In each region, the layers are assigned identical fluid and rock properties and a very high crossflow parameter. The responses were generated for different mobility ratios and Figure 2.5 shows a good match between the two solutions. Figure 2.6 shows a comparison of the results of this study with Ambastha and Ramey's⁶⁴ pressure derivative solution for a single-layer, two-region, composite reservoir. Again, Figure 2.6 shows a good match between the two solutions. Figure 2.7 shows a comparison of this study with Ambastha

and Ramey's solution⁴⁵ for a three-region composite reservoir. The three-region composite reservoir response was generated by dividing a 2-layer reservoir into three regions and setting different fluid properties for each region. The layers were assigned identical fluid and rock properties in each region and very high crossflow parameters. Figure 2.7 shows pressure derivative responses for different mobility ratios between zones one and two and the responses show a good match between the two solutions.

Figure 2.8 shows the effect of crossflow on pressure transient responses for a two-layer reservoir. The upper and the lower straight lines represent commingled and homogeneous reservoir responses, respectively. Initially, the reservoir behaves like a commingled reservoir. Then, depending on the crossflow parameter λ , there is a transition period during which the crossflow effect becomes important and the responses change from those for a commingled reservoir to those for a homogeneous reservoir. At late time, the reservoir behaves like an equivalent homogeneous system. The transition from commingled reservoir behaviour to homogeneous reservoir behaviour depends on the crossflow parameter. The higher the crossflow parameter, the earlier the transition occurs. The above observation is consistent with layered reservoir behaviour reported in the literature.

Figure 2.9 shows the pressure drawdown responses of a partially-penetrating well in a two-layer reservoir subject to bottom-water drive. The upper layer is open to flow and the lower layer is closed. For a penetration ratio of 0.5, the two curves show the responses for two different crossflow parameters. Both curves show radial flow characteristics until the effect of the constant-pressure boundary becomes dominant. Similar observations have been made by Streltsova-Adams⁴⁶ and Buhidma and Raghavan⁴⁷. For a lower crossflow parameter, it takes a longer time for the constant pressure boundary to have a dominant effect on the pressure drawdown responses.

2.5 Future Possibilities

In this study, a general analytical solution for an n-layer, composite reservoir with pseudosteady state interlayer crossflow has been developed and validated. Formation crossflow has been modelled as pseudosteady state interlayer crossflow. This method is very general and computationally efficient. This method has an advantage over the finite difference method in that this method does not require extensive discretization like the finite difference method.

A reservoir undergoing a thermal recovery process has been idealized as a single-layer, composite reservoir for a long time^{63,64,68-71}. This new model can be used to analyze more general scenarios of heterogeneous reservoirs undergoing thermal recovery processes. Effects of gravity override or underride, viscous fingering, and so forth, on a discontinuity boundary can be treated as a tilted or any other irregularly-shaped front and its effects on pressure transient responses can be studied. Pressure transient analysis of both drawdown and buildup tests can be studied with this model.

This new model can also accommodate the situation where each layer has a different outer boundary distance, r_{oi} . This can be done by vertically extending the outer boundary of each layer, the same way as has been done for the discontinuity boundaries. This will create some mathematical zones (which do not exist) which will be taken care of by assigning very small horizontal and vertical permeabilities to them.

Another possibility is to use automated type-curve matching to analyze rate and pressure measurements from different layers of layered, composite reservoirs. The effect of a gas cap or bottom-water can be included by properly specifying pressure and semi-permeabilities at the appropriate boundary to yield a constant-pressure boundary at the top or bottom, respectively. Transient pressure responses of a partially-penetrating well in a

layered reservoir subject to the effects of a bottom-water and/or a gas cap can be investigated with this model. The proposed analytical solution may also lead to new and/or improved methods for analyzing well test data from multi-layered, composite reservoirs with formation crossflow. Efforts are underway to develop some simplified type-curves for the system under study.

2.6 Conclusions

- 1. A general, analytical solution for pressure transient responses for an n-layer, composite reservoir with pseudosteady state interlayer crossflow has been developed and validated.**
- 2. The new, analytical solution developed in this study is a more efficient and versatile solution than presently-available solutions in the literature.**
- 3. The new analytical solution of this study offers new possibilities to analyze more complicated well-testing scenarios than the possibilities offered by presently-available solutions.**

References

- 1. Jacquard, P.: "Etude Mathematique du Drainage d'un Reservoir Heterogene," *Revue de l'Institut Francais du Petrole*, Vol. XV, No. 10 (1960) 1384-1400.**
- 2. Tempelaar-Lietz, W.: "Effect of the Rate of Oil Production Upon the Performance of Wells Producing from more than One Horizon," *SPEJ* (March 1961) 26-31.**
- 3. Lefkovits, H.C. et al.: "A Study of the Behavior of Bounded Reservoirs Composed of Stratified Layers," *SPEJ* (March 1961) 43-58; *Trans., AIME*, 222.**
- 4. Duvaut, G.: "Drainage des systems heterogenes," *Rev. Inst. Fran. Petrole* (1961) 16, No. 10, 1164-1170.**

5. Pelissier, F. and Seguiers, P.: "Analysis numerique des equations des bicouches," *Rev. Inst. Fran. Petrole* (1961) 16, No. 10, 1182--87.
6. Pottier, J.: "Modeles heterogenes avec communications," *Rev. Inst. Fran. Petrol.* (1961) 16, No.10, 1127-46.
7. Polubarinova-Kocina, P.Ya.: *Theory of Groundwater Movement* , Translated from Russian by J.M. Roger de Weist, Princeton U. Press, Princeton, NJ, (1962) 381-95.
8. Russell, D.G. and Prats, M.: "Performance of Layered Reservoirs with Crossflow: Single-Compressible -Fluid Case," *JPT* (March 1962) 53-57; *Trans.*, AIME, 225.
9. Russell, D.G. and Prats, M.: "The Practical Aspects of Interlayer Crossflow," *JPT* (June 1962) 589-92.
10. Katz, M.L. and Tek, M.R.: "A Theoretical Study of Pressure Distribution and Fluid Flux in Bounded Stratified Porous Systems With Crossflow," *SPEJ* (March 1962) 68-82; *Trans.*, AIME, 225.
11. Pendergrass, J.D. and Berry, V.J.: "Pressure Transient Performance of a Multilayered Reservoir with Crossflow," *SPEJ* (Dec. 1962) 347-50; *Trans.*, AIME, 225.
12. Kazemi, H. and Seth, M.S.: "Effect of Anisotropy and Stratification on Pressure Transient Analysis of Wells with Restricted Flow Entry," *JPT* (May 1969) 639-47; *Trans.*, AIME, 246.
13. Kazemi, H.: "Pressure Buildup in Reservoir Limit Testing of Stratified Systems," *JPT* (April 1970) 943-49; *Trans.*, AIME, 249.
14. Woods, E.G.: "Pulse-Test Response of a Two-Zone Reservoir," *SPEJ* (Sept. 1970) 245-50; *Trans.*, AIME, 249.

15. Cobb, W.M., Ramey, H.J., Jr., and Miller, F.G.: "Well-Test Analysis for Wells Producing Commingled Zones," *JPT* (Jan. 1972) 27-37; Trans. AIME, 253.
16. Earlougher, R.C., Jr., Kersch, K.M., and Kunzman, W.J.: "Some Characteristics of Pressure Buildup Behavior in Bounded Multiple-Layered Reservoirs without Crossflow," *JPT* (Oct. 1974) 1178-86; Trans., AIME, 257.
17. Raghavan, R. et al.: "Well-Test Analysis for Wells Producing From Two Commingled Zones of Unequal Thickness," *JPT* (Sept. 1974) 1035-40; Trans., AIME, 257.
18. Tariq, S.M., and Ramey, H.J., Jr.: "Drawdown Behavior of a Well with Storage and Skin Effect Communicating With Layers of Different Radii and Other Characteristics," paper SPE 7453 presented at the 1978 Annual Meeting, Houston, TX, Oct. 1-3.
19. Chu, W.C. and Raghavan, R.: "The Effect of Noncommunicating Layers on Interference Test Data," *JPT* (Feb. 1981) 370-82.
20. Larsen, L.: "Wells Producing Commingled Zones with Unequal Initial Pressures and Reservoir Properties," paper SPE 10325 presented at the 1981 Annual Meeting, San Antonio, TX, Oct. 5-7.
21. Satman, A.: "An Analytical Study of Transient Flow in Stratified Systems with Fluid Banks," paper SPE 10264 presented at the 1981 Annual Meeting, San Antonio, TX, Oct. 5-7.
22. Bennett, C.O., Reynolds, A.C., and Raghavan, R.: "Analysis of Finite Conductivity Fractures Intercepting Multilayer Reservoirs," *SPEFE* (June 1986) 259-74.

23. Larsen, L.: "Determination of Skin Factor and Flow Capacities of Individual Layers in Two-Layered Reservoir," paper SPE 11138 presented at the 1982 Annual Meeting, New Orleans, Sept. 26-29.
24. Prats, M.: "Interpretation of Pulse Tests in Reservoirs with Crossflow Between Contiguous Layers," *SPEFE* (Oct. 1983) 511-20.
25. Niko, H.: "Well Test Interpretation of Heterogeneous Reservoirs With Skin and Afterflow: Some New Theoretical Solutions and General Field Experience," paper SPE 11964 presented at the 1983 Annual Meeting, San Francisco, CA, Oct. 5-8.
26. Gao, C.: "Crossflow Behaviour in a Partially Penetrated Two-Layer Reservoir : the Evaluation of Reservoir Parameters by Transient Well Tests," paper SPE 11875 presented at the 1983 Annual Meeting, San Francisco, CA, Oct. 5-8.
27. Javandel, I., and Witherspoon, P.A.: "Analytical Solution of Partial Penetration in a Two-Layer Aquifer," *Water Resource Res.* (April 1983) 19, 567-78.
28. Gao, C.: "Single-Phase Fluid Flow in a Stratified Porous Medium with Crossflow," *SPEJ* (Feb. 1984) 97-106.
29. Streltsova-Adams, T. D.: "Buildup Analysis for Interference Tests in Stratified Formations," *JPT* (Feb. 1984) 301-10.
30. Lee, S.T., Chien, M.C.H., and Culham, W.E.: "Vertical Single-Well Pulse Testing of a Three-Layer Stratified Reservoir," paper SPE 13249 presented at the 1984 Annual Meeting, Houston, TX, Sept. 16-19.
31. Bourdet, D.: "Pressure Behavior of Layered Reservoirs with Crossflow," paper SPE 13628 presented at the 1985 California Reg. Mtg., CA March 27-29.

32. Bremer, R.E., Winston, H. and Vela, S.: "Analysis Model for Vertical Interference Tests Across Low-Permeability Zones," *SPEJ* (June 1985) 407-18.
33. Prijambodo, R., Raghavan, R. and Reynolds, A.C.: "Well Test Analysis for Well Producing Layered Reservoir with Crossflow," *SPEJ* (June 1985) 380-96.
34. Satman, A. and Oskay, M.M.: "Effect of a Tilted Front on Well Test Analysis," paper SPE 14701 available from SPE (1985).
35. Ehlig-Economides, C.A., and Ayoub, J.: "Vertical Interference Testing Across a Low Permeability Zone," *SPEFE* (Oct. 1986) 497-510.
36. Kucuk, F., Karakas, M., and Ayestaran, L.: "Well Test Analysis Techniques for Layered Reservoirs," *SPEFE* (Aug. 1986) 342-54.
37. Ehlig-Economides, C.A. and Joseph, J.: "Evaluation of Single Layer Transients in a Multilayer System," paper SPE presented at the 1986 European Pet. Conference, London, Oct. 20-22.
38. Kucuk, F., Karakas, M., and Ayestaran L.: "Well Test Analysis of Commingled Zones Without Crossflow," paper SPE 15419 presented at the 1986 Annual Meeting, New Orleans, Oct. 5-8.
39. Mavor, M.J. and Walkup, G.W., Jr.: "Application of Parallel Resistance Concept to Well Test Analysis of Multilayered Reservoirs," paper SPE 15117 presented at the 1986 California Regional Meeting, Oakland, CA, April 2-4.
40. Joseph, J. et al.: "A Study of Pressure Transient Behavior in Bounded Two-Layered Reservoirs: Shengli Field, China," paper SPE 15418 presented at the 1986 Annual Meeting, New Orleans, LA, Oct. 5-8.

41. Chen, T.: "Pressure Drawdown in a Layered Reservoir with Linear Boundaries," paper SPE 16767 presented at the 1987 Annual Meeting, Dallas, TX, Sept 27-30.
42. Gao, C.: "Determination of Parameters for Individual Layer Properties in a Multilayer Reservoir," *SPEFE* (Sept. 1987) 43-65.
43. Ehlig-Economides, C. A. and Joseph, J.A.: "A New Test for Determination of Individual Layer Properties in a Multilayered Reservoir," *SPEFE* (Sept. 1987) 261-83.
44. Morris, C.: "Case Study of a Gulf Coast Layered Reservoir Using Multirate Transient Testing," paper SPE 16762 presented at the 1987 Annual Meeting, Dallas, TX, Sept. 27-30.
45. Hatzignatiou, D.G., Ogbe, D.O., Dehghani, K. and Economides, M.J.: "Interference Behavior in Multilayered Composite Reservoirs," paper SPE 16766 presented at the 1987 Annual Meeting, Dallas, TX, Sept. 27-30.
46. Gao, C. and Deans, H. A.: "Pressure Transients and Crossflow Caused by Diffusivities in Multilayer Reservoirs," *SPEFE* (June 1988) 438-48.
47. Larsen, L.: "Similarities and Differences in Methods Currently used to Analyze Pressure-Transient Data From Layered Reservoirs," paper SPE 18122 presented at the 1988 Annual Meeting, Houston, TX, Oct. 2-5.
48. Larsen, L.: "Boundary Effects in Pressure-Transient Data From Layered Reservoirs," paper SPE 19797 presented at the 1989 Annual Meeting, San Antonio, TX, Oct. 8-11.
49. Park, H., and Horne, R.N.: "Well Testing Analysis of a Multilayered Reservoir With Formation Crossflow," paper SPE 19800 presented at the 1989 Annual Meeting, San Antonio, TX, Oct. 8-11.

50. Olarewaju, J.S. and Lee, W.J.: "Pressure Buildup Behavior of Partially Completed Wells in Layered Reservoirs," paper SPE 18876 presented at the 1989 Production Operation Symposium, Oklahoma City, Oklahoma, March 13-14.
51. Olarewaju, J.S. and Lee, W.J.: "Pressure Behavior of Layered and Dual-Porosity Reservoirs in the Presence of Wellbore Effects," *SPEFE* (Sept. 1989) 397-405.
52. Raghavan, R.: "Behavior of Wells Completed in Multiple Producing Zones," *SPEFE* (June 1989) 219-230.
53. Yeh, N., and Reynolds, A.C.: "Analysis of Pressure Data From a Restricted Entry Well in a Multilayer Reservoir," *SPEFE* (March 1989) 81-89.
54. Yeh, N., and Reynolds, A.C.: "Computation of the Pseudoskin Factor Caused by a Restricted-Entry Well Completed in a Multilayer Reservoir," *SPEFE* (June 1989) 253-263.
55. Anbarci, K., Grader, A.S., and Ertekin, T.: "Determination of Front Locations in Multilayer Composite Reservoir," paper SPE 19799 presented at the 1989 Annual Meeting, San Antonio, TX, Oct. 8-11.
56. Olarewaju, J.S. and Lee, W.J.: "Rate Performance of a Layered Reservoir with Unsteadystate Interlayer Crossflow," *SPEFE* (March 1990) 46-52.
57. Mishra, S. and Ramey, H.J. Jr.: "A Comparison of Pressure-Transient and Tracer-Concentration/Time Data for Layered Reservoirs Under Injection," *SPEFE* (March 1990) 60-66.

58. Spath, J.B., Ozkan, E. and Raghavan, R.: "An Efficient Algorithm for Computation of Well Responses in a Commingled Reservoir," paper CIM/SPE 90-1 presented at the 1990 International Tech. Meeting , Calgary, AB, June 10-13.
59. Kiome, I.: "Pressure Transient Behaviour for a Well in a Multi-Layered Composite Reservoir with an Inclined Front," M.Sc. Thesis, University of Alberta, Edmonton, AB (March 1991) 132 pp.
60. User's Manual, IMSL Math/Library, version 1.0 (April 1987) pp. 13 and 329.
61. Stehfest, H.: "Algorithm 368, Numerical Inversion of Laplace Transforms, D-5," *Comm. of ACM*, 13, No.1 (Jan. 1970) 49.
62. Agarwal, R. G., Al-Hussainy, R., and Ramey, H. J., Jr.: "An Investigation of Wellbore Storage and Skin effect in Unsteady Liquid Flow," *SPEJ* (Sept.1970) 279-290.
63. Eggenschwiler, M., Ramey, H.J., Jr., Satman, A., and Cinco-Ley, H.: "Interpretation of Injection Well Pressure Transient Data in Thermal Oil Recovery," paper SPE 8908 presented at the 1980 Reg. Mtg., Los Angeles, CA, April 9-11.
64. Ambastha, A. K. and Ramey, H.J., Jr.: "Thermal Recovery Well Test Design and Interpretation," *SPEFE* (June 1989) 173-180.
65. Ambastha, A. K. and Ramey, H.J., Jr.: "Pressure Transient Analysis for a Three-Region Composite Reservoir," paper SPE 24378 presented at the 1992 Rocky Mountain Reg. Mtg., Wyoming, May 18-21.
66. Streksova-Adams, T. D.: "Pressure Drawdown in a Well with Limited Flow Entry," *JPT* (Nov. 1977) 1469-76.

67. Buhidma, I. M. and Raghavan, R.: "Transient Pressure Behavior of Partially Penetrating Wells Subject to Bottomwater Drive," *JPT* (July 1980) 1251-61.
68. Walsh, J.W., Ramey, H.J., Jr., and Brigham, W.E.: "Thermal Injection Well Falloff Testing," paper SPE 10227 presented at the 1981 Annual Meeting, San Antonio, TX, Oct. 5-7.
69. Da Prat, G., Bockh, A., and Prado, L.: "Use of Pressure Falloff Tests to Locate the Burning Front in the Miga Field, Eastern Venezuela," paper SPE 13667 presented at the 1985 Reg. Mtg., Bakersfield, CA, March 27-29.
70. Stanislav, J.F., Easwaran, C.V., and Kokal, S.L.: "Interpretation of Thermal Injection Well Testing," *SPEFE* (June 1989) 181-86.
71. Fassihi, M.R.: "Evaluation of An Analytical Technique for Estimating Swept Volume from Thermal Pressure Falloff Tests in Heterogeneous Systems," *SPEFE* (June 1988) 449-458.

Table 2.1: Published Results on Layered Reservoirs
(Based on the list by Economides and Joseph (43))

Year	Author(s)	Solution Method(s)					No. of Layers	Innerlayer Flow(s)			Well Specifications(s)				Well Control(s)			Outer Boundary(s)			Composite Reservoir(s)	
		L	H	F	PD	O		NOC	F	PSS	FWS	LS	VF	C	g	q	P	IA	NP	CP	C	NC
1960	Jacquot (1)	.					2
1961	Tompson-Lane (2)	.					2
1961	Lafayette et al. (3)	.					2
1961	Drewitt (4)	.					2
1961	Politzer and Segura (5)	.					2
1961	Patzer (6)	.					2
1962	Pulgarino-Economides (7)	.					2
1962	Russell and Pratt (8)	.	.				2
1962	Russell and Pratt (9)	.	.				2
1962	Koz and Teh (10)	.		.			2
1962	Pandey and Berry (11)	.				.	2
1969	Koz and Seth (12)	.				.	2
1970	Koz (13)	.				.	2
1970	Woods (14)	.				.	2
1972	Cobb et al. (15)	.					2
1974	Barling et al. (16)	.					2
1974	Raghavan et al. (17)	.					2
1976	Torq and Roney (18)	.					2
1981	Chu and Raghavan (19)	.				.	2
1981	Loren (20)	.					2
1981	Semen (21)	.					2
1982	Semen et al. (22)	.		.			2
1982	Loren (23)	.					2
1983	Pratt (24)	.	.	.			2
1983	Nito (25)	.					2
1983	Geo (26)	.					2
1983	Javaheri and Wahneken (27)	.	.				2
1984	Geo (28)	.				.	2
1984	Srinivas (29)	.					2
1984	Lee et al. (30)	.					2
1985	Boudin (31)	.					2
1985	Brown et al. (32)	.					2
1985	Pignatelli et al. (33)	.		.			2
1985	Semen and Okey (34)	.					2
1985	Eding-Economides and Aymeh (35)	.					2
1986	Koz et al. (36)	.					2
1986	Eding-Economides and Joseph (37)	.					2
1986	Koz et al. (38)	.				.	2
1986	Meyer and Walsh (39)	.					2
1986	Joseph et al. (40)	.					2
1987	Chu (41)	.					2
1987	Geo (42)	.				.	2
1987	Eding-Economides and Joseph (43)	.					2
1987	Morris (44)	.					2
1987	Margaret et al. (45)	.					2
1988	Geo and Dunn (46)	.		.			2
1988	Loren (47)	.					2
1989	Loren (48)	.					2
1989	Park and Morris (49)	.					2
1989	Oliver and Lee (50)	.					2
1989	Oliver and Lee (51)	.					2
1989	Raghavan (52)	.					2
1989	Veh and Reynolds (53)	.		.			2
1989	Veh and Reynolds (54)	.					2
1989	Ahmed et al. (55)	.					2
1989	Oliver and Lee (56)	.					2
1989	Morris and Roney (57)	.					2
1989	Speth et al. (58)	.					2
1991	Koz (59)	.					2

a.
L = Laplace transform
H = Heaviside transform
F = Fourier transform
PD = Partial Derivative
O = Other

b.
NOCF = No formation crossflow
T = Transient crossflow
PSS = Pseudo-steady-state crossflow

c.
FWS = Finite wellbore
LS = Line source
VF = Vertical fracture
C = Wellbore storage
g = Skin
Δ = Partial penetration skin

d.
q = Constant rate
p = Constant pressure
P = Pulse rate

e.
C = Composite NC = Noncomposite

f.
IA = Infinite acting
NP = No flow
CP = Constant pressure

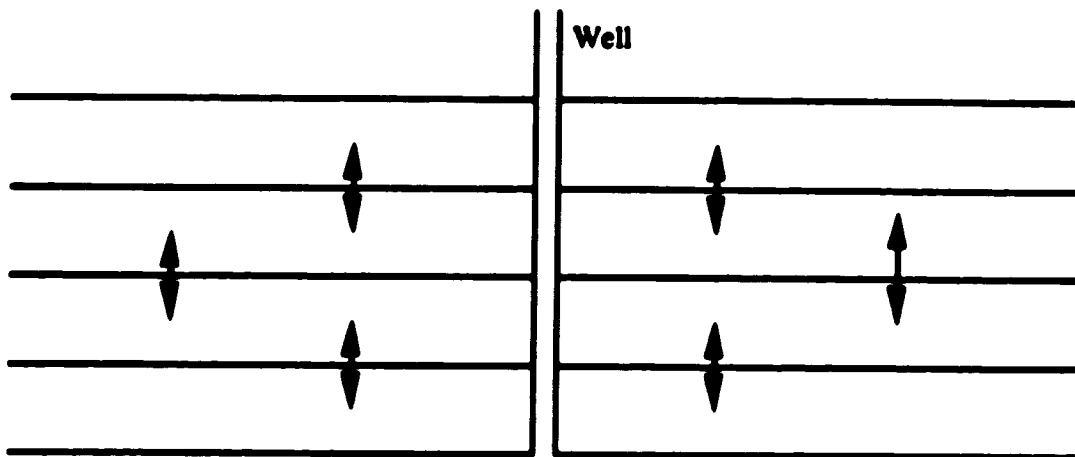


Figure 2.1a : Layered reservoir with interlayer crossflow.

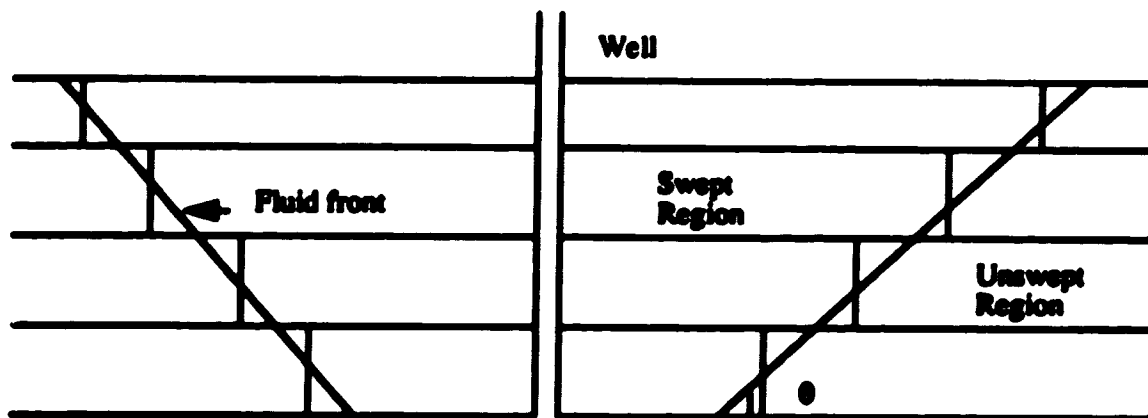


Figure 2.1b : Radial, layered composite reservoir with a tilted front.

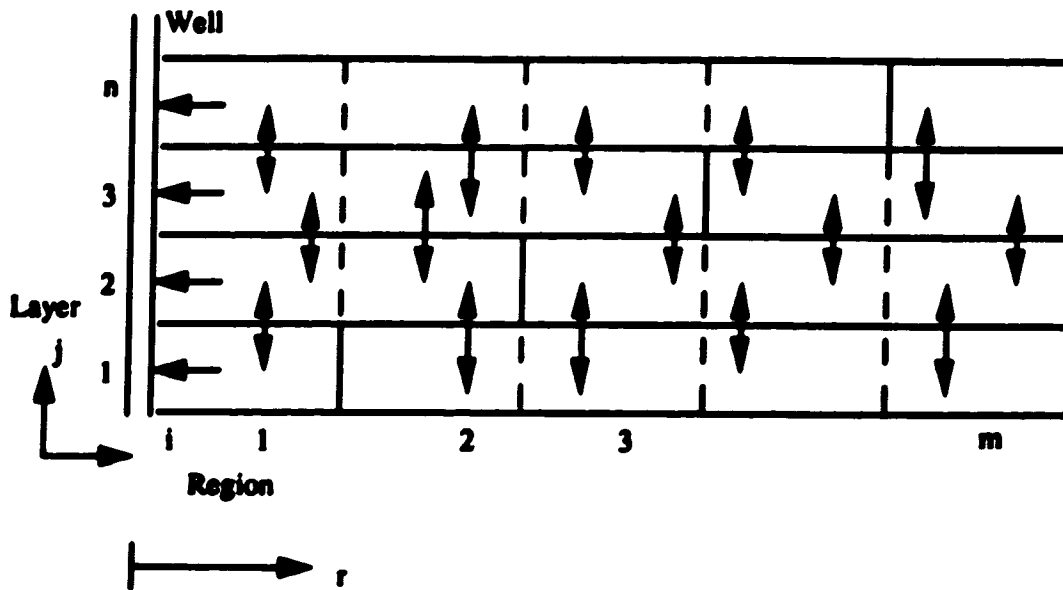


Figure 2.2: Schematic of an n -layer composite reservoir in a radial geometry with two different rock and/or fluid types in each layer.

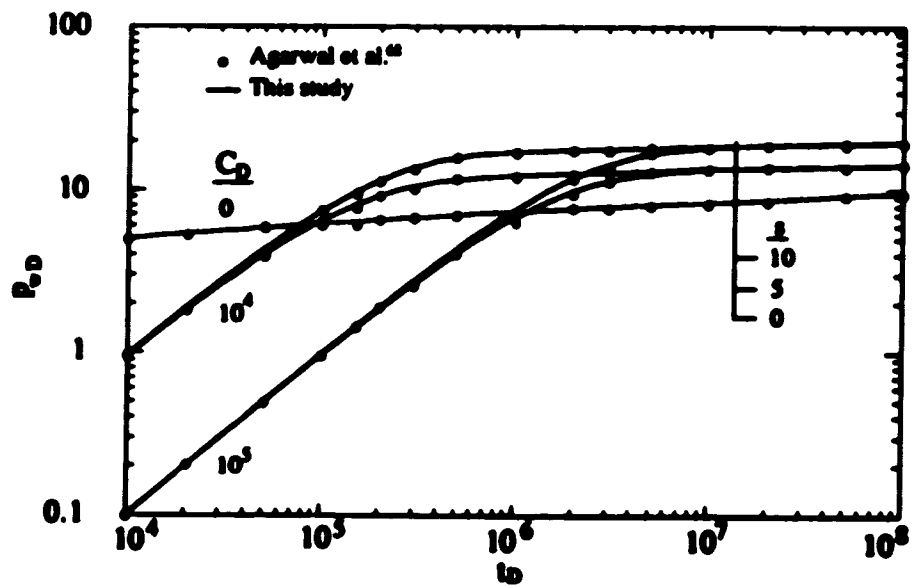


Figure 2.3: Comparison of this study with Agarwal et al.⁴⁸ solution for a homogeneous reservoir.

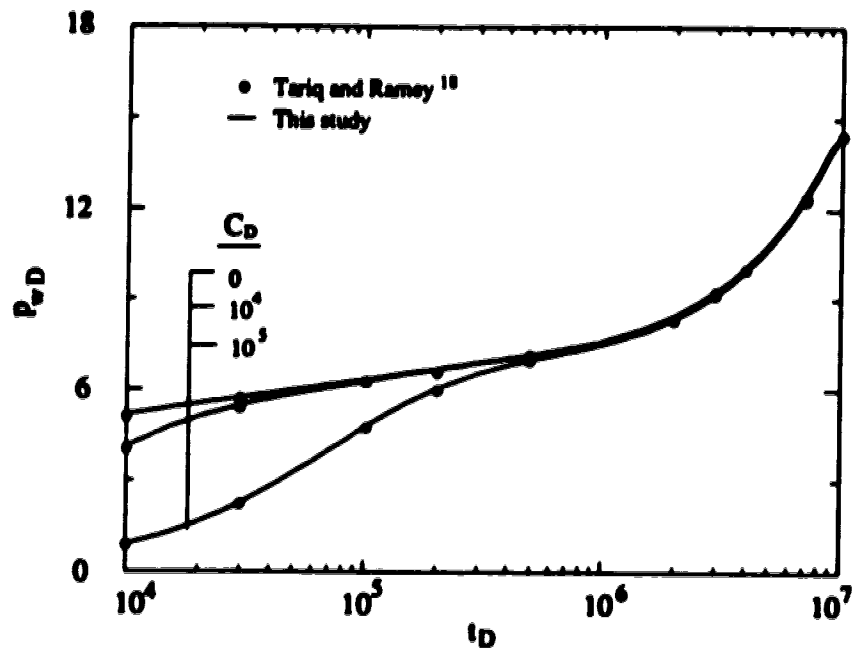


Figure 2.4: Comparison of this study with Tariq and Ramey's¹⁸ solution for a two-layer reservoir with a closed outer boundary.

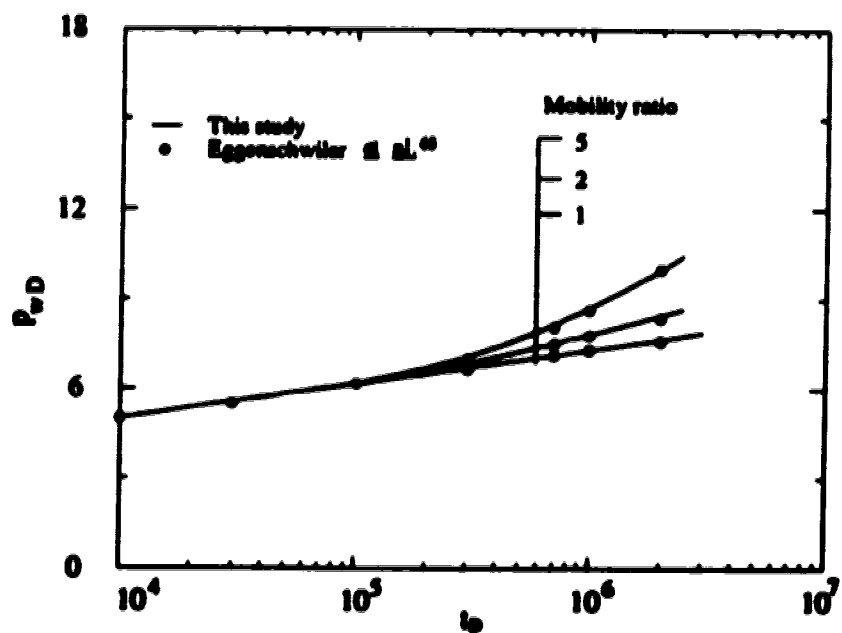


Figure 2.5: Comparison of this study with Eggenschwiler et al.⁴⁰ solution for a two-region composite reservoir.

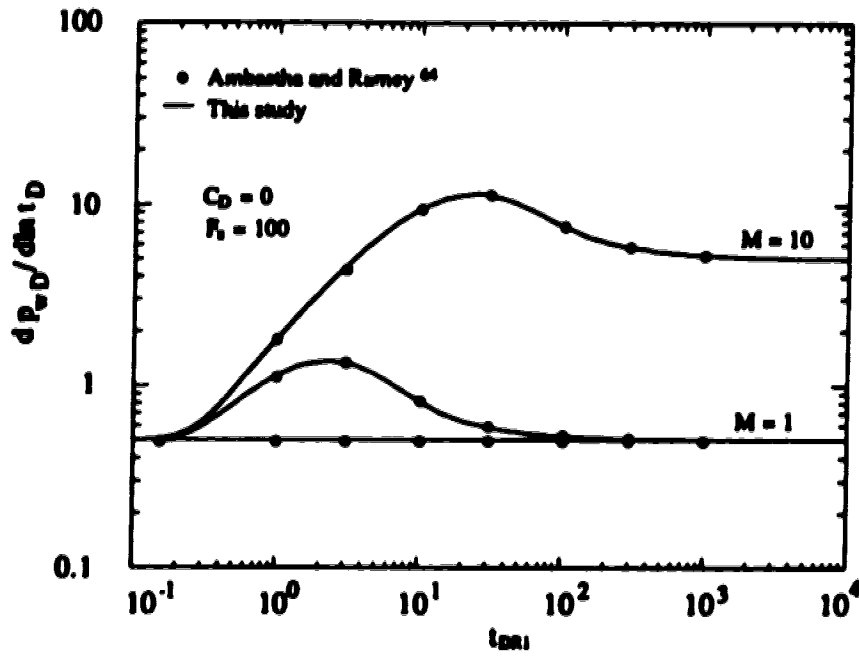


Figure 2.6: Comparison of this study with Ambastha and Ramey's⁶⁴ study for a two-region, composite reservoir.

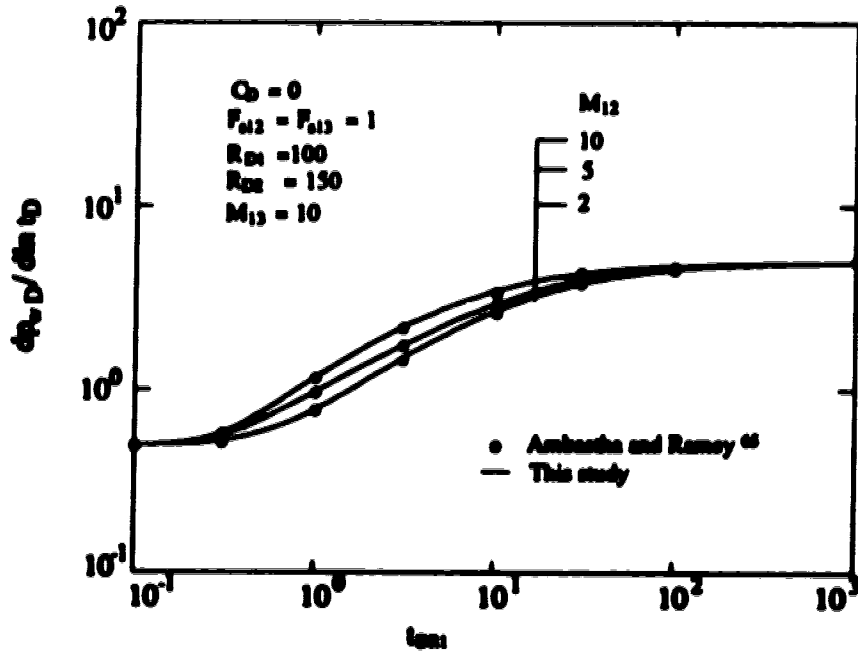


Figure 2.7: Comparison of this study with Ambastha and Ramey's⁶⁵ study for an infinitely large, three-region, composite reservoir.

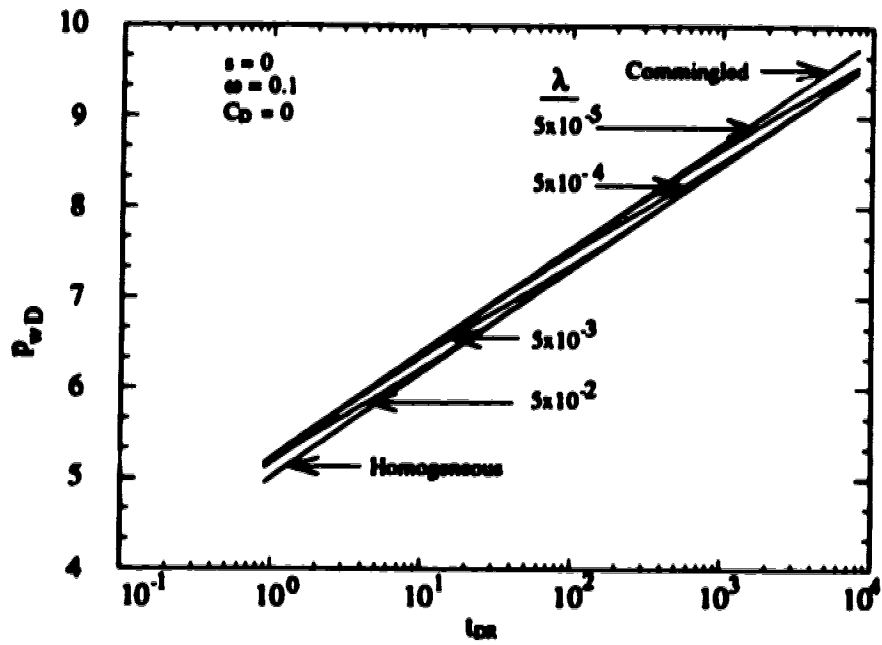


Figure 2.8: Effect of crossflow on wellbore pressure for a two-layer reservoir.

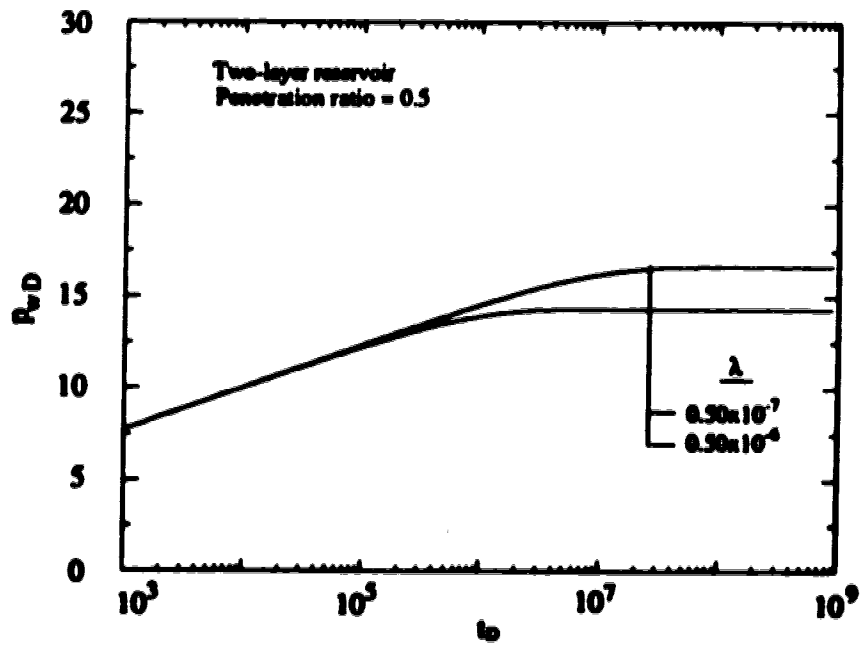


Figure 2.9: Pressure drawdown responses of a partially-penetrating well in a two-layer reservoir subject to bottom-water drive.

3.0 WELL TEST ANALYSIS FOR THERMAL RECOVERY SYSTEMS

3.1 Introduction

Most reservoirs are heterogeneous in nature. The presence of layers and zones of different fluid and/or rocks is a common cause for reservoir heterogeneity. Figures 3.1a and 3.1b show a layered reservoir and a layered composite reservoir, respectively. The horizontal lines show the layering and the arrows show the presence of crossflow. The layers may be communicating or non-communicating. Formation crossflow is present when the layers are communicating. When the layers do not communicate with each other, except through the wellbore, then the reservoir is termed a "commingled reservoir". A layered, composite reservoir situation occurs when all or some of the layers have two or more regions of different rock and/or fluid properties.

Thermal recovery processes, such as steam-flooding, are widely used in heavy-oil reservoirs. As a result of steam-flooding, a swept region is created in the reservoir. A layered reservoir resembles a layered composite reservoir because of steam-flooding. Usually, the fluid front in such a reservoir is not vertical, but tilted or inclined because of the gravity override effect. The tilted line in Figure 3.1b shows the discontinuity boundary or the fluid front and θ is the angle of inclination. A tilted front can also occur in a thick, homogeneous reservoir due to gravity override effects.

Numerous studies have been reported in the literature on layered reservoirs. Among many researchers, Leftkovits et. al.¹, Tariq and Ramsy² and Bourdet³ have conducted some significant studies on layered reservoirs. Gomes and Ambastha⁴ have done an extensive literature review on layered and composite reservoirs. Responses of layered reservoirs may be summarized as follows: initially, a crossflow system and a commingled system have the same response; then there is a transition period and,

finally, the crossflow system behaves like an equivalent homogeneous system. Eggenschwiler et al.⁵ have developed an analytical solution for a single-layer, composite reservoir and used the pseudosteady-state analysis method to estimate the swept volume. Ambastha⁶ has presented an extensive study on single-layer, composite reservoirs based on pressure derivative responses. The responses of a single-layer, composite reservoir, without wellbore storage and skin effects, consist of the following steps: initially, the responses show a first radial flow period corresponding to the swept region (inner region); then, there is a transition period during which the swept region may show pseudosteady-state flow behaviour if the mobility contrast between the swept and the unswept regions is sufficiently large; and finally, the responses show a second radial (pseudo-radial) flow period corresponding to the unswept (outer) region, if the reservoir is large enough.

A limited number of studies have been conducted on multilayered, composite reservoirs. Satman⁷ presented injectivity and falloff responses for a commingled, multilayered composite reservoir. In his model, Satman⁷ considered different discontinuity boundary radii for different layers. He introduced the concept of a tilted front for layered, composite reservoirs, because the fluid front would propagate at different rates in different layers. Satman⁷ described the methods to estimate the properties of the swept region, distance to the nearest boundary, and the swept volume from transient pressure responses. But he did not consider the effect of the discontinuity boundary shape in his study. For enhanced recovery processes, such as steam flooding, Satman and Okay⁸ considered the discontinuity boundary as a tilted front (inclined front) to account for the gravity override effect and modelled the reservoir as a multi-layer, composite reservoir without formation crossflow. They concluded that the tilted front model is a better representation of the actual reservoir than the sharp-front model when the gravity override effect is present. For an inclined-front

reservoir, Satman and Oskay⁸ observed that the time to reach pseudosteady-state (pss) can be much longer than that for a sharp-front reservoir, and conventional pss analysis results in considerable underestimation of the swept volume. Hatzignatiou *et al.*⁹ presented a solution for interference pressure transient behaviour in a two-layer, composite reservoir having pseudosteady-state formation crossflow and described a type-curve matching technique to estimate the reservoir parameters from the active and from the observation well data. Anbarci *et al.*¹⁰ presented an analytical solution for a two-layer, composite reservoir. They included wellbore storage and skin, and considered pseudosteady-state crossflow between the layers. They conducted a limited sensitivity study and used a type-curve matching technique to locate the front in a particular layer.

The preceding discussion shows that a systematic and in-depth study for the transient pressure behaviour of an inclined-front, multilayered, composite reservoir with crossflow has not been conducted yet. Especially, for steam-flooding, in which the gravity override effect is important, and which can be modelled as a multilayered, composite reservoir with an inclined front, a detailed study has not been carried out. The analytical solution developed by Gomes and Ambastha⁴ has been used to conduct a systematic and in-depth study of the transient pressure behaviour of a multilayered, composite reservoir with pseudosteady-state formation crossflow. Although not a limitation of the model, this study assumes that all the layers of the reservoir are of equal thickness. The inclined front has been represented by a minimum front radius and an angle of inclination. The inclined front in each layer has been approximated by an equivalent vertical front (Figure 3.1b). In the absence of actual physical layers, a number of mathematical layers is assumed to be present in the reservoir for the step approximation of the inclined front. In this study, the well is a fully-penetrating well, unless mentioned otherwise. Wellbore storage and skin effects are neglected. All layers

in the swept region are assigned a constant value of mobility, and all layers in the unswept region are assigned a different, but constant, value of mobility corresponding to a specified mobility ratio. Assignment of storativities is carried out in exactly the same manner as the mobilities. Appendix A shows the calculation procedure of various front radii using a minimum front radius, layer thicknesses, total reservoir thickness, and the angle of inclination. A representation of an inclined front, as shown in Figure 3.2, has been used in Appendix A. Appendix B describes the derivation of the average front radius for inclined front reservoirs. Appendices A and B follow the approach presented by Klome¹¹.

3.2 Effect of Front Angle

When an enhanced recovery process, such as steam-flooding, is applied to a multi-layer reservoir, the discontinuity boundary may be tilted because of the gravity override effect. Satman⁷ modelled a tilted front in a two-layer, commingled reservoir by locating the two discontinuity boundaries at two different locations. Later, Satman and Oskay⁸ studied the effect of a tilted front in a multi-layer, composite reservoir without formation crossflow. They conducted a limited study by varying the front angle as well as the minimum front radius to investigate the effect on transient pressure responses. For tilted fronts, Satman and Oskay⁸ observed that the swept volume is underestimated when calculated from the Cartesian slope after the first radial-flow period. They also observed that it takes a longer time to reach pseudosteady-state for reservoirs with tilted fronts compared to those with sharp fronts. They recommended a type-curve matching technique for locating the pseudosteady-state period.

Figures 3.3 through 3.7 show the effect of front angle on pressure derivative responses. These responses are for a three-layer reservoir with a mobility ratio $M=10$, storativity ratio $F_v=1$, and a fully-penetrating well. Wellbore storage and the skin effect

are neglected. The minimum discontinuity boundary distance is the same for all responses and is $R_{Dmin} = 500$. Figures 3.3 through 3.5 show the responses when crossflow is present between the layers, and Figures 3.6 and 3.7 show the responses of a commingled reservoir. These figures show that the transient responses of a layered, composite reservoir with a tilted front consist of the following flow regime sequences: a radial-flow period corresponding to the swept region, a transition period which depends on the front angle, total reservoir thickness, as well as the mobility and the storativity contrast between the swept and the unswept regions, and a second radial-flow period corresponding to the unswept region. After the second radial-flow period, boundary effects will be observed for finite reservoirs. However, this study is limited to infinite reservoirs as well tests for thermal recovery situations are seldom run long enough to observe the effects of outer boundaries. Figures 3.3 and 3.6 show the responses for very thick reservoirs with $h_{LD} = 1000$. For thick reservoirs, the effect of the front angle is more apparent and for smaller front angles, deviation from the first, radial-flow period occurs later than for the sharp-front reservoirs. Figure 3.5 shows that the transient pressure responses of very thin reservoirs do not exhibit much effect due to the front angle and therefore transient pressure analysis of thin reservoirs can be performed with a sharp-front model. This conclusion is consistent with Klome's¹¹ observation for thin, commingled, composite reservoirs with a tilted front, where he observed very little effect of the front angle on the transient, wellbore pressure.

A comparison of Figures 3.3 and 3.4 with Figures 3.6 and 3.7, respectively, shows that crossflow does not make a significant difference in these particular situations with $k_u/k = 0.1$ for the crossflow system. When the well is partially penetrated and k_u/k is not very small, crossflow must be taken into consideration to generate proper responses. Figures 3.8 and 3.9 show the effect of crossflow on pressure-derivative responses of a fully- and partially-penetrating well, respectively. In Figure 3.8, the

solid line represents a commingled reservoir, and the data points represent various crossflow cases. In Figure 3.8, k_w/k has been varied between 0.01 and 10. Figure 3.8 shows that the crossflow system responses are the same as commingled system responses for fully-penetrating wells. For partially-penetrating wells, Figure 3.9 shows the effect of crossflow on wellbore responses. In Figure 3.9, the penetration ratio is 0.5 and k_w/k has been varied as 0.01, 0.1 and 1. Initially, the crossflow systems and the commingled system have the same response. Then, for crossflow systems, the fluid starts flowing from the closed section to the open section of the reservoir. For the commingled system, there is no fluid flow from the closed section to the open section and the wellbore pressure is not affected by the closed section of the reservoir. At late time, the pressure derivative approaches $M/2$ for crossflow systems. For a commingled system, the late-time pressure derivative approaches $Mh_w/2h_i$, where h_w/h_i represents the penetration ratio. Although not shown, the aforementioned observations regarding Figures 3.8 and 3.9 hold true for different cases of front angle, dimensionless reservoir thickness, mobility ratio, storativity ratio, and dimensionless minimum front radius.

3.3 Layer Refinement Effect

In this study, a composite reservoir with an inclined or tilted front has been approximated by a multi-layer, composite reservoir with a step approximation of the inclined front. The layer refinement effect is studied by varying the number of mathematical layers in a particular reservoir and observing the transient pressure responses. Figures 3.10 and 3.11 show the effect of layer refinement on the pressure derivative responses. These figures show the responses for a multi-layer, composite reservoir with a mobility ratio $M = 10$, a minimum discontinuity distance $R_{Dmin} = 500$, and a dimensionless reservoir thickness $h_D = 500$. The number of layers have been varied as 2, 3, 5 and 10 layers. All the layers in the swept zone have been assigned the same properties with a mobility contrast of $M = 10$ between the swept and the unswept

zones. Pseudosteady-state crossflow is present between the layers with $k_v/k = 0.1$. Figures 3.10 and 3.11 show responses for front angles of 30° and 60° , respectively. From these two figures, it is observed that the smaller the front angle is, the more apparent the layer refinement effects are. Layer refinement effects also depend on the reservoir thickness. Very thin reservoirs and reservoirs with sharp fronts do not show any layer refinement effect. This observation is also consistent with Kiome's¹¹ findings for commingled, composite reservoirs. Layer refinement effects occur because by increasing the number of layers, the definition of the fluid front is improved. Figures 3.10 and 3.11 also show that increasing the number of layers from 5 to 10 makes very little change in the responses. Therefore, for a particular reservoir situation, there is a maximum number of layers beyond which the layer refinement effect would not improve the responses significantly. Larsen¹² has reported a similar layer refinement effect. To minimize the layer refinement effect, a reservoir consisting of five layers is considered for the rest of this study.

3.4 Effect of Mobility and Storativity Ratio

Figures 3.12 through 3.14 show the effect of mobility ratio on semi-log pressure derivative responses. Figures 3.12, 3.13 and 3.14 are for front angles of 30° , 60° and 90° , respectively. For all these figures, the dimensionless minimum front radius (R_{Dmin}) = 500, the dimensionless time is calculated based on the minimum front radius, and the mobility ratio is varied between 1 and 1000. Initially, the reservoir behaves like an infinite-acting radial flow system with a semi-log pressure derivative of 0.5. Then, there is a transition period, the duration of which depends on the mobility ratio. The higher the mobility ratio, the longer the duration of the transition period. At late time, the responses show a second, radial-flow period with a constant semi-log derivative of 0.5M. For all mobility ratios, the time, at which the first radial flow ends, depends on the front angle. This is more evident from Figure 3.15 which shows the effect of front

angles for a reservoir with a mobility ratio of 100. Figure 3.15 shows that a reservoir with a sharp front (90°) deviates from the first radial flow period earlier than the tilted front reservoirs and this deviation depends on the front angle. The higher the front angle is, the earlier the response deviates from the first radial flow period. This happens because in a tilted front reservoir, when the pressure response reaches the minimum front, for the rest of the layers, the pressure response still corresponds to the first radial flow period. Since the wellbore response is the combined effect of the responses from all the layers, the wellbore still senses the response as the first radial flow period, although the pressure response has already reached the minimum front radius. In a sharp front reservoir, the pressure response in all the layers reaches the front at the same time and, thus, the wellbore response deviates earlier. For tilted front cases, Table 3.1 shows that the delay in deviation from the first radial flow period and the delay in time to the occurrence of the maximum semi-log slope (for $F_s > 1$) during the transition period are equal to the ratio of the average front radius to the minimum front radius. In Table 3.1, the mobility ratio is varied between 10 and 1000 and the storativity ratio is varied between 1 and 1000. For a fixed minimum front radius, as the front angle becomes smaller, the average radius becomes larger. Therefore, the design equation for the end of the first radial flow period and for the maximum semi-log slope for sharp-front reservoirs should be modified for the tilted front cases. Thus, the design equations derived by Ambastha and Ramey¹³ are modified as follows:

$$(t_{DR1})_{end} = 0.18 \frac{R_{Davg}}{R_{Dmin}} \quad (3.1)$$

$$(t_{DR})_{max} = (1.8 + 0.4 \log F_s) M \frac{R_{Davg}}{R_{Dmin}} \quad (3.2)$$

where, $(t_{DR1})_{end}$ and $(t_{DR})_{max}$ are the time to the end of the first, radial-flow period and the time of the maximum semi-log pressure derivative during the transition period, respectively.

For a sharp-front reservoir, R_{Davg} and R_{Dmin} are identical. Although Table 3.1 shows results for $R_{Dmin} = 500$, Equations (3.1) and (3.2) have been tested for R_{Dmin} values of 300 through 1000 with satisfactory results. Equation (3.1) is important, since it shows that for tilted front reservoirs, the end of the first radial flow period occurs later than it does for sharp-front reservoirs. Thus, the deviation time method can not be used to locate the minimum discontinuity boundary as is currently believed⁶. According to Equation (3.1), the end of the first, radial-flow period occurs at a dimensionless time of 0.18, and this dimensionless time is based on the geometric mean of R_{Dmin} and R_{Davg} , not on R_{Dmin} . A similar modification can be made to the other design equations for the end of the first, radial-flow period developed by Sosa et al.¹⁴ and Tang¹⁵, which are based on pressure data, instead of pressure derivative data.

Figures 3.16 through 3.18 show the effect of the storativity ratio, F_s , on the semi-log pressure derivative responses. Figure 3.16, 3.17 and 3.18 are for front angles of 30°, 60° and 90°, respectively. These figures show that the effect of the storativity ratio is somewhat similar to that of the mobility ratio, but, unlike the mobility ratio, the storativity ratio does not affect the duration significantly of the transition period between the first and the second radial flow periods.

3.5 Pseudosteady-State (pes) Analytical Method

During the pseudosteady-state period, if the mobility contrast is large enough, the swept region of a composite reservoir acts like a closed reservoir for some time and the transient pressure responses are similar to the late-time responses of a closed reservoir.

Ramey and Cobb¹⁶ derived the equation for the variation of the dimensionless pressure with dimensionless time during the pes flow period for a well in a single-layer, homogeneous, closed reservoir as:

$$p_{wD} = 2\pi t_{DA} + \frac{1}{2} \ln(A/r_w^2) + \frac{1}{2} \ln(2.2458/C_A) \quad (3.3)$$

Here, the dimensionless time, t_{DA} , is based on the swept area. Equation (3.3) shows that during the pss period, pressure is linearly related with time and, thus, the Cartesian slope of pressure versus time will be a constant.

Eggenschwiler *et al.*⁵ developed the solution for the transient-pressure responses of a single-layer, composite reservoir and used the slope of the Cartesian, straight line to estimate the swept volume. From material balance, Eggenschwiler *et al.*⁵ derived the relationship between the swept volume and the Cartesian slope as:

$$V_s = \frac{qB}{m_i c_i} \quad (3.4)$$

Eggenschwiler *et al.*⁵ also pointed out that estimation of the swept volume from Equation (3.4) is independent of the geometry of the swept volume. Thus, the pss analytical method might be applicable for multilayered, composite reservoirs with inclined fronts and with any other irregularly-shaped fronts.

3.6 Pseudosteady-state Analysis

Figures 3.19 through 3.21 show the Cartesian pressure derivative responses for a five-layered, tilted-front composite reservoir. The Cartesian derivatives have been calculated with respect to $t_{DA,avg}$, which is defined as $t_{DA,avg} = t_D/R_{DA,avg}^2$. Here $R_{DA,avg}$ is the dimensionless average front radius of the swept region and is defined in Appendix B. All these figures are for a mobility ratio $M = 1000$ and a storativity ratio $F_s = 1$. Figure 3.19 is graphed for a dimensionless reservoir thickness $h_D = 400$ and front angles of 30° , 45° , 60° , and 90° . When the front is at 90° , the discontinuity boundary moves as a piston and the front is called a sharp front. In the case of a sharp front, the average radius of the swept region is equal to the minimum front radius, R_{Dmin} . During the

pseudosteady-state period, the Cartesian slope is constant and if the dimensionless time is based on the swept area, the Cartesian slope should be 2π for vertical or sharp-front swept boundaries. When dimensionless time is based on the average front radius, the Cartesian slope should be 2 for sharp-front cases. In Figure 3.19, at early times the Cartesian derivatives form a single straight line with a slope of -1 for all front angles, and this corresponds to the first infinite-acting radial flow period. Then the Cartesian slopes tend to become constant, which represents the pseudosteady-state period. At late times all the responses form another straight line of slope -1, which represents the second radial flow period. Figure 3.19 shows that, during the pseudosteady-state flow period, the Cartesian slopes for different front angles are approximately constant, but depend on the front angle. This can be explained with reference to Figure 3.1b. When the well starts producing, the pressure transient starts to move away from the well. Assuming that the layer diffusivities do not vary much from layer to layer, the pressure transient will reach the closest front (i.e., the bottom layer front) first, while in most of the layers, the pressure transient will still be propagating through the swept region. Similarly, by the time the pressure transient reaches the front in the top layer (i.e., the farthest layer), the pressure transient in the bottom layer (the layer with the closest front) has already travelled into the unswept region. This phenomenon becomes more significant for more acute front angles. Thus, in the true sense, pseudosteady-state flow never happens for an inclined front. For an inclined front case, pseudosteady-state flow occurs only in some average sense and, thus, it is not possible to get a constant Cartesian slope from pes analysis which is independent of the front angle. For a sharp-front reservoir (90°), the value of the Cartesian slope is 2.0 during the pseudosteady-state period when dimensionless time is based on the average front radius. For tilted-front reservoirs, the slopes are higher than the slope for the sharp-front reservoir. The smaller the front angle, the higher the value of the Cartesian slope. This means that, for tilted front reservoirs, if the swept volume is estimated from the Cartesian slope of

the pseudosteady-state period, the calculated swept volume will be considerably underestimated. One way to solve this problem is to develop a correction factor which, when multiplied with the underestimated swept volume, will result in the correct swept volume. Table 3.2 shows the equivalence between the ratios of R_{Davg}/R_{Dmin} and m_w/m_{wf} , where m_{wf} is the Cartesian slope for a sharp-front reservoir. In Table 3.2, h_{LD} has been varied between 100 and 400 and R_{Dmin} has been varied between 300 and 1000. For tilted-front reservoirs, $R_{Davg}/R_{Dmin} = m_w/m_{wf} = m_w/2$, since $m_{wf} = 2$. This means that for tilted-front reservoirs, the Cartesian slope of the ps flow period increases by a factor of R_{Davg}/R_{Dmin} more than that for the sharp-front reservoirs. Thus, the underestimated swept volume can be corrected by multiplying it by a correction factor, $f_c = R_{Davg}/R_{Dmin}$. Figures 3.20 and 3.21 also show that the Cartesian slope during the pseudosteady-state flow period is affected by reservoir thickness as well. Figures 3.20 and 3.21 show the responses for a dimensionless reservoir thickness of 300 and 100, respectively. As the reservoir thickness decreases, the effect of front angles on the Cartesian slope also decreases. Table 3.2 shows the relationship between R_{Davg}/R_{Dmin} and m_w/m_{wf} for different average radii and reservoir thicknesses. For the same front angle, the ratio R_{Davg}/R_{Dmin} will depend on the reservoir thickness. The definition of the average swept radius, R_{Davg} , takes into account both the front angle and the reservoir thickness. To use the correction factor, f_c , knowledge of the reservoir thickness, the front angle, and the minimum and average front radii are required a priori. The reservoir thickness can be estimated from drilling and log data, and from geological information. An approximate value of the angle can be assumed from the available geological data, and from the reservoir and injected fluid properties. The minimum and average front radii can be obtained using a trial-and-error method. A minimum front radius is first assumed, and using the reservoir thickness and front angle, the average front radius is calculated following the method described in Appendix B. The geometric mean of R_{Dmin} and R_{Davg} is calculated and is compared with that obtained from the

deviation time method based on Equation (3.1). If the two geometric means do not agree, the assumed value of R_{Dmin} is adjusted and the above procedure is repeated until agreement between the two geometric means is achieved.

Figures 3.22 through 3.24 show the effect of reservoir thickness on pseudosteady-state analysis. These figures show responses for a five-layered reservoir and for different front angles. For the same front angle, as the reservoir thickness decreases, the ratio of R_{Davg}/R_{Dmin} also decreases. Since it has been shown before that $R_{Davg}/R_{Dmin} = m/m_{inf}$, as the reservoir thickness decreases, the responses come closer to the sharp-front response. For the conditions specified in Figures 3.22 through 3.24, the responses for $h_D = 100$ are very close to the sharp-front reservoir and, thus, a reservoir with $h_D = 100$ or less can be considered as a thin reservoir for pseudosteady-state analysis. Therefore, for all front angles, a thin reservoir can be analyzed as a sharp-front reservoir. But for thick reservoirs, the assumption of a sharp front will cause significant error in pseudosteady-state analysis. Figures 3.22 through 3.24 also show that as the front angle increases, the effect of the reservoir thickness decreases, since for a particular reservoir thickness, as the front angle increases, the ratio R_{Davg}/R_{Dmin} decreases and the responses become closer to the sharp-front response.

Figures 3.25 and 3.26 show the effect of front angle on Cartesian derivative responses for R_{Dmin} of 300 and 1000, respectively. For the same front angle and reservoir thickness, as R_{Dmin} becomes smaller, the ratio R_{Davg}/R_{Dmin} becomes larger and thus deviation from the sharp-front response is also larger. Although Figure 3.26 shows results for $h_D = 400$ ($h_D = 300$ in Figure 3.25), the ratios R_{Davg}/R_{Dmin} for various front angles are smaller for the responses shown on Figure 3.26 as compared to Figure 3.25, since $R_{Dmin} = 1000$ in Figure 3.26.

Figures 3.27 and 3.28 show the effect of mobility ratio on the Cartesian pressure derivatives. Figures 3.27 and 3.28 describe responses for front angles of 45° and 60° , respectively. Both of these figures are for a storativity ratio, $F_s = 1$. Figures 3.27 and 3.28 show that the mobility ratio does not change the Cartesian slope. An increase in the mobility ratio increases the length of the pseudosteady-state period and delays the beginning of the second radial flow period. For a pss analysis to be possible, the mobility ratio, M , should be significantly greater than 10 for $F_s=1$. A comparison between Figures 3.27 and 3.28 shows that as the front angle moves closer to 90° , the Cartesian slope moves closer to 2.

Figures 3.29 and 3.30 show the effect of the storativity ratio, F_s , on the Cartesian derivatives. Figures 3.29 and 3.30 are for front angles of 45° and 60° , respectively. Like the mobility ratios, the higher storativity ratios increase the length of the pseudosteady-state flow period and the storativity ratios do not change the Cartesian slope of the pseudosteady-state period. Thus, Figures 3.27 through 3.30 suggest that the correction factor developed in Table 3.2 applies for most-commonly encountered mobility and storativity ratios for thermal recovery processes.

3.7 Conclusions

For multi-layer, composite reservoirs with tilted fronts, the following conclusions have been drawn from this study:

1. Design equations for the end of the first, radial-flow period for sharp front reservoirs are inadequate for tilted-front reservoirs. Modified design equations have been developed for the end of the first, radial-flow period and for the time to the maximum derivative for tilted-front reservoirs.

2. The deviation time method yields an estimate of the geometric mean of the minimum front radius and the average front radius of the swept region.
3. For inclined fronts, traditional pseudosteady-state analysis does not produce a constant Cartesian slope which is independent of the front angle and the reservoir thickness. For an inclined-front reservoir, pseudosteady-state flow exists in some average sense.
4. A correction factor has been developed to estimate the correct swept volume from the pseudosteady-state analysis for situations where a tilted front is suspected to occur. This correction factor should apply for most-commonly encountered thermal recovery situations.
5. For the cases studied in this paper, thermal well test responses obtained from a crossflow system can be analyzed using a commingled system solution for a fully-penetrating well. However, crossflow must be taken into account for proper analysis of thermal well test responses for partially-penetrating wells.

References

1. Lefkovits, H.C., Hazebroek, P., Allen, E.E., and Matthews, C.S.: "A Study of the Behavior of Bounded Reservoirs Composed of Stratified Layers," *SPEJ* (March 1961) 43-58; *Trans., AIME*, 222.
2. Tariq, S.M., and Ramey, H.J. Jr.: "Drawdown Behavior of a Well with Storage and Skin Effect Communicating With Layers of Different Radii and Other Characteristics," paper SPE 7453 presented at the 1978 SPE Annual Meeting Houston, TX, Oct. 1-3.

3. Bourdet, D.: "Pressure Behavior of Layered Reservoirs with Crossflow," paper SPE 13628 presented at the 1985 California Regional Meeting, CA, March 27-29.
4. Gomes, E. and Ambastha, A.K.: "An Analytical Pressure-Transient Model for Multilayered, Composite Reservoirs with Pseudosteady-State Formation Crossflow," paper SPE 26049 presented at the 1993 Western Regional Meeting, Anchorage, AK, May 26-28; see also *AOSTRA Journal of Research*, Vol. 8, No.2 (Spring 1992) 63-77.
5. Eggenschwiler, M., Ramey, H.J. Jr., Satman, A., and Cinco-Ley, H.: "Interpretation of Injection Well Pressure Transient Data in Thermal Oil Recovery," paper SPE 8908 presented at the 1980 California Regional Meeting, Los Angeles, CA, April 9-11.
6. Ambastha, A.K.: "Pressure Transient Analysis for Composite Systems," Ph.D. Thesis, Stanford University, Stanford, CA (Oct. 1988) 193 pp.
7. Satman, A.: "An Analytical Study of Transient Flow in Stratified Systems with Fluid Banks," paper SPE 10264 presented at the 1981 Annual Meeting, San Antonio, TX, Oct. 5-7.
8. Satman, A. and Oskay, M.M.: "Effect of a Tilted Front on Well Test Analysis," paper SPE 14701 available from SPE (1985).
9. Hatzignatiou, D.G., Ogbe, D.O., Dehghani, K. and Economides, M.J.: "Interference Behavior in Multilayered Composite Reservoirs," paper SPE 16766 presented at the 1987 Annual Meeting, Dallas, TX, Sept. 27-30.

10. Anbarci, K., Grader, A.S., and Ertekin, T.: "Determination of Front Locations in Multilayer Composite Reservoir," paper SPE 19799 presented at the 1989 Annual Meeting, San Antonio, TX, Oct. 8-11.
11. Kiome, I.: "Pressure Transient Behaviour for a Well in a Multi-Layered Composite Reservoir with an Inclined Front," M.Sc. Thesis, University of Alberta, Edmonton, AB (March 1991) 132 pp.
12. Larsen, L.: "Similarities and Differences in Methods Currently Used to Analyze Pressure-Transient Data From Layered Reservoirs," paper SPE 18122 presented at the 1988 Annual Meeting, Houston, TX, Oct. 2-5.
13. Ambastha, A. K. and Ramey, H.J. Jr.: "Thermal Recovery Well Test Design and Interpretation," *SPEFE* (June 1989) 173-180.
14. Sosa, A., Raghavan, R., and Limon, T.J.: "Effect of Relative Permeability and Mobility Ratio on Pressure Falloff Behavior," *JPT* (June 1981) 1125-35.
15. Tang, R.W.K.: "Transient Pressure Analysis in Composite Reservoirs," SUPRI-A Technical report 31, U.S. DOE Report no. DOE/ET/12056-31 (Aug. 1982).
16. Ramey, H.J. Jr., and Cobb, W.M.: "A General Pressure Buildup Theory for a Well in a Closed Drainage Area," *JPT* (December, 1971) 1493-1505.

Table 3.1: Effect of front angle on $(t_{DR})_{end}$ and $(t_{DR})_{max}$ for various mobility and storativity ratios.

M	F_s	θ	R_{Davg}	$(t_{DR})_{end}$	$(t_{DR})_{max}$	$\frac{R_{Davg}}{R_{Dmin}}$	$\frac{(t_{DR})_{end}}{(t_{DR})_{end of}}$	$\frac{(t_{DR})_{max}}{(t_{DR})_{max of}}$
10	1	30°	628.8	0.23		1.258	1.277	
		45°	572.8	0.21		1.146	1.166	
		60°	541.4	0.2		1.083	1.111	
		90°	500	0.18		1	1	
100	1	30°	628.8	0.225		1.258	1.25	
		45°	572.8	0.21		1.146	1.166	
		60°	541.4	0.2		1.083	1.111	
		90°	500	0.18		1	1	
1000	1	30°	628.8	0.225		1.258	1.25	
		45°	572.8	0.21		1.146	1.166	
		60°	541.4	0.2		1.083	1.111	
		90°	500	0.18		1	1	
100	10	30°	628.8	0.225	310	1.258	1.25	1.291
		45°	572.8	0.21	280	1.146	1.166	1.166
		60°	541.4	0.2	260	1.083	1.111	1.083
		90°	500	0.18	240	1	1	1
100	100	30°	628.8	0.225	340	1.258	1.25	1.299
		45°	572.8	0.21	310	1.146	1.166	1.148
		60°	541.4	0.2	290	1.083	1.111	1.074
		90°	500	0.18	270	1	1	1
100	1000	30°	628.8	0.225	380	1.258	1.25	1.266
		45°	572.8	0.21	350	1.146	1.166	1.166
		60°	541.4	0.2	320	1.083	1.111	1.066
		90°	500	0.18	300	1	1	1

Table 3.2: Equivalence between the ratios of R_{Davg}/R_{Dmin} and m_e/m_{ref} for inclined front reservoirs (for $M=1000$ and $F_i=1$).

Case	Front Angle	R_{Davg}	m_e	R_{Davg}/R_{Dmin}	m_e/m_{ref}
$h_D = 400$ $R_{Dmin} = 500$	30°	753.5	2.95	1.51	1.48
	45°	642.3	2.52	1.28	1.27
	60°	580.3	2.33	1.16	1.17
	90°	500.0	2.0	1.0	1.0
$h_D = 300$ $R_{Dmin} = 500$	30°	687.3	2.68	1.37	1.34
	45°	605.4	2.45	1.21	1.23
	60°	559.7	2.28	1.12	1.14
	90°	500.0	2.0	1.0	1.0
$h_D = 100$ $R_{Dmin} = 500$	30°	559.7	2.26	1.12	1.13
	45°	534.0	2.12	1.07	1.06
	60°	519.5	2.08	1.04	1.04
	90°	500	2.0	1.0	1.0
$h_D = 300$ $R_{Dmin} = 300$	30°	492.4	3.19	1.64	1.59
	45°	407.9	2.71	1.36	1.35
	60°	360.8	2.42	1.20	1.21
	90°	300	2.0	1.0	1.0
$h_D = 400$ $R_{Dmin} = 1000$	30°	1244.9	2.46	1.24	1.23
	45°	1138.5	2.28	1.14	1.14
	60°	1078.8	2.20	1.08	1.10
	90°	1000	2.0	1.0	1.0

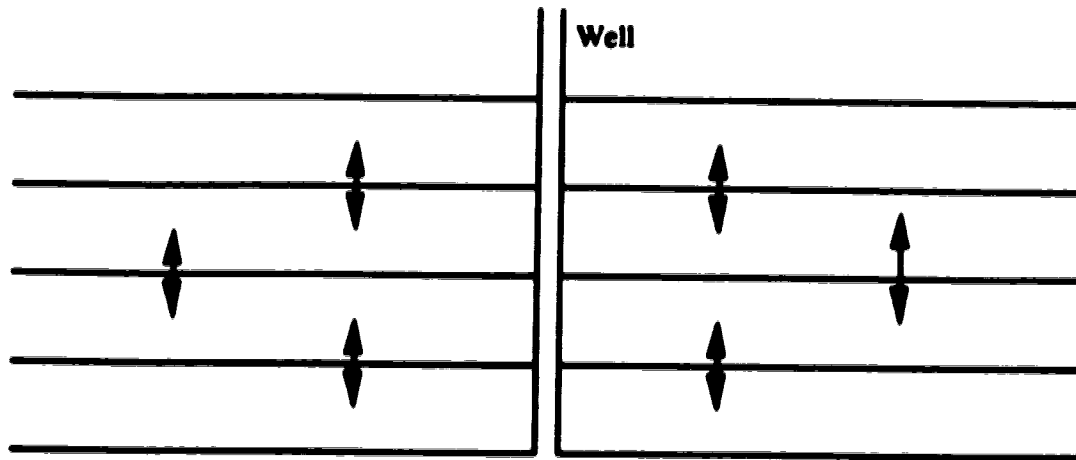


Figure 3.1a : Layered reservoir with interlayer crossflow.

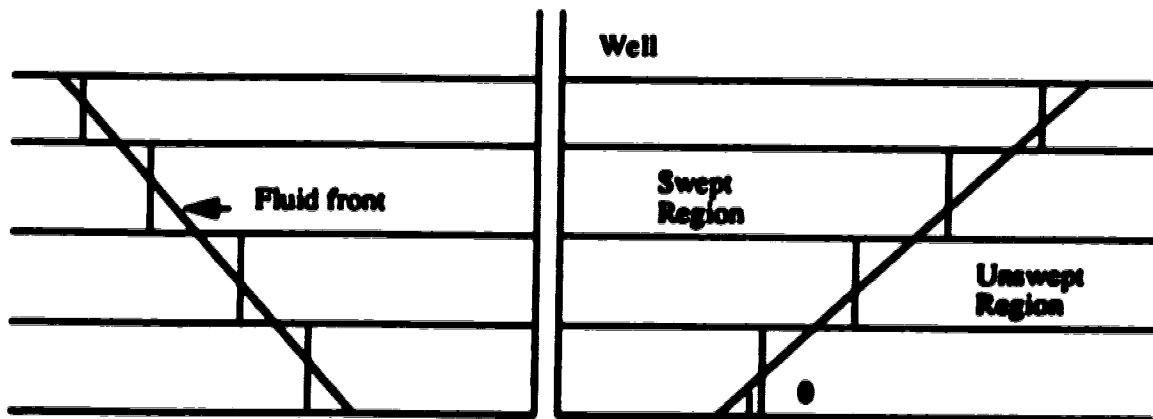


Figure 3.1b : Radial, layered composite reservoir with a tilted front.

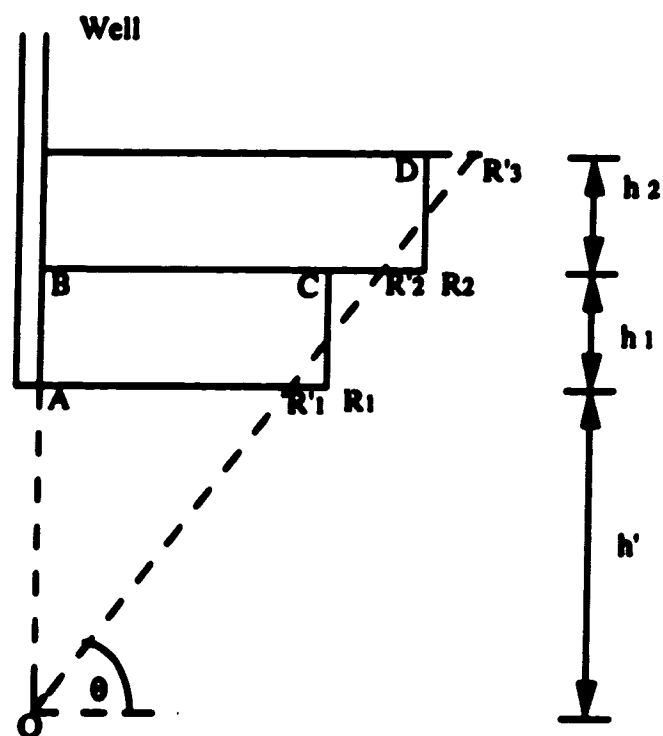


Figure 3.2: Schematic of the swept section of a two-layer composite reservoir.

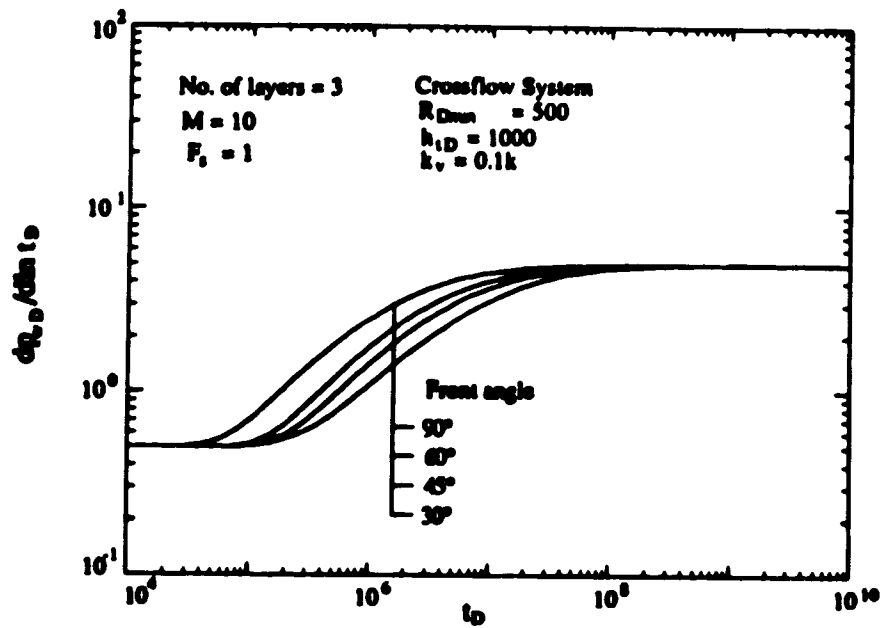


Figure 3.3: Effect of front angle on pressure derivative responses for $h_{1D} = 1000$.

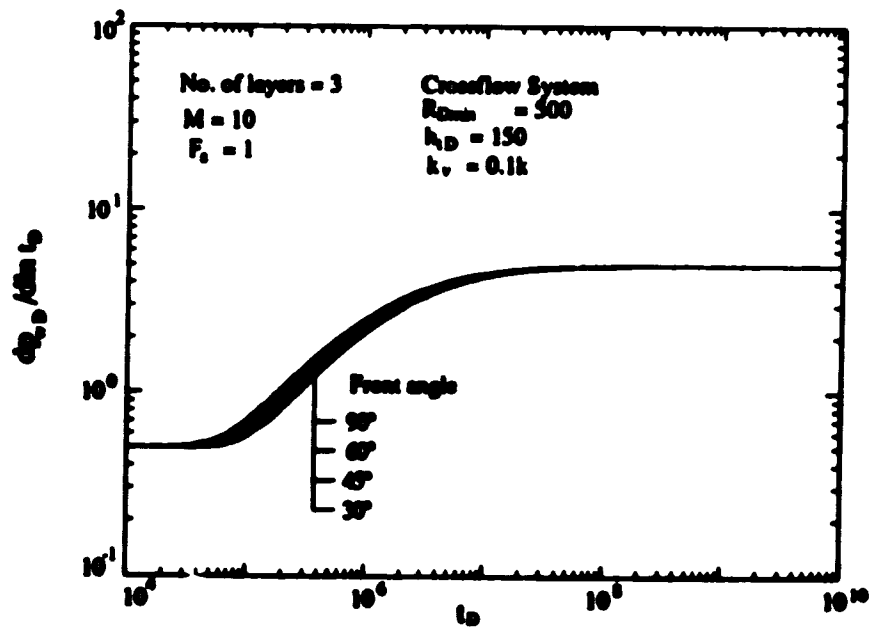


Figure 3.4: Effect of front angle on pressure derivative responses for $h_{1D} = 150$.

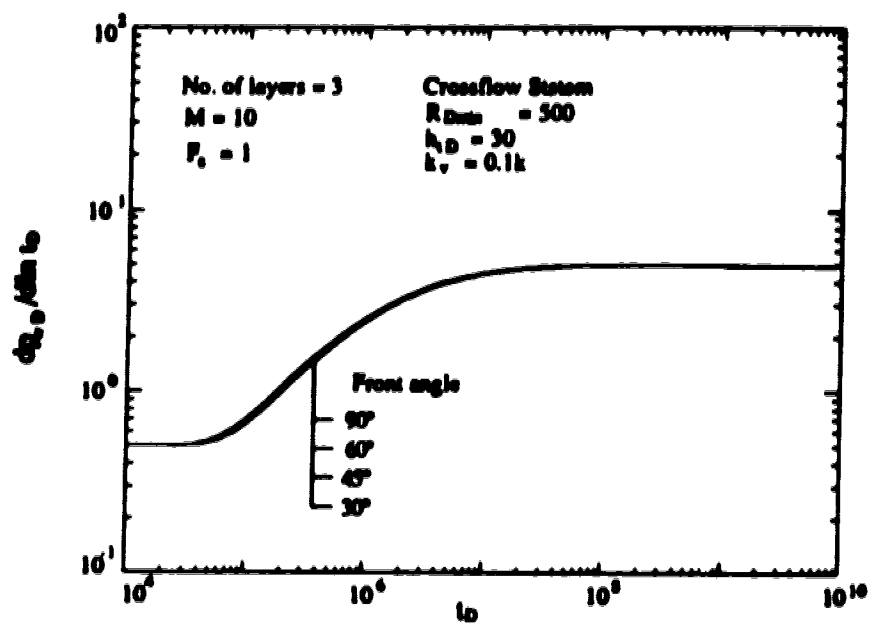


Figure 3.5: Effect of front angle on pressure derivative responses for $h_{1D} = 30$.

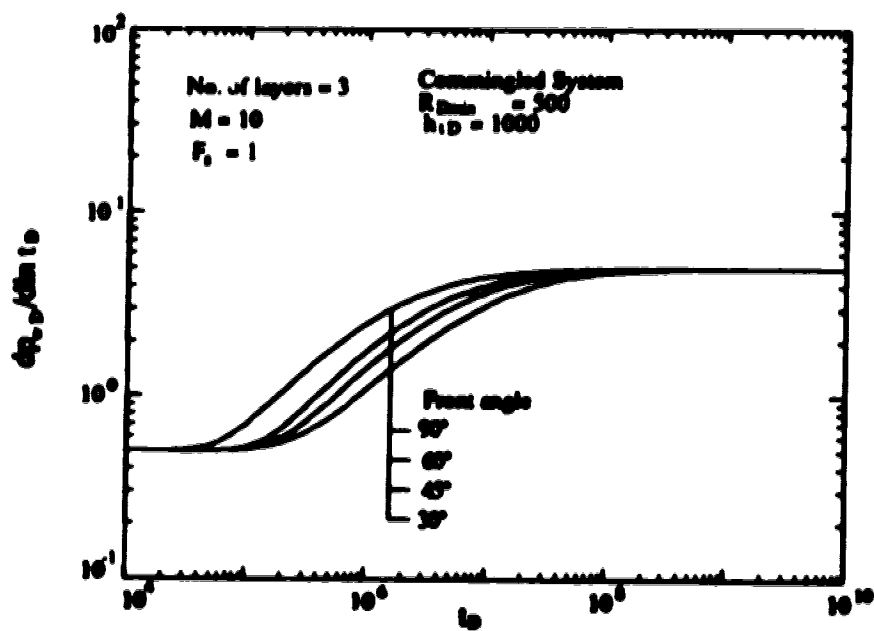


Figure 3.6: Effect of front angle on pressure derivative responses for $h_{1D} = 1000$.

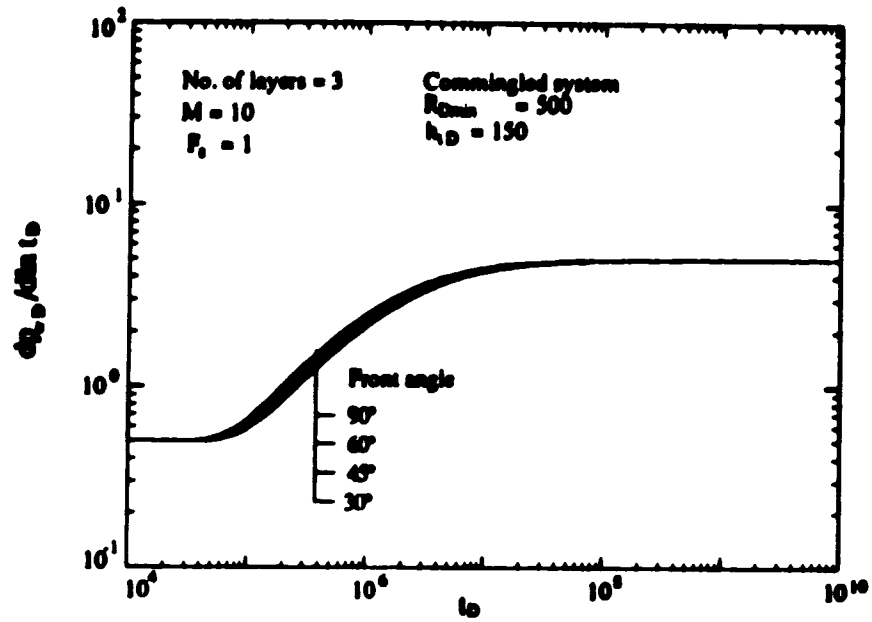


Figure 3.7: Effect of front angle on pressure derivative responses for $h_{iD} = 150$.

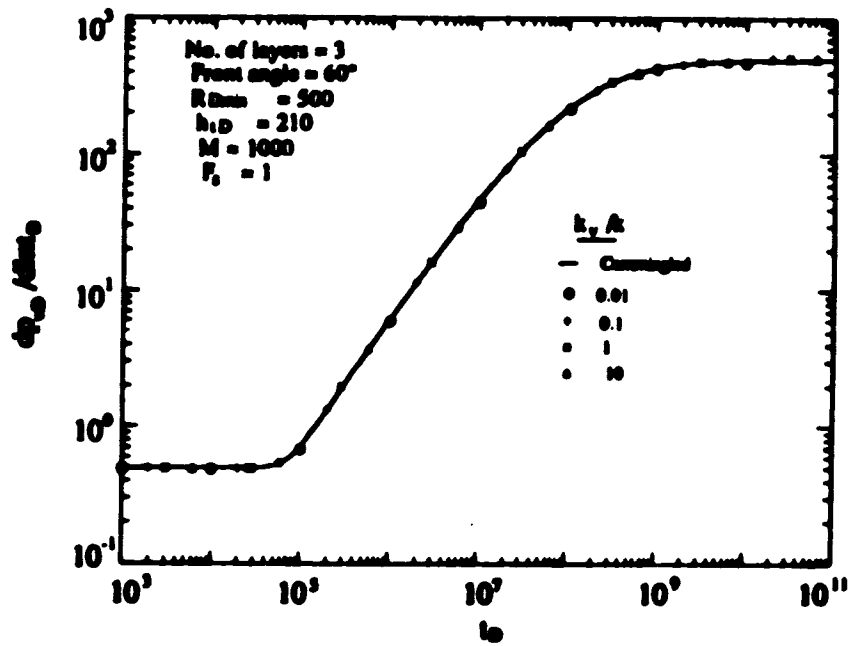


Figure 3.8: Effect of crossflow on pressure derivative responses for a fully-penetrating well.

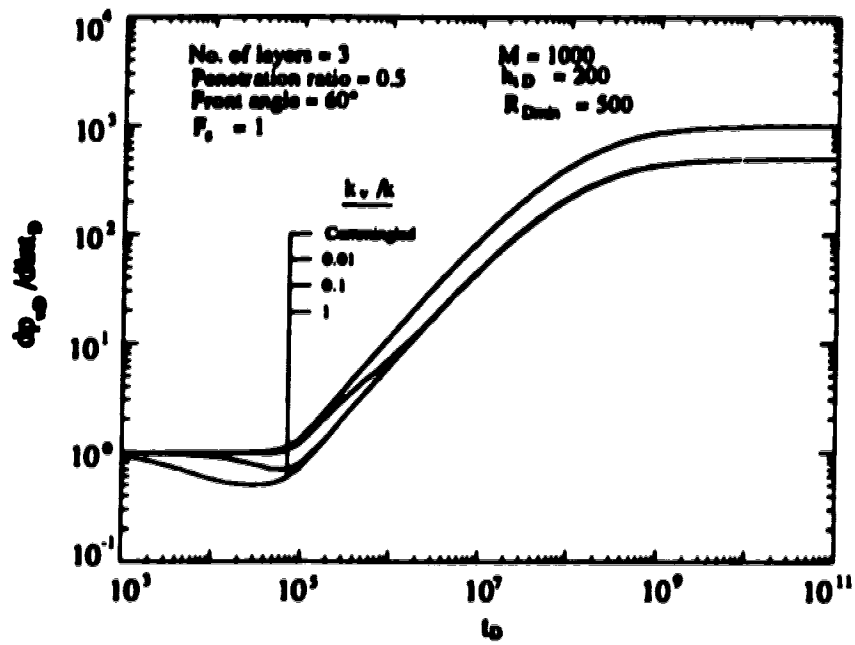


Figure 3.9: Effect of crossflow on pressure derivative responses of a partially-penetrating well.

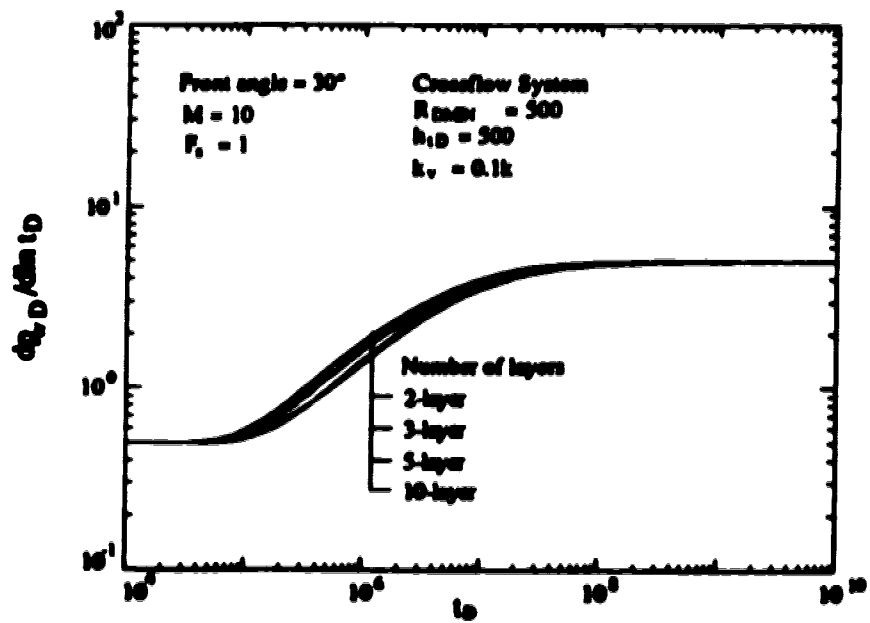


Figure 3.10: Effect of layer refinement on pressure derivative responses for a front angle = 30° .

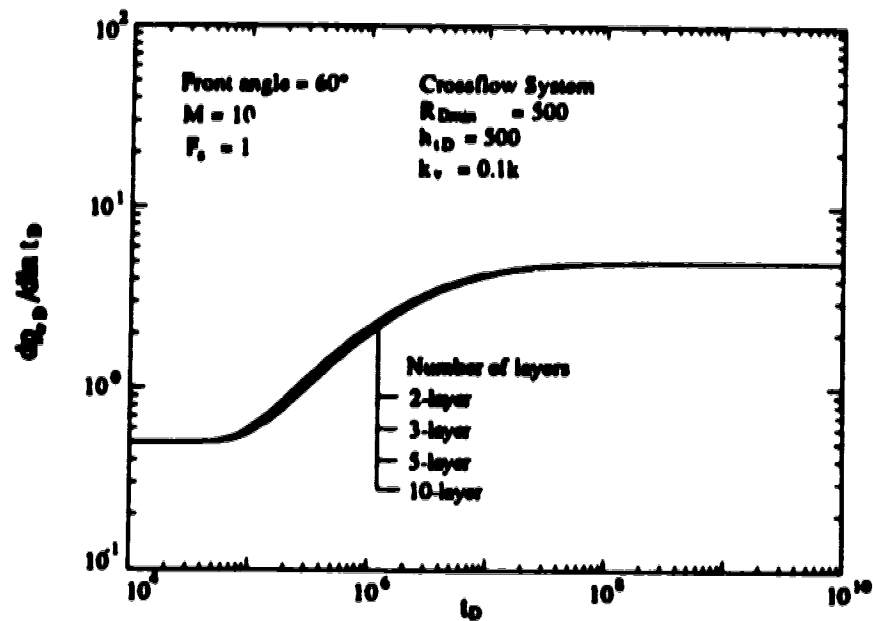


Figure 3.11: Effect of layer refinement on pressure derivative responses for a front angle = 60° .

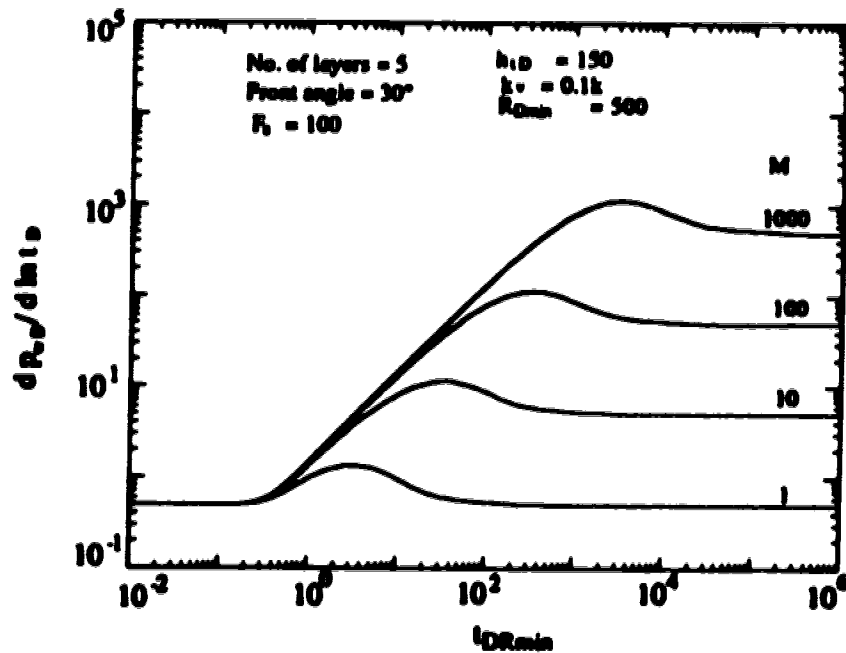


Figure 3.12: Effect of mobility ratio on pressure derivative responses for a front angle = 30° .

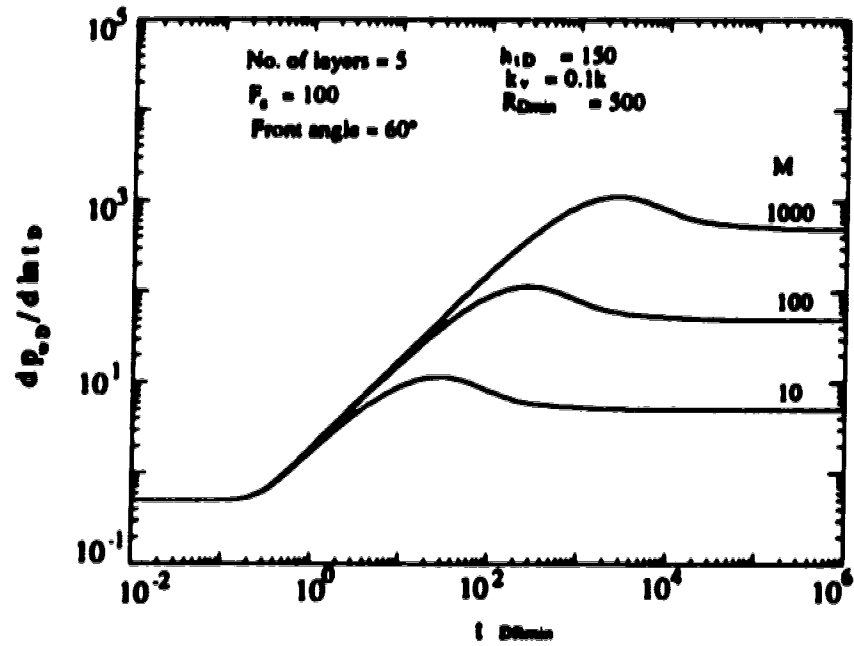


Figure 3.13: Effect of mobility ratio on pressure derivative responses for a front angle = 60° .

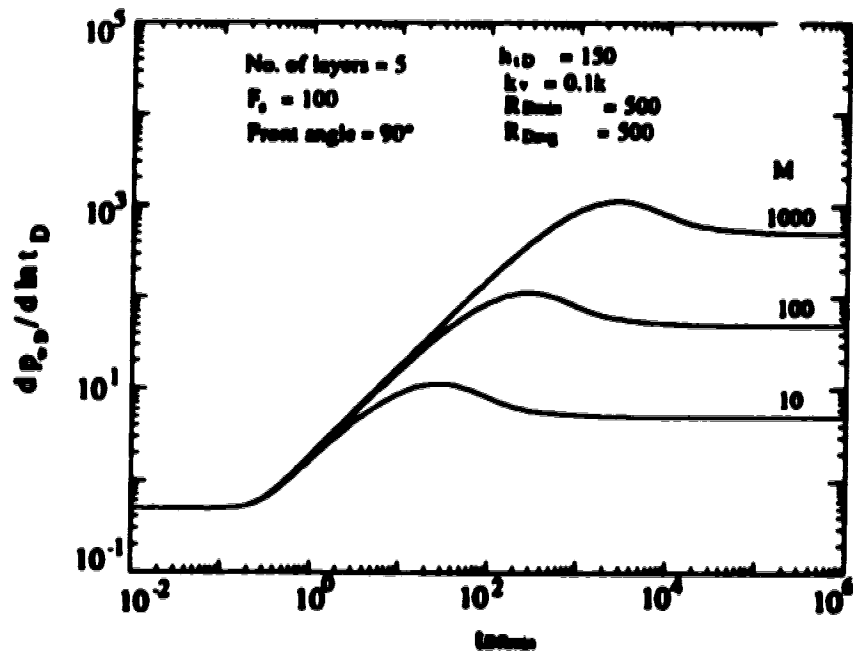


Figure 3.14: Effect of mobility ratio on pressure derivative responses for a sharp front reservoir.

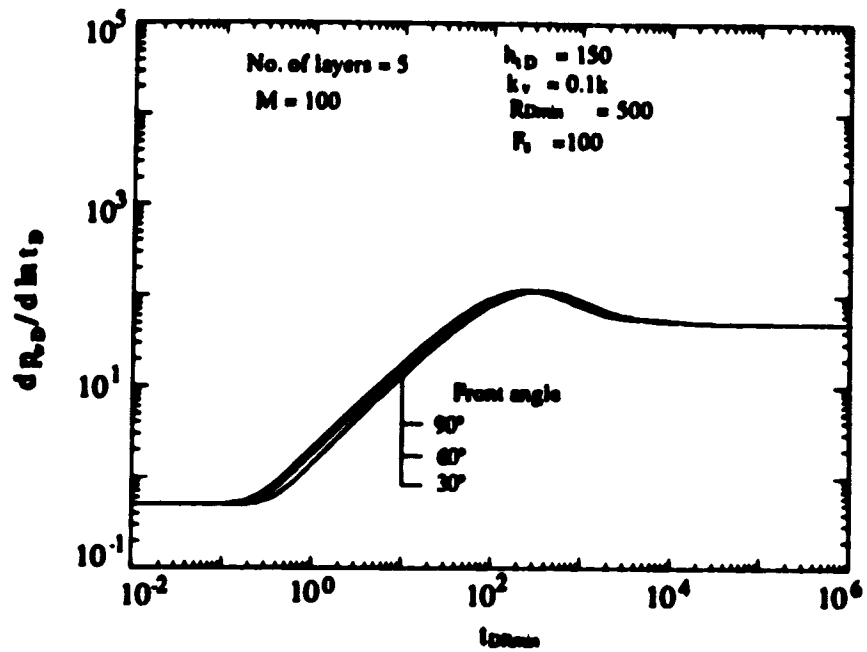


Figure 3.15: Effect of front angle on pressure derivative responses.

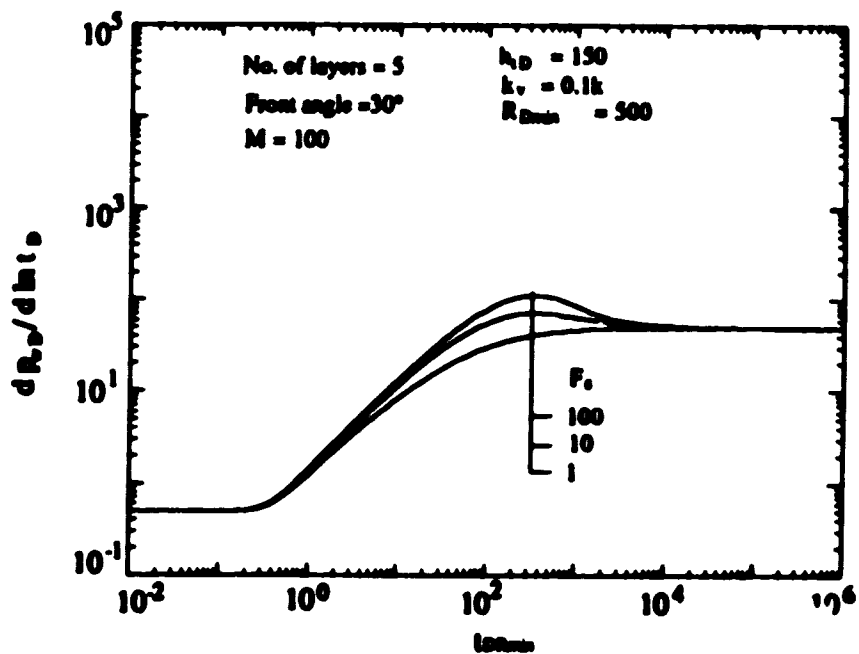


Figure 3.16: Effect of storativity ratio on pressure derivative responses for a front angle = 30° .

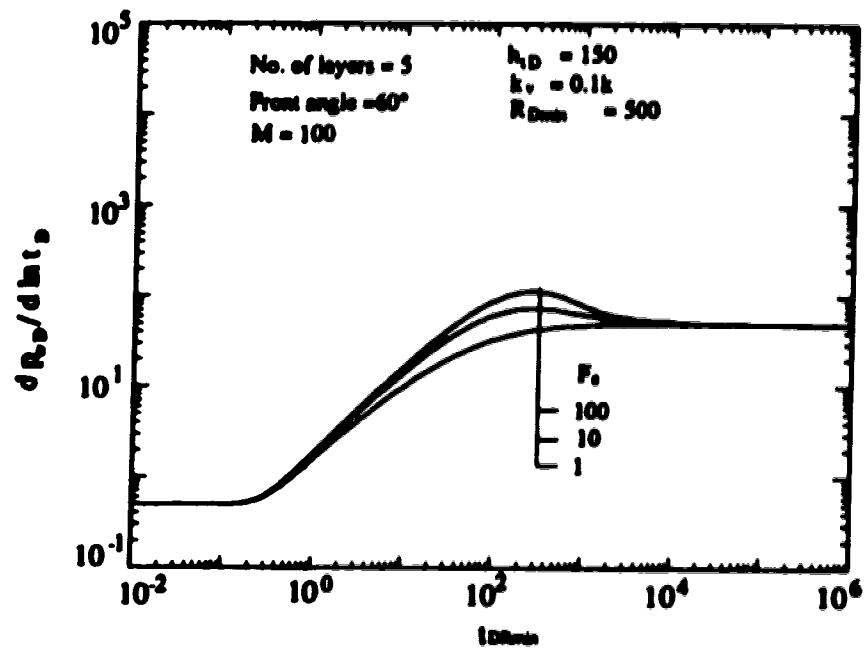


Figure 3.17: Effect of storativity ratio on pressure derivative responses for a front angle = 60° .

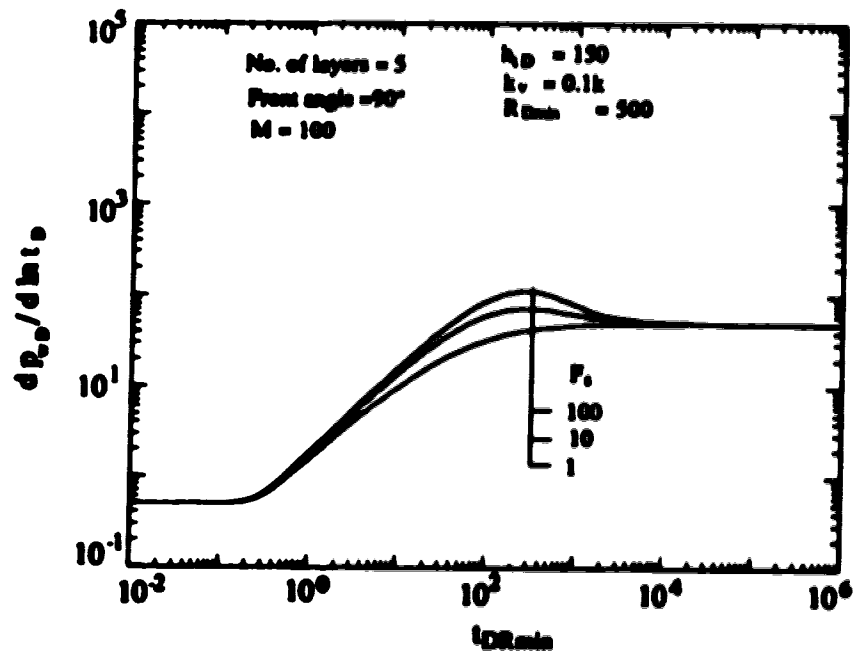


Figure 3.18: Effect of storativity ratio on pressure derivative responses for a sharp front reservoir.

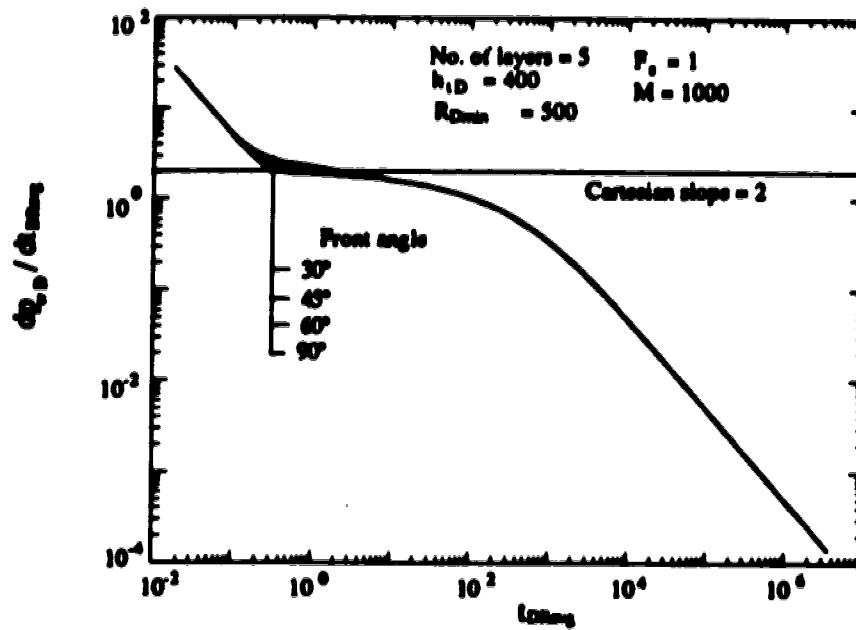


Figure 3.19: Effect of front angle on pseudosteady-state analysis for $h_{1D} = 400$.

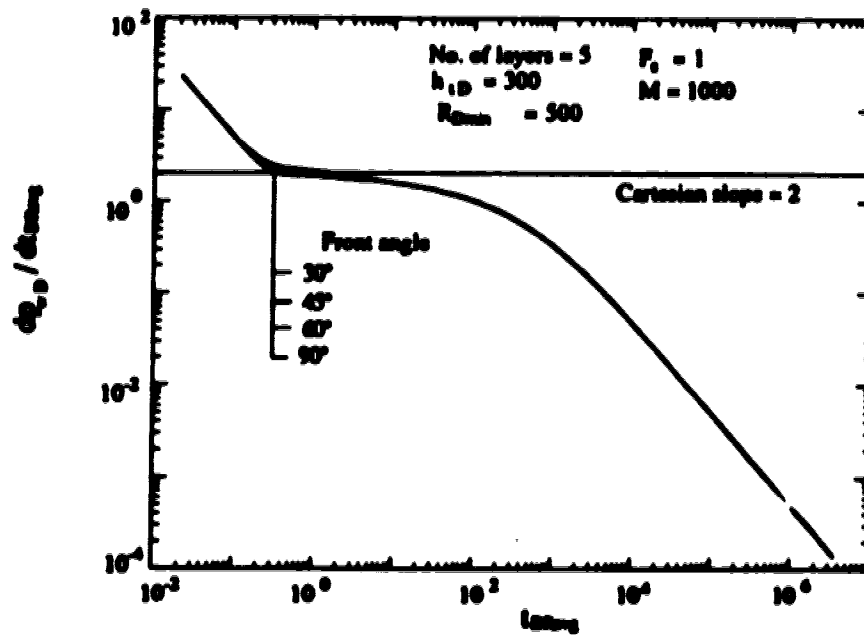


Figure 3.20: Effect of front angle on pseudosteady-state analysis for $h_{1D} = 300$.

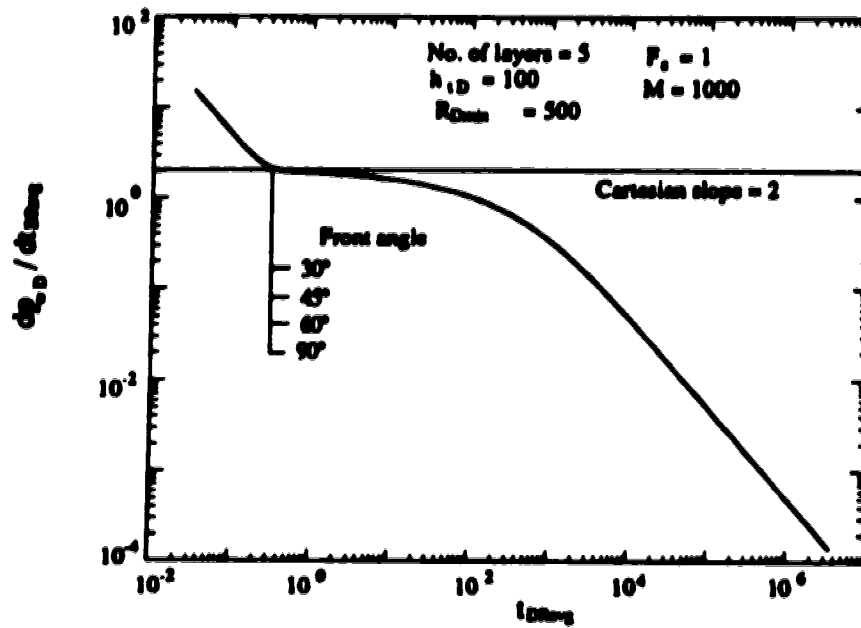


Figure 3.21: Effect of front angle on pseudosteady-state analysis for $h_{1D} = 100$.

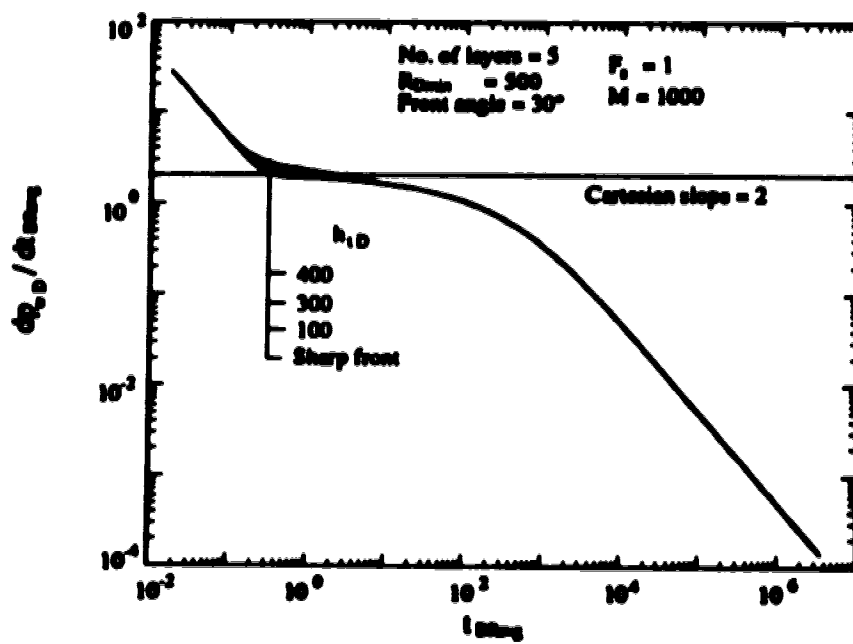


Figure 3.22: Effect of reservoir thickness on pseudosteady-state analysis for a front angle = 30°.

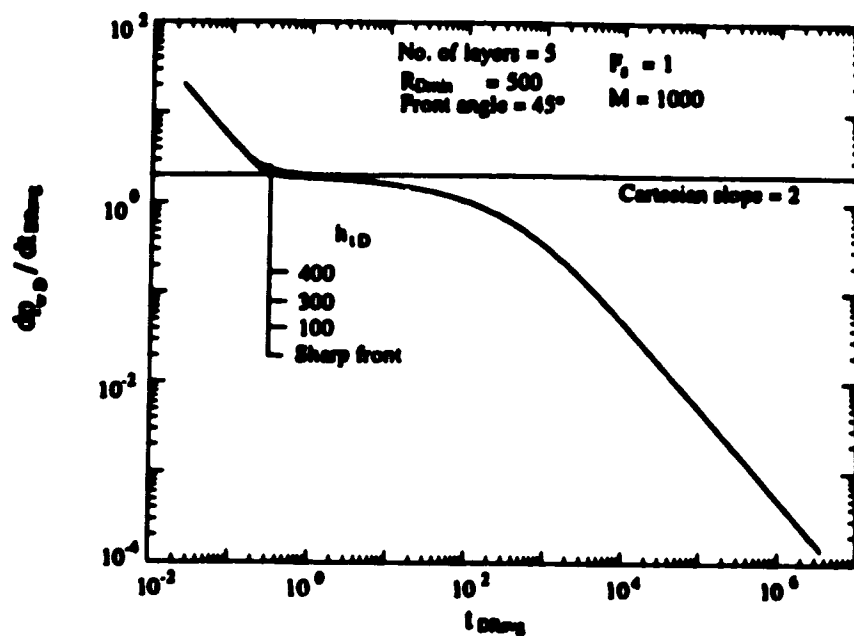


Figure 3.23: Effect of reservoir thickness on pseudosteady-state analysis for a front angle = 45° .

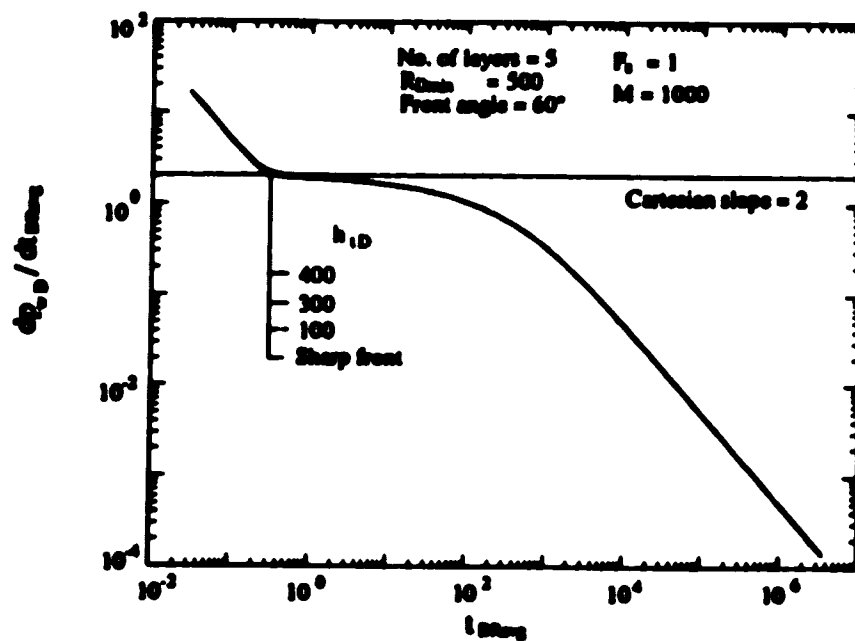


Figure 3.24: Effect of reservoir thickness on pseudosteady-state analysis for a front angle = 60° .

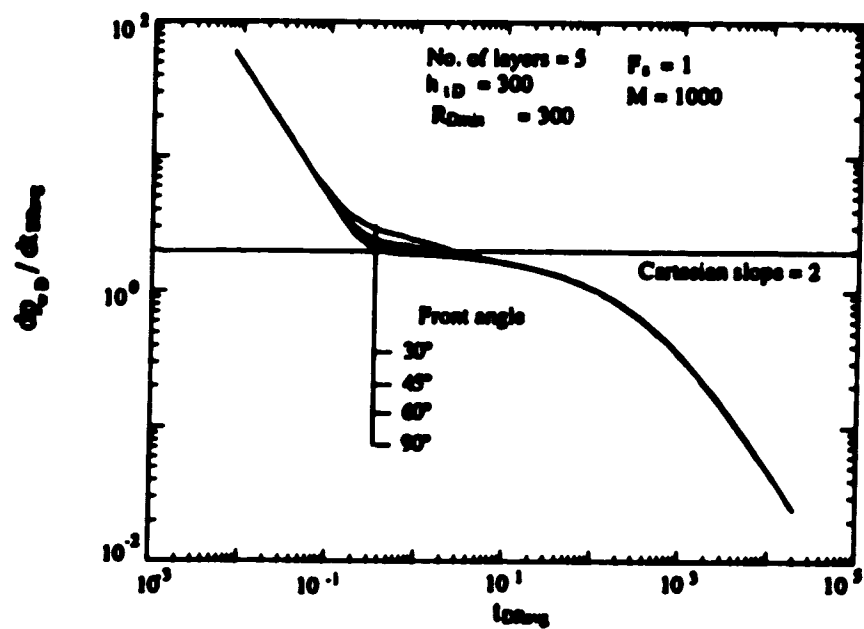


Figure 3.25: Effect of front angle on pseudosteady-state analysis for $R_{0min} = 300$.

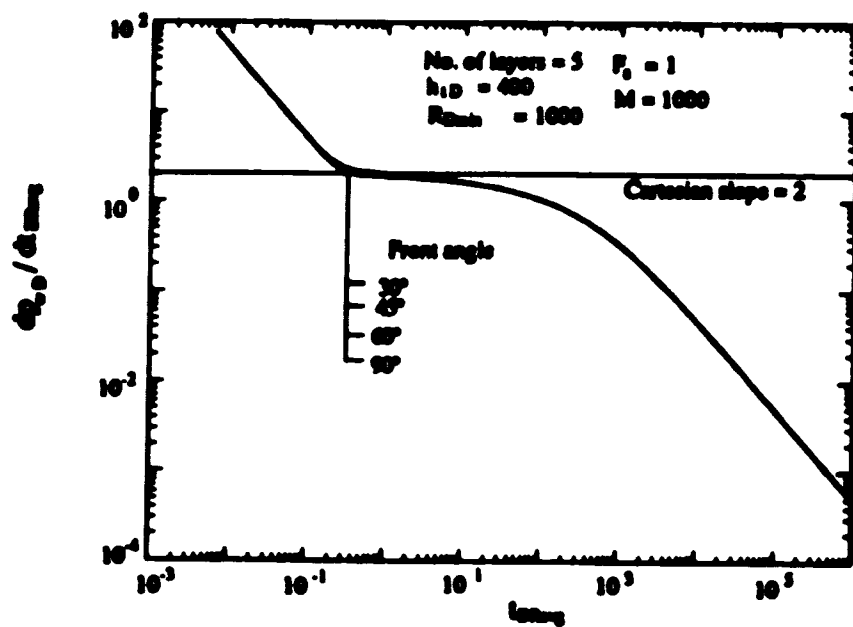


Figure 3.26: Effect of front angle on pseudosteady-state analysis for $R_{0min} = 1000$.

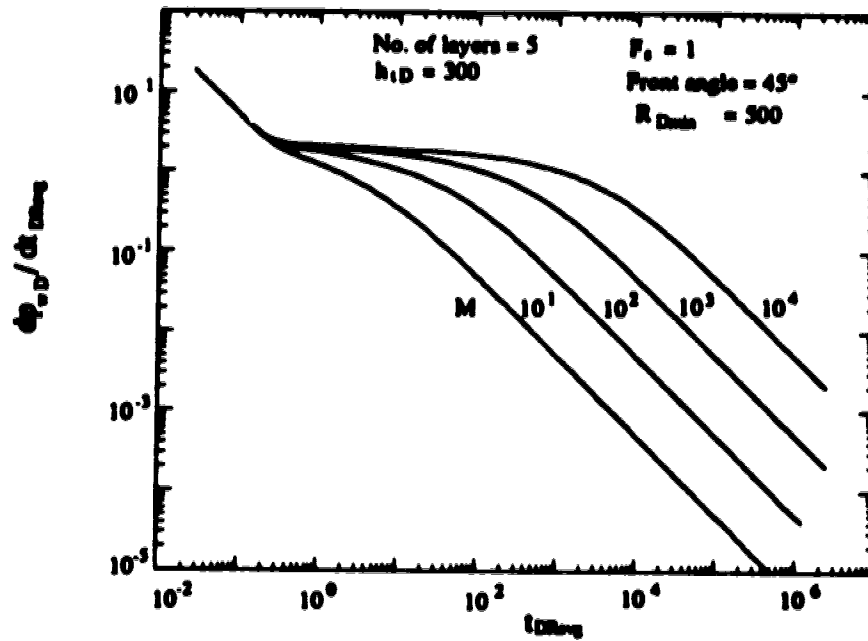


Figure 3.27: Effect of mobility ratio on pseudosteady-state analysis for a front angle = 45° .

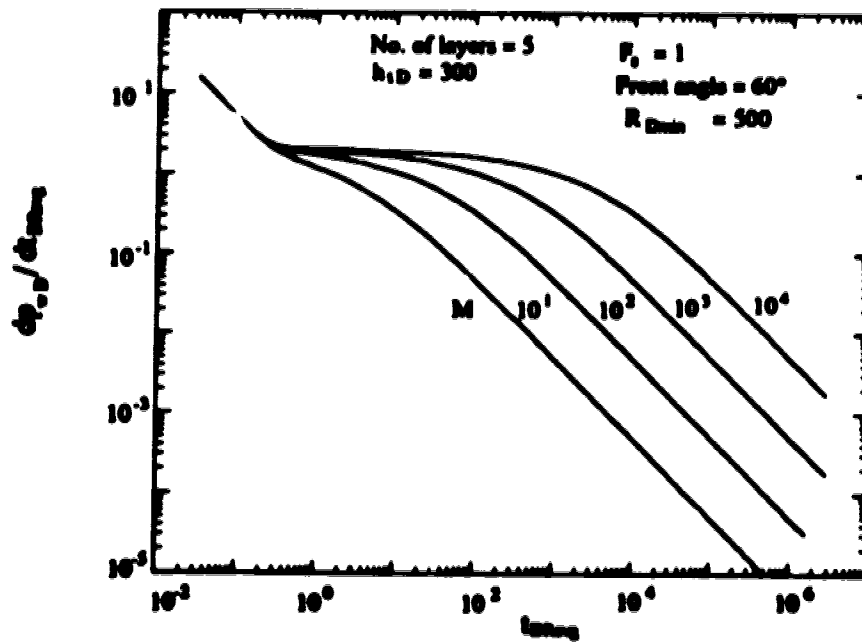


Figure 3.28: Effect of mobility ratio on pseudosteady-state analysis for a front angle = 60° .

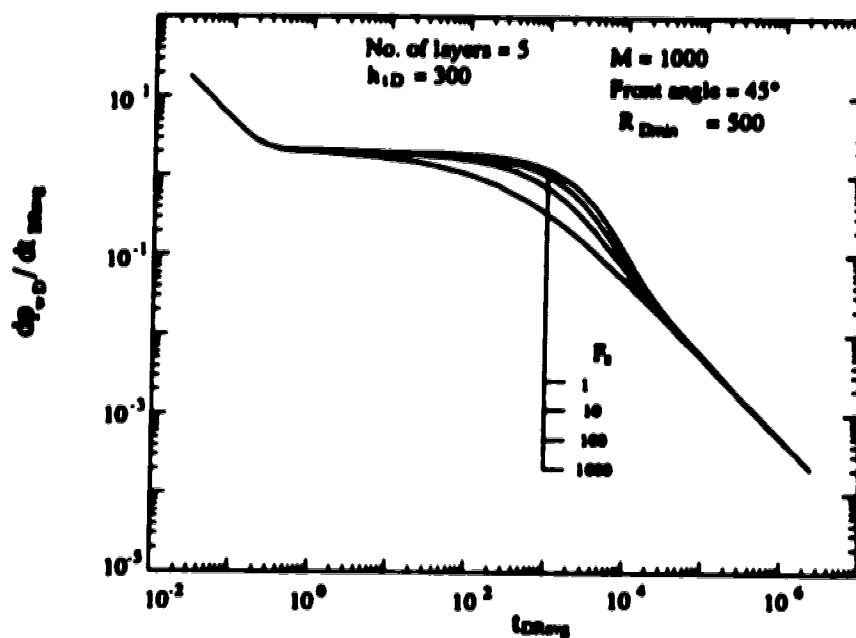


Figure 3.29: Effect of storativity ratio on pseudosteady-state analysis for a front angle = 45°.

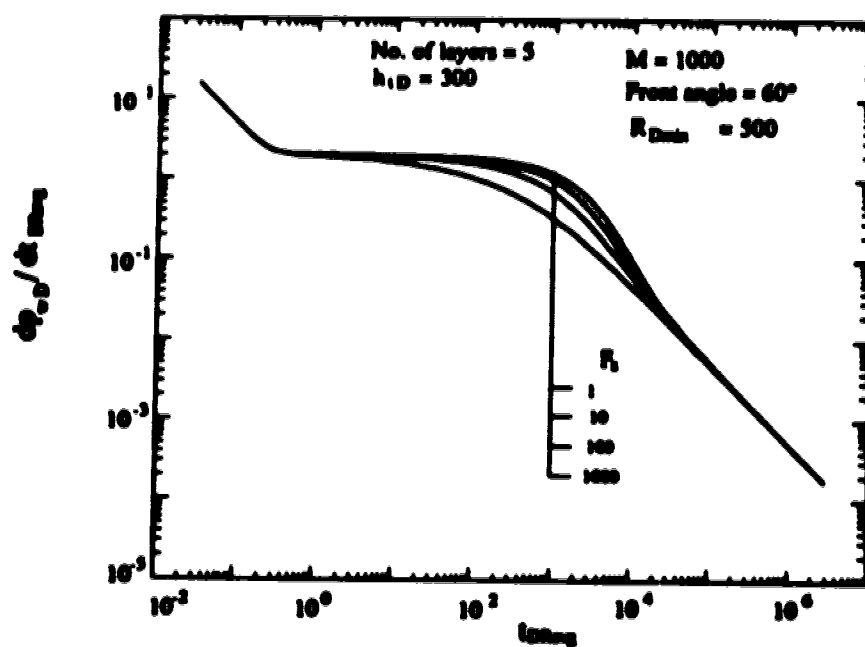


Figure 3.30: Effect of storativity ratio on pseudosteady-state analysis for a front angle = 60°.

4.0 PSEUDOSKIN UNDER VARIOUS RESERVOIR CONDITIONS

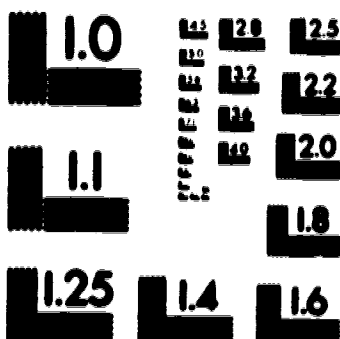
4.1 Introduction

Reservoir deposition occurs over a geologic period of time and, because of this, many reservoirs are layered instead of being homogeneous. Oil reservoirs are often accompanied by a bottom-water zone and/or a gas cap. In such situations, wells are completed over a fraction of the productive zone to delay water and/or gas coning. These wells are known as partially-penetrating wells. Because of partial penetration, pressure transient responses show an additional pressure drop in comparison to the pressure drop for a fully-penetrating well. This additional pressure drop is referred to as pseudoskin. Partially-penetrating wells have their own characteristic responses which, if not properly evaluated, may lead to errors in the interpretation of well-test data. The purpose of this paper is to study the pressure transient responses and the pseudoskin factor in a partially-penetrated, multi-layer reservoir with or without a bottom-water zone or a gas cap.

Muskat¹ studied partially-penetrating wells in single-layer reservoirs under steady-state conditions using the method of images and estimated the productivity loss because of partial penetration. Nisile² presented buildup pressure transient responses for a partially-penetrating well in a single-layer homogeneous reservoir. He considered a partially-penetrating well in an infinite slab and used the method of images to solve the problem. He observed two different straight lines for early and late time pressure buildup responses and used the ratio of the slopes of these two straight lines to estimate the penetration ratio. Brons and Marting³ observed three sequences in pressure transient responses of a partially-penetrating well in a single-layer isotropic reservoir: a radial flow period with a slope corresponding to the open interval thickness, a transition period, and a pseudoradial flow period with a slope corresponding to the total formation thickness. They presented an empirical expression for the pseudoskin factor, s_p . But they did not consider the variation

2

PM-1 3 1/2"x4" PHOTOGRAPHIC MICROCOPY TARGET
NBS 1815a ANSI/ISO #2 EQUIVALENT



PRECISIONSM RESOLUTION TARGETS

in the horizontal and the vertical permeabilities when defining dimensionless wellbore thickness and their pseudoskin factor had to be numerically evaluated.

Bilhartz and Ramey⁴ used a two-dimensional, finite-difference model to study wellbore storage and skin effects in a single-layer, partially-penetrated reservoir. They concluded that the radial flow period and the transition to pseudoradial flow period may be masked in the presence of significant wellbore storage. They extended the Brons and Marting³ pseudoskin expression to anisotropic reservoirs and discussed methods to estimate horizontal and vertical permeabilities.

Streltsova-Adams⁵ used Laplace and Hankel transformations to solve the partial-penetration problem in a single-layer reservoir and derived an expression for the pseudoskin factor in terms of infinite sine and cosine series. She considered the presence of a gas cap as a constant-pressure boundary in her solution. She investigated the effect of open interval (penetrated portion) location on the pseudoskin factor and concluded that the pseudoskin factor is minimum for centrally-located open intervals, other parameters remaining unchanged. She also observed that for a reservoir with a gas cap, the pseudoskin factor is lower than that for a reservoir with no gas cap, when the open interval is adjacent to the constant-pressure boundary. Saidikowski⁶ investigated the combined effect of wellbore damage and partial penetration on transient pressure analysis and presented a relationship for the total skin obtained from transient pressure analysis with wellbore skin and pseudoskin. Buhidma and Raghavan⁷ studied drawdown and buildup behaviour of a partially-penetrating well in a square reservoir subject to bottom-water drive. Using Green's function to obtain the solution, they concluded that, under bottom-water drive, pseudoradial flow does not exist and the pseudoskin factor can not be calculated by the methods presented by Brons and Marting³ and other researchers. Although a pseudoradial flow period does not exist under bottom-water or gas-cap drive, the expression for pseudoskin developed in this study can be used to estimate the pseudoskin factor under

these reservoir conditions.

Using a two-dimensional finite-difference simulator, Reynolds *et al.*⁸ graphically presented the pressure transient responses of a partially-penetrated, two-layer reservoir. Analyzing the steady-state analytical solution, they identified the correlating parameters and then obtained a correlation for the pseudoskin factor by regression analysis. They also concluded that by using different layers for different fluid regions, a multi-phase flow system can be approximated by a layered, single-phase flow system.

Papatzacos⁹ used the method of images to solve the partial-penetration problem for a single-layer, homogeneous reservoir and derived an expression for the pseudoskin factor in terms of the dimensionless open interval, its location and the dimensionless wellbore radius.

Olarewaju and Lee¹⁰ studied the buildup pressure behaviour of a partially-penetrating well in a two-layer reservoir with closed top and bottom boundaries. Of the two layers they considered, one layer is open to flow and the other layer is closed. In the closed layer, they considered flow only in the vertical direction, neglecting the radial component of the flow, which may limit the applicability of their model. Olarewaju and Lee¹⁰ considered crossflow as a time-dependent source term for the open layer based on the vertical flow component for the closed layer. By regression analysis, they developed a series of expressions correlating the pseudoskin factor with the penetration ratio for various k_1/k_2 values.

Using a numerical simulator, Yeh and Reynolds¹¹ presented some type-curves for partially-penetrated, multi-layer reservoirs with transient crossflow. Using the same numerical model, Yeh and Reynolds¹² graphically presented pseudoskin factors for a partially-penetrated, multi-layer reservoir. Using regression analysis, they obtained an expression for the pseudoskin factor.

Vrbik¹³ derived a simplified approximate expression for a single-layer, homogeneous

reservoir in terms of three correlating parameters which are related to the dimensionless open interval length, its location and the dimensionless wellbore radius. Ding and Reynolds¹⁴ extended Papatzacos⁹ expression for the pseudoskin for a single-layer reservoir to that for a multi-layer reservoir and reported a good match with simulated results.

Shah and Thambynayagam¹⁵ presented an analytical solution for a two-layer, partially-penetrated reservoir by successive application of Laplace and Hankel transformations. They considered transient crossflow between the two layers and the presence of a gas-cap drive. They presented some pressure transient responses for fully- and partially-penetrating wells and they did not study the pseudoskin factor because of the partial penetration.

Table 4.1 summarizes most of the studies¹⁻²⁰ conducted on partially-penetrated reservoirs and on the pseudoskin factor. Table 4.1 shows that most of the studies considered single-layer reservoirs and only a limited number of studies have focussed on partially-penetrated, multi-layer reservoirs. The partially-penetrated, multi-layer reservoir problem has been studied either by using a numerical simulator with graphical presentation of pressure transient responses and pseudoskin values (Yeh and Reynolds^{11,12}), or by extending the single-layer expression of pseudoskin to the multi-layer case by redefining some of the parameters (Ding and Reynolds¹⁴). Table 4.1 also shows that very few studies have been conducted for a partially-penetrated reservoir subject to a bottom-water or a gas-cap drive.

This study attempts to give some new insights into understanding partially-penetrated, multi-layer reservoirs and covers both pressure transient responses and pseudoskin factors in situations where the top and bottom boundaries are closed and where one of the boundaries is at a constant pressure because of a bottom-water or a gas-cap drive.

4.2 Pseudoskin Factor Expression for Closed Top and Bottom Boundaries

Figure 4.1 schematically shows a two-layer, partially-penetrated reservoir . In this study, the layers are numbered from the bottom to the top. Thus, layer 1 is always the bottom-most layer. In Figure 4.1, Layer 1 is penetrated and Layer 2 is closed at the wellbore. The upper boundary of Layer 2 and the lower boundary of Layer 1 are considered as closed boundaries. Pseudosteady-state crossflow is considered between the two layers. Appendix C shows a detailed derivation of the pressure transient solution and the late-time limiting solution for this case. From the late-time limiting solution, we obtain the expression for pseudoskin as:

$$s_b = \frac{(1 - \kappa)}{\kappa} \frac{K_0\left(\sqrt{\frac{\lambda_A}{\kappa(1 - \kappa)}}\right)}{\sqrt{\frac{\lambda_A}{\kappa(1 - \kappa)}} K_1\left(\sqrt{\frac{\lambda_A}{\kappa(1 - \kappa)}}\right)} \quad (4.1)$$

where s_b denotes the pseudoskin, and λ_A and κ denote the dimensionless crossflow parameter and the mobility-thickness ratio of the open interval, respectively. Equation (4.1) can be extended for a multi-layer reservoir by appropriately defining λ_A and κ as:

$$s_b = \frac{(1 - \bar{\kappa})}{\bar{\kappa}} \frac{K_0\left(\sqrt{\frac{\bar{\lambda}_A}{\bar{\kappa}(1 - \bar{\kappa})}}\right)}{\sqrt{\frac{\bar{\lambda}_A}{\bar{\kappa}(1 - \bar{\kappa})}} K_1\left(\sqrt{\frac{\bar{\lambda}_A}{\bar{\kappa}(1 - \bar{\kappa})}}\right)} \quad (4.2)$$

where, $\bar{\kappa}$ = total mobility-thickness ratio of the open interval

$\bar{\lambda}_A$ = average crossflow parameter

Equation (4.2) is applicable for a multi-layer reservoir having any arbitrary number of layers making up the open interval and any arbitrary location of the open interval. In Equation (4.2), $\bar{\kappa}$ and $\bar{\lambda}_A$ are calculated by adding the individual layer mobility-thickness ratio of the open interval, and by adding the bottom and the top boundary crossflow parameters of the open interval, respectively. For multi-layer reservoirs, instead of

considering the crossflow parameters of each and every layer, only the top and bottom boundary crossflow parameters of the open interval are considered in defining the average crossflow parameter. This was done because Equation (4.2) gives better results with an average crossflow parameter defined in this manner, rather than with an average crossflow parameter which considers the crossflow parameters of each and every layer. A similar observation is made by Ding and Reynolds¹⁴ in defining the average vertical permeability. Irrespective of the number of layers in the reservoir, only two parameters (that is, $\bar{\kappa}$ and $\bar{\lambda}_A$) are required to estimate the pseudoskin using Equation (4.2).

For a single-layer, anisotropic reservoir, the mobility-thickness ratio, κ , and the crossflow parameter, λ_A , reduce to the penetration ratio (b) and $2b^2/h_D^2$, respectively. With these simplifications, Equation (4.1) reduces to:

$$s_b = \frac{h_D}{\sqrt{2}} \left(\frac{1-b}{b} \right)^{\frac{3}{2}} \frac{K_0 \left(\sqrt{\frac{2b}{h_D^2(1-b)}} \right)}{K_1 \left(\sqrt{\frac{2b}{h_D^2(1-b)}} \right)} \quad (4.3)$$

$$\text{where, } h_D = \frac{h_w}{r_w} \sqrt{\frac{\kappa}{k_v}} \quad (4.4)$$

Equation (4.3) estimates the pseudoskin factor for a single-layer, anisotropic reservoir with closed top and bottom boundaries. Equation (4.3) is also applicable for homogeneous reservoirs with an appropriate change (that is, $\kappa = k_v$) in the definition of h_D .

4.3 Pseudoskin Factor Expression for a Gas-Cap or a Bottom-Water Drive

Figure 4.2 schematically shows a two-layer, partially-penetrated reservoir subject to a gas cap drive. The gas cap is considered to be very large compared to the size of the reservoir and the boundary between the reservoir and the gas cap is considered as a constant pressure boundary. An infinitely-large bottom-water zone can be treated in a similar fashion. A finite gas-cap or bottom-water zone can be modelled as a layer of finite thickness with

appropriate properties, and a partially penetrating well in such a reservoir can be treated in the same way as in the previous section. Layer 1 is penetrated and Layer 2 is closed at the wellbore. The upper boundary of Layer 2 is considered as a constant-pressure boundary because of the gas cap, whereas the lower boundary of Layer 1 is considered as a closed boundary. Pseudosteady-state crossflow is considered between the two layers. Appendix D shows a detailed derivation of the pressure transient solution and late-time limiting solution. From the late-time limiting solution, the pseudoskin expression can be obtained as:

$$s_b = \frac{a_{2L}K_0(\sigma_{2L})}{(a_{2L}-a_{1L})\kappa\sigma_{2L}K_1(\sigma_{2L})} + \frac{a_{1L}K_0(\sigma_{1L})}{(a_{2L}-a_{1L})\kappa\sigma_{1L}K_1(\sigma_{1L})} + \frac{(a_{2L}-a_{1L})K_0(\sigma_{1L})K_0(\sigma_{2L})}{b_L} \quad (4.5)$$

where s_b denotes the pseudoskin factor, and σ_{1L} , σ_{2L} , a_{1L} , a_{2L} , and b_L are late-time limiting values defined by Equations (D.22) through (D.26) and (D.30) in Appendix D. The variable, λ_C , in Equations (D.22) through (D.26), is the crossflow parameter between the reservoir and the gas cap and this parameter is required to calculate the late-time limiting values in Equation (4.5). Equation (4.5) estimates the pseudoskin in a two-layer, partially-penetrated reservoir subject to a gas-cap or a bottom-water drive. Equation (4.5) is also applicable for a multi-layer reservoir having any arbitrary number of layers representing the open interval and any arbitrary location of the open interval, provided κ and λ_A are calculated by adding the individual layer mobility-thickness ratio of the open interval, and by adding the top and bottom boundary crossflow parameters of the open interval, respectively. Irrespective of the number of layers in the reservoir, only three parameters (that is, $\bar{\kappa}$, $\bar{\lambda}_A$ and λ_C) are required to estimate the pseudoskin. An effort was made to simplify Equation (4.5) for a single-layer reservoir without much success.

4.4 Accuracy of Pseudoskin Factor Expressions

For multilayered reservoirs, Table 4.2 compares the estimated pseudoskins using the simplified expressions of Equations (4.2) and (4.5) with those calculated using the actual

analytical solutions. Layered reservoirs with different numbers of layers are considered. Various cases of reservoir configuration in Table 4.1 are considered in Table 4.3. In Table 4.2, for a particular reservoir, s_{bc} denotes the actual 'correct' pseudoskin from the analytical solution of Gomes and Ambastha³ which is the late-time dimensionless pressure difference between the response of the partially penetrating well and that of the fully-penetrating well at a particular time whereas s_{estA} denotes the estimated pseudoskin using the simplified expressions of Equation (4.2) and (4.5). For different values of open interval mobility-thickness ratio ($\bar{\kappa}$) and crossflow parameter ($\bar{\lambda}_A$) and for different open interval locations, pseudoskin factors are estimated for layered reservoirs having a different number of layers. For both the closed top and bottom boundaries and the bottom-water zone, Table 4.2 shows an excellent match between the estimated and the actual pseudoskins for all the different cases considered.

4.5 Comparison with Reference 3

Figure 4.3 compares the pseudoskin factors estimated using Equation (4.3) of this study with those from Figure 2 of the Brons and Marting³ study for a single-layer, homogeneous reservoir. Figure 4.3 shows that, except for small penetration ratios ($b < 0.3$), the pseudoskin factors estimated using Equation (4.3) are very close to those estimated in the Brons and Marting³ study. The difference between the two pseudoskin values increases with a decrease in penetration ratios. Also, pseudoskin factors calculated from Equation (4.3) are consistently higher than those from the Brons and Marting³ study. The reason for the differences in pseudoskin values may be the difference in crossflow modelling in the two studies. For the pseudoskin factor comparison shown in Figure 4.3, Figure 4.4 shows the ratio of the pseudoskin factor obtained from the Brons and Marting³ study to that obtained from this study. When the penetration ratio is not very small ($b > 0.2$), the pseudoskin ratio for a particular h/r_w is approximately constant. Thus, the pseudoskin factor obtained from this study can be corrected to the Brons and Marting³ pseudoskin

value by multiplying by the pseudoskin ratio.

4.6 Comparison with References 12 and 14

Table 4.4 compares the pseudoskin factors estimated from this study with those estimated from the Yeh and Reynolds¹² and Ding and Reynolds¹⁴ studies. Various cases in Table 4.4 refer to different data sets. The cases in Table 4.4 are not related to the cases in Table 4.3. Table 4.4 shows data for a three-layer reservoir with closed top and bottom boundaries and with layer 3 open to flow. These data are taken from the Ding and Reynolds¹⁴ study. In Table 4.4, s_{bYR} and s_{bDR} denote the pseudoskin obtained from the Yeh and Reynolds¹² study and the Ding and Reynolds¹⁴ study, respectively. Table 4.4 shows that the pseudoskins obtained in this study are very close to those of the Ding and Reynolds¹⁴ study, and of the Yeh and Reynolds¹² study. Ding and Reynolds¹⁴ reported a good match between their pseudoskin and that obtained from the numerical simulator. In most cases, pseudoskin factors obtained from the analytical solution as well as from the simplified expression developed in this study are observed to be greater than those obtained from the Ding and Reynolds¹⁴ study, and from the Yeh and Reynolds¹² study. This is probably because of the pseudosteady state crossflow assumption in the development of the analytical model of this study. The significance of this assumption is that the resistance to vertical flow is assumed to be limited in the interlayer area instead of uniformly dispersed in the vertical direction. This pseudosteady state crossflow assumption is more applicable when shale streaks are present in the interlayer areas.

4.7 Development of New Time Criteria and Comparison with Reference 4

Figure 4.5 shows the effect of the crossflow parameter, λ_A , on the pressure derivative responses of a two-layer reservoir with different open interval mobility-thickness ratios, κ . The crossflow parameter (λ_A) has been varied between 0.5×10^{-5} and 0.5×10^{-7} , and the mobility-thickness ratio (κ) has been varied between 0.25 and 0.75. For all values of the

crossflow parameter and mobility-thickness ratio, the early time responses show radial flow behaviour with a constant semi-log slope of $0.5/\kappa$. At very early times, the semi-log slopes are slightly lower than their constant value because of the numerical errors introduced in solving the system of equations. After some time, the responses show a transition from radial flow behaviour, and the time at which the transition occurs is a strong function of the crossflow parameter and the mobility-thickness ratio. At late times, all responses show pseudoradial flow behaviour with a semi-log slope of 0.5. Again, the time to the beginning of the pseudoradial flow is a function of the crossflow parameter and the mobility-thickness ratio. The higher the crossflow parameters are, the sooner the radial flow period ends and the sooner the pseudoradial flow period begins. The lower the mobility-thickness ratio is, the earlier the radial flow period ends and the later the pseudoradial flow period begins. Analysis of the pressure derivative responses shown in Figure 4.5 results in the following criteria for the end of the radial flow period and the beginning of the pseudoradial (second radial) flow-period:

$$t_{D1} = 0.0196 \kappa^2 / \lambda_A \quad (4.6)$$

and

$$t_{D2} = 0.658 / (\lambda_A \sqrt{\kappa}) \quad (4.7)$$

Equations (4.6) and (4.7) describe the times at which the semi-log pressure derivatives are within 5% of the correct slope values. Equations (4.6) and (4.7) have been extended for reservoirs having more than two layers by replacing λ_A and κ by $\bar{\lambda}_A$ and $\bar{\kappa}$, respectively, and have been shown to be applicable for three-layer and five-layer reservoirs. Table 4.5 shows the data used to obtain Equations (4.6) and (4.7). Figures 4.6 and 4.7 show the verification of the accuracy of Equations (4.6) and (4.7), respectively.

Bilhartz and Ramey⁴ used a two-dimensional, finite-difference model to study the pressure

transient responses of a partially-penetrating well with wellbore storage and skin effects. Based on an analysis of the pressure responses, they developed the time criteria for the end of radial flow and the beginning of the pseudoradial flow periods as follow:

$$t_{D1} = 0.02 h_D^2 \quad (4.8)$$

and

$$t_{D2} = h_D^2 \left(\frac{h}{h_w \pi} \right)^2 \left[\ln \left\{ \frac{2}{\pi} \sin \left(\frac{\pi h_w}{h} \right) \cos \left(\frac{\pi h_w}{2h} \right) \cos \left(\frac{3\pi h_w}{4h} \right) \right\} - \ln (0.02) \right] \quad (4.9)$$

where, h_D is defined by Equation (4.4).

For a single-layer reservoir, Equations (4.6) and (4.7) degenerate to the following forms:

$$t_{D1} = 0.0098 h_D^2 \quad (4.10)$$

and

$$t_{D2} = 0.329 \frac{h_D^2}{b^{3/2}} \quad (4.11)$$

The time for the end of the first radial flow period given by Equation (4.10) is about half of that given by Equation (4.8). Thus, the first radial flow period ends earlier as predicted by Equation (4.10) than by Equation (4.8). For a single-layer reservoir, Equation (4.11) estimates the time for the beginning of the second radial flow period, $t_{D2} = 837,500$ with a crossflow parameter $\lambda_A = 1.11 \times 10^{-6}$ and a penetration ratio of 0.5. For the same data, Equation (4.9) estimates $t_{D2} = 196,500$. Analysis with some other values of the crossflow parameter and penetration ratio showed that the time for the beginning of the second radial flow period estimated from Equation (4.11) is approximately 2 to 4 times greater than that estimated from Equation (4.9). Thus, according to the time criteria obtained in this study, the first radial flow period ends earlier and the second radial flow period begins later than

the times predicted by Bilhartz and Ramey's⁴ correlations. Some of the differences in these time criteria may be attributed to different ways of modelling the crossflow in these two studies. However, a smaller t_{D1} and a larger t_{D2} based on pressure derivative responses (Equations (4.10) and (4.11)) than those based on pressure responses (Equations (4.8) and (4.9)) are consistent with the general observations regarding time criteria based on pressure and pressure derivative responses presented by Ambastha²².

Figure 4.8 compares the correlations for the time to the beginning of the second radial flow period from this study (Equation 4.11) and that from the Bilhartz and Ramey⁴ study (Equation 4.9) for a single-layer reservoir. Equation (4.9) is not applicable for all penetration ratios. Equation (4.9) becomes meaningless for $b \geq 2/3$ because $\cos(3\pi h_w/4h)$ becomes zero or negative. However computationally, Equation (4.9) is applicable for $b < 0.64$, because beyond this penetration ratio, t_{D2} becomes negative. To the best of my knowledge, this limitation of Equation (4.9) has not been pointed out in the literature. But Equation (4.11) has been derived for $0.1 \leq b \leq 0.8$ and for h_p between 100 and 10,000. Although there is no mathematical or computational limitation to Equation (4.11), t_{D2} value calculated at $b = 1$ becomes physically meaningless, since there is no pseudoradial flow in this case.

Figure 4.9 compares the pressure transient responses from this study with those from Figure 3 of Bilhartz and Ramey's⁴ study. Figure 4.9 graphs dimensionless wellbore pressure against dimensionless time for penetration ratios of 0.25 and 0.5. Initially, the responses show a straight line corresponding to the first radial flow period with a semi-log slope of $0.5/b$. After the first radial flow period, there is a transition period after which, the responses again show straight lines corresponding to the second radial (pseudoradial) flow period with a slope of 0.5. Since pseudoskin factors obtained from this study are slightly higher than those obtained from Bilhartz and Ramey's⁴ study, pressure responses for the second radial flow period are slightly higher than those of Bilhartz and Ramey⁴. For

penetration ratios of 0.25 and 0.5, pseudoskin factors obtained from this study are 19.6 and 5.98, respectively, whereas those obtained from Bilhartz and Ramey's⁴ study are 17.83 and 5.47, respectively. Thus, the pseudoskin factors obtained from the two studies are very close.

4.8 Effects of Gas-Cap (or Bottom-Water) Drive on Pseudoskin and Comparison with Reference 5

Table 4.6 shows the effects of a gas cap on the pseudoskin factor for a three-layer reservoir with $k_1 = k_2 = k_3 = 4.9346 \times 10^{-14} \text{ m}^2$ and with $h = 200 \text{ m}$. The various cases of reservoir configuration in Table 4.6 are explained in Table 4.3. Cases 1 and 2 show pseudoskins when there is no gas cap and Cases 3 and 4 show pseudoskins when the reservoir is subject to a gas-cap drive. In the absence of the gas cap, the pseudoskin is lower when the open interval is away from the top or the bottom boundary than when the open interval is located adjacent to the top or the bottom boundary. This happens because the crossflow parameter, $\bar{\lambda}_A$, is higher when the open interval is away from the top or bottom boundary. But Case 3 shows that when the gas cap is present, the pseudoskin is smaller when the open interval is adjacent to the constant-pressure boundary than when the open interval is away from the constant-pressure boundary. This happens because, when the open interval is adjacent to the constant-pressure boundary, the wellbore pressure stabilizes faster than when the open interval is away from the constant-pressure boundary. Similar observations were also made by Streltsova-Adams⁵. The above observations are also valid for the corresponding cases when the reservoir is accompanied by a bottom-water zone.

Figure 4.10 compares the pseudoskin factors from this study with those from the Streltsova-Adams⁵ study for a partially-penetrating well in a reservoir subject to a gas-cap drive. The gas-oil contact has been modelled as a constant pressure boundary in both studies. Figure 4.10 compares pseudoskin factors with those from Figure 9 of the

Streltsova-Adams⁵ study. The solid lines in Figure 4.10 show the pseudoskin factors estimated from Equation (4.5) of this study for various penetration ratios and under a gas-cap condition. Streltsova-Adams⁵ estimated the pseudoskin by taking the difference between the late-time pressure responses of a partially-penetrating well and a fully-penetrating well in a particular reservoir. Figure 4.10 shows that the pseudoskin factors estimated in this study differ only slightly from those obtained in the Streltsova-Adams⁵ study, except for small penetration ratios ($b < 0.3$). Pseudoskin factors estimated in this study are slightly higher than those obtained in the Streltsova-Adams⁵ study. This is likely due to the different ways of modelling the crossflow in the two studies. For the pseudoskin factor comparison shown in Figure 4.10, Figure 4.11 shows the ratio of the pseudoskin factor obtained in the Streltsova-Adams⁵ study to that obtained in this study. Although the pseudoskin factors obtained from the two studies are very close, the pseudoskin factor obtained from this study can be corrected to that of Streltsova-Adams⁵ pseudoskin value by multiplying by the pseudoskin ratio.

4.9 Comparison with Reference 10

Figure 4.12 shows a comparison of the pseudoskin factors obtained from Equation (4.1) of this study with those obtained from Figure 8 of Olarewaju and Lee's¹⁰ study. Figure 4.12 graphs the pseudoskin factors against various penetration ratios for a two-layer reservoir with layer two open to flow and layer one closed. Note that because of the reverse order of the numbering of the layers, k_2/k_1 of this study is equal to k_1/k_2 in Olarewaju and Lee's¹⁰ study. Figure 4.12 shows that the pseudoskin factors obtained from this study are significantly higher (more than double when $k_2/k_1 = 1$) than those obtained from Olarewaju and Lee's¹⁰ study. The reason for this may be the assumption that Olarewaju and Lee¹⁰ made in developing their model. They assumed that there is no radial flow component in the closed layer (that is, layer one). Because of this restriction, fluid particles travel shorter distances and only vertically to move from the closed layer to the open layer (layer two). If

there were a radial flow component in the closed layer, fluid particles would have travelled longer distances to move from the closed layer to the open layer and this would have caused higher pressure drops; that is, higher pseudoskin factors. Thus, neglecting the radial flow component in the closed layer may not be a satisfactory assumption while studying pressure-transient responses for partially-penetrating wells.

4.10 Effect of Layer Refinement on Pseudoskin Factor

Table 4.7 shows the effects of layer refinement on the pseudoskin factor. For a particular reservoir thickness and open interval, the reservoir is divided into a number of mathematical layers to study the effect of layer refinement on the pseudoskin factor. In Table 4.7, Cases 1 through 3 represent a reservoir height of 30 m with an open interval thickness of 10 m, and Cases 4 through 6 represent a reservoir thickness of 100 m with an open interval thickness of 20 m, respectively. For both reservoir thicknesses of 30 m and 100 m, the open interval is considered as a single layer, and the closed interval of the reservoir is divided into 1, 2 and 4 layers. The results in Table 4.7 show a small decrease in the pseudoskin factor as the number of mathematical layers increases and this decrease in pseudoskin factor is greater when the reservoir thickness is larger. But the value of the pseudoskin factor stabilizes as the number of mathematical layers is further increased. This layer refinement effect occurs because of the pseudosteady-state crossflow assumption. The layer refinement effect has also been observed by Larsen²³.

4.11 Conclusions

1. Pressure transient responses and pseudoskin factors for a partially-penetrated, multi-layer reservoir can be studied analytically by a pseudosteady-state crossflow model.
2. Simplified expressions for the pseudoskin factor have been derived for a partially-penetrated, multi-layer reservoir with or without a bottom-water or a gas-cap drive and

the pseudoskin factors can be estimated from these expressions with reasonable accuracy.

3. Times for the end of the radial flow period and the beginning of the pseudoradial flow period depend on the crossflow parameter and the mobility-thickness ratio of the open interval. Simplified expressions have been derived for these time criteria.
4. Pseudoskin factors obtained from this study have been compared with those obtained from other studies in the literature and these comparisons have shown good matches with all but one of the studies.

References

1. Muskat, M.: *Physical Principles of Oil Production*, McGraw-Hill Book Co. Inc., New York City (1949) 259-70.
2. Nisle, R. G.: "The Effect of Partial Penetration on Pressure Build-Up in Oil Wells," *Trans.*, AIME (1958), Vol. 213, 85-90.
3. Brons, F. and Marting, V. E.: "The Effect of Restricted Flow Entry on Well Productivity," *JPT* (Feb. 1961) 172-74.
4. Bilhartz, H. L. and Ramey, H. J., Jr.: "The Combined Effect of Storage, Skin, and Partial Penetration on Well Test Analysis," paper SPE 6753 presented at the 1977 Annual Meeting, Denver, Colorado, Oct. 9-12.
5. Streltsova-Adams, T. D.: "Pressure Drawdown in a Well with Limited Flow Entry," *JPT* (Nov. 1978) 1469-76.
6. Saidikowski, R.M.: "Numerical Simulations of the Combined Effects of Wellbore Damage and Partial Penetration," paper SPE 8204 presented at the 1979 Annual Meeting, Las Vegas, Nevada, Sept. 23-26.
7. Buhidma, I. M. and Raghavan, R.: "Transient Pressure Behavior of Partially Penetrating Wells Subject to Bottomwater Drive," *JPT* (July 1980) 1251-61.

8. Reynolds, A. C., Chen, J. C. and Raghavan, R.: "Pseudoskin Factor Caused by Partial Penetration," *JPT* (Dec. 1984) 2197-2210.
9. Papatzacos, P.: "Approximate Partial-Penetration Pseudoskin for Infinite-Conductivity Wells," *SPEE* (May 1987) 227-34.
10. Olufuwaju, J.S. and Lee, W.J.: "Pressure Buildup Behavior of Partially Completed Wells in Layered Reservoirs," paper SPE 18876 presented at the 1989 Production Operations Symposium, Oklahoma, March 13-14.
11. Yeh, N.S. and Reynolds, A. C.: "Analysis of Pressure Data From a Restricted-Entry Well in a Multilayer Reservoir," *SPEFE* (March 1989) 81-89.
12. Yeh, N.S. and Reynolds, A. C.: "Computation of Pseudoskin Factor Caused by a Restricted-Entry Well Completed in a Multilayer Reservoir," *SPEFE* (June 1989) 253-63.
13. Vrbik, J.: "A Simple Approximation to the Pseudoskin Factor Resulting from Restricted Entry," *SPEFE* (Dec. 1991) 444-46.
14. Ding, W. and Reynolds, A. C.: "Computation of the Pseudoskin Factor for a Restricted-Entry Well," paper SPE 21705 presented at the 1991 Production Operation Symposium, Oklahoma, April 7-9.
15. Shah, P. C. and Thambynayagam, R. K. M.: "Transient Pressure Response of a Well with Partial Completion in a Two-Layer Crossflowing Reservoir," paper SPE 24681 presented at the 1992 Annual Meeting, Washington, DC, Oct. 4-7.
16. Odeh, A. S.: "Steady-State Flow Capacity of Wells with Limited Entry to Flow," *SPEJ* (March 1968) 43-51.
17. Seth, M. S.: "Unsteady-State Pressure Distribution in a Finite Reservoir with Partial Well-Bore Opening," *JCPT* (Oct. 1968) 153-63.
18. Kazemi, H. and Seth, M. S.: "Effect of Anisotropy and Stratification on Pressure Transient Analysis of Wells with Restricted Flow Entry," *JPT* (May 1969) 639-47.
19. Grigariuc, A. C. and Ramey, H. J., Jr.: "An Approximate Infinite Conductivity Solution for a Partially Penetrating Line-Source Well," *SPEJ* (April 1975) 140-48.

20. Vrbik, J.: "Calculating the Pseudo-skin Factor due to Partial Well Completion," *JCPT* (Sept.-Oct. 1986) 57-61.
21. Gomes, E. and Ambastha, A.K.: "An Analytical Pressure-Transient Model for Multilayered, Composite Reservoirs with Pseudosteady-State Formation Crossflow," paper SPE 26049 presented at the 1993 Western Regional Meeting, Alaska, May 26-28; also accepted for publication in the *AOSTRA Journal of Research* (Nov. 13, 1992).
22. Ambastha, A.K.: "Pressure Transient Analysis in Composite Systems," Ph.D. Thesis, Stanford University (Oct. 1988) 193 pp.
23. Larsen, L.: "Boundary Effects in Pressure-Transient Data From Layered Reservoirs," paper SPE 19797 presented at the 1989 Annual Meeting, San Antonio, TX, Oct. 8-11.
24. Bourdet, D.: "Pressure Behavior of Layered Reservoirs With Crossflow," paper SPE 13628 presented at the 1985 Regional Meeting, California, March 27-29.
25. Stehfest, H.: "Algorithm 368, Numerical Inversion of Laplace Transformations, D-5," *Comm. of ACM*, 13, No.1 (Jan. 1970) 47-49.

Table 4.1: Summary of Studies on Partially-Penetrating Wells.

Year	Author(s)	Ref. no.	Solution Method(s)							Number of Layers	Gas Cap or Botm-Water(b)			Pseudoskin Estimation(c)			
			I	F	L	H	G	S	N		C	B	G	O	R	E	A
1949	Muskat	1	*							1	*			*			
1958	Nisio	2	*							1	*			*			
1961	Brons and Marting	3	*							1	*					*	
1968	Odeh	16		*						1	*			*			
1968	Seth	17		*	*					1	*			*			
1969	Kazemi and Seth	18						*		1	*			*			
1975	Gringarten and Ramey	19					*			1	*			*			
1977	Bilharz and Ramey	4						*		1	*			*			
1978	Strekoova-Adams	5				*				1	*		*	*			*
1979	Saidikowski	6						*		1	*				*	*	*
1980	Buhidma and Raghavan	7				*				1		*		*			
1984	Reynolds et. al.	8						*		2	*				*		
1986	Vrbik	20						*		1	*						*
1987	Papatzacos	9	*							1	*						*
1989	Olarowaju and Lee	10			*					2	*				*		
1989	Yeh and Reynolds	11						*		n	*			*			
1989	Yeh and Reynolds	12						*		n	*			*			
1991	Vrbik	13						*		1	*						*
1991	Ding and Reynolds	14	*							n	*						*
1992	Shah and Thambynayagam	15			*	*				2	*	*		*			
1993	This study				*					n	*	*	*				*

a.
 I=Method of images
 F=Fourier transform
 L=Laplace transform
 H=Hankel transform
 G=Green's function
 S=Separation of variables
 N=Numerical method

b.
 C=Gas cap
 G=Gas cap
 B=Bottom-water

c.
 O=Graphical
 R=Regression
 E=Empirical
 A=Analytical

Table 4.2: Comparison of pseudoskin factors estimated from the simplified expression with those from the actual analytical solution.

Reservoir Configuration Case (see Table 4.3)	$\bar{\kappa}$	$\bar{\lambda}_A \times 10^7$	Closed top and bottom boundaries		$\bar{\lambda}_C \times 10^7$	Bottom-Water	
			s_{DA}	s_C		s_{DA}	s_C
1	0.601	4.80	5.196	5.197	5.97	5.628	5.628
1	0.702	4.18	3.321	3.323	5.97	3.680	3.679
2	0.429	0.375	10.577	10.650	4.74	10.977	11.150
3	0.333	6.525	15.273	15.280	4.74	15.555	15.470
4	0.763	0.277	2.476	2.492	4.74	2.830	2.860
5	0.640	0.648	4.310	4.380	0.222	4.490	4.620
6	0.480	1.292	7.966	7.980	0.222	8.086	8.110

Table 4.3: Reservoir configurations considered in Tables 4.2 and 4.6.

Case	No. of layers	Penetrated layer
1	2	2
2	3	3
3	3	2
4	3	2 & 3
5	5	4 & 5
6	5	3 & 4

Table 4.4: Comparison of pseudoskin factors estimated from this study with those estimated from other studies for a three-layer reservoir with closed top and bottom boundaries and with layer 3 open to flow ($h = 200$ m and $k_1 = 4.9346 \times 10^{-14}$ m²)

Case	1	2	3	4	5
h_1/h	0.50	0.10	0.10	0.49	0.10
h_2/h	0.40	0.10	0.10	0.02	0.60
k_1/k_2	100	0.25	0.25	0.41	0.857
k_1/k_3	0.10	1.60	1.60	0.26	1.5
k_1/k_{s1}	10.0	1.0	1.0	1.04	4.0
k_2/k_{s2}	1.0	0.16	0.16	625.0	0.544
k_3/k_{s3}	100.0	0.39	39.06	1.58	177.78
h_1/r_w	400.0	50.0	50.0	50.0	50.0
η_C	16.31	33.89	36.03	20.28	41.50
η_{GA}	15.68	32.90	32.90	19.15	40.30
η_{YR}	13.38	26.36	26.36	20.03	34.44
η_{DR}	13.47	26.33	26.33	20.03	34.41

Table 4.5: Data for the development of Equations (4.6) and (4.7)

l_{D1}	κ^2 / λ_A	l_{D2}	$1/(\kappa^{1/2} \lambda_A)$
325	12500	1.500×10^5	2.309×10^5
900	50000	1.800×10^5	2.828×10^5
1500	1.125×10^5	2.200×10^5	4.000×10^5
2500	1.250×10^5	1.500×10^6	2.309×10^6
12000	5.000×10^5	1.950×10^6	2.828×10^6
21000	1.125×10^6	2.800×10^6	4.000×10^6
25000	1.250×10^6	1.500×10^7	2.309×10^7
100000	5.000×10^6	1.850×10^7	2.828×10^7
220000	1.125×10^7	2.650×10^7	4.000×10^7

Table 4.6: Effect of gas cap (bottom-water) on pseudoskin factor (three-layer reservoir, $h = 270$ m, $k_1 = k_2 = k_3 = 4.9346 \times 10^{-14}$ m²)

Case	Reservoir Configuration Case (see Table 4.3)	$\bar{\kappa}$	$\bar{\lambda}_A \times 10^7$	Presence of gas cap	$\bar{\lambda}_C \times 10^7$	Pseudoskin, s_p
1	2	0.333	0.47	No	-	15.26
2	3	0.333	1.50	No	-	14.44
3	2	0.333	0.47	Yes	1.50	13.51
4	3	0.333	1.50	Yes	1.50	14.66

Table 4.7: Effect of layer refinement on pseudoskin factor ($k = 2.9477 \times 10^{-14} \text{ m}^2$, $k_v = 2.9477 \times 10^{-15} \text{ m}^2$)

Case	Total reservoir thickness, m	Open interval thickness, m	Number of Layers	Pseudoskin Factor, s_p
1	30	10	2	11.74
2	30	10	3	11.47
3	30	10	5	11.39
4	100	20	2	27.65
5	100	20	3	26.89
6	100	20	5	26.55

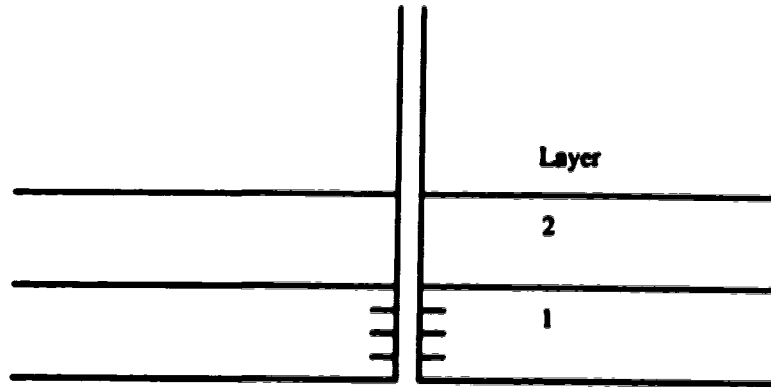


Figure 4.1: Schematic of a two-layer, partially-penetrated reservoir with closed top and bottom boundaries.

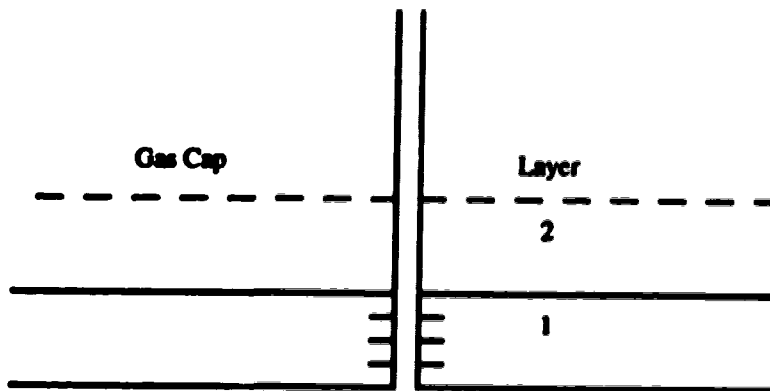


Figure 4.2: Schematic of a two-layer, partially-penetrated reservoir with a gas cap.

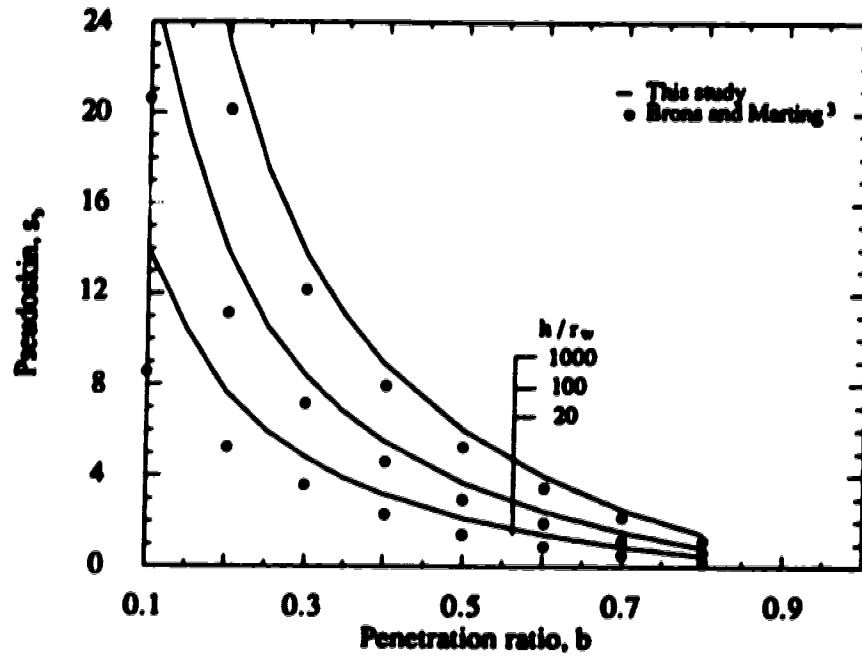


Figure 4.3: Comparison of pseudoskin factor from this study with that from Brons and Marting.³

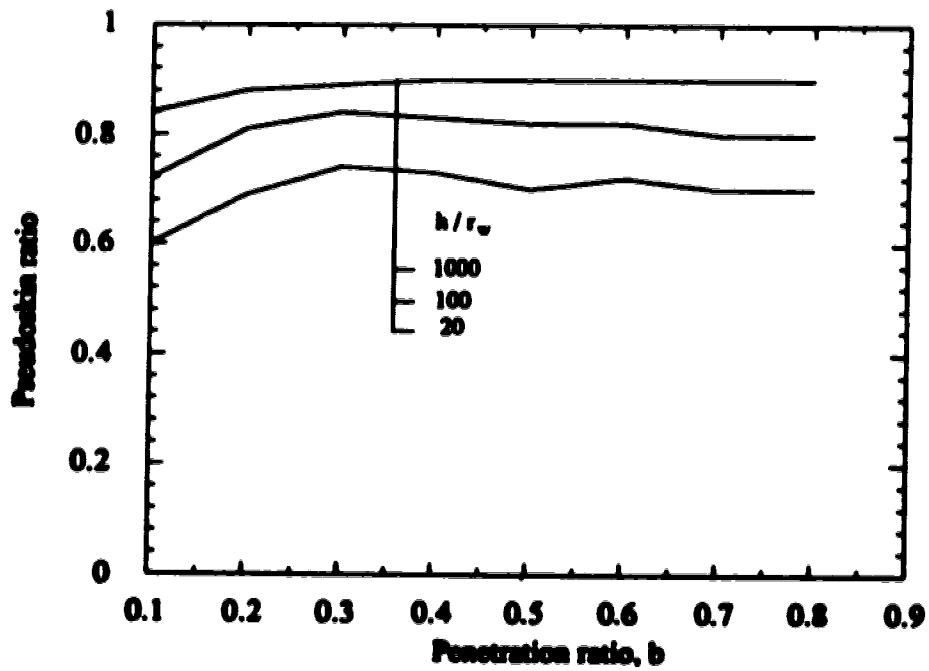


Figure 4.4: Ratio of pseudoskin factor from the Brons and Marting³ study to that of this study.

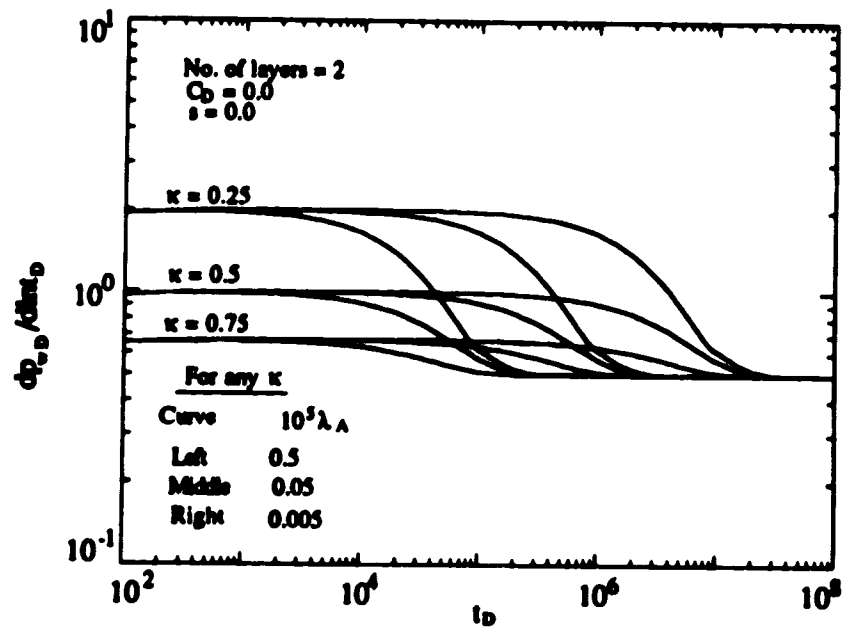


Figure 4.5: Effect of the crossflow parameter and the mobility-thickness ratio on pressure derivative responses.

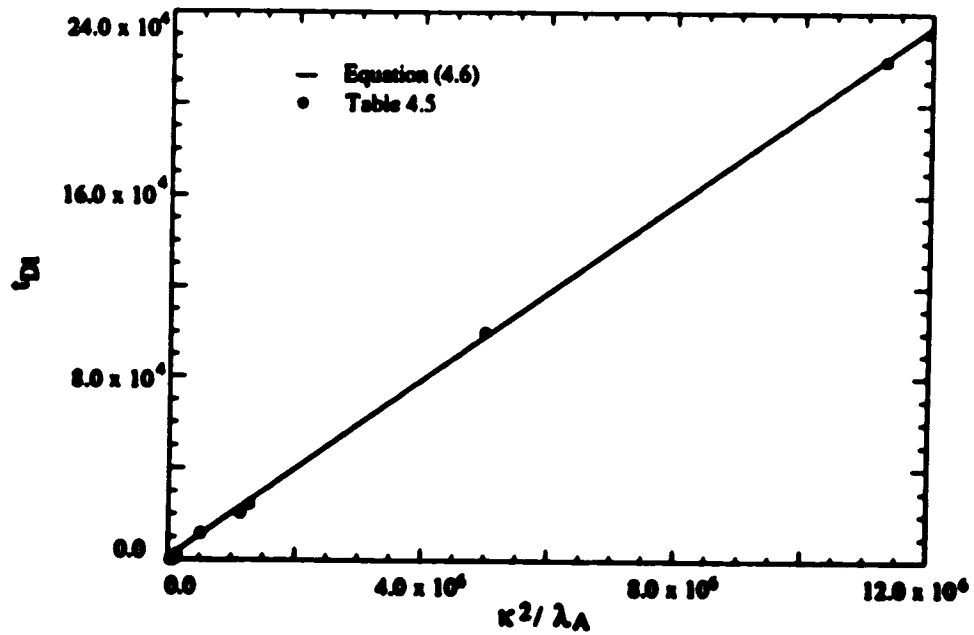


Figure 4.6: Verification of the accuracy of Equation (4.6).

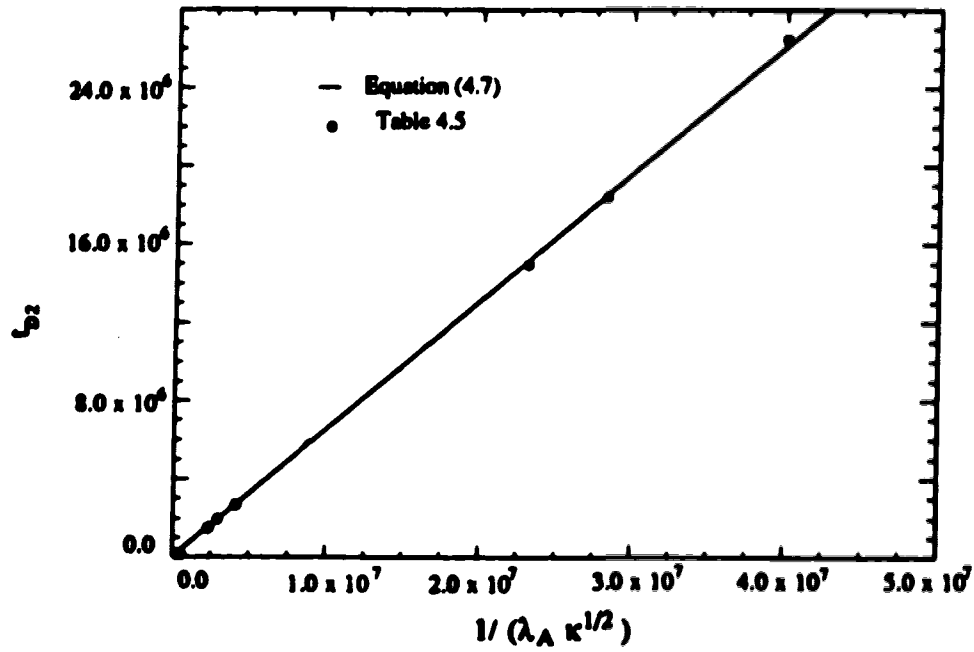


Figure 4.7: Verification of the accuracy of Equation (4.7)

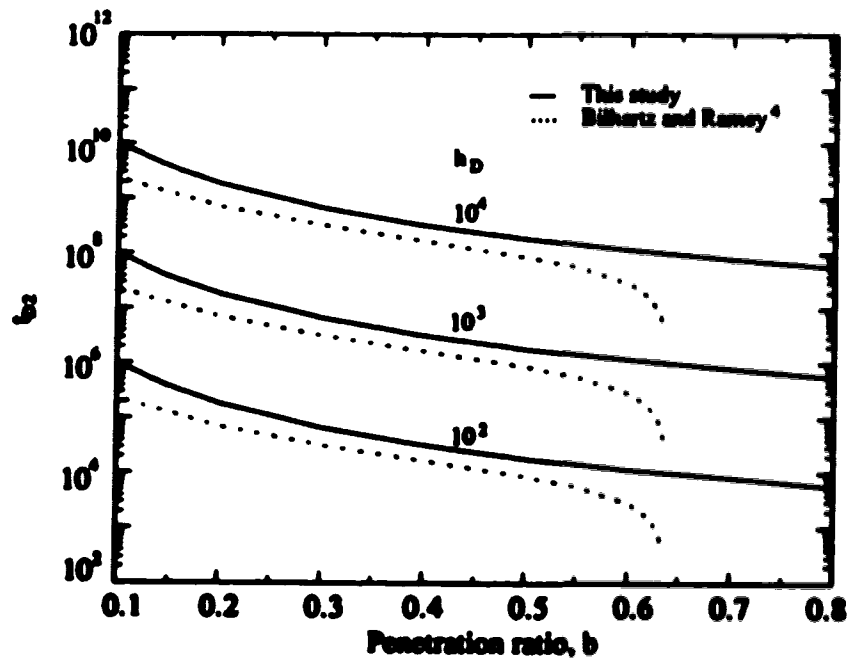


Figure 4.8: Comparisons of the correlation for the time to the beginning of the second radial flow from this study with those from Reference 4.

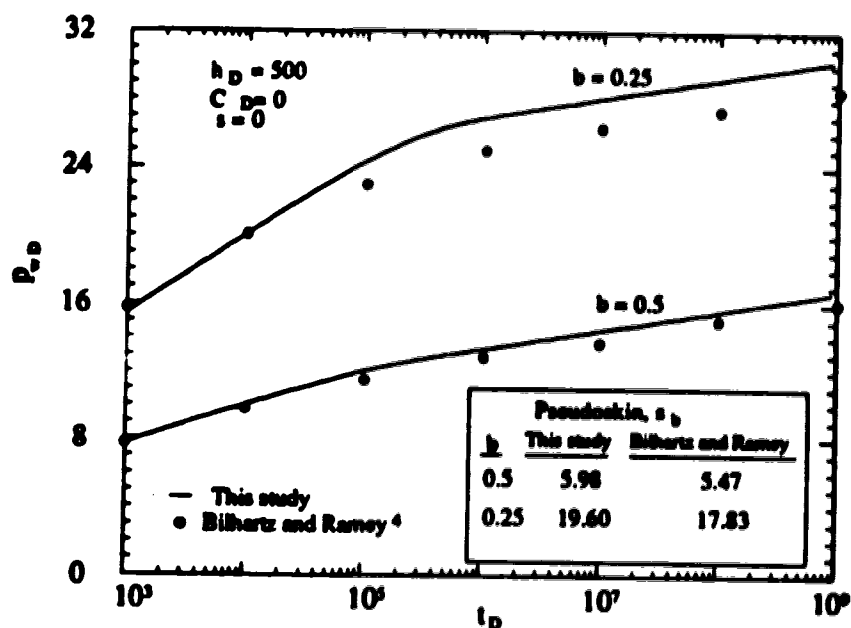


Figure 4.9: Comparison of pseudoskin and dimensionless pressure from this study with those from the Bilhartz and Ramey⁴ study.

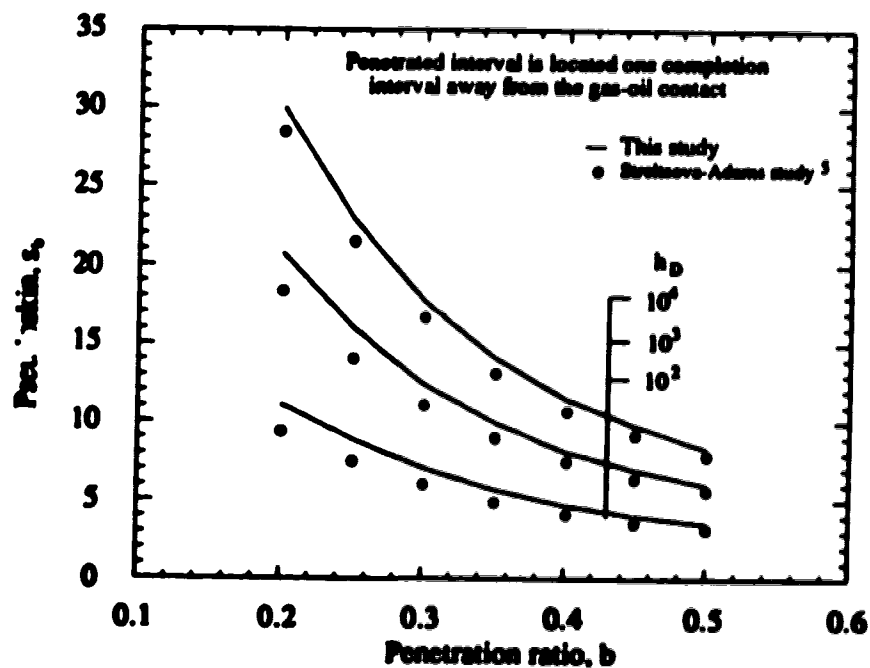


Figure 4.10: Comparison of the pseudoskin factor from this study with that from the Strekova-Adams⁵ study for a reservoir with a gas cap.

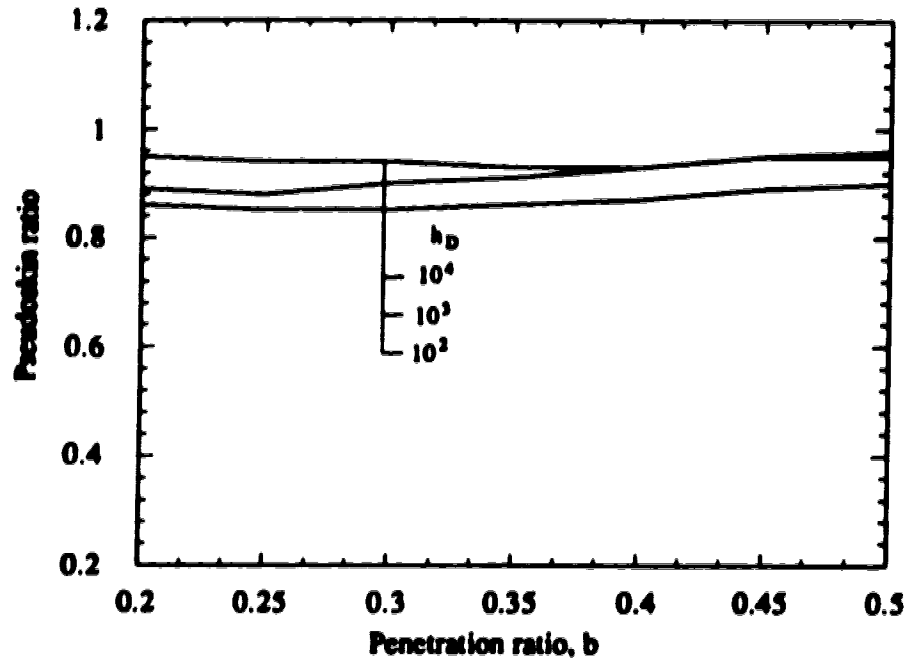


Figure 4.11: Ratio of the pseudoskin factor from the Streletsova-Adams⁷ study to that of this study.

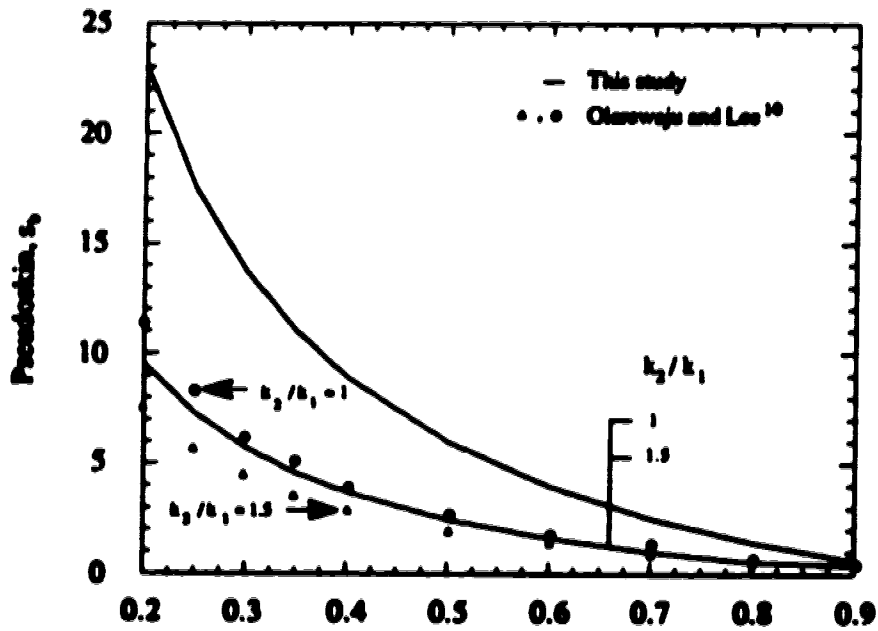


Figure 4.12: Comparison of the pseudoskin factor from this study with that from the Olarowaju and Lee¹⁰ study.

5.0 THERMAL WELL TEST ANALYSIS UNDER BOTTOM-WATER CONDITIONS

5.1 Introduction

The steam injection process is widely used in heavy oil recovery operations. As a result of steam injection, at least two regions of different fluid properties are created and the reservoir resembles a composite reservoir. Because of the gravity override effect, an inclined fluid front is created between the hot and the cold zones. In many cases, heavy oil reservoirs are accompanied by a bottom-water zone. The purpose of this study is to investigate the transient pressure behaviour of a steam-stimulated heavy oil reservoir under bottom-water conditions.

A reservoir undergoing a thermal recovery process has been idealized as a composite reservoir for a long time¹⁻⁴. But most of the studies consider piston-like movement of the fluid front, neglecting the gravity-override effect. Satman⁷ used the concept of a tilted (inclined) front in the pressure transient analysis of a two-layer composite reservoir. He suggested that the fluid front would propagate at different rates in different layers. For steam flooding, Satman and Oskay⁸ considered the discontinuity boundary as a tilted front to account for the gravity override effect and modelled the reservoir as a multi-layer composite reservoir without crossflow. They concluded that the tilted-front model is a better representation of the actual reservoir.

According to published reports on steam-drive projects^{9,10}, the gravity override effect is a common phenomenon which results in a tilted front between the swept and the unswept zones. If the gravity override effect is not taken into consideration, the predicted performance of the steam flooding project may be quite different than the actual one. Singhal¹¹ conducted some scaled physical model studies of a steam-flood in a reservoir

containing heavy oil. He presented some temperature profiles obtained from his model which showed a very strong gravity override effect. Blevins et al.⁹ discussed the application of steam-flooding for light oil reservoirs. They mentioned that the gravity override effect also exists for light oil reservoirs, although it is less prominent than that for heavy oil reservoirs.

Recently, Nasr and Pierce¹² studied steamflooding in a scaled, oil-sand reservoir through a bottom-water zone. They presented some temperature profiles with time and observed steam underrunning in the bottom-water zone and the gravity override effect in the oil-sand zone.

Many times, heavy oil reservoirs are accompanied by a bottom-water zone. In such a situation, both the stimulation well (with good injectivity) and the producing well are partially perforated to avoid injecting the steam into the bottom-water region and to avoid a water-coning problem, respectively. For a partially-penetrating well, transient pressure responses show additional pressure drop around the wellbore because of flow convergence. This additional pressure drop is referred to as a "pseudoskin" in the literature. Streletsova-Adams¹³ investigated the pseudoskin under bottom-water or gas cap conditions, in which she graphically presented the pseudoskin factor. Gomes and Ambastha¹⁴ presented simplified expressions for pseudoskin factors both for closed top and bottom boundaries and for a bottom-water condition. They also presented an extensive literature review on partially penetrating wells.

The objective of this study is to investigate the transient pressure responses for a heavy oil reservoir undergoing steam flooding under bottom-water conditions. Both finite and infinite bottom-water zones have been considered. A new analytical solution developed by Gomes and Ambastha¹⁵ for multi-layer composite reservoirs has been used to generate the responses.

5.2 Modelling of Infinite and Finite Bottom-Water Zones

Figures 5.1 and 5.2 show two different bottom-water situations, where a heavy-oil reservoir has undergone a steam-flooding process. Though there is no limitation to the number of layers that can be used in the analytical model, this study uses two layers to represent the reservoir and one layer to represent the finite bottom-water zone (for the finite bottom-water case) unless mentioned otherwise. Wellbore storage and skin are neglected in this study. In Figure 5.1, the bottom-water zone is very large compared to the size of the reservoir. Thus, the boundary between the the bottom-water zone and the reservoir has been approximated as a constant-pressure boundary. Because of the bottom-water zone, the well has been partially penetrated to avoid or delay the water coning problem. In Figure 5.1, Zones 1 and 3 represent the swept zone, and Zones 2 and 4 represent the unswept zone. Because of the gravity override effect, Zone 3 extends a longer distance than does Zone 1. Thus, the swept front has propagated further in Zone 3 than in Zone 1. Although Zone 1 is considered as a part of the swept zone, it may have different fluid properties than Zone 3. In Figure 5.1, a discontinuity boundary between Zones 1 and 2 is denoted as R_1 . The discontinuity boundary between Zones 3 and 4 is denoted as R_2 . In dimensionless form, R_1 and R_2 , have been represented by R_{D1} and R_{D2} , respectively. In reality, a bottom-water zone may not be very large for all reservoirs. Figure 5.2 shows a heavy-oil reservoir with a finite bottom-water zone. As in Figure 5.1, Zones 1 and 3 represent the swept zone and Zones 2 and 4 represent the unswept zone. Because of the gravity override effect, the swept fronts have been located at different positions in Zones 1 and 2. In Figure 5.2, R_{D1} and R_{D2} represent the dimensionless discontinuity boundary radii between Zones 1 and 2 and between Zones 3 and 4, respectively.

5.3 Infinitely Large Bottom-Water Zone and No Bottom-Water Zone Cases

The reservoir configuration considered in this section is shown schematically in Figure 5.1. Since the aquifer is very large, the water-oil contact has been represented as a constant-pressure boundary. R_{D1} and R_{D2} are the dimensionless discontinuity boundary radii between Zones 1 and 2, and between Zones 3 and 4, respectively. For an infinite bottom-water condition, λ_A represents the crossflow parameter between layers 1 and 2 and λ_C represents the crossflow between Layer 1 and the bottom-water layer. Figure 5.3 shows the effect of mobility-thickness ratio on wellbore pressure. The mobility-thickness ratio has been defined as:

$$\kappa = \frac{\left(\frac{kh}{\mu}\right)_{\text{penetrated}}}{\left(\frac{kh}{\mu}\right)_{\text{total}}} \quad (5.1)$$

In defining the mobility-thickness ratio, reservoir and fluid properties of the swept zone (Zones 1 and 3) have been used. For example, for the case depicted by Figure 5.1, $(kh/\mu)_{\text{penetrated}} = (kh/\mu)_{\text{Zone 1}}$ and $(kh/\mu)_{\text{total}} = (kh/\mu)_{\text{Zone 1}} + (kh/\mu)_{\text{Zone 3}}$. In a limiting case, where the penetrated and the non-penetrated sections in the swept zone have the same reservoir and fluid properties, the mobility-thickness ratio becomes the penetration ratio. The mobility-thickness ratio has been varied by changing the thickness of Layer 1 for a fixed thickness of Layer 2. Changing the mobility-thickness ratio in this way also changes the crossflow parameter because the thickness of Layer 1 appears in the definitions of both λ_A and λ_C . Figure 5.3 shows that, initially, the responses show the radial flow period corresponding to the swept zone mobility of the penetrated interval of the reservoir. After some time, the well feels the presence of the bottom-water zone and the wellbore responses show constant pressure values. The smaller the mobility-thickness ratio is, the longer it takes for the wellbore pressure to attain the constant value. This late-time constant p_{∞}

value includes the additional pressure drop that occurs at the wellbore because of the partial penetration. This additional pressure drop is known as the "pseudoskin factor". The pseudoskin factor depends on the mobility-thickness ratio. A mathematical expression for this "pseudoskin" has been presented in Reference 14.

Figures 5.4 through 5.6 show the effect of mobility-thickness ratio on the semi-log pressure derivative responses. Figures 5.4, 5.5 and 5.6 show responses for mobility ratios of 10, 100, and 1000, respectively. For all these figures, the properties of Zones 1 and 3 are assumed to be the same, and R_{D1} and R_{D2} are assumed to be 500 and 600, respectively. Initially, semi-log pressure derivatives are constant, which corresponds to the first radial-flow period. The relationship between the dimensionless semi-log slope for the first radial flow period (m) and the mobility-thickness ratio (κ) is :

$$m = \frac{0.5}{\kappa} \quad (5.2)$$

In Equation 5.2, the constant 0.5 is the dimensionless semi-log slope for a fully-penetrating well. For a homogeneous reservoir, the mobility-thickness ratio becomes the penetration ratio. In Figures 5.4 through 5.6, the initial constant values of the semi-log slopes decrease because of the influence of the bottom-water zone. When the transient effects reach the front boundary, the semi-log slopes increase because of the mobility difference between the swept and the unswept regions. The effect of the discontinuity boundary and, therefore, mobility ratio is more pronounced when the mobility-thickness ratio is less than 0.5. However, the effects of the constant-pressure bottom boundary ultimately cause the semi-log pressure derivative to sharply decline toward zero, which is equivalent to attainment of a constant p_{wD} value at late time.

To understand how the responses for an infinite bottom-water zone differ from those for a no bottom-water zone situation, Figure 5.7 shows the effect of the mobility-thickness ratio on semi-log pressure derivative responses when there is no bottom-water zone. In this

case, both the bottom and the top boundaries are closed and the responses graphed are for $M = 10$. Initially, the responses show the first radial flow period with a semi-log slope $= 0.5/\kappa$. Then there is a transition flow period. During the transition period, the effect of the bottom-water zone would have been felt, if a bottom-water zone had been present. Then all the responses show the second radial-flow (pseudoradial-flow) period corresponding to the unswept region with a dimensionless semi-log slope $m = 0.5M$. A comparison of Figure 5.7 with Figures 5.4 through 5.6 shows that the transition flow period does not develop completely in the presence of the bottom-water zone. This is especially true for higher mobility-thickness ratio cases ($\kappa > 0.5$). For a mobility-thickness ratio of 0.5 or smaller, the transition flow period develops to a certain extent and, thus, pseudosteady-state analysis may be possible. As expected, the second radial flow period does not occur in the presence of a bottom-water zone.

Figures 5.8 through 5.10 show the effect of mobility-thickness ratio on Cartesian pressure derivatives. Figures 5.8, 5.9, and 5.10 are for mobility ratios of 10, 100, and 1000, respectively. For these figures, dimensionless time is based on the discontinuity boundary distance between Zones 3 and 4 (R_{D2}). In Figure 5.8 ($M=10$), the transition flow period is of very short duration and, thus, a pseudosteady-state flow period with a constant Cartesian derivative value has not developed at all. Theoretically, the dimensionless slope of the Cartesian graph, m_c , should be equal to $2/\kappa$, where 2 is the dimensionless Cartesian slope for a fully-penetrating well with a sharp front. The preceding statement is true when the swept front is vertical (sharp), and when the top and the bottom boundaries of the reservoir are closed. But in Figures 5.8 through 5.10, both Zones 1 and 3 represent the swept zone, and the front is a tilted front (see Figure 5.1) and the reservoir is under an infinitely-large bottom-water condition. An in-depth investigation of pseudosteady-state behaviour for a tilted front has been presented in Reference 16. In Figures 5.9 and 5.10, Cartesian slopes for the pseudosteady-state flow period tend to flatten at a value smaller

than the value of $2/\kappa$ discussed before, because of the effects of the bottom-water zone and the tilted-front.

To understand the differences between the Cartesian derivative responses for an infinite bottom-water zone and no bottom-water zone, Figure 5.11 shows the effect of the mobility-thickness ratio on the Cartesian pressure derivative for a reservoir with no bottom-water zone. Here, after the first radial flow period (initial -1 slope line), the transition flow period is more developed in comparison to the responses shown on Figure 5.8, and after the transition flow period, all responses merge to another -1 slope line corresponding to the second radial (pseudoradial) flow period.

In the preceding discussion, the mobility-thickness ratio has been varied by changing the thickness of Layer 1 for a fixed thickness of Layer 2. Changing the mobility-thickness ratio in this way also changes the crossflow parameters since the thickness of Layer 1 appears in the definitions of the crossflow parameters. By changing the horizontal permeability of the penetrated layer (that is, Layer 2 in Figure 5.1), the mobility-thickness ratio of the penetrated interval can be varied without changing the crossflow parameters. However, the vertical permeability of the penetrated layer has not been changed while changing the horizontal permeability, since it will affect the crossflow parameter. Figure 5.12 shows the effect of the mobility-thickness ratio on semi-log pressure derivative responses, when the mobility-thickness ratio has been varied by changing the horizontal permeability of the penetrated layer (Layer 2). Thus, in Figure 5.12, the mobility-thickness ratio has been varied independently, without varying the crossflow parameters. A comparison of Figure 5.12 with Figure 5.5 shows that the pressure derivative responses are different when the mobility-thickness ratio is varied independently without affecting the crossflow parameters. For small mobility-thickness ratios ($\kappa < 0.6$), Figure 5.12 shows that the wellbore responses are dominated by the bottom-water zone before the front boundary is felt. This happens because small mobility-thickness ratios in Figure 5.12 have been obtained by

assigning a small horizontal permeability to Layer 2. Thus, the pressure transient can move more easily (because of less resistance) in the vertical direction than in the horizontal direction for small mobility-thickness ratios. However, when a small mobility-thickness ratio is obtained because of a small penetrated thickness (as in the case of Figures 5.5 and 5.6), the responses reach the front boundary before the wellbore responses are dominated by the bottom-water zone.

Figure 5.13 shows the effect of storativity ratio on the semi-log pressure derivative responses. Figure 5.13 is for a mobility ratio $M = 100$, and a mobility-thickness ratio $\kappa = .5$. The storativity ratio influences the responses during the intermediate time period after the end of the first radial flow period. But for the reservoir parameters utilized in Figure 5.13, increasing the storativity ratio above 10 does not affect the wellbore responses due to the presence of a bottom-water zone .

Figure 5.14 shows the effect of the dimensionless discontinuity radius in Layer 1 (R_{D1}) on the semi-log pressure derivative responses. Responses in Figure 5.14 have been generated for $M = 100$, $F_1 = 100$, and $\kappa = 0.5$. The discontinuity radius, R_{D1} , has been varied as 300, 500 and 1000. When $R_{D1} = 300$, the responses reach the fluid front before the bottom-water zone dominates the wellbore pressure. But when $R_{D1} = 1000$, the wellbore responses do not feel the fluid front, because the wellbore response is dominated by the bottom-water zone after the end of the first radial flow period.

Figures 5.15 and 5.16 show the effect of the crossflow parameters on the semi-log pressure derivative responses. As mentioned before, the variables λ_A and λ_C denote the crossflow parameter between the penetrated and the non-penetrated section of the reservoir, and the crossflow parameter between the reservoir and the aquifer, respectively. Crossflow parameters have been varied by changing the vertical permeability of Zone 1 of Figure 5.1. Everywhere else in the reservoir, $k_v = 0.1k$. The crossflow parameter ranges shown on

Figures 5.15 and 5.16 correspond to vertical permeabilities of $2.4 \times 10^{-15} \text{ m}^2$ (2.4 mD) to $9.5 \times 10^{-18} \text{ m}^2$ (0.001 mD). Figures 5.15 and 5.16 are for mobility ratios of 100 and 1000, respectively, and for $\kappa = 0.5$. Figures 5.15 and 5.16 show that, as the crossflow parameters decrease, the transition flow period after the first radial flow period becomes longer, and it takes a longer time for the pressure transient to reach the bottom-water zone. Figures 5.17 and 5.18 show the corresponding Cartesian derivative graphs. In Figures 5.17 and 5.18, dimensionless time has been computed based on R_{D2} . For small crossflow parameters, the responses in Figures 5.17 and 5.18 show some flattening of the Cartesian derivative and thus, some modification of traditional pseudosteady-state analysis may be possible. In Figures 5.17 and 5.18, a horizontal line corresponding to a Cartesian derivative of 4 (that is, $2/\kappa$) has been shown for comparison purposes. A Cartesian derivative of 4 is expected when $\kappa = 0.5$ and for a sharp-front reservoir with no bottom-water zone. When the front is tilted, the Cartesian slope is higher (for small crossflow parameters) than that for a sharp-front reservoir and the swept volume obtained from pseudosteady-state analysis is underestimated. This has been explained in more detail in Chapter 3.

5.4 Finite Aquifers

In reality, most of the aquifers accompanying the reservoirs are finite in size. Figure 5.2 schematically shows a finite bottom-water zone accompanying a reservoir. Figures 5.19 and 5.20 show the effect of aquifer mobility-thickness ratio on the semi-log pressure derivative responses. Aquifer mobility-thickness ratio has been defined as:

$$\kappa_a = \frac{\left(\frac{kh}{\mu} \right)_{\text{aquifer}}}{\left(\frac{kh}{\mu} \right)_{\text{reservoir}}} \quad (5.3)$$

Figures 5.19 and 5.20 are for mobility ratios of 100 and 1000, respectively. For both the reservoir and the aquifer, $k_v = 0.1k$. Figures 5.19 and 5.20 show that after the first radial flow period, wellbore responses are affected by the non-penetrated section of the reservoir and the aquifer. At late time, the responses show a second radial flow period corresponding to the total mobility-thickness ratio of the reservoir and the aquifer. As the aquifer size becomes larger (that is, κ_a becomes larger), the response for a reservoir with a finite bottom-water zone approaches that for a reservoir with an infinite bottom-water zone. In Figures 5.19 and 5.20, after the transition flow period, semi-log slopes become constant at late times. For higher values of κ_a ($\kappa_a > 0.1$), the value of this constant semi-log slope is $0.5/\kappa_a$. This happens because, at late times, the pressure transient response is dominated by the bottom-water zone because of the much higher mobility in the bottom-water zone compared to the mobility in the reservoir. However, when κ_a becomes smaller ($\kappa_a < 0.1$), the pressure transient response is also affected by the unswept region of the reservoir and, thus, the semi-log derivative is affected by the mobility contrast between the swept and the unswept zones of the reservoir. To quantify the relative effects of κ_a and M on the late-time semi-log slope requires more sensitivity studies.

In Figures 5.19 and 5.20, the responses have been presented when Layer 2 is penetrated and Layer 1 is closed (see Figure 5.2). However, when the reservoir does not possess sufficient injectivity, the well is penetrated closer to the bottom-water zone to take advantage of the higher injectivity of the bottom-water zone. Figure 5.21 shows the semi-log pressure derivative responses when Layer 1 is penetrated instead of Layer 2, and Layer 2 is closed. A comparison of Figures 5.21 and 5.19 shows the effect of the bottom-water zone is felt earlier in Figure 5.21 as compared to that in Figure 5.19. This is expected because, in Figure 5.21, Layer 1 is penetrated which is closer to the bottom-water zone than Layer 2. However, late-time responses in Figure 5.21 are the same as those of Figure

5.19, because, at late-time, responses are dominated by the bottom-water zone for the both cases.

In the preceding discussion of a finite aquifer, the bottom-water zone has been represented by a single layer as shown in Figure 5.2. This may not be adequate for large bottom-water zones. Figure 5.22 shows the effect of layering in the bottom-water zone on the semi-log pressure derivative responses. Figure 5.22 shows responses for an aquifer mobility-thickness ratio (κ_a) of 50. A very large κ_a value has been chosen to enforce the layering effect. In Figure 5.22, the solid line represents responses when the bottom-water zone consists of a single layer. The solid circles and triangles represent the responses when the bottom-water zone consists of two layers and three layers, respectively. Figure 5.22 shows that the responses for a two-layer and a three-layer bottom-water zone are almost identical with that for a single-layer bottom-water zone. Thus, for the analysis done in this study, the bottom-water zone can be adequately represented by a single layer without causing significant error.

Figures 5.23 and 5.24 show the effect of a closed outer boundary on wellbore responses for a reservoir with a finite bottom-water zone. In Figures 5.23 and 5.24, the well is partially-penetrating with $\kappa = 0.5$ and $\kappa_a = 1$. Figure 5.23 shows the effect of the outer boundary on the wellbore pressure. The dimensionless outer boundary radius, r_{oD} , has been varied as 10000, 20000 and 50000. The outer boundaries of the reservoir and the aquifer are assumed to be at the same distance. Initially, the responses show the first radial flow period corresponding to the penetrated section of the reservoir. Though not obvious on Figure 5.23, after the end of the first radial flow period, the wellbore pressure is affected sequentially by the pressure transient in the non-penetrated section of the reservoir, by the fluid front between the swept and the unswept zones of the reservoir, and by the pressure transient in the aquifer before the effect of the outer boundary is felt. This is more clearly shown in Figure 5.24, which shows the corresponding semi-log pressure derivative

responses. Initially, the responses show the first radial flow period corresponding to the penetrated section of the reservoir with a semi-log slope of 1.0 (that is, $0.5/\kappa$). As the pressure transient propagates into the non-penetrated section, the semi-log slope decreases before the pressure transient reaches the fluid front, when the semi-log slope increases because of the mobility contrast. Then, because the pressure transient responses at the wellbore are dominated by the aquifer, the semi-log slope decreases again and reaches a constant value of $0.5/\kappa_a$ before the effects of the outer boundaries of the reservoir and the aquifer are felt. In this particular case, the semi-log slope reaches a value of 0.5 when the transient pressure responses at the wellbore are dominated by the bottom-water zone, because the mobility-thickness ratio of the bottom-water zone, κ_a , equals 1.0. The aforementioned flow regimes and their sequences depend on a particular aquifer-reservoir system and the properties of the reservoir and the aquifer.

5.5 Conclusions

1. Bottom-water conditions, both finite and infinite, can be represented by the multi-layer composite reservoir model used in this study. The effects of mobility-thickness ratio of the penetrated section, crossflow parameters and the mobility-thickness ratio of the aquifer (for a finite aquifer) on transient pressure behaviour have been investigated.
2. The presence of the bottom-water zone is felt before the pseudosteady-state flow period occurs when the reservoir has a high vertical permeability. But if the vertical permeability is very small compared to the horizontal permeability, a brief pseudosteady-state flow period may be observed.
3. For a finite aquifer in a multi-layer, composite reservoir with closed outer boundary, the occurrence of various flow regimes and their sequences depend on the particular aquifer-reservoir system and its properties.

References

1. Eggenschwiler, M., Ramey, H.J., Jr., Satman, A., and Cinco-Ley, H.: "Interpretation of Injection Well Pressure Transient Data in Thermal Oil Recovery," paper SPE 8908 presented at the 1980 Regional Meeting, Los Angeles, CA, April 9-11.
2. Ambastha, A. K. and Ramey, H.J., Jr.: "Thermal Recovery Well Test Design and Interpretation," *SPEFE* (June 1989) 173-180.
3. Walsh, J.W., Ramey, H.J., Jr., and Brigham, W.E.: "Thermal Injection Well Falloff Testing," paper SPE 10227 presented at the 1981 Annual Meeting, San Antonio, TX, Oct. 5-7.
4. Da Prat, G., Bockh, A., and Prado, L.: "Use of Pressure Falloff Tests to Locate the Burning Front in the Miga Field, Eastern Venezuela," paper SPE 13667 presented at the 1985 Regional Meeting, Bakersfield, CA, March 27-29.
5. Stanislav, J.F., Easwaran, C.V., and Kokal, S.L.: "Interpretation of Thermal Injection Well Testing," *SPEFE* (June 1989) 181-86.
6. Fassihi, M.R.: "Evaluation of An Analytical Technique for Estimating Swept Volume from Thermal Pressure Falloff Tests in Heterogeneous Systems," *SPEFE* (June 1988) 449-458.
7. Satman, A.: "An Analytical Study of Transient Flow in Stratified Systems with Fluid Banks," paper SPE 10264 presented at the 1981 Annual Meeting, San Antonio, TX, Oct. 5-7.
8. Satman, A. and Oakay, M.M.: "Effect of a Tilted Front on Well Test Analysis," paper SPE 14701 available from SPE (1985).

9. Blevins, T.R., Aseltine, R.J., and Kirk, R.S.: "Analysis of a Steam-Drive Project, Inglewood Field, California," *JPT* (Sept. 1969) 1141-50.
10. Myhill, N.A. and Stegemier, G.L.: "Steam-Drive Correlation and Prediction." *JPT* (Feb. 1978) 173-82.
11. Singhal, A.K.: "Physical Model Study of Inverted Seven-Spot Steamfloods in a Pool Containing Conventional Heavy Oil," *JCPT* (July 1980) 123-34.
12. Nasr, T.N. and Pierce, G.E.: "Steamflooding Cold Lake Oil Reservoirs Through a Bottomwater Zone: A Scaled Physical Model Study," *SPERE* (may 1993) 94-100.
13. Streltsova-Adams, T.D.: "Pressure Drawdown in a Well with Limited Flow Entry," *JPT* (Nov. 1978) 1469-76.
14. Gomes, E. and Ambastha, A.K.: "Analytical Expressions for Pseudoskin for Partially-Penetrating Wells Under Various Reservoir Conditions" paper SPE 26484 presented at the 1993 Annual Meeting, Houston, TX, Oct. 3-6.
15. Gomes, E. and Ambastha, A.K.: "An Analytical Pressure-Transient Model for Multilayered, Composite Reservoirs with Pseudosteady-State Formation Crossflow" *AOSTRA Journal of Research*, Vol. 8, no. 2, (1992) p. 63-77; also paper SPE 26049 presented at the 1993 Western Regional Meeting, Anchorage, AK, May 26-28.

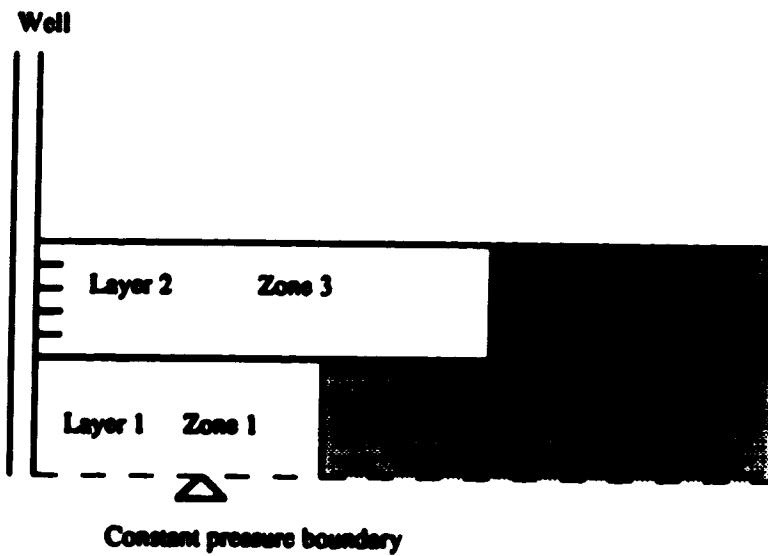


Figure 5.1: Steam-flooded heavy oil reservoir with an infinitely-large bottom-water region.

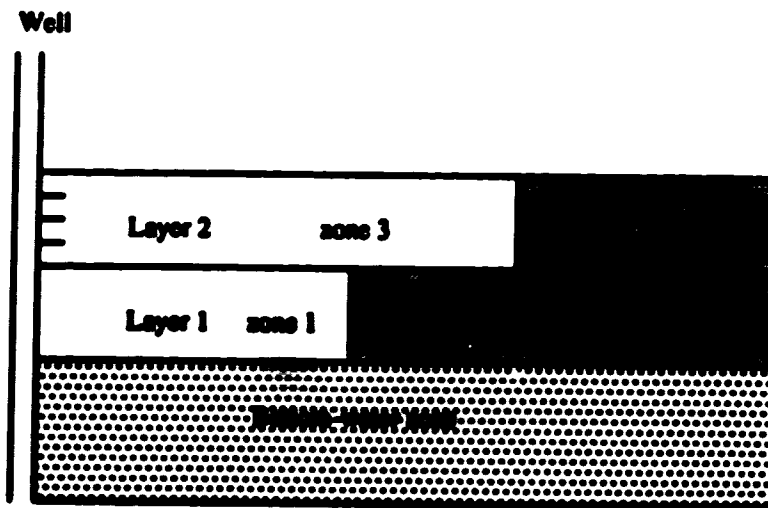


Figure 5.2: Steam-flooded heavy oil reservoir with a finite bottom-water zone.

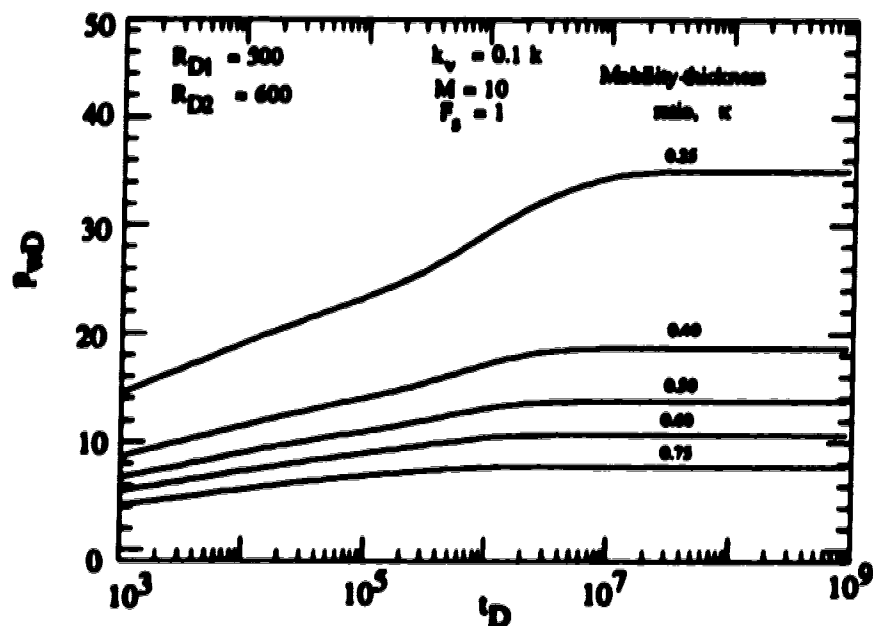


Figure 5.3 : Effect of mobility-thickness ratio on pressure responses of a partially-penetrating well for $M = 10$.

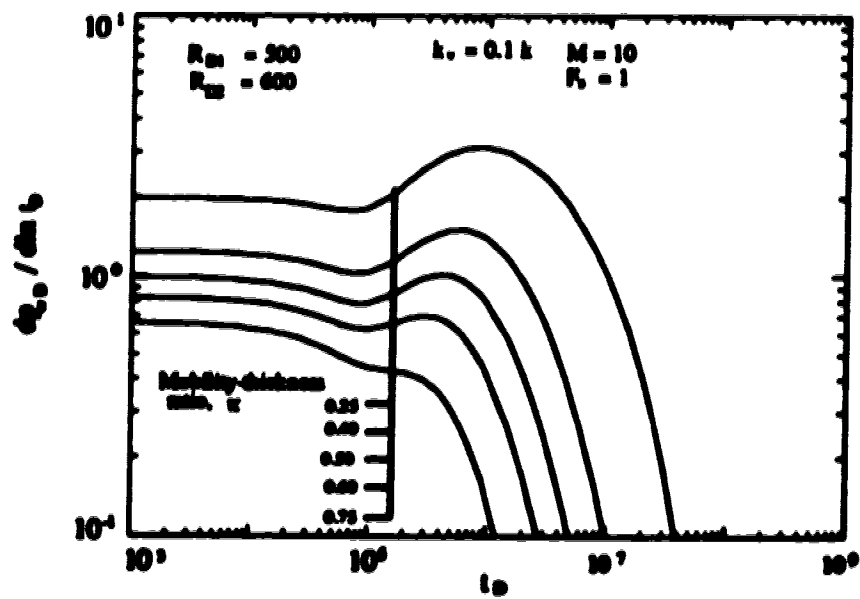


Figure 5.4 : Effect of mobility-thickness ratio on pressure derivative responses of a partially-penetrating well for $M = 10$.

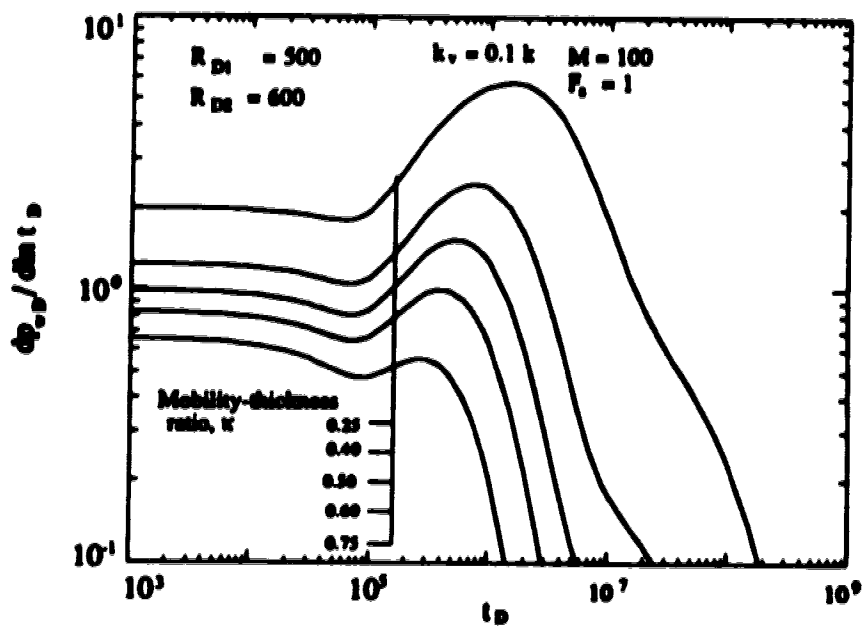


Figure 5.5: Effect of mobility-thickness ratio on pressure derivative responses of a partially-penetrating well for $M = 100$.

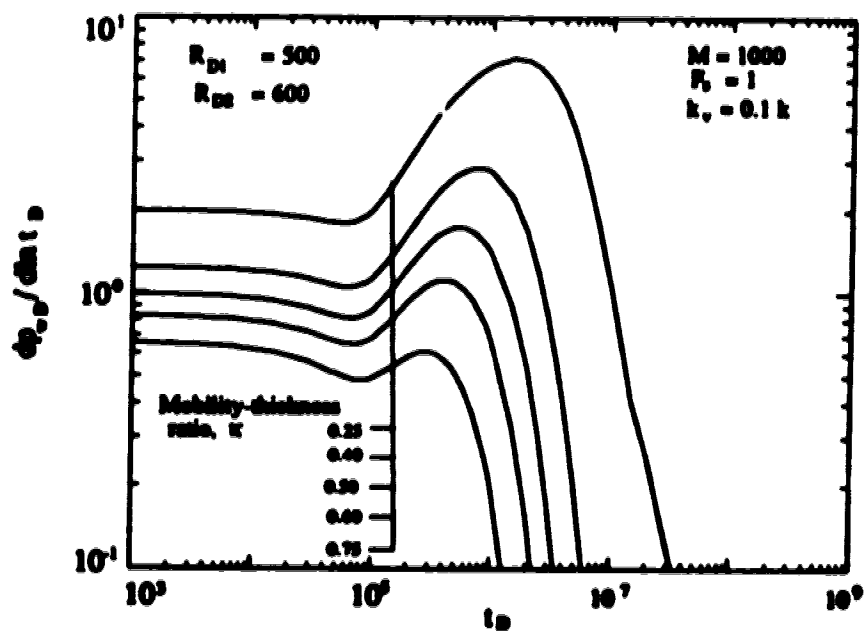


Figure 5.6: Effect of mobility-thickness ratio on pressure derivative responses of a partially-penetrating well for $M = 1000$.

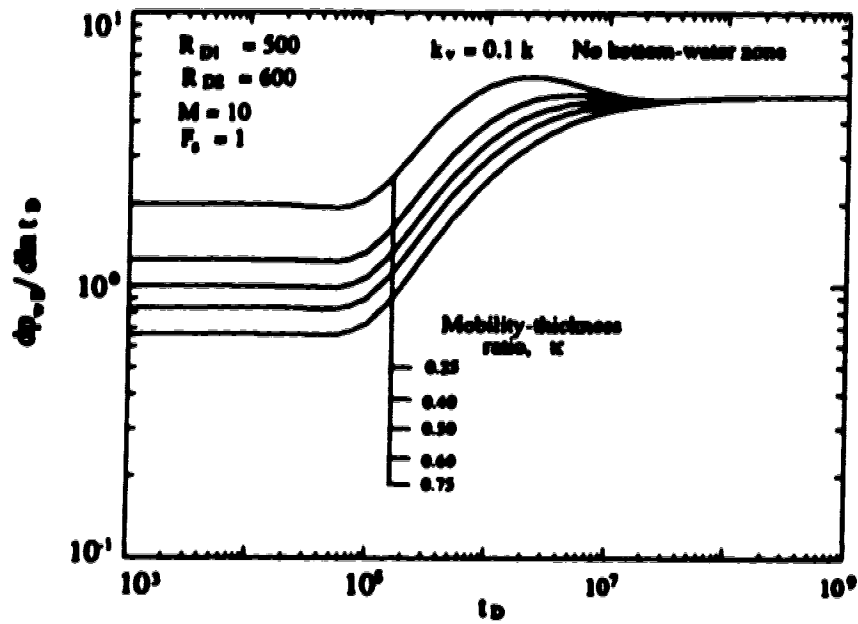


Figure 5.7 : Effect of mobility-thickness ratio on pressure derivative responses of a composite reservoir with no bottom-water zone.

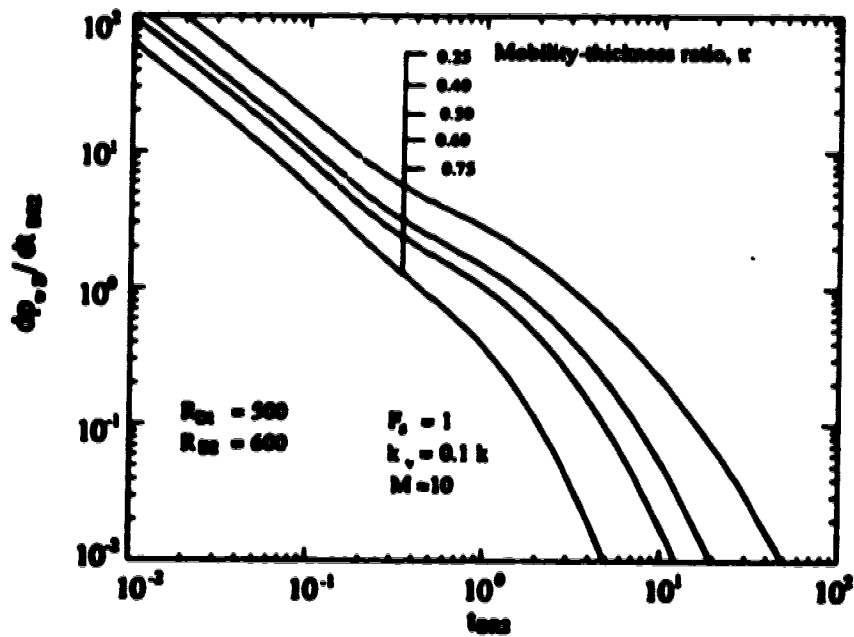


Figure 5.8: Effect of mobility-thickness ratio on the Cartesian pressure derivative of a partially-penetrating well for $M = 10$.

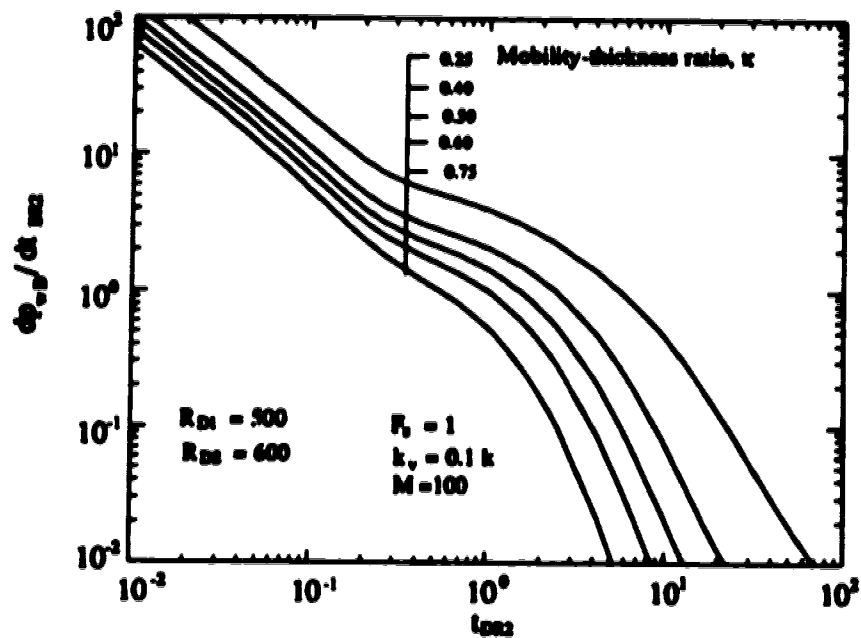


Figure 5.9: Effect of mobility-thickness ratio on the Cartesian pressure derivative of a partially-penetrating well for $M = 100$.

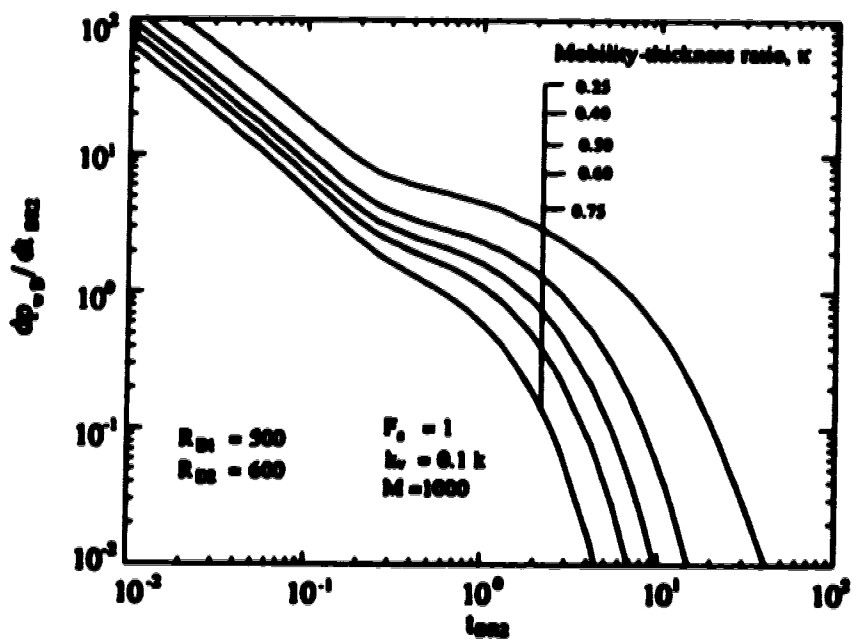


Figure 5.10: Effect of mobility-thickness ratio on the Cartesian pressure derivative of a partially-penetrating well for $M = 1000$.

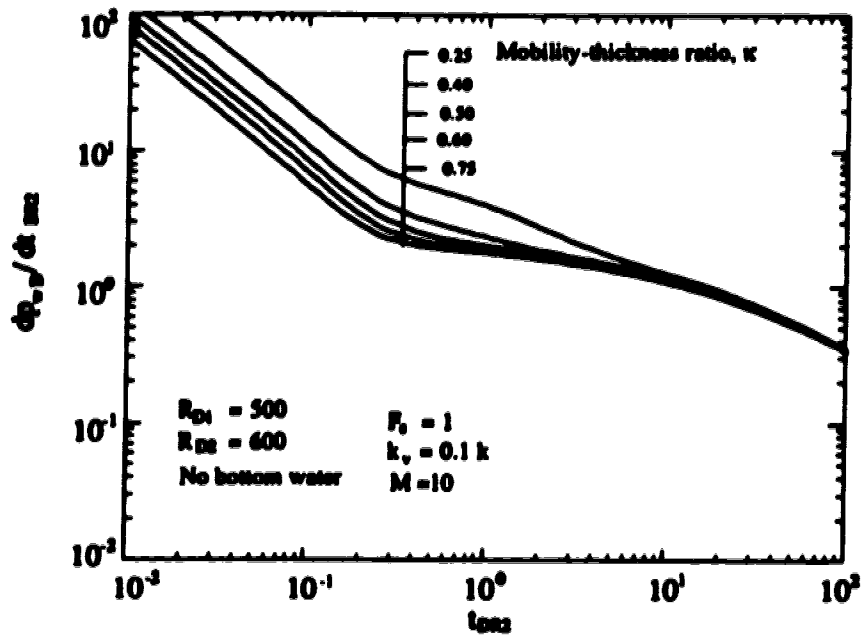


Figure 5.11: Effect of mobility-thickness ratio on the Cartesian pressure derivative of a partially-penetrating well with no bottom-water zone.

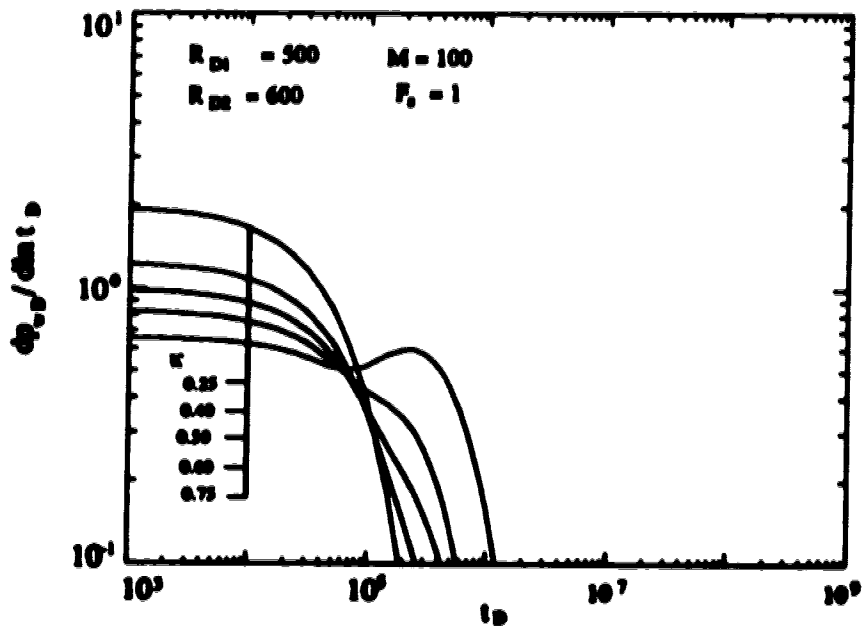


Figure 5.12: Effect of mobility-thickness ratio on pressure derivative responses when the mobility-thickness ratio has been varied by changing the permeability of the penetrated layer.

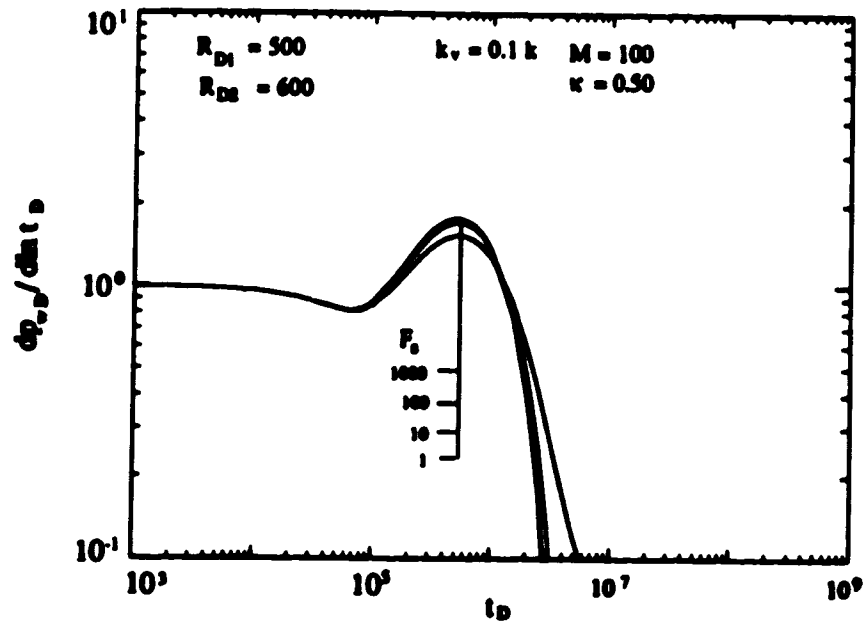


Figure 5.13: Effect of the storativity ratio on pressure derivative responses of a partially-penetrating well for $M = 100$.

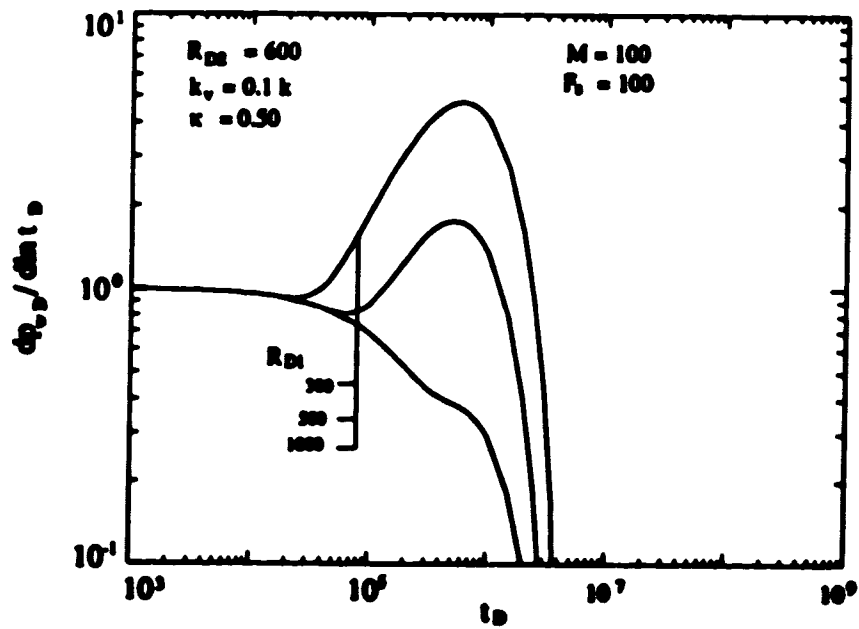


Figure 5.14: Effect of the dimensionless discontinuity radius in Layer 1 on pressure derivative responses of a partially-penetrating well.

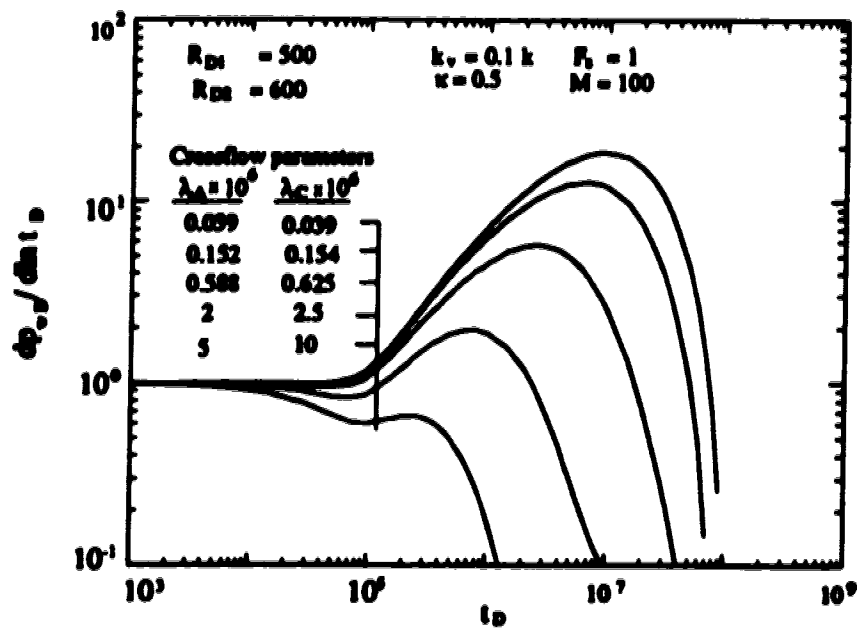


Figure 5.15: Effect of the crossflow parameters on the semi-log pressure derivative responses for $M = 100$.

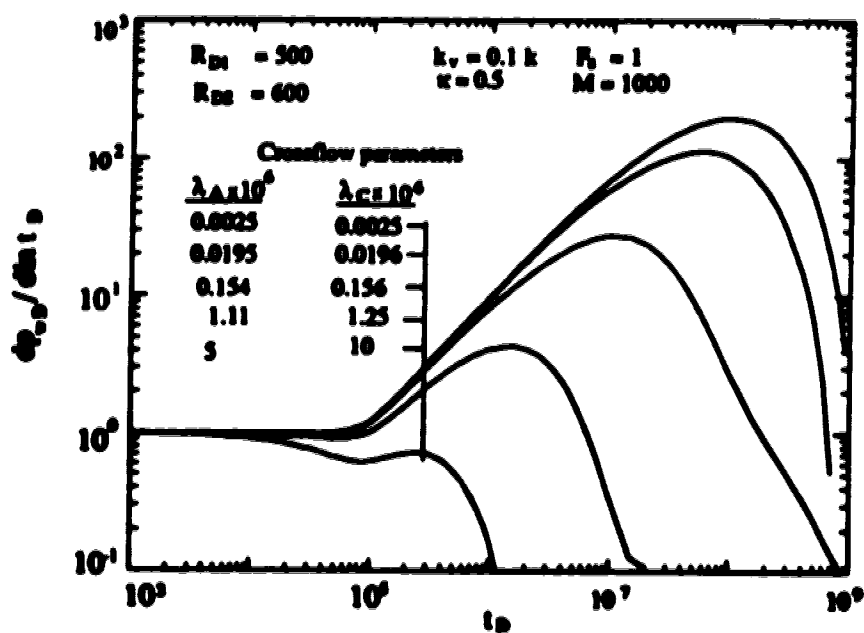


Figure 5.16: Effect of the crossflow parameters on the semi-log pressure derivative responses for $M = 1000$.

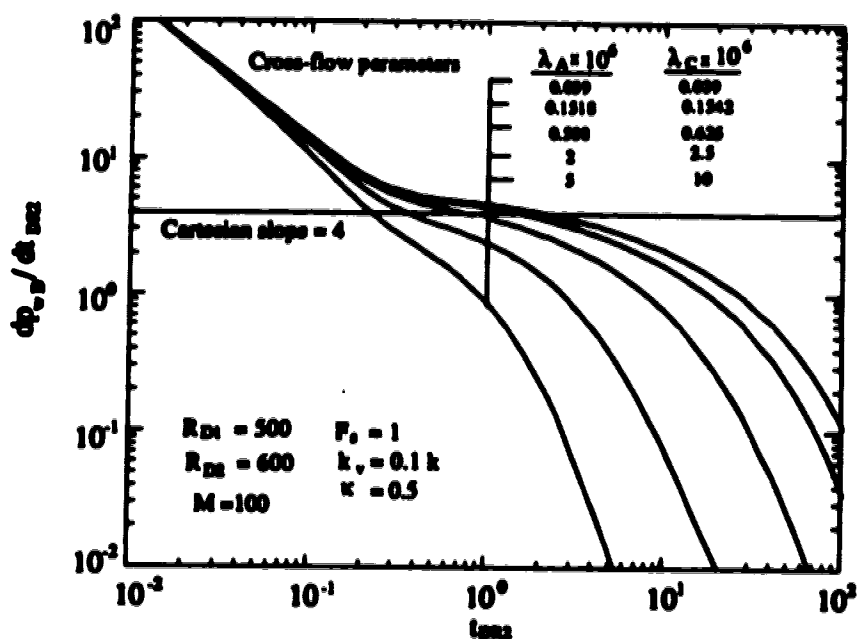


Figure 5.17: Effect of the crossflow parameters on the Cartesian pressure derivative for $M = 100$.

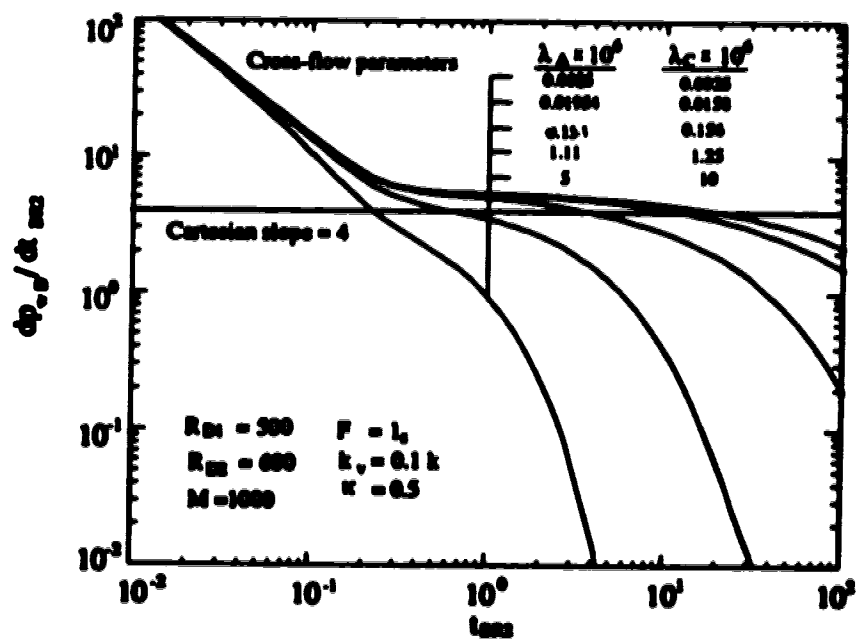


Figure 5.18: Effect of the crossflow parameter on the Cartesian pressure derivative for $M = 1000$.

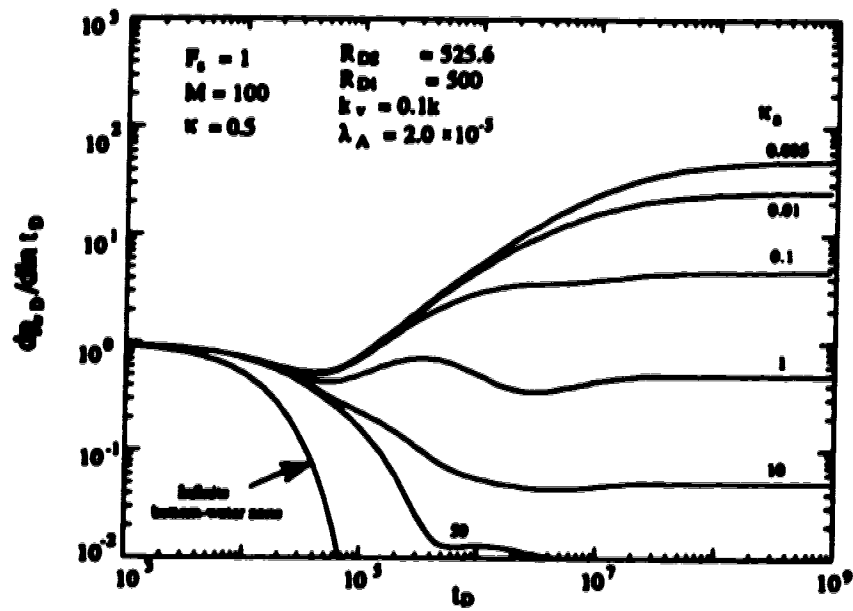


Figure 5.19: Effect of the aquifer mobility-thickness ratio on the semi-log pressure derivative responses for $M = 100$.

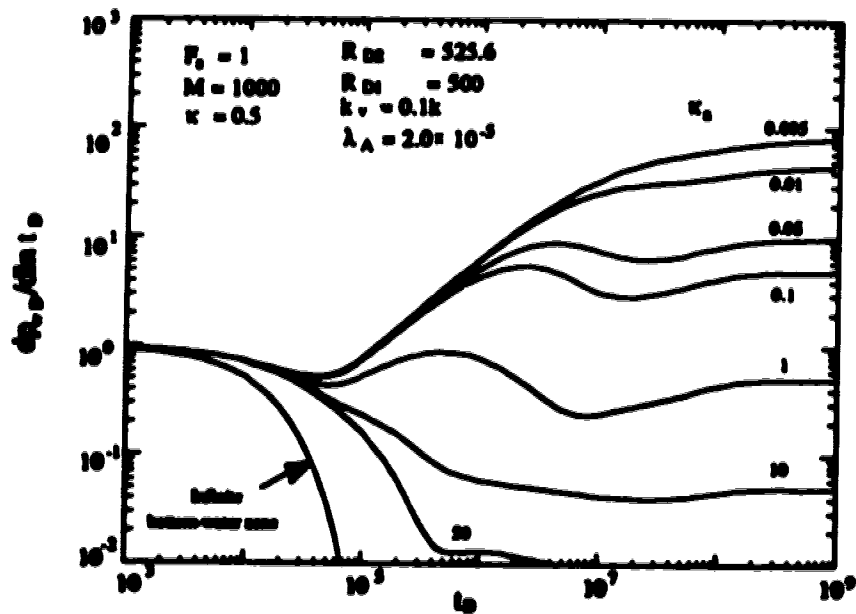


Figure 5.20: Effect of the aquifer mobility-thickness ratio on the semi-log pressure derivative responses for $M = 1000$.

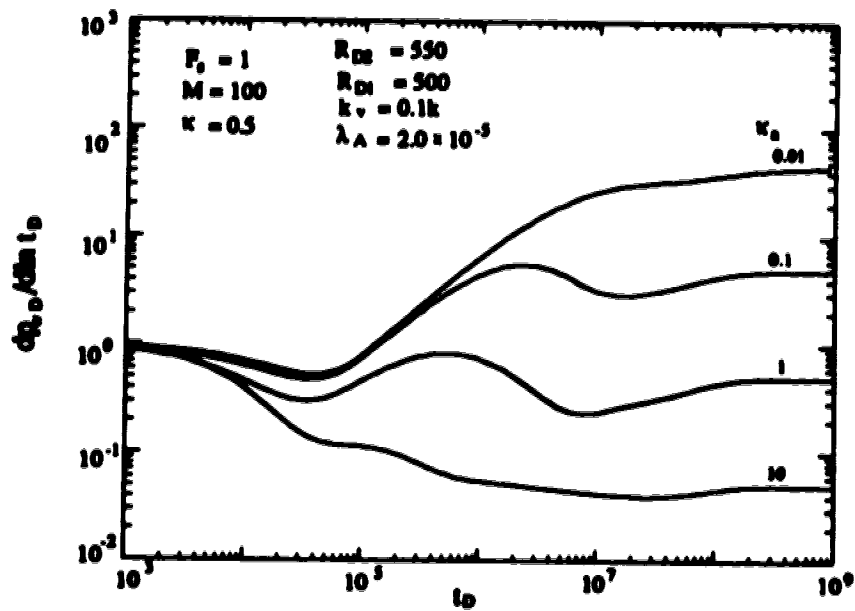


Figure 5.21: Effect of the aquifer mobility-thickness ratio on the semi-log pressure derivative responses when Layer 1 is penetrated.

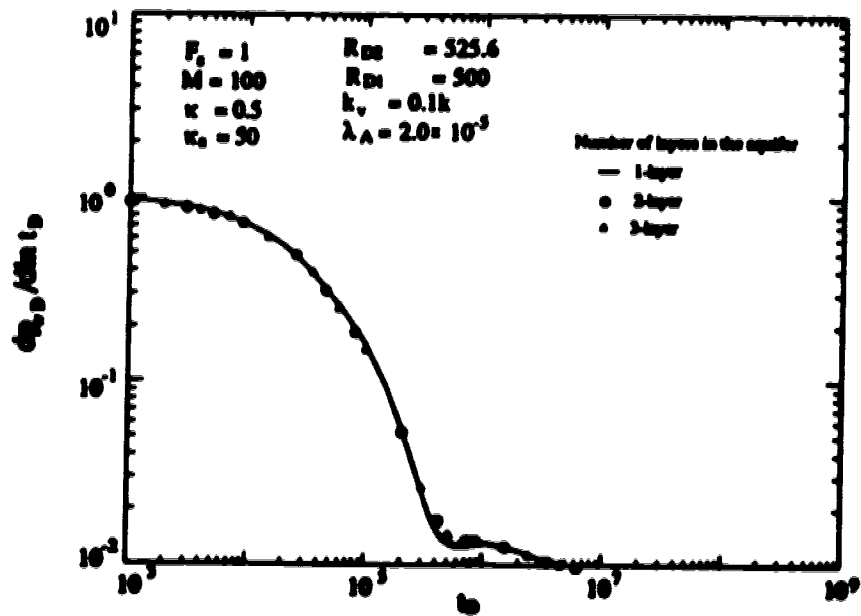


Figure 5.22: Effect of layering in the aquifer on the semi-log pressure derivative responses for $M = 100$.

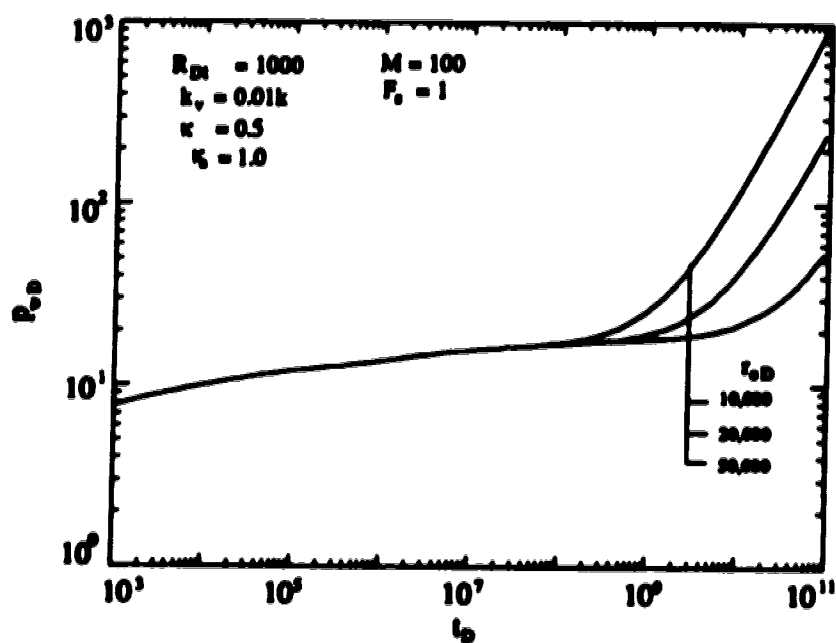


Figure 5.23: Effect of the dimensionless outer boundary on the wellbore pressure of a reservoir with a finite aquifer.

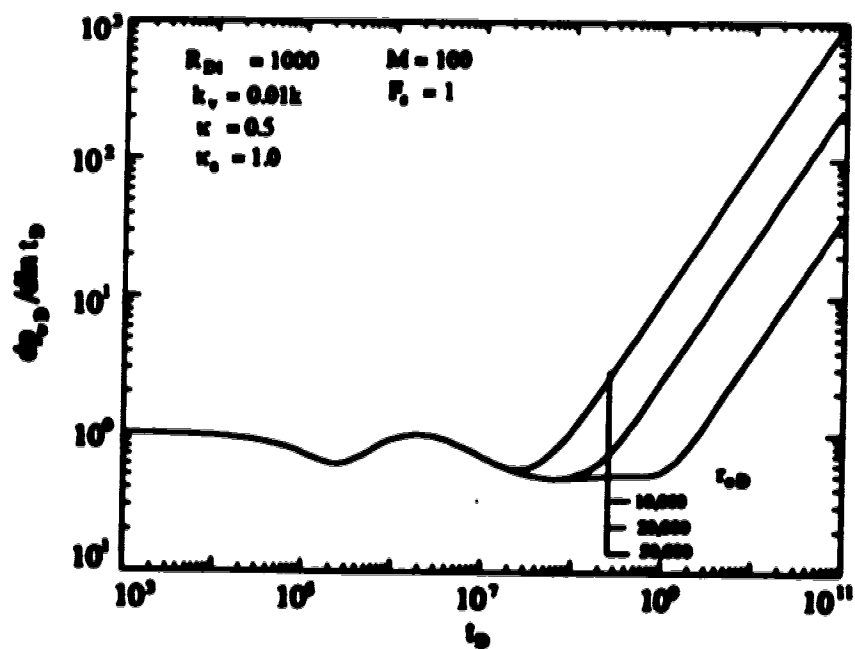


Figure 5.24: Effect of the dimensionless outer boundary radius on the semi-log pressure derivative of a reservoir with a finite aquifer.

6.0 AN ANALYTICAL PRESSURE-TRANSIENT MODEL FOR COMPLEX RESERVOIR SCENARIOS

6.1 Introduction

Reservoir heterogeneity is usually described by layers and zones of different rock and/or fluid properties. When a secondary recovery method, such as steam-flooding, is applied, the reservoir resembles a composite reservoir. Because of reservoir heterogeneity and gravity override effects, the fluid front can have very complex shape. The presence of aquifers and gas caps can further complicate the situation. Numerous studies have been reported in the literature on layered and composite reservoirs. Gomes and Ambastha¹ have presented an extensive literature review on layered and composite reservoirs. These studies are limited in that they can not model the aforementioned complex situations analytically. This paper considers a multi-layer, composite reservoir with pseudosteady-state crossflow and presents a new and efficient model for the analytical treatment of such complex scenarios.

6.2 Model Description

In this study an n -layer, radial, composite reservoir as shown in Figure 6.1 has been considered. A symmetrically located well fully penetrates the reservoir. The well produces at a constant flow rate and pseudosteady-state formation crossflow is present between the layers. In Figure 6.1, the discontinuity boundary in each layer is represented by a vertical solid line. These discontinuity boundaries have been vertically extended across all the layers. As a result, depending on the total number of discontinuity boundaries and their locations, an n -layered reservoir may have m number of zones in each layer. Therefore, the reservoir is divided into $n \times m$ zones and each

zone may be identified by (i,j) , in which i and j denote the zone and the layer, respectively. Each zone may have different rock and/or fluid properties, and can have a variable length in the radial direction, depending on the discontinuity boundary locations. In an actual reservoir, $n \times m$ zones of different rock and/or fluid properties may not be needed. In Figure 6.1, the shaded and non-shaded areas represent two different fluid and/or rock types. Each layer has only two different rock and/or fluid types separated by a discontinuity boundary. In each layer, the discontinuity boundary is placed at a different location to simulate a tilted-front discontinuity boundary for the reservoir and for this particular situation, $m=n+1$. Though layers of equal thicknesses throughout the reservoir are shown in Figure 6.1, non-uniform layer thicknesses are accounted for in the model presented in this paper.

The pseudosteady-state crossflow between layers within the reservoir is modelled as in the semi-permeable wall model proposed by Gao². Thus, the crossflow resistance is assumed to be confined to the interlayer boundary and flow in each layer is horizontal. The upper boundary of the top layer and the lower boundary of the bottom layer are considered closed, when there is no aquifer or gas cap present. If an aquifer or a gas cap exists, crossflow across the bottom or top boundary should be considered. In the presence of an aquifer or a gas cap, the well is partially perforated to delay water or gas coning. Transient pressure responses for partially-penetrating wells can also be studied using the model discussed in this paper.

6.3 Solution Description

The diffusivity equations for all zones (i,j) in a cylindrical coordinate system has been considered. This system has been treated as a generalized eigenvalue system. From the boundary conditions of the various zones, a system of simultaneous, linear equations has been derived and solved to obtain transient pressure responses for each zone.

Details of this solution have been presented by Gomes and Ambastha¹. A general solution for dimensionless pressure in Laplace space ($\bar{P}_{D,i,j}$) for zone(i,j) has been obtained as:

$$\bar{P}_{D,i,j} = \sum_{k=1}^n \left[A_i^k E_{i,j}^k K_0(\sigma_i^k r_D) + B_i^k E_{i,j}^k I_0(\sigma_i^k r_D) \right], \quad (6.1)$$

where σ_i^k and $E_{i,j}^k$ are the eigenvalues and the eigenvector, respectively, for Region i and Layer j. Constants A_i^k and B_i^k are to be determined from the boundary conditions. The boundary conditions are: the inner boundary condition (wellbore condition), the outer boundary condition, and the interface conditions, which are pressure and flowrate continuity conditions between zones. Equation (6.1) contains $2n \times m$ constants to be evaluated from the boundary conditions. The variable r_D represents dimensionless radius. To evaluate the transient pressure response at the wellbore, the solution represented in Equation (6.1) is evaluated at $r_D=1$. As discussed in Gomes and Ambastha¹, this new solution uses the eigenvalues and eigenvectors of the system and is computationally more efficient than other methods proposed in the literature.

6.4 Solution Algorithm

The computer program for the solution has been written in FORTRAN 77 and Appendix F shows the complete source code. The following logical sequence has been utilized in writing the source code:

Main Program: GENERAL

1. open output files to store results
2. read all the necessary input data from an input data file
3. call Subroutine TAB to compute front radii, if required
4. compute the average front radius, RDAV
5. non-dimensionalize the wellbore and front radii

6. compute transmissibilities, $TS(i,j)$, and storativities, $ST(i,j)$, of each zone
7. compute crossflow parameters, $XA(i,j)$ and $XB(i,j)$, of each zone
8. generate a set of time vectors, TD
9. call Subroutine INVERT to invert the results from Laplace space to real space

Subroutine INVERT

- 9.1 Subroutine Invert uses the Stehfest³ algorithm to invert results from Laplace space to real space
- 9.2 call Subroutine LAP to compute results in Laplace space

Subroutine LAP

- 9.2.1 set up the coefficient matrices, $A(j,j)$ and $BB(j,j)$, and compute the eigenvalues and eigenvectors from the IMSL.Math Library⁴
- 9.2.2 set up the augmented matrices, $AA(k,k)$ and $B(k)$, from the boundary conditions and solve the resulting system of equations using the IMSL.Math Library⁴
- 9.2.3 compute the wellbore pressure and its derivative in Laplace space and transfer it to Subroutine INVERT
- 9.3 invert the pressure and the pressure derivative to real space and transfer it to the Main Program

10. compute the semi-log and Cartesian derivatives and generate buildup results
11. write and store the results in the Output files

The computational process involves repeated calculations of Bessel's functions. Very small and large arguments of Bessel's functions create an overflow problem during the computational process. This problem is overcome by using a dimensionless radius, r_D , based on the minimum front radius, instead of the wellbore radius, and by calculating

Bessel's functions in exponentiated form. Because of the exponentiation of Bessel's functions, equations obtained from the boundary conditions are multiplied by exponentiation factors, and if this is not corrected, the solution will generate erroneous results. During computation of the wellbore pressure, the results are divided by the corresponding exponentiation factors to reverse the exponentiation effects.

6.5 Model Validation

The new analytical solution has been validated by generating some well-known transient-pressure responses for various cases of homogeneous, composite, and layered reservoirs, which are subsets of the general solution developed. Results obtained from this solution have been compared against Agarwal *et al.*⁵ type-curves for homogeneous reservoirs, Tariq and Ramey's⁶ study on layered reservoirs, Eggenschwiler *et al.*⁷ study on composite reservoirs, and Ambastha and Ramey's^{8,9} study on two- and three-region, composite reservoirs. These comparisons have shown excellent matches of the results obtained from this new solution with those obtained from other studies. Gomes and Ambastha¹ have presented details of this validation. The model discussed in this paper is capable of generating transient pressure responses for partially-penetrating wells. A study regarding partially-penetrating wells using the model of this paper is presented in Gomes and Ambastha¹⁰.

6.6 Reservoirs with Complex Front Shapes

One of the important advantages of this new analytical solution is its versatility in use. This new model can accommodate complex reservoir scenarios resulting from reservoir heterogeneity and from thermal recovery or other fluid injection operations. Figures 6.2 and 6.3 schematically show two reservoir situations where, because of the very high permeability contrast between layers, the shapes of the swept zones are complex or irregularly-shaped. These front shapes can not be described by a sharp front, or a tilted

front by specifying a front angle and a minimum front radius. Both reservoirs shown in Figures 6.2 and 6.3 consist of three layers. The non-shaded and the shaded areas represent the swept and the unswept regions, respectively. In Figure 6.2, Layer 2 has a very high permeability compared to the other layers and, thus, the swept front in Layer 2 propagates the maximum distance. In Figure 6.3, Layer 3 has a very high permeability, whereas Layer 2 has a very low permeability resulting in a complex front shape. Although, the swept fronts in Figures 6.2 and 6.3 have very different shapes, the swept zones in both these figures have equal swept volumes and minimum front radii. Thus, the two reservoirs have identical average front radii.

Figures 6.4 and 6.5 show the responses for the reservoirs described by Figures 6.2 and 6.3. Figure 6.4 shows the wellbore pressure responses with time. The line and the solid circles represent the responses corresponding to Figures 6.2 and 6.3, respectively. The two responses follow each other very closely. Figure 6.5 shows the corresponding semi-log pressure derivative responses. Figures 6.4 and 6.5 show that, when the minimum front radius and swept volume are equal, the transient pressure and pressure derivative responses are not very sensitive to the shape of the swept zones. This example represents one application of this new, multi-purpose pressure-transient model, which should become increasingly useful to the petroleum engineering community in the foreseeable future.

6.7 Summary

A computer program has been developed on the basis of an analytical solution to generate transient pressure responses for a multi-layer, composite reservoir with pseudosteady-state formation crossflow. This computer program can generate transient pressure responses for various complicated reservoir situations. The usefulness of the

computer program has been demonstrated by considering transient pressure behaviour for reservoirs with complex front shapes.

References

1. Gomes, E. and Ambastha, A.K., "An Analytical Pressure-Transient Model for Multilayered, Composite Reservoirs with Pseudosteady-State Formation Crossflow" *AOSTRA J. of Research*, (April 1992) p. 63-77; also paper SPE 26049 presented at the 1993 Western Regional Meeting of SPE of AIME, Anchorage, AK, May 26-28.
2. Gao, C., "Single-Phase Fluid Flow in a Stratified Porous Medium with Crossflow" *SPEJ* (Feb. 1984) p. 97-106.
3. Stehfest, H. "Algorithm 368, numerical inversion of Laplace transforms, D-5" *Comm. of ACM* (Jan. 1970) p. 47-49.
4. Anon., "User's manual, IMSL Math/Library: version 1.0 (April 1987) p. 13 and 329.
5. Agarwal, R. G., Al-Hussainy, R., and Ramey, H. J., Jr., "An Investigation of Wellbore Storage and Skin Effect in Unsteady Liquid Flow" *SPEJ* (Sept. 1970) p. 279-290.
6. Tariq, S.M., and Ramey, H.J. Jr., "Drawdown Behavior of a Well with Storage and Skin Effect Communicating with Layers of Different Radii and Other Characteristics" paper SPE 7453 presented at the 1978 Annual Technical Conference and Exhibition of SPE of AIME, Houston, TX, Oct. 1-3.

7. **Eggenschwiler, M., Ramey, H.J., Jr., Satman, A., and Cinco-Ley, H., "Interpretation of Injection Well Pressure Transient Data in Thermal Oil Recovery" paper SPE 8908 presented at the 1980 California Regional Meeting, Los Angeles, CA, April 9-11.**
8. **Ambastha, A. K. and Ramey, H.J., Jr.: "Thermal Recovery Well Test Design and Interpretation" *SPEFE* (June 1989) p. 173-180.**
9. **Ambastha, A. K. and Ramey, H.J., Jr.: "Pressure Transient Analysis for a Three-Region Composite Reservoir" paper SPE 24378 presented at the 1992 Rocky Mountain Regional Meeting , Casper, Wyoming, May 18-21.**
10. **Gomes, E. and Ambastha, A.K.: "Analytical Expressions for Pseudoskin for Partially-Penetrating Wells Under Various Reservoir Conditions" paper SPE 26484 presented at the 1993 Annual Meeting , Houston, TX, Oct. 3-6.**

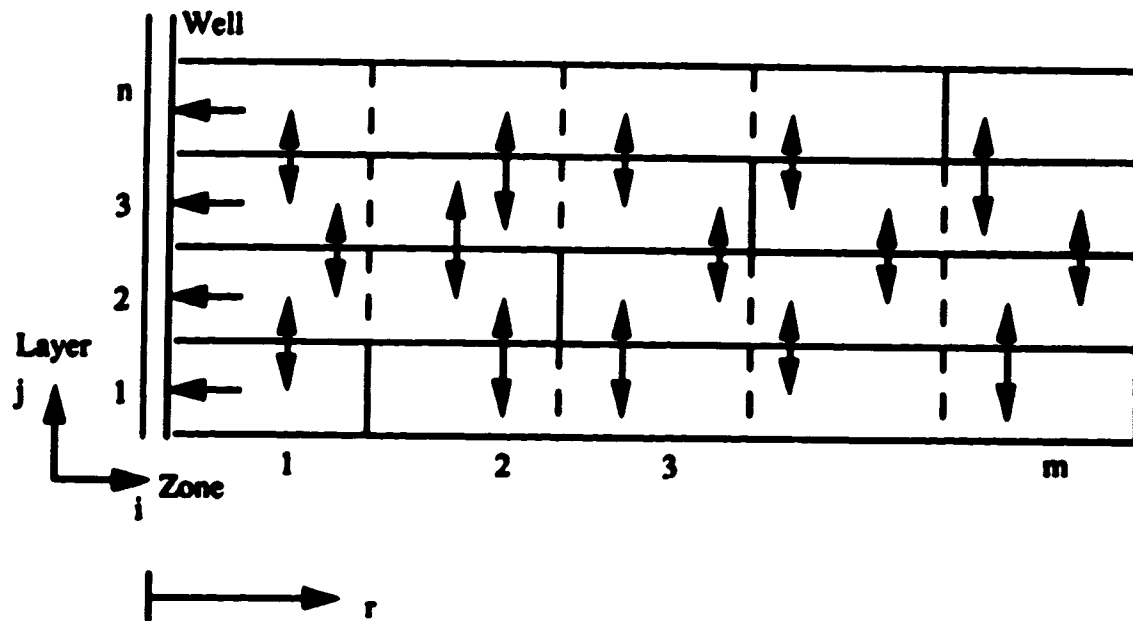


Figure 6.1: Schematic of an n -layer, composite reservoir in radial geometry with two different rock and/or fluid types in each layer.

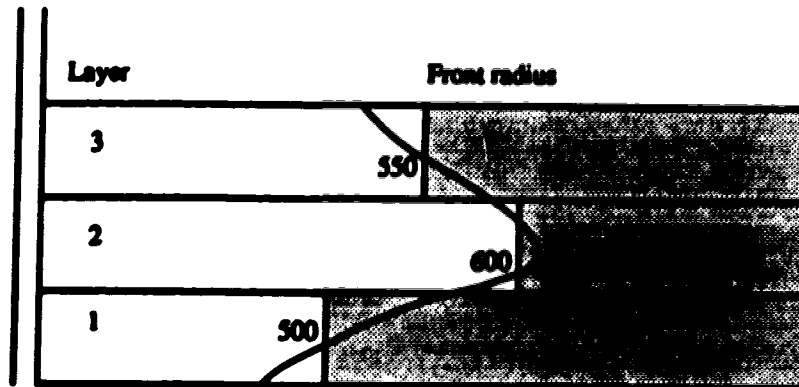


Figure 6.2: Complex swept zones resulting from very high permeability in Layer 2.

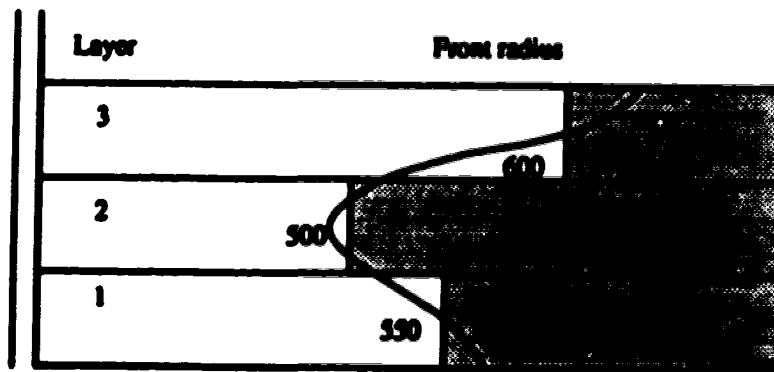


Figure 6.3: Complex swept zones resulting from very high permeability in Layer 3 and very low permeability in Layer 2.

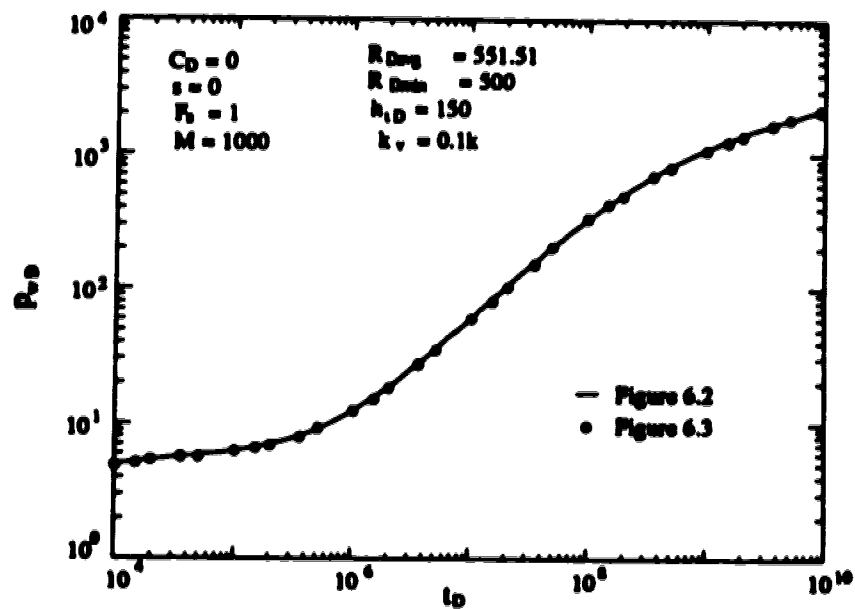


Figure 6.4: Effect of a complex front shape on transient wellbore pressure.

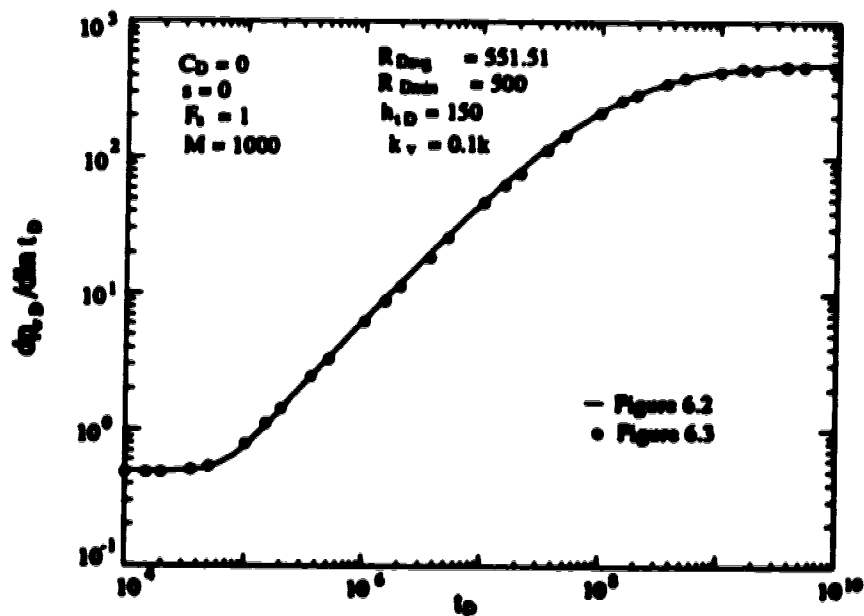


Figure 6.5: Effect of a complex front shape on semi-log pressure derivative responses.

7.0 DISCUSSION, CONCLUSIONS, AND RECOMMENDATIONS

7.1 Discussion

In this study, an analytical solution for a multi-layer, composite reservoir with pseudosteady-state formation crossflow has been developed and validated. The new analytical solution is applicable for tilted or irregularly-shaped fluid fronts, multiple composite regions, and for closed, constant pressure and infinite outer boundary conditions. This new solution is computationally very efficient and requires solution of an order of magnitude fewer equations as compared to the other methods in the literature. The new solution is very versatile and can treat partially-penetrating wells subject to finite and infinite bottom-water conditions for well testing purposes.

In steam-flooding projects, because of the gravity override effect, the fluid front of the swept region is not vertical, but tilted or inclined. For tilted front reservoirs, this study shows that transient pressure responses are sensitive to the front shape. The time to the end of the first radial flow period and the responses for the transition flow period between the first and the second radial flow period are affected by the shape of the fluid front. This study shows that design equations for the end of the first radial flow period applicable for a sharp-front, single-layer reservoir are not adequate for tilted front reservoirs. Based on pressure derivative responses, modified design equations have been derived for the end of the first radial flow period and for the time to the maximum semi-log pressure derivative during the transition flow period. For tilted front cases and with sufficient mobility and storativity contrast between the swept and the unswept zones, this study shows that the pseudosteady-state (pes) flow period exists in some average sense and that pes analysis assuming a sharp front will result in considerable underestimation of the swept volume. A correction factor has been developed to correct the estimated swept volume from the pes analysis.

For reservoirs under bottom-water or gas-cap drives, the wells are partially-penetrated to avoid or delay water or gas production. For partially-penetrating wells in multi-layer reservoirs, this study has developed new analytical expressions for pseudoskin for both closed top and bottom boundaries and for bottom-water or gas cap conditions. These analytical expressions are simple and easy to use. The estimated pseudoskin factors are very close to the actual pseudoskin factors obtained from the complete analytical solution. These new analytical expressions are also applicable to the corresponding homogeneous and single-layer cases. For partially-penetrating wells in multi-layer reservoirs, time criteria have been derived for the end of the first radial flow period and for the beginning of the second radial flow period.

Many times, heavy-oil reservoirs undergoing steam-flooding are underlain by a bottom-water zone. Because of the gravity override effect, the fluid front is not vertical but tilted or inclined. Such reservoirs have been studied using the multi-layer composite reservoir model developed in this study. Both finite and infinite bottom-water conditions have been considered. A finite aquifer has been modelled as a layer of finite thickness having appropriate properties, and an infinite aquifer has been modelled as a constant-pressure boundary. The solution developed in this study can model adequately both finite and infinite bottom-water conditions for transient pressure analysis purposes. Both pressure and pressure derivative responses have been investigated to determine the effects of aquifer size, penetration ratio and the vertical permeability on wellbore responses. As the aquifer size increases, the response approaches that of an infinite aquifer. As expected, the presence of the bottom-water zone is felt before the pseudosteady-state flow period occurs when the reservoir has a very high vertical permeability. But when the vertical permeability (that is, the crossflow parameter) is small, a brief period of pseudosteady-state flow behaviour is observed for small penetration ratios and pseudosteady-state analysis, with some modification, may be possible.

7.2 Conclusions

In this study, the transient pressure behaviour of a multi-layer, composite reservoir has been investigated. To accommodate the gravity override effect, tilted and irregularly-shaped fluid fronts have been considered. The behaviour of partially-penetrating wells in reservoirs with finite and infinite bottom-water conditions has been investigated. Based on this study, the following has been concluded:

New Analytical Solution

1. A general analytical solution for transient pressure responses for an n-layered, composite reservoir with pseudosteady-state formation crossflow has been developed and validated.
2. The new analytical solution developed in this study is computationally more efficient and versatile in use than presently-available solutions in the literature.
3. The new analytical solution offers new possibilities to analyze more complicated well-testing scenarios than the possibilities offered by presently-available solutions.

Tilted Front Reservoirs

1. Design equations for the time to the end of the first radial flow period for a sharp-front reservoir are inadequate for the tilted-front reservoirs. For tilted-front reservoirs, modified design equations have been developed for the time to the end of the first radial flow period, and for the time to the occurrence of the maximum semi-log slope during the transition flow period.
2. The deviation time method yields an estimate of the geometric mean of the minimum front radius and the average front radius of the swept region.

3. For inclined front reservoirs, pseudosteady-state (pss) occurs in some average sense and pss analysis results in a considerable underestimation of the swept volume.
4. A correction factor has been developed to estimate the correct swept volume from the pseudosteady-state analysis for situations where a tilted front is suspected.
5. For the cases considered in this study, thermal well test responses obtained from a crossflow system can be analyzed using a commingled system solution for a fully-penetrating well. However, crossflow must be taken into account for a proper analysis of thermal well test responses for partially-penetrating wells.

Partially-Penetrating Wells and Pseudoskin

1. Transient pressure responses and pseudoskin factors for a partially-penetrating well in a multi-layer reservoir can be studied analytically by a pseudosteady-state crossflow model.
2. Simplified expressions for pseudoskin factors have been derived for multi-layer reservoirs with or without bottom-water or a gas-cap drive and pseudoskin factors can be estimated from these expressions with reasonable accuracy.
3. Times for the end of the radial flow period and the beginning of the pseudoradial flow period depend on the crossflow parameter and the mobility-thickness ratio of the open interval. Simplified expressions have been derived for these time criteria .
4. Pseudoskin factors obtained from this study have been compared with those obtained from other studies in the literature and these comparisons have shown good matches with most of the studies.

Composite Reservoirs Under Bottom-Water Conditions

- 1. Bottom-water conditions, both finite and infinite, can be represented by the multi-layer composite reservoir model used in this study. Effects of various parameters of the reservoir-aquifer system on transient pressure behaviour have been investigated.**
- 2. The presence of the bottom-water zone is felt before the pseudosteady-state flow period occurs when the reservoir has a high vertical permeability. However, if the vertical permeability is very small compared to the horizontal permeability, a short pseudosteady-state flow period may be observed.**
- 3. For a finite aquifer in a multi-layer, composite reservoir with a closed outer boundary, the occurrence of various flow regimes and their sequences depend on the particular reservoir-aquifer system and its properties.**

Irregularly-Shaped Fronts

- 1. For irregularly-shaped fronts, when the minimum front radius and the swept volume are equal, pressure and pressure derivative responses are not very sensitive to the shape of the swept zones.**

7.3 Recommendations

Future studies in multi-layer, composite reservoir should address the following:

- 1. Pressure falloff data for multi-layer, composite reservoirs with tilted and irregularly-shaped fluid fronts can be studied using this new analytical model.**
- 2. The new analytical model can be used for automatic type-curve matching for complex reservoir scenarios.**

3. Extension of this new model to multi-phase well-testing situations will make this model more general.

APPENDICES

Appendix A: Calculation of Layer Front Radii for Inclined Front Reservoirs (after Klome¹¹)

This appendix describes the calculation procedure of various layer front radii for inclined front reservoirs (see Chapter 3) provided the minimum front radius (R_1), layer thicknesses (h_i), total number of layers (n), and the angle of inclination (θ) are known. An expression for the layer front radius has been obtained following the approach presented by Klome¹¹.

Figure 3.2 shows the swept section of a two-layer composite reservoir. The parameters, R_1 and θ , are the minimum front radius and the angle of inclination, respectively. Layers are numbered from bottom to top. For Layer 1, line $R'_1 R'_2$ is drawn in such a way that the half-cylinder $ABCR_1$ and the cone frustum $ABR'_1 R'_2$ have the same volume. The dotted line $R'_1 R'_2$ represents the inclined front, while line CR_1 represents the step approximation of the inclined front.

Considering the half-cones OBR'_2 and OAR'_1 ,

$$\tan \theta = \frac{h'}{R'_1} = \frac{h' + h_1}{R'_2} = \frac{h_1}{R'_2 - R'_1} \quad (\text{A.1})$$

Rearranging Equation (A.1) yields:

$$h' = R'_1 \tan \theta \quad (\text{A.2})$$

$$R'_2 = R'_1 + h_1 \cot \theta \quad (\text{A.3})$$

$$R'_2 = (h' + h_1) \cot \theta \quad (\text{A.4})$$

The volume of the half cone frustum $ABR'_1 R'_2$ is:

$$V_{cf} = \frac{1}{2} \cdot \frac{\pi}{3} [R_2'^2 (h' + h_1) - R_1'^2 h'] \quad (A.5)$$

Equations (A.1) and (A.5) yield:

$$V_{cf} = \frac{\pi}{6} \tan \theta [R_2'^3 - R_1'^3] \quad (A.6)$$

Equating the volume of the half-cylinder $ABCR_1$ and the half-cone frustrum, V_{cf} yields:

$$R_1'^2 = \frac{\tan \theta}{3 h_1} (R_2'^3 - R_1'^3) \quad (A.7)$$

Making use of Equation (A.3) in Equation (A.7) yields:

$$R_1'^2 + (h_1 \cot \theta) R_1' + \left[\frac{h_1^2 \cot^2 \theta}{3} - R_1'^2 \right] = 0 \quad (A.8)$$

For a specified minimum front radius R_1 and a front angle θ , it can be written:

$$R_1' = \frac{-(h_1 \cot \theta) + \sqrt{(h_1 \cot \theta)^2 + 4 \left(R_1'^2 - (h_1 \cot \theta)^2 / 3 \right)}}{2} \quad (A.9)$$

For any Layer j , Equation (A.9) can be written as:

$$R_j' = \frac{-(h_j \cot \theta) + \sqrt{(h_j \cot \theta)^2 + 4 \left(R_j'^2 - (h_j \cot \theta)^2 / 3 \right)}}{2} \quad (A.10)$$

For any Layer j , Equations (A.3) and (A.7) can be written as:

$$R_{j+1}' = R_j' + h_j \cot \theta \quad (A.11)$$

$$R_j = \sqrt{\frac{\tan \theta}{3 h_j} (R_{j+1}'^3 - R_j'^3)} \quad (A.12)$$

For a particular Layer j with a layer thickness h_j , and with an angle of inclination θ , Equations (A.11) and (A.12) can be used to calculate the front radius R_j .

Appendix B: Defining an Average Radius for a Multi-layered, Composite Reservoir with an Inclined Front (after Klome¹¹)

This appendix describes the calculation procedure of the average front radius for a tilted-front reservoir for Chapter 3. The swept volume of a multi-layer, composite reservoir with an inclined front can be represented by an equivalent swept volume in a single-layer, composite reservoir with a sharp front. This is done by equating the pore volume-compressibility products for the corresponding reservoirs. The expression for the average radius has been derived following Klome's¹¹ approach .

Consider an n-layer, composite reservoir (Figure 3.1b) with a layer front radius R_j and swept volume storativity $(\phi c_i h)_j$, where j represents the layer number. Let the equivalent single-layer reservoir have a storativity of $(\phi c_i)_{\text{err}}$ per unit reservoir thickness. Equating the storativity values for the two reservoirs gives:

$$\sum_{j=1}^n (\phi c_i h)_j = (\phi c_i)_{\text{err}} \sum_{j=1}^n h_j \quad (\text{B.1})$$

where h_j is the thickness of Layer j . Rearranging Equation (B.1) yields:

$$(\phi c_i)_{\text{err}} = \sum_{j=1}^n (\phi c_i h)_j / h_t \quad (\text{B.2})$$

where $h_t = \sum_{j=1}^n h_j$.

To obtain an appropriate definition of the average front radius, R_{avg} , the summation of the layer pore volumes and the compressibility product for all the layers has to be equal to the pore volume-compressibility product of the single-layer system. Thus:

$$\sum_{j=1}^n (\phi c_i \pi R_j^2 h)_j = (\phi c_i)_{\text{err}} \pi R_{\text{avg}}^2 h_t \quad (\text{B.3})$$

Rearranging Equation (B.3) yields:

$$R_{avg}^2 = \frac{\sum_{j=1}^n (\phi_{ci} R^2 h)_j}{(\phi_{ci})_{eff} h_i} \quad (B.4)$$

Substituting for $(\phi_{ci})_{eff}$ from Equation (B.2) into Equation (B.4) yields:

$$R_{avg} = \sqrt{\frac{\sum_{j=1}^n (\phi_{ci} R^2 h)_j}{\sum_{j=1}^n (\phi_{ci} h)_j}} \quad (B.5)$$

The transient-pressure responses of a multi-layer, composite reservoir can be compared with that of a single-layer, composite reservoir having equivalent reservoir properties. For example, transient-pressure responses of a multi-layer, composite reservoir having an inclined front with an average front radius of R_{avg} can be compared with that of a single-layer, composite reservoir having a sharp front located at R_{avg} . This definition of the average radius has been used in obtaining a correction factor for the estimation of the correct swept volume from the pseudosteady-state analysis. However, for this study, swept-region $\phi_{ci}h$ products for all layers are the same, and, thus, a simpler expression for R_{avg} is obtained from Equation (B.5) as:

$$R_{avg} = \sqrt{\sum_{j=1}^n R_j^2 / n} \quad (B.6)$$

Equation (B.6) describes R_{avg} as a root-mean-square front radius. Satman and Oskay⁶ proposed the square root of the sum of the square of the nearest and the farthest distances to the front as the representative average front radius. Such an approximation is inadequate for reservoirs having more than two layers and for irregularly-shaped fronts.

Appendix C: Pseudoskin Factor for Closed Top and Bottom Boundaries

This appendix shows the derivation of the late-time pressure and the pseudoskin factor expressions when the top and the bottom boundaries are closed for multi-layer reservoirs. This pseudoskin expression has been discussed in Chapter 4.

Late-Time Behaviour of a Partially-Penetrating Well in a Two-layer Reservoir with Pseudosteady-State Crossflow.

Figure 4.1 schematically shows a two-layer, partially-penetrated reservoir. Layer 1 is penetrated and Layer 2 is closed at the wellbore. The upper boundary of Layer 2 and the lower boundary of Layer 1 are considered as closed boundaries. Pseudosteady-state crossflow is considered between the two layers. The problem is solved following the steps taken by Bourdet²⁰. The diffusivity Equations for the two layers are:

$$\left(\frac{kh}{\mu}\right)_1 \left(\frac{\partial^2 p_1}{\partial r^2} + \frac{1}{r} \frac{\partial p_1}{\partial r} \right) = (\phi c_1 h)_1 \frac{\partial p_1}{\partial t} + X_A(p_1 - p_2) \quad (C.1)$$

$$\left(\frac{kh}{\mu}\right)_2 \left(\frac{\partial^2 p_2}{\partial r^2} + \frac{1}{r} \frac{\partial p_2}{\partial r} \right) = (\phi c_1 h)_2 \frac{\partial p_2}{\partial t} + X_A(p_2 - p_1) \quad (C.2)$$

$$\text{Initial condition: } p_1 = p_2 = p_m \quad (C.3)$$

$$\text{Outer boundary condition: } \lim_{r \rightarrow \infty} p_1 = \lim_{r \rightarrow \infty} p_2 = p_{ia} \quad (C.4)$$

Inner boundary condition: Assuming Layer 1 is penetrated and Layer 2 is closed, and neglecting wellbore storage and skin yield:

$$p_1 = p_w \quad \text{for } r = r_w \quad (C.5)$$

$$\left(\frac{\partial p_2}{\partial r} \right)_{r=r_w} = 0 \quad (C.6)$$

$$q = 2\pi \left(\frac{kh}{\mu} \right)_1 \left(r \frac{\partial p_1}{\partial r} \right)_{r=r_0} \quad (C.7)$$

Dimensionless variables are defined as follows:

$$p_{D1,2} = \frac{2\pi}{q} \left(\frac{kh}{\mu} \right) (p_{in} - p_{1,2}) \quad (C.8)$$

$$t_D = \frac{\left(\frac{kh}{\mu} \right)}{(\phi c_i h)} \frac{1}{r_w^2} \quad (C.9)$$

$$\text{where, } \left(\frac{kh}{\mu} \right) = \left(\frac{kh}{\mu} \right)_1 + \left(\frac{kh}{\mu} \right)_2, \text{ and} \quad (C.10)$$

$$(\phi c_i h) = (\phi c_i h)_1 + (\phi c_i h)_2 \quad (C.11)$$

All other dimensionless parameters are defined in the Nomenclature.

The differential Equations and the boundary conditions can be written in dimensionless form as:

$$\kappa \nabla^2 p_{D1} = \omega \frac{\partial p_{D1}}{\partial t_D} + \lambda_A (p_{D1} - p_{D2}) \quad (C.12)$$

$$(1 - \kappa) \nabla^2 p_{D2} = (1 - \omega) \frac{\partial p_{D2}}{\partial t_D} + \lambda_A (p_{D2} - p_{D1}) \quad (C.13)$$

$$\text{Initial condition: } p_{D1}(r_D, 0) = p_{D2}(r_D, 0) = 0 \quad (C.14)$$

$$\text{Outer boundary condition: } \lim_{r_D \rightarrow \infty} p_{D1} = \lim_{r_D \rightarrow \infty} p_{D2} = 0 \quad (C.15)$$

$$\text{Inner boundary condition: } p_{D1}(1, t_D) = p_{wD} \quad (C.16)$$

$$\left(\frac{\partial p_{D2}}{\partial r_D} \right)_{r_D=1} = 0 \quad (C.17)$$

$$1 = -\kappa \left(\frac{\partial p_{D1}}{\partial r_D} \right)_{r_D=1} \quad (C.18)$$

Taking the Laplace transform of Equations (C.12) through (C.18) yields:

$$\kappa \nabla^2 \bar{p}_{D1} = \omega \bar{p}_{D1} + \lambda_A (\bar{p}_{D1} - \bar{p}_{D2}) \quad (C.19)$$

$$(1 - \kappa) \nabla^2 \bar{p}_{D2} = (1 - \omega) \bar{p}_{D2} + \lambda_A (\bar{p}_{D2} - \bar{p}_{D1}) \quad (C.20)$$

$$\text{Outer boundary condition: } \lim_{r_D \rightarrow \infty} \bar{p}_{D1} = \lim_{r_D \rightarrow \infty} \bar{p}_{D2} = 0 \quad (C.21)$$

$$\text{Inner boundary condition: } \bar{p}_{D1}(1, s) = \bar{p}_{wD} \quad (C.22)$$

$$\left(\frac{\partial \bar{p}_{D2}}{\partial r_D} \right)_{r_D=1} = 0 \quad (C.23)$$

$$\frac{1}{l} = -\kappa \left(\frac{\partial \bar{p}_{D1}}{\partial r_D} \right)_{r_D=1} \quad (C.24)$$

Solutions of Equations (C.19) and (C.20) are modified Bessel's functions, $I_0(\sigma r_D)$ and $K_0(\sigma r_D)$, where σ is the eigenvalue of the system. For an infinite system, only the $K_0(\sigma r_D)$ function applies. Therefore,

$$\bar{p}_{D1} = A' K_0(\sigma r_D) \quad (C.25)$$

$$\bar{p}_{D2} = B' K_0(\sigma r_D) \quad (C.26)$$

Equations (C.19) and (C.20) together with Equations (C.25) and (C.26) yield:

$$\kappa \sigma^2 A' K_0(\sigma r_D) = \omega A' K_0(\sigma r_D) + \lambda_A [A' K_0(\sigma r_D) - B' K_0(\sigma r_D)] \quad (C.27)$$

$$(1 - \kappa) \sigma^2 B' K_0(\sigma r_D) = (1 - \omega) B' K_0(\sigma r_D) + \lambda_A [B' K_0(\sigma r_D) - A' K_0(\sigma r_D)] \quad (C.28)$$

Equations (C.27) and (C.28) reduce to:

$$[\kappa \sigma^2 - \omega - \lambda_A] A' + \lambda_A B' = 0 \quad (C.29)$$

$$\lambda_A A' + [(1 - \kappa) \sigma^2 - (1 - \omega) - \lambda_A] B' = 0 \quad (C.30)$$

Non-trivial solutions are possible, if the determinant is zero, that is,

$$(\kappa\sigma^2 - \omega l - \lambda_A)[(1 - \kappa)\sigma^2 - (1 - \omega)l - \lambda_A] - \lambda_A^2 = 0 \quad (\text{C.31})$$

Equation (C.31) can be reorganized as:

$$\sigma^4 - \left[\frac{(1 - \omega)l + \lambda_A}{1 - \kappa} + \frac{\omega l + \lambda_A}{\kappa} \right] \sigma^2 + \frac{[\omega l (1 - \omega) + \lambda_A]l}{\kappa(1 - \kappa)} = 0 \quad (\text{C.32})$$

This polynomial has two positive roots and they are:

$$\sigma_1^2 = \frac{1}{2} \left[\left(\frac{(1 - \omega)l + \lambda_A}{1 - \kappa} + \frac{\omega l + \lambda_A}{\kappa} \right) + \Delta \right] \quad (\text{C.33})$$

$$\sigma_2^2 = \frac{1}{2} \left[\left(\frac{(1 - \omega)l + \lambda_A}{1 - \kappa} + \frac{\omega l + \lambda_A}{\kappa} \right) - \Delta \right] \quad (\text{C.34})$$

$$\text{where, } \Delta = \left[\left(\frac{(1 - \omega)l + \lambda_A}{1 - \kappa} - \frac{\omega l + \lambda_A}{\kappa} \right)^2 + \frac{4\lambda_A^2}{\kappa(1 - \kappa)} \right]^{\frac{1}{2}} \quad (\text{C.35})$$

Putting σ_1^2 and σ_2^2 from Equations (C.33) and (C.34), respectively, into Equation (C.30) and rearranging yield:

$$a_1 = \frac{A_1}{B_1} = 1 + \frac{1}{\lambda_A} [(1 - \omega)l - (1 - \kappa)\sigma_1^2] \quad (\text{C.36})$$

$$a_2 = \frac{A_2}{B_2} = 1 + \frac{1}{\lambda_A} [(1 - \omega)l - (1 - \kappa)\sigma_2^2] \quad (\text{C.37})$$

Putting $A_1 = a_1 B_1$ and $A_2 = a_2 B_2$ in Equations (C.25) and (C.26) yields:

$$F_{D1} = a_1 B_1 K_0(\sigma_1 r_D) + a_2 B_2 K_0(\sigma_2 r_D) \quad (\text{C.38})$$

$$F_{D2} = B_1 K_0(\sigma_1 r_D) + B_2 K_0(\sigma_2 r_D) \quad (\text{C.39})$$

Equations (C.38) and (C.39) together with Equations (C.22) and (C.23) yield:

$$B_1 = - \frac{B_2 \sigma_2 K_1(\sigma_2)}{\sigma_1 K_1(\sigma_1)} \quad (C.40)$$

Equations (C.38) and (C.39) together with Equation (C.24) yields:

$$\frac{1}{\kappa l} = a_1 B_1 \sigma_1 K_1(\sigma_1) + a_2 B_2 \sigma_2 K_1(\sigma_2) \quad (C.41)$$

Equations (C.40) and (C.41) yields:

$$B_1 = - \frac{1}{(a_2 - a_1) \kappa l \sigma_1 K_1(\sigma_1)} \quad (C.42)$$

$$B_2 = \frac{1}{(a_2 - a_1) \kappa l \sigma_2 K_1(\sigma_2)} \quad (C.43)$$

Now, Equation (C.38) becomes:

$$\bar{p}_{wD} = - \frac{a_1 K_0(\sigma_1)}{(a_2 - a_1) \kappa l \sigma_1 K_1(\sigma_1)} + \frac{a_2 K_0(\sigma_2)}{(a_2 - a_1) \kappa l \sigma_2 K_1(\sigma_2)} \quad (C.44)$$

Equation (C.44) represents the pressure transient responses of a partially-penetrating well in a two-layer reservoir in Laplace space and these responses are numerically inverted to real space using the Stehfest algorithm²⁸.

Late-Time Behaviour for a Partially-Penetrating Well with No Bottom-Water Zone or Gas Cap

At late time $t_D \rightarrow \infty$ and $l \rightarrow 0$, and Equations (C.33) through (C.37) become:

$$\lim_{l \rightarrow 0} \Delta = \lim_{l \rightarrow 0} \left[\left(\frac{\lambda_A}{1 - \kappa} + \frac{\lambda_A}{\kappa} \right)^2 + l[\dots] + l^2[\dots] \right]^{\frac{1}{2}} = \frac{\lambda_A}{\kappa(1 - \kappa)} \quad (C.45)$$

$$\lim_{l \rightarrow 0} \sigma_1^2 = \lim_{l \rightarrow 0} \left[\frac{\lambda_A}{1 - \kappa} + \frac{\lambda_A}{\kappa} + l[\dots] + l^2[\dots] \right] = \frac{\lambda_A}{\kappa(1 - \kappa)} \quad (C.46)$$

$$\lim_{l \rightarrow 0} \sigma_2^2 = \lim_{l \rightarrow 0} \frac{1}{2} \left[\frac{1 - \kappa}{1 - \kappa} + \frac{\kappa}{\kappa} \cdot \frac{1 - \kappa}{1 - \kappa} + \frac{\kappa}{\kappa} \right] = 1 \quad (C.47)$$

Appendix E shows the simplification proposed in Equation (C.47) in detail.

$$\lim_{l \rightarrow 0} a_1 = \lim_{l \rightarrow 0} \left[1 + \frac{(1 - \omega)l - (1 - \kappa) \sigma_1^2}{\lambda_A} \right] = \frac{\kappa - 1}{\kappa} \quad (C.48)$$

$$\lim_{l \rightarrow 0} a_2 = \lim_{l \rightarrow 0} \left[1 + \frac{(1 - \omega)l - (1 - \kappa) \sigma_2^2}{\lambda_A} \right] = 1 \quad (C.49)$$

Using the late-time limits shown in Equations (C.45) through (C.49), Equation (C.44) may be written as:

$$P_{wD} = \frac{(1 - \kappa)}{\kappa l} \frac{K_0 \left(\sqrt{\frac{\lambda_A}{\kappa(1 - \kappa)}} \right)}{\sqrt{\frac{\lambda_A}{\kappa(1 - \kappa)}} K_1 \left(\sqrt{\frac{\lambda_A}{\kappa(1 - \kappa)}} \right)} + \frac{K_0(\sqrt{l})}{l \sqrt{l} K_1(\sqrt{l})} \quad (C.50)$$

The first term in Equation (C.50) is a constant and it represents the additional pressure drop because of partial penetration, which is usually known as pseudoskin. The second term in Equation (C.50) represents the equivalent infinite, homogeneous reservoir response for the whole reservoir. So, for a two-layer reservoir, the expression for pseudoskin is:

$$s_p = \frac{(1 - \kappa)}{\kappa} \frac{K_0 \left(\sqrt{\frac{\lambda_A}{\kappa(1 - \kappa)}} \right)}{\sqrt{\frac{\lambda_A}{\kappa(1 - \kappa)}} K_1 \left(\sqrt{\frac{\lambda_A}{\kappa(1 - \kappa)}} \right)} \quad (C.51)$$

Equation (C.51) can be extended for a multi-layer reservoir by appropriately defining κ and λ_A :

$$s_p = \frac{(1 - \bar{\kappa})}{\bar{\kappa}} \frac{K_0 \left(\sqrt{\frac{\bar{\lambda}_A}{\bar{\kappa}(1 - \bar{\kappa})}} \right)}{\sqrt{\frac{\bar{\lambda}_A}{\bar{\kappa}(1 - \bar{\kappa})}} K_1 \left(\sqrt{\frac{\bar{\lambda}_A}{\bar{\kappa}(1 - \bar{\kappa})}} \right)} \quad (C.52)$$

where, $\bar{\kappa}$ = Total mobility-thickness ratio of the open interval

$\bar{\lambda}_A$ = Total crossflow parameter

Equation (C.52) is applicable for a multi-layer reservoir having any arbitrary number of layers making up the open interval and any arbitrary location of the open interval. In Equation (C.52), $\bar{\kappa}$ and $\bar{\lambda}_A$ are calculated by adding the individual layer mobility-thickness ratio of the open interval and by adding the lower and the upper boundary crossflow parameters, respectively. Irrespective of the number of layers in the reservoir, only two parameters are required to estimate the pseudoskin. A similar treatment for a reservoir subject to a gas-cap drive (or a bottom-water drive) is shown in Appendix D.

Appendix D: Pseudoskin Factor for a Gas-Cap Condition

This appendix shows the derivation of the late-time pressure and the pseudoskin factor expressions when the multi-layer reservoir is under an infinitely-large gas-cap drive. This pseudoskin expression has been discussed in Chapter 4.

Late-Time Behaviour of a Partially-Penetrated Well in a Two-layer Reservoir Subject to a Gas-Cap Drive.

Figure 4.2 schematically shows a two-layer, partially-penetrated reservoir subject to a gas-cap drive. The gas cap is assumed to be very large compared to the size of the reservoir and the boundary between the reservoir and the gas cap is considered to be at constant pressure. Layer 1 is penetrated and Layer 2 is closed at the wellbore. The upper boundary of Layer 2 is considered as a constant-pressure boundary because of gas cap, whereas the lower boundary of Layer 1 is considered as a closed boundary. Pseudosteady-state crossflow is considered between the two layers. The diffusivity Equations for the two layers are:

$$\left(\frac{kh}{\mu}\right)_1 \left(\frac{\partial^2 p_1}{\partial r^2} + \frac{1}{r} \frac{\partial p_1}{\partial r} \right) = (\phi c_1 h)_1 \frac{\partial p_1}{\partial t} + X_A(p_1 - p_2) \quad (D.1)$$

$$\left(\frac{kh}{\mu}\right)_2 \left(\frac{\partial^2 p_2}{\partial r^2} + \frac{1}{r} \frac{\partial p_2}{\partial r} \right) = (\phi c_1 h)_2 \frac{\partial p_2}{\partial t} + X_A(p_2 - p_1) + X_C(p_2 - p_{in}) \quad (D.2)$$

Inner and outer boundary conditions, and the initial condition are the same as in Appendix C. In dimensionless form, the differential equations and the boundary conditions can be written as:

$$\kappa \nabla^2 p_{D1} = \omega \frac{\partial p_{D1}}{\partial t_D} + \lambda_A(p_{D1} - p_{D2}) \quad (D.3)$$

$$(1 - \kappa) \nabla^2 p_{D2} = (1 - \omega) \frac{\partial p_{D2}}{\partial t_D} + \lambda_A(p_{D2} - p_{D1}) + \lambda_C p_{D2} \quad (D.4)$$

$$\text{Initial condition: } p_{D1}(r_D, 0) = p_{D2}(r_D, 0) = 0 \quad (\text{D.5})$$

$$\text{Outer boundary condition: } \lim_{r_D \rightarrow \infty} p_{D1} = \lim_{r_D \rightarrow \infty} p_{D2} = 0 \quad (\text{D.6})$$

$$\text{Inner boundary condition: } p_{D1}(1, t_D) = p_{wD} \quad (\text{D.7})$$

$$\left(\frac{\partial p_{D1}}{\partial r_D} \right)_{r_D=1} = 0 \quad (\text{D.8})$$

$$1 = -\kappa \left(\frac{\partial p_{D1}}{\partial r_D} \right)_{r_D=1} \quad (\text{D.9})$$

Following the same steps as in Appendix C, one can obtain:

$$[\kappa\sigma^2 - \omega' - \lambda_A]A + \lambda_A B = 0 \quad (\text{D.10})$$

$$\lambda_A A + [(1 - \kappa)\sigma^2 - (1 - \omega)' - \lambda_A - \lambda_C]B = 0 \quad (\text{D.11})$$

Non-trivial solutions are possible, if the determinant is zero, that is,

$$(\kappa\sigma^2 - \omega' - \lambda_A)[(1 - \kappa)\sigma^2 - (1 - \omega)' - \lambda_A - \lambda_C] - \lambda_A^2 = 0 \quad (\text{D.12})$$

Equation (D.12) can be reorganized as:

$$\sigma^4 - \left[\frac{(1 - \omega)' + \lambda_A + \lambda_C}{1 - \kappa} + \frac{\omega' + \lambda_A}{\kappa} \right] \sigma^2 + \frac{(\omega' + \lambda_A)[(1 - \omega)' + \lambda_A + \lambda_C] - \lambda_A^2}{\kappa(1 - \kappa)} = 0 \quad (\text{D.13})$$

This polynomial has two positive roots and these are:

$$\sigma_1^2 = \frac{1}{2} \left[\left(\frac{(1 - \omega)' + \lambda_A + \lambda_C}{1 - \kappa} + \frac{\omega' + \lambda_A}{\kappa} \right) + \Delta \right] \quad (\text{D.14})$$

$$\sigma_2^2 = \frac{1}{2} \left[\left(\frac{(1 - \omega)' + \lambda_A + \lambda_C}{1 - \kappa} + \frac{\omega' + \lambda_A}{\kappa} \right) - \Delta \right] \quad (\text{D.15})$$

$$\text{where, } \Delta = \left[\left(\frac{(1-\omega)\lambda + \lambda_A + \lambda_C}{1-\kappa} + \frac{\omega\lambda + \lambda_A}{\kappa} \right)^2 - \frac{4(\omega\lambda + \lambda_A)[(1-\omega)\lambda + \lambda_A + \lambda_C] - \lambda_A^2}{\kappa(1-\kappa)} \right]^{\frac{1}{2}} \quad (\text{D.16})$$

Putting σ_1^2 and σ_2^2 from Equations (D.14) and (D.15), respectively, into Equation (D.11) and rearranging, one can write:

$$a_1 = \frac{A_1}{B_1} = 1 + \frac{\lambda_C}{\lambda_A} + \frac{1}{\lambda_A} [(1-\omega)\lambda - (1-\kappa)\sigma_1^2] \quad (\text{D.17})$$

$$a_2 = \frac{A_2}{B_2} = 1 + \frac{\lambda_C}{\lambda_A} + \frac{1}{\lambda_A} [(1-\omega)\lambda - (1-\kappa)\sigma_2^2] \quad (\text{D.18})$$

As in Appendix A, putting $A_1 = a_1 B_1$ and $A_2 = a_2 B_2$ in the solution yields:

$$\bar{p}_{D1} = a_1 B_1 K_0(\sigma_1 r_D) + a_2 B_2 K_0(\sigma_2 r_D) \quad (\text{D.19})$$

$$\bar{p}_{D2} = B_1 K_0(\sigma_1 r_D) + B_2 K_0(\sigma_2 r_D) \quad (\text{D.20})$$

Again, following the same steps as in Appendix C, one can obtain the expression for the wellbore pressure as:

$$\bar{p}_{wD} = - \frac{a_1 K_0(\sigma_1)}{(a_2 - a_1)\omega' \sigma_1 K_1(\sigma_1)} + \frac{a_2 K_0(\sigma_2)}{(a_2 - a_1)\omega' \sigma_2 K_1(\sigma_2)} \quad (\text{D.21})$$

Equation (D.21) represents pressure transient responses in Laplace space of a partially-penetrating well in a two-layer reservoir subject to a gas-cap drive and these responses are numerically inverted to real space using the Stehfest Algorithm²⁸.

Late-Time Behaviour for a Partially-Penetrating Well Under a Gas-cap Drive

At late time $t_D \rightarrow \infty$ and $l \rightarrow 0$, and Equations (D.14) through (D.18) become:

$$\lim_{t \rightarrow 0} \sigma_1^2 = \sigma_{1L}^2 = \frac{1}{2} \left[\frac{\lambda_A + \lambda_C}{1 - \kappa} + \frac{\lambda_A}{\kappa} + \left(\left(\frac{\lambda_A + \lambda_C}{1 - \kappa} + \frac{\lambda_A}{\kappa} \right)^2 - \frac{4\lambda_A\lambda_C}{(1 - \kappa)\kappa} \right)^{\frac{1}{2}} \right] \quad (D.22)$$

$$\lim_{t \rightarrow 0} \sigma_2^2 = \sigma_{2L}^2 = \frac{1}{2} \left[\frac{\lambda_A + \lambda_C}{1 - \kappa} + \frac{\lambda_A}{\kappa} - \left(\left(\frac{\lambda_A + \lambda_C}{1 - \kappa} + \frac{\lambda_A}{\kappa} \right)^2 - \frac{4\lambda_A\lambda_C}{(1 - \kappa)\kappa} \right)^{\frac{1}{2}} \right] \quad (D.23)$$

$$\lim_{t \rightarrow 0} \Delta = \left[\left(\frac{\lambda_A + \lambda_C}{1 - \kappa} + \frac{\lambda_A}{\kappa} \right)^2 - \frac{4\lambda_A\lambda_C}{(1 - \kappa)\kappa} \right]^{\frac{1}{2}} \quad (D.24)$$

$$\lim_{t \rightarrow 0} a_1 = a_{1L} = 1 + \frac{\lambda_C}{\lambda_A} - \frac{(1 - \kappa)}{2\lambda_A} \left[\frac{\lambda_A + \lambda_C}{1 - \kappa} + \frac{\lambda_A}{\kappa} + \left(\left(\frac{\lambda_A + \lambda_C}{1 - \kappa} + \frac{\lambda_A}{\kappa} \right)^2 - \frac{4\lambda_A\lambda_C}{(1 - \kappa)\kappa} \right)^{\frac{1}{2}} \right] \quad (D.25)$$

$$\lim_{t \rightarrow 0} a_2 = a_{2L} = 1 + \frac{\lambda_C}{\lambda_A} - \frac{(1 - \kappa)}{2\lambda_A} \left[\frac{\lambda_A + \lambda_C}{1 - \kappa} + \frac{\lambda_A}{\kappa} - \left(\left(\frac{\lambda_A + \lambda_C}{1 - \kappa} + \frac{\lambda_A}{\kappa} \right)^2 - \frac{4\lambda_A\lambda_C}{(1 - \kappa)\kappa} \right)^{\frac{1}{2}} \right] \quad (D.26)$$

Using the late-time limits shown in Equations (D.22) through (D.26), Equation (D.21) may be written as:

$$P_{wDPL} = - \frac{a_{1L}K_0(\sigma_{1L})}{(a_{2L} - a_{1L})\omega\sigma_{1L}K_1(\sigma_{1L})} + \frac{a_{2L}K_0(\sigma_{2L})}{(a_{2L} - a_{1L})\omega\sigma_{2L}K_1(\sigma_{2L})} \quad (D.27)$$

Equation (D.27) denotes the limiting pressure drop in Laplace space for a partially-penetrating well subject to a gas-cap drive. Taking the inverse Laplace transform of Equation (D.27), one can obtain the corresponding pressure drop in the real space as:

$$P_{wDPL} = - \frac{a_{1L}K_0(\sigma_{1L})}{(a_{2L} - a_{1L})\omega\sigma_{1L}K_1(\sigma_{1L})} + \frac{a_{2L}K_0(\sigma_{2L})}{(a_{2L} - a_{1L})\omega\sigma_{2L}K_1(\sigma_{2L})} \quad (D.28)$$

Performing the same treatment for a fully-penetrating well in a two-layer reservoir subject to a gas-cap drive, one can obtain:

$$p_{wDFL} = \frac{(a_{2L} - a_{1L})K_0(\sigma_{1L}) K_0(\sigma_{2L})}{b_L} \quad (D.29)$$

where,

$$b_L = (1 - a_{1L})(\kappa a_{2L} + 1 - \kappa)\sigma_{2L}K_0(\sigma_{1L})K_1(\sigma_{2L}) - (1 - a_{2L})(\kappa a_{1L} + 1 - \kappa)\sigma_{1L}K_0(\sigma_{2L})K_1(\sigma_{1L}) \quad (D.30)$$

The difference between Equations (D.28) and (D.29) is the additional pressure drop because of the partial penetration of a two-layer reservoir subject to a gas-cap drive. Therefore, the expression for the pseudoskin for this case is:

$$s_b = \frac{a_{2L}K_0(\sigma_{2L})}{(a_{2L} - a_{1L})\kappa\sigma_{2L}K_1(\sigma_{2L})} - \frac{a_{1L}K_0(\sigma_{1L})}{(a_{2L} - a_{1L})\kappa\sigma_{1L}K_1(\sigma_{1L})} - \frac{(a_{2L} - a_{1L})K_0(\sigma_{1L}) K_0(\sigma_{2L})}{b_L} \quad (D.31)$$

Equation (D.31) estimates the pseudoskin in a two-layer, partially-penetrated reservoir subject to a gas-cap or a bottom-water drive. Equation (D.31) is also applicable for a multi-layer reservoir having any arbitrary number of layers making up the open interval and any arbitrary location of the open interval, provided κ and λ_A are calculated by adding the individual layer mobility-thickness ratio of the open interval and by adding the lower and the upper boundary crossflow parameters of the open interval, respectively. Parameter, λ_C , is the crossflow parameter between the reservoir and the gas cap or the bottom-water zone. Irrespective of the number of layers in the reservoir, only three parameters (κ , λ_A , λ_C) are required to estimate the pseudoskin factor.

Appendix E: Late-Time Approximation of σ_2^2

This appendix shows the simplification proposed in Equation (C.47) of Appendix C in detail.

From Appendix C,

$$\sigma_2^2 = \frac{1}{2} \left[\left(\frac{\lambda_A}{1-\kappa} + \frac{\lambda_A}{\kappa} + \left(\frac{1-\omega}{1-\kappa} + \frac{\omega}{\kappa} \right) l \right) \cdot \Delta \right] \quad (\text{E.1})$$

$$\text{and, } \lim_{l \rightarrow \infty} \Delta = \lim_{l \rightarrow \infty} \left[\left(\frac{(1-\omega)l + \lambda_A}{1-\kappa} - \frac{\omega l + \lambda_A}{\kappa} \right)^2 + \frac{4\lambda_A^2}{\kappa(1-\kappa)} \right]^{\frac{1}{2}} \quad (\text{E.2})$$

Equation (E.2) can be written as:

$$\lim_{l \rightarrow \infty} \Delta = \lim_{l \rightarrow \infty} \left[\left(\frac{\lambda_A}{1-\kappa} - \frac{\lambda_A}{\kappa} \right)^2 \left\{ 1 + \frac{\frac{1-\omega}{1-\kappa} - \frac{\omega}{\kappa}}{2} l + \left(\frac{\frac{1-\omega}{1-\kappa} - \frac{\omega}{\kappa}}{2} \right)^2 l^2 \right\} + \frac{4\lambda_A^2}{\kappa(1-\kappa)} \right]^{\frac{1}{2}} \quad (\text{E.3})$$

Neglecting the term containing l^2 and rearranging Equation (E.3) yields:

$$\lim_{l \rightarrow \infty} \Delta = \lim_{l \rightarrow \infty} \left(\frac{\lambda_A}{1-\kappa} + \frac{\lambda_A}{\kappa} \right) \left[1 + \frac{\left(\frac{1-\omega}{1-\kappa} - \frac{\omega}{\kappa} \right) \left(\frac{\lambda_A}{1-\kappa} - \frac{\lambda_A}{\kappa} \right)}{\left(\frac{\lambda_A}{1-\kappa} + \frac{\lambda_A}{\kappa} \right)^2} l \right]^{\frac{1}{2}} \quad (\text{E.4})$$

Expanding Equation (E.4) using the binomial theorem yields:

$$\lim_{l \rightarrow \infty} \Delta = \lim_{l \rightarrow \infty} \left(\frac{\lambda_A}{1-\kappa} + \frac{\lambda_A}{\kappa} \right) \left[1 + \frac{\left(\frac{1-\omega}{1-\kappa} - \frac{\omega}{\kappa} \right) \left(\frac{\lambda_A}{1-\kappa} - \frac{\lambda_A}{\kappa} \right)}{\left(\frac{\lambda_A}{1-\kappa} + \frac{\lambda_A}{\kappa} \right)^2} l - (\dots) l^2 + (\dots) l^3 - \dots \right] \quad (\text{E.5})$$

Neglecting the higher order terms in l in Equation (E.5) yields:

$$\Delta = \left[\frac{\lambda_A}{1-\kappa} + \frac{\lambda_A}{\kappa} + \left(\frac{1-\omega}{1-\kappa} - \frac{\omega}{\kappa} \right) (2\kappa - 1) \gamma \right] \quad (\text{E.6})$$

At late times, the reservoir behaves like a fully-penetrated, equivalent homogeneous system with s pseudoskin. Thus, at late time, $\kappa = \omega = 1$, and Equation (E.6) becomes:

$$\Delta = \left[\frac{\lambda_A}{1-\kappa} + \frac{\lambda_A}{\kappa} + \left(\frac{1-\omega}{1-\kappa} - \frac{\omega}{\kappa} \right) \gamma \right] \quad (\text{E.7})$$

Now, Equation (E.1) becomes:

$$\sigma_2^2 = \frac{\omega}{\kappa} = 1 \quad (\text{E.8})$$

Appendix F: Computer Program

This appendix shows the computer program for the analytical solution developed in this study. This computer program has been described in Chapter 6.

SOURCE CODE FOR THE PROGRAM: GENERAL

```
*****
C   Source code for program GENERAL to generate the transient pressure responses for a
C   well in a multi-layered, composite reservoir
C   (This program is written in FORTRAN 77 and in SI units)
C
C   PROGRAM GENERAL
C
C   Major assumptions are :
C   Single phase flow in a radial flow geometry
C   Layered system with communicating strata
C
C   Constant total surface rate
C   Constant wellbore storage coefficient
C   A given layer is of constant thickness across different zones for that layer, but
C   different layers can be of different thicknesses
C   Slightly compressible fluid with constant viscosity and compressibility
C   Instantaneous sand face pressure at the wellbore location is the same for all the
C   layers
C
C   *****
C   Variable identification list
C   *****
C   CD --- Wellbore storage
C   CT(I,J) --- Compressibility for zone i and layer j
C   H(J) --- Thickness for the jth layer
C   HT --- Total reservoir thickness
C   NLAYER --- Number of layers in the reservoir
C   NFL(J) --- Codes for penetration for layer j
```

C RD(J) --- Wellbore radius (j=1) and front radii (j=2,3,...)
 C RDAV --- Average front radius
 C SK(J) --- Wellbore skin at the jth layer
 C ST(I,J) --- Storativity for zone i and layer j
 C TD --- Dimensionless time
 C TPD --- Dimensionless producing time
 C TS(I,J) --- Transmissibility for layer j and zone i
 C TTS --- Total transmissibility
 C TST --- Total storativity
 C XA(I,J) --- Crossflow parameter for zone i and layer j and j+1
 C XB(I,J) --- Crossflow parameter for zone i and layer j and j-1

C
 C

```

IMPLICIT REAL*8(A-H,O-Z)
  DIMENSION TD(20),H(3),RED(3),RK(4,3),RMU(4,3),PHI(4,3),RKV(4,3
+ ),CT(4,3)
  COMMON/GM1/ CD,RD(5),SK(3),ST(4,3),TS(4,3),RM(3,3),JCODE,
+ NLayer,XA(4,3),XB(4,3),JWELL,LCODE,NPL(3)
  
```

C

C Opening output files

C

C For drawdown

C

C PD --- Contains PWD as a function of TD data

C PDP --- Contains semi-log slope as a function of TD data

C PDC --- Contains Cartesian slope as a function of TD data

C

C For buildup

C

C PD --- Contains PWDS as a function of delta TDE data

C PDP --- Contains Agarwal slope as a function of TDE data

C PDC --- Contains Cartesian slope as a function of delta TDA data

C PDH --- Contains MDH slope as a function of delta TDE data

C

```

OPEN(UNIT=7,FILE='PD',STATUS='OLD')
  
```

```

OPEN(UNIT=8,FILE='PDP',STATUS='OLD')
  
```

```
OPEN(UNIT=9,FILE='PDC',STATUS='OLD')
OPEN(UNIT=10,FILE='PDH',STATUS='OLD')
```

C Unformatted read section

```
PRINT*, 'GIVE THE VALUE OF NLAYER'
READ(5,*)NLAYER
NN=NLAYER+1
PRINT*, 'GIVE THE LAYER NUMBER, JWELL, FOR WHICH WELLBORE
PRESSURE WILL BE CALCULATED'
READ(5,*)JWELL
PRINT*, 'READ THE VALUE OF CD AND SKIN'
READ(5,*)CD, (SK(I), I=1, NLAYER)
PRINT*, '# OF CYCLES OF DATA REQUIRED'
READ(5,*)NC
PRINT*, 'GIVE FIRST VALUE OF TD (BASED ON MINIMUM FRONT RADIUS)'
READ(5,*)TD1
PRINT*, 'NUMBER OF TERMS TO BE USED IN STEHFEST'
READ(5,*)NTF&M
```

C

C Read codes for drawdown or buildup response

```
PRINT*, 'RESPONSE FUNCTION CODES:'
PRINT*, '1 --- DRAWDOWN'
PRINT*, '2 --- BUILDUP'
READ(5,*)ICODE
```

C

C Read codes for the outer boundary condition

```
PRINT*, 'SUPPLY OUTER BOUNDARY CONDITION CODES'
PRINT*, '1 --- INFINITE'
PRINT*, '2 --- CLOSED'
PRINT*, '3 --- CONSTANT PRESSURE'
READ(5,*)JCODE
```

C

C Read codes for the bottom water or gas cap

```
PRINT*, 'SUPPLY CODES FOR GAS CAP AND BOTTOM WATER'
PRINT*, '1 --- NO GAS CAP OR BOTTOM WATER'
PRINT*, '2 --- GAS CAP'
```

```

PRINT*, '3 --- BOTTOM WATER'
READ(5,*)KCODE
C
IF(ICODE.EQ.2)THEN
  PRINT*, 'DIMENSIONLESS PRODUCING TIME(BASED ON RW)'
  READ(5,*)TPD
ENDIF
C
IF(JCODE.NE.1)THEN
  PRINT*, 'DIMENSIONLESS OUTER RADIUS '
  READ(5,*)RD(NLAYER+2)
ELSE
C   For infinite reservoir a fictitious radius is supplied
RD(NLAYER+2)=1.0D30
ENDIF
PRINT*, 'READ THE VALUES OF PERMEABILITIES RK(I,J), I=ZONE,
      J=LAYER'
READ(5,*)(RK(I,J),I=1,NN),J=1,NLAYER)
PRINT*, 'READ THE VALUES OF VERTICAL PERMS RKV(I,J)'
READ(5,*)(RKV(I,J),I=1,NN),J=1,NLAYER)
PRINT*, 'READ THE VALUES OF VISCOSITIES, RMU(I,J)'
READ(5,*)(RMU(I,J),I=1,NN),J=1,NLAYER)
PRINT*, 'READ THE VALUES OF POROSITIES , PHI(I,J)'
READ(5,*)(PHI(I,J),I=1,NN),J=1,NLAYER)
PRINT*, 'READ THE VALUES OF COMPRESSIBILITIES, CT(I,J)'
READ(5,*)(CT(I,J),I=1,NN),J=1,NLAYER)
PRINT*, 'READ THE VALUES OF LAYER THICKNESS H(J) AND HT,'
READ(5,*)HT,(H(J),J=1,NLAYER)
PRINT*, 'OPTION FOR RDAVG CALC., IRDAV=1 OR 0'
READ(5,*)IRDAV
PRINT*, 'OPTION FOR FRONT RADII CALC., IRADII=1 OR 0'
READ(5,*)IRADII
IF(IRADII.EQ.1)THEN
PRINT*, 'PRINT WELLBORE RADIUS, MINIMUM FRONT RADIUS AND THE
      FRONT ANGLE'
READ(5,*)RD(1),RD(2),ANGLE

```

```

ELSE
PRINT*, 'PRINT WELLBORE RADIUS AND THE FRONT RADII'
READ(5,*)(RD(J),J=1,NN)
ENDIF
PRINT*, 'ENTER CODE , LCODE, FOR FULLY- OR PARTIALLY
        PENETRATING WELL, 0 = FULL 1 = PARTIAL PENETRATION'
READ(5,*)LCODE
IF(LCODE.EQ.1)THEN
PRINT*, 'GIVE CODES NPL(J) FOR PENETRATION FOR LAYER J'
PRINT8, 'NPL(J)=0 (NONPENETRATED), NPL(J)=1 (PENETRATED)'
READ(5,*)(NPL(J),J=1,NLAYER)
ENDIF
C
C ***** Input section ends *****
C
C Subroutine TAB calculates front radii when minimum front radius and front angle are
C supplied
IF(IRADII.EQ.1)THEN
CALL TAB(NLAYER,ANGLE,H(J),HT,RD)
ENDIF
C
C Calculation of average front radius, RDAV
IF(IRDAV.EQ.1)THEN
SUM1=0.0D00
SUM2=0.0D00
DO 31 J=1,NLAYER
C1=PHI(1,J)*CT(1,J)*H(J)
C2=C1*RD(J+1)*RD(J+1)
SUM1=SUM1+C1
SUM2=SUM2+C2
31 CONTINUE
C3=SUM2/SUM1
RDAV=DSQRT(C3)
RDAV=RDAV/RD(1)
PRINT*, ' AVERAGE RADIUS RDAV=',RDAV
ENDIF

```

```

C   Non-dimensionalize the radii based on minimum front radius, RD(2)
      A2=RD(2)
      A1=RD(1)
      DO 4 I=1,NN+1
        RD(I)=RD(I)/A2
      4 CONTINUE
C
C   Compute the transmissibilities, TS(I,J) and storativities, ST(I,J)
      DO 18 J=1,NLAYER
        DO 18 I=1,NN
          TS(I,J)=RK(I,J)*H(J)/RMU(I,J)
          ST(I,J)=PHI(I,J)*CT(I,J)*H(J)
        18 CONTINUE
C   Compute crossflow parameter, XA(I,J)
      DO 12 I=1,NN
        DO 12 J=1,NLAYER
          IF(J.EQ.NLAYER)THEN
            IF(KCODE.EQ.2)THEN
              XA(I,J)=2.00D00*RKV(I,J)/(H(J)*RMU(I,J))
            ELSE
              XA(I,J)=0.0D00
            ENDIF
          ELSE
            XA(I,J)=2.0D00*RKV(I,J)*RKV(I,J+1)/(H(J)*RMU(I,J)
            + *RKV(I,J+1)+H(J+1)*RMU(I,J+1)*RKV(I,J))
          ENDIF
        12 CONTINUE
C   Compute crossflow parameter, XB(I,J)
      DO 13 I=1,NN
        DO 13 J=1,NLAYER
          IF(J.BQ.1)THEN
            IF(KCODE.BQ.3)THEN
              XB(I,J)=2.00D00*RKV(I,J)/(H(J)*RMU(I,J))
            ELSE
              XB(I,J)=0.0D00
            ENDIF
          
```

```

ELSE
  XB(I,J)=2.0D00*RKV(I,J)*RKV(I,J-1)/(H(J)*RMU(I,J)
+ *RKV(I,J-1)+H(J-1)*RMU(I,J-1)*RKV(I,J))
ENDIF
13 CONTINUE
C  PRINT*,((XA(I,J), I=1,NN),J=1,NLAYER)
C  PRINT*,((XB(I,J), I=1,NN),J=1,NLAYER)
C    Calculate mobility ratios, RM(I,J)
  DO 14 I=1,NLAYER
    DO 14 J=1,NLAYER
      RM(I,J)=TS(I+1,J)/TS(I,J)
14 CONTINUE
C    Calculate the total transmissibility and storativity
  TTS=0.0D00
  TST=0.00D00
  DO 15 J=1,NLAYER
    TTS=TTS+TS(1,J)
    TST=TST+ST(1,J)
15 CONTINUE
C    Non-dimensionalize the storativities and transmissibilities
  DO 16 I=1,NN
    DO 16 J=1,NLAYER
      TS(I,J)=TS(I,J)/TTS
      ST(I,J)=ST(I,J)/TST
16 CONTINUE
  DO 17 I=1,NN
C    Non-dimensionalize the crossflow parameters
    DO 17 J=1,NLAYER
C    A1=Wellbore radius
      XA(I,J)=A1*A1*XA(I,J)/TTS
      XB(I,J)=A1*A1*XB(I,J)/TTS
17 CONTINUE
C  PRINT*,((XA(I,J), I=1,NN),J=1,NLAYER)
C  PRINT*,((XB(I,J), I=1,NN),J=1,NLAYER)
M=777
PI=2.*ASIN(1.0)

```

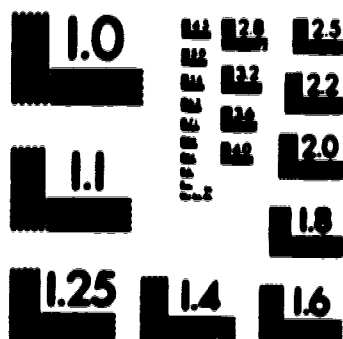
```

C
C   Generate the first set of TD vector
TD(1)=TD1
TD(2)=1.5*TD1
TD(3)=2.0*TD1
TD(4)=2.5*TD1
TD(5)=3.0*TD1
TD(6)=3.5*TD1
TD(7)=4.0*TD1
TD(8)=4.5*TD1
TD(9)=5.0*TD1
TD(10)=6.0*TD1
TD(11)=7.0*TD1
TD(12)=8.0*TD1
TD(13)=9.0*TD1
C   Generate and print the pressure transient responses
IF(ICODE.EQ.2)THEN
  CALL INVERT(TPD,NTERM,PD1,PDP1)
ENDIF
DO 1 I=1,NC
DO 2 J=1,13
  SPC=TD(J)
  IF(ICODE.EQ.2)THEN
    SPC1=SPC+TPD
    CALL INVERT(SPC1,NTERM,PD2,PDP2)
  ENDIF
  CALL INVERT(SPC,NTERM,PD,PDP)
  IF(ICODE.EQ.1)PDC=PDP
  IF(ICODE.EQ.2)THEN
    PD=PD1+PD-PD2
    PDC=PDP-PDP2
    PDH=SPC1/TPD*SPC*PDC
  ENDIF
  FDP=SPC*PDC
  IF(ICODE.EQ.2)THEN
    SPCH=SPC1/SPC

```


3 of/de 3

PM-1 3 1/4" x 4" PHOTOGRAPHIC MICROCOPY TARGET
NBS 1010a ANSI/ISO #2 EQUIVALENT



PRECISIONTM RESOLUTION TARGETS

```

      ENDIF
C   Report the results
C   Convert dimensionless time on the basis of wellbore radius
      SPC=SPC*A2*A2/A1/A1
      PDC=PDC
      WRITE(7,9)SPC,PD
      WRITE(8,9)SPC,PDP
C   For Cartesian derivative report time based on RDAV
      WRITE(9,9)SPC/RDAV/RDAV,PDC
      IF(ICODE.EQ.2,WRITE(10,9)SPC,PDH
      TD(J)=10.*TD(J)
2  CONTINUE
1  CONTINUE
9  FORMAT(2X,F20.6,2X,F20.6)
      STOP
      END
C*****
C   This subroutine LAP calculates eigenvalues, eigenvectors and Bessel functions from
C   IMSL.MATH Library. It calculates all coefficients and solves a system of
C   simultaneous linear equations using IMSL.MATH Library. Finally, it calculates the
C   wellbore pressure and its derivative
C
      SUBROUTINE LAP(S,PWDL,PDPL)
      IMPLICIT REAL*8(A-H,O-Z)
      DIMENSION A(3,3),EVAL(3),EVEC(3,3),AEI(4,3,3),
      + AA(21,21),B(21),X(21),SGMA(4,3),BB(3,3)
      COMMON/GM1/ CD,RD(5),SK(3),ST(4,3),TS(4,3),RM(3,3),JCODE,
      + NLAYER,XA(4,3),XB(4,3),JWELL,LCODE,NPL(3)
C
C   Set up the coefficient matrix A(I,J) for eigenvalue calculation
C   NODA and IPATH are codes for IMSL.MATH Library
C   Convert crossflow parameters on the basis of minimum front radius
      NN=NLAYER+1
      DO 19 I=1,NN
      DO 19 J=1,NLAYER
      XA(I,J)=XA(I,J)/RD(1)/RD(1)

```

```

      XB(I,J)=XB(I,J)/RD(1)/RD(1)
19  CONTINUE
      NCODA=1
      LDA=NLAYER
      LDB=NLAYER
      N=NLAYER
      LDEVEC=NLAYER
      IPATH=1
      DO 100 I=1,NN
      DO 11 J=1,NLAYER
      DO 11 J1=1,NLAYER
      BB(J,J1)=0.0D00
      A(J,J1)=0.00D00
11  CONTINUE
      DO 12 J=1,NLAYER
      IF(J.EQ.1)THEN
      A(J,J+1)=-XA(I,J)
      ELSEIF(J.EQ.NLAYER)THEN
      A(J,J-1)=-XB(I,J)
      ELSE
      A(J,J+1)=-XA(I,J)
      A(J,J-1)=-XB(I,J)
      ENDIF
      A(J,J)=ST(I,J)*S+XA(I,J)+XB(I,J)
      BB(J,J)=TS(I,J)
12  CONTINUE
C   Calculate eigenvalues(EVAL(J)) and eigenvector(EVEC(J,J))
      CALL DQVCSP(N,A,LDA,BB,LDB,EVAL,EVEC,LDEVEC)
C
C   Store eigenvalues and eigenvectors
      DO 13 J=1,NLAYER
      DO 13 J1=1,NLAYER
      AEI(I,J,J1)=EVEC(J,J1)
13  CONTINUE
      DO 14 J=1,NLAYER
      SGMA(I,J)=EVAL(J)

```

```

      SGMA(I,J)= DSQRT(SGMA(I,J))
14  CONTINUE
100 CONTINUE
C
C   Initialize the augmented matrix
C
      NN1=2*N*NN-N
      DO 15 I1=1,NN1
      DO 15 I2=1,NN1
      AA(I1,I2)=0.0D00
      B(I1)=0.00D00
15  CONTINUE
C   Setting up the matrices AA(I,J) and B(J) from
C   boundary conditions
      N1=N-1
C   Wellbore condition
C   For full penetration
      IF(LCODE.EQ.0)THEN
      I=1
      DO 16 J=1,N-1
      DO 16 K=1,N
      AA(J,K)=AEI(I,J,K)*DBSK0E(SGMA(I,K)*RD(1))
+      +SK(J)*RD(1)*AEI(I,J,K)*SGMA(I,K)*DBSK1E(SGMA(I,K)*RD
+      (1))
+      -AEI(I,J+1,K)*DBSK0E(SGMA(I,K)*RD(1))
+      -SK(J+1)*AEI(I,J+1,K)*SGMA(I,K)*DBSK1E(SGMA(I,K)*RD(
+      1))*RD(1)
      N2=N*N+N+K
      AA(J,N2)=AEI(I,J,K)*DBSK0E(SGMA(I,K)*RD(1))
+      -SK(J)*RD(1)*AEI(I,J,K)*SGMA(I,K)*DBSK1E(SGMA(I,K)*RD
+      (1))
+      -AEI(I,J+1,K)*DBSK0E(SGMA(I,K)*RD(1))
+      +SK(J+1)*AEI(I,J+1,K)*SGMA(I,K)*DBSK1E(SGMA(I,K)*RD(1
+      ))*RD(1)
16  CONTINUE
      DO 18 K=1,N

```

```

SUM1=0.0D00
SUM2=0.00D00
DO 17 J=1,N
  S1=TS(I,J)*RD(1)*AEI(I,J,K)*SGMA(I,K)*DBSK1E(SGMA(I,K)*RD(1))
  SUM1=SUM1+S1
  S2=-TS(I,J)*RD(1)*AEI(I,J,K)*SGMA(I,K)*DBSK1E(SGMA(I,K)*RD(1))
  SUM2=SUM2+S2
17 CONTINUE
  AA(N,K)=SUM1
  N3=N*N+N+K
  AA(N,N3)=SUM2
18 CONTINUE
  B(N)=1.00D00/S
C
C   For partial penetration
  ELSEIF(LCODE.EQ.1)THEN
    I=1
    DO 20 J=1,NLAYER
      DO 20 K=1,N
        IF(NPL(J).EQ.0)THEN
          AA(J,K)=-AEI(I,J,K)*DBSK1E(SGMA(I,K)*RD(1))*RD(I)*SGMA(I,K)
          N2=N*N+N+K
          AA(J,N2)=AEI(I,J,K)*DBSK1E(SGMA(I,K)*RD(1))*RD(I)*SGMA(I,K)
        ENDIF
20 CONTINUE
      DO 16 J=1,N-1,1
        DO 16 K=1,N
          IF(NPL(J).EQ.1.AND.NPL(J+1).EQ.1)THEN
            AA(J,K)=AEI(I,J,K)*DBSK0E(SGMA(I,K)*RD(1))
            +   +SK(J)*RD(1)*AEI(I,J,K)*SGMA(I,K)*DBSK1E(SGMA(I,K)*RD
            +   (1))
            +   -AEI(I,J+1,K)*DBSK0E(SGMA(I,K)*RD(1))
            +   -SK(J+1)*AEI(I,J+1,K)*SGMA(I,K)*DBSK1E(SGMA(I,K)*RD(
            +   1))*RD(1)
            N2=N*N+N+K
            AA(J,N2)=AEI(I,J,K)*DBSK0E(SGMA(I,K)*RD(1))

```

```

+      -SK(J)*RD(1)*AEI(I,J,K)*SGMA(I,K)*DBSI1E(SGMA(I,K)*RD
+      (1))
+      -AEI(I,J+1,K)*DBSI0E(SGMA(I,K)*RD(1))
+      +SK(J+1)*AEI(I,J+1,K)*SGMA(I,K)*DBSI1E(SGMA(I,K)*RD(1
+      ))*RD(1)
      ENDIF
16 CONTINUE
      DO 18 K=1,N
      SUM1=0.0D00
      SUM2=0.00D00
      DO 17 J=1,N
      IF(NPL(J).EQ.1)THEN
      S1=TS(I,J)*RD(1)*AEI(I,J,K)*SGMA(I,K)*DBSK1E(SGMA(I,K)*RD(1))
      SUM1=SUM1+S1
      S2=-TS(I,J)*RD(1)*AEI(I,J,K)*SGMA(I,K)*DBSI1E(SGMA(I,K)*RD(1))
      SUM2=SUM2+S2
      ENDIF
17 CONTINUE
      AA(N,K)=SUM1
      N3=N*N+N+K
      AA(N,N3)=SUM2
18 CONTINUE
      B(N)=1.00D00/S
      ENDIF
C
C **** Setting up equations from interface boundary conditions
C
      DO 200 I=1,N
      DO 200 J=1,N
      DO 200 K=1,N
      IF(LLT.N)THEN
      N3=I*N+J
      N4=N*(I-1)+K
      ARG1=SGMA(I,K)*RD(I)
      ARG2=SGMA(I+1,K)*RD(I)
      FACTOR1=SGMA(I,K)*(RD(I)-RD(I+1))

```

```

      IF(FACTOR1.LT.-174.0D00)FACTOR1=-170.0D00
C
C   Equations from pressure continuity condition
C
      AA(N3,N4)=AEI(I,J,K)*DBSK0E(SGMA(I,K)*RD(I+1))*DEXP(FACTOR1)
      N5=N+N*(I-1)+K
      AA(N3,N5)=-AEI(I+1,J,K)*DBSK0E(SGMA(I+1,K)*RD(I+1))
      N6=N*N+N+N*(I-1)+K
      AA(N3,N6)=AEI(I,J,K)*DBSI0E(SGMA(I,K)*RD(I+1))*DEXP(-FACTOR1)
      N7=N+N6
      AA(N3,N7)=-AEI(I+1,J,K)*DBSI0E(SGMA(I+1,K)*RD(I+1))
C
C   Equations from flow continuity condition
C
      N8=N*N+I*N+J
      AA(N8,N4)=AEI(I,J,K)*SGMA(I,K)*DBSK1E(SGMA(I,K)*RD(I+1))*DEXP(
+   FACTOR1)
      AA(N8,N5)=-AEI(I+1,J,K)*SGMA(I+1,K)*DBSK1E(SGMA(I+1,K)*RD(I+1)
+   )*RM(I,J)
      AA(N8,N6)=-AEI(I,J,K)*SGMA(I,K)*DBSI1E(SGMA(I,K)*RD(I+1))*DEXP
+   (-FACTOR1)
      AA(N8,N7)=AEI(I+1,J,K)*SGMA(I+1,K)*DBSI1E(SGMA(I+1,K)*RD(I+1))
+   *RM(I,J)
      ELSE
      N3=I*N+J
      N4=N*(I-1)+K
      ARG1=SGMA(I,K)*RD(I)
      ARG2=SGMA(I+1,K)*RD(I)
      FACTOR1=SGMA(I,K)*(RD(I)-RD(I+1))
      IF(FACTOR1.LT.-174.0D00)FACTOR1=-170.0D00
C
C   Equations from pressure continuity condition
C
      AA(N3,N4)=AEI(I,J,K)*DBSK0E(SGMA(I,K)*RD(I+1))*DEXP(FACTOR1)
      N5=N+N*(I-1)+K
      AA(N3,N5)=-AEI(I+1,J,K)*DBSK0E(SGMA(I+1,K)*RD(I+1))

```

```

      N6=N*N+N+N*(I-1)+K
      AA(N3,N6)=AEI(I,J,K)*DBSI0E(SGMA(I,K)*RD(I+1))*DEXP(-FACTOR1)
C
C      Equations from flow continuity condition
C
      N7=N+N6
      N8=N*N+I*N+J
      AA(N8,N4)=AEI(I,J,K)*SGMA(I,K)*DBSK1E(SGMA(I,K)*RD(I+1))*DEXP(
+   FACTOR1)
      AA(N8,N5)=-AEI(I+1,J,K)*SGMA(I+1,K)*DBSK1E(SGMA(I+1,K)*RD(I+1)
+   )*RM(I,J)
      AA(N8,N6)=-AEI(I,J,K)*SGMA(I,K)*DBSI1E(SGMA(I,K)*RD(I+1))*DEXP
+   (-FACTOR1)
      ENDIF
200 CONTINUE
C
C      Outer boundary conditions
C
C      For infinite outer boundary
      IF(JCODE.EQ.1)THEN
C
      ELSEIF(JCODE.EQ.2)THEN
C      For closed outer boundary
      DO 25 J=1,N
      DO 25 K=1,N
      N9=2*N*N+N+J
      N10=N*N+K
      ARG3=SGMA(N+1,K)*RD(NN)
      FACTOR2=SGMA(N+1,K)*(RD(NN)-RD(NN+1))
      IF(FACTOR2.LT.-174.0D00)FACTOR2=-170.0D00
      AA(N9,N10)=AEI(N+1,J,K)*SGMA(N+1,K)*DBSK1E(SGMA(N+1,K)*RD(NN+1
+   ))*DEXP(FACTOR2)
      N11=2*N*N+N+K
      AA(N9,N11)=-AEI(N+1,J,K)*SGMA(N+1,K)*DBSI1E(SGMA(N+1,K)*RD(NN+
+   1))*DEXP(-FACTOR2)
25 CONTINUE

```



```

C
  ELSEIF(JCODE.EQ.3)THEN
C    For constant pressure outer boundary
  DO 25 J=1,N
    DO 25 K=1,N
      N9=2*N*N+N+J
      N10=N*N+K
      ARG3=SGMA(N+1,K)*RD(NN)
      FACTOR2=SGMA(N+1,K)*(RD(NN)-RD(NN+1))
      AA(N9,N10)=AEI(N+1,J,K)*DBSK0E(SGMA(N+1,K)*RD(NN+1
+    ))*DEXP(FACTOR2)
      N11=2*N*N+N+K
      AA(N9,N11)=AEI(N+1,J,K)*DBSK0E(SGMA(N+1,K)*RD(NN+
+    1))*DEXP(-FACTOR2)
25  CONTINUE
    ENDIF
C    Solve the system of equations using IMSL.MATH Library
    NEQ=2*N*(N+1)-N
    LDA2=NEQ
    CALL DLSARG(NEQ,AA,LDA2,B,IPATH,X)
C
C    PRINT*,THE SOLN=,',(X(I),I=1,12)
C
C    Calculate the wellbore pressure
    FACT1=0.00D00
    SUM=0.00D00
    J=JWELL
    I=1
    DO 220 K=1,N
      N12=N*N+N+K
      PW= AEI(I,J,K)*DBSK0(SGMA(I,K)*RD(I))*X(K)*DEXP(SGMA(I,K)*RD(
+    I))
      + AEI(I,J,K)*DBSK0(SGMA(I,K)*RD(I))*X(N12)*DEXP(-SGMA(I,K)
+    *RD(I))
      + SK(J)*AEI(I,J,K)*SGMA(I,K)*DBSK1(SGMA(I,K)*RD(I))*X(K)
      + *DEXP(SGMA(I,K)*RD(I))*RD(I)

```

```

      + -SK(J)*AEI(I,J,K)*SGMA(I,K)*DBSI1(SGMA(I,K)*RD(I))*X(N12)
      + *DEXP(-SGMA(I,K)*RD(I))*RD(I)
      SUM=SUM+PW
220 CONTINUE
      PWDL=SUM
      PWDL=PWDL/(1.0D00+CD*S*S*PWDL)
      PDPL=S*PWDL
      RETURN
      END
*****
      SUBROUTINE INVERT(TD,N,PD,PDP)
C   THIS subroutine inverts PWD and PDP from Laplace space to real space using
C   Stehfest algorithm
      IMPLICIT REAL*8(A-H,O-Z)
C
      DIMENSION G(50),V(50),H(25)
C   Now if the array V(I) was calculated before the program goes directly to the end
C   of the subroutine
      M=777
      IF(N.EQ.M) GO TO 17
      M=N
      DLOGTW=0.6931471805599
      NH=N/2
C   The factorials of 1 TO N are calculated into array G
      G(1)=1
      DO 1 I=2,N
        G(I)=G(I-1)*I
1    CONTINUE
C   Terms with K only are calculated into array H
      H(1)=2./G(NH-1)
      DO 6 I=2,NH
        FI=I
        IF(I-NH)4,5,6
4     H(I)=FI**NH*G(2*I)/(G(NH-I)*G(I)*G(I-1))
        GO TO 6
5     H(I)=FI**NH*G(2*I)/(G(I)*G(I-1))

```

```

6 CONTINUE
C
C The terms  $-1^{*}NH+1$  are calculated
C First the term for  $I=1$ 
   $SN=2*(NH-NH/2*2)-1$ 
C
C The rest of the SN'S are calculated in the main routine
C The array  $V(I)$  is calculated
  DO 7 I=1,N
C First set  $V(I)=0$ 
   $V(I)=0.$ 
C The limits for K are established
C The lower limit is  $K1=INTEG((I+1/2))$ 
   $K1=(I+1)/2$ 
C The upper limit is  $K2=MIN(I,N/2)$ 
   $K2=I$ 
  IF(K2-NH)8,8,9
9 K2=NH
C The summation term in  $V(I)$  is calculated
8 DO 10 K=K1,K2
  IF(2*K-I)12,13,12
12 IF(I-K)11,14,11
11  $V(I)=V(I)+H(K)/(G(I-K)*G(2*K-I))$ 
  GO TO 10
13  $V(I)=V(I)+H(K)/G(I-K)$ 
  GO TO 10
14  $V(I)=V(I)+H(K)/G(2*K-I)$ 
10 CONTINUE
C
C The  $V(I)$  array is finally calculated by weighting according to SN

   $V(I)=SN*V(I)$ 
C The term SN changes its sign each iteration
   $SN=-SN$ 
7 CONTINUE
C The numerical approximation is calculated

```

```

17 PD=0.0
   PDP=0.0
   A=DLOGTW/TD
   DO 15 I=1,N
   ARG=A*I
   CALL LAP(ARG,PWDL,PDPL)
   PD=PD+V(I)*PWDL
   PDP=PDP+V(I)*PDPL
15 CONTINUE
   PD=PD*A
   PDP=PDP*A
   RETURN
   END

C
*****

   SUBROUTINE TAB(NLAYER,ANGLE,H,HT,RD)
C   This subroutine computes the front radii when front angle and minimum front
C   radius are supplied
   IMPLICIT REAL*8(A-H,O-Z)
   DIMENSION RD(NLAYER),H(NLAYER)
   PI=2.0*ASIN(1.0)
C   Converting the angle to radians
   THETA=PI*ANGLE/180.0
   STEP=H/DTAN(THETA)
   F1=RD(2)*RD(2)-STEP*STEP/3.0
   BOTTOMR=(DSQRT(F1*4.0+STEP*STEP)-STEP)/2.0
   TOPR=BOTTOMR+STEP
C   Calculate the radii
C
   DO 12 I=2,NLAYER,1
   IF(ANGLE.EQ.90.0)THEN
   RD(I+1)=RD(I)
   ELSE
   BOTTOMR=TOPR
   TOPR=BOTTOMR+STEP
   RD(I+1)=DSQRT((TOPR**3-BOTTOMR**3)*DTAN(THETA)/(3.0*H))

```

```
ENDIF  
12 CONTINUE  
PRINT*,RD  
RETURN  
END
```

Appendix G: Published Paper From Chapter 2

This appendix shows the published paper from Chapter 2 of this study in *AOSTRA Journal of Research*, Volume 8, Number 2 , Spring 1992. This paper was originally presented as SPE 26049 at the 1993 SPE Western Regional Meeting, held in Anchorage, AK, May 26-28, 1993.

An Analytical Pressure-Transient Model for Multi-Layered, Composite Reservoirs With Pseudosteady-State Formation Crossflow

Edmond Gomes and Anil K. Ambastha*

Mining, Metallurgical, and Petroleum Engineering Department, University of Alberta, Edmonton, Alberta, Canada T6G 2G6. Received September 22, 1992; in revised form, May 4, 1993.

* To whom correspondence should be addressed.

Abstract. Reservoir deposition occurs over geologic periods of time. Although reservoirs are assumed homogeneous for simplicity of analysis, most reservoirs are heterogeneous in nature. Some common forms of heterogeneity are the presence of layers and the presence of different zones of fluids and/or rocks in the formation.

In this study, a new analytical solution for multi-layered composite reservoirs with pseudosteady-state interlayer crossflow has been developed. Fluid flow in the reservoir has been treated as a generalized eigenvalue problem. The developed analytical solution for an n -layered composite reservoir is applicable for any irregularly-shaped discontinuity boundary, and for closed, constant-pressure and infinite outer boundary conditions. This new solution is computationally very efficient. Using eigenvalues and eigenvectors of the system, this method requires solution of an order-of-magnitude fewer simultaneous equations as compared to other methods proposed in the literature. This method is also very versatile and can handle multiple composite regions (more than two), and partially-penetrating wells subject to bottom-water and/or gas-cap drives for well testing purposes. This analytical model has been validated by comparing the results with those of some simple, well-known models in the well-testing literature. Solution methodology and future possibilities of the new solution are also discussed.

Keywords: Pressure-transient model/layered reservoirs/composite reservoirs/formation crossflow.

INTRODUCTION

Most reservoirs are heterogeneous in nature. The presence of layers and zones of different fluid and/or rocks is a common cause for reservoir heterogeneity. Figures 1a and 1b show a layered reservoir and a layered composite reservoir, respectively. The horizontal lines show the layering and the arrows show the presence of crossflow. The layers may be communicating or non-communicating. Formation crossflow is present when the layers are communicating. When the layers do not communicate with each other, except through the wellbore, then the reservoir is termed a "commingled reservoir." A layered, composite reservoir may result because of artificial as well as natural processes.

Enhanced oil recovery processes such as steam flooding, CO₂ flooding, *in-situ* combustion, tectonic movements, phase changes, acidizing, and temperature differences may cause a reservoir to behave as a composite reservoir. The tilted line in Figure 1b shows the discontinuity boundary or the fluid front. A layered, composite reservoir situation occurs when all or some of the layers have two or more regions of different rock and/or fluid properties.

Numerous studies have been reported in the literature on layered reservoirs and Table 1 lists relevant papers on layered reservoirs. One aspect in which the studies differ is the way they model crossflow between the layers. Formation crossflow has been modelled mainly by two methods: pseudosteady-state crossflow

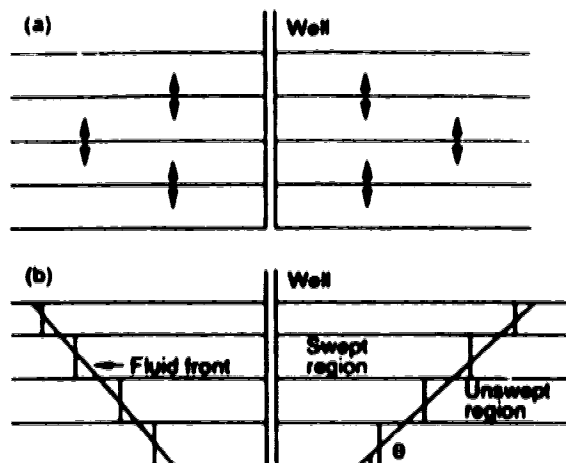


Figure 1. (a) Layered reservoir with interlayer crossflow; (b) radial, layered composite reservoir with a tilted front.

and transient crossflow. Pseudosteady-state crossflow assumes that the resistance to crossflow is confined to the interlayer boundary and the flow is horizontal within each layer. This assumption reduces a two-dimensional problem to a one-dimensional problem. Transient crossflow utilizes the two-dimensional diffusivity equation for each layer. Table 1 also shows that, although numerous studies have appeared on layered reservoirs with formation crossflow, very little work has been reported for layered, composite reservoirs with formation crossflow. Responses of layered reservoirs may be summarized as follows: for commingled reservoirs, the time needed to reach pseudosteady-state is an order of magnitude higher than that for homogeneous reservoirs; semi-log analysis can be used to estimate the average permeability-thickness product and the skin effect; initially, a crossflow system and a commingled system have the same responses; then there is a transition period and, finally, the crossflow system behaves like an equivalent homogeneous system.

Satman [22] presented drawdown and buildup responses for a commingled, multi-layered composite reservoir. In his model, he considered different discontinuity boundary radii for different layers. He used the concept of a tilted front for layered composite reservoirs, because the fluid front would propagate at different rates in different layers. For enhanced recovery processes, such as steam flooding, Satman and Utkay [35] considered the discontinuity boundary as a tilted front to

account for the gravity override effect and modelled the reservoir as a multi-layered composite reservoir without crossflow. They concluded that the tilted front model is a better representation of the actual reservoir than the sharp-front model when the gravity override effect is present. Hatzignatiou *et al* [45] presented a solution for interference pressure transient behaviour in a two-layered reservoir having pseudosteady-state formation crossflow and described a type-curve matching technique to estimate the reservoir parameters. Anbarci *et al*. [55] presented an analytical solution for a two-layer, composite reservoir. They included wellbore storage and skin, and considered pseudosteady-state crossflow between the layers. They conducted a limited sensitivity study and used a type-curve matching technique to locate the front location in a particular layer. The preceding discussion shows that a general solution for an n -layer composite reservoir with crossflow is yet to be developed. In this study, we present an analytical solution and its validation for multi-layered, composite reservoirs with formation crossflow. We also discuss the usefulness of this solution for future studies.

MODEL DEVELOPMENT

We consider an n -layer, radial, composite reservoir as shown in Figure 2. A symmetrically located well fully penetrates the reservoir. The well produces at a constant flow rate and pseudosteady-state formation crossflow is present between the layers. The problem is solved following the approach of Anbarci *et al*. [55]. In Figure 2, the discontinuity boundary in each layer is represented by a vertical solid line. These discontinuity boundaries have been vertically extended across all the

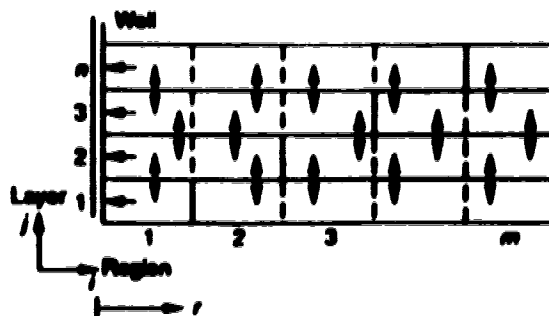


Figure 2. Schematic diagram of an n -layered composite reservoir in radial geometry with two different rock and/or fluid types in each layer.

Table 1. Published results on layered reservoirs (extended beyond Ehlig-Economides and Joseph [1]).

Year	Author	Solution method ^a					No. of layers	Interlayer flow ^b			Well specifications ^c					Well control ^d			Outer boundary ^e			Composite reservoir ^f	
		L	H	F	FD	O		NOCF	T	PSS	FWB	LS	VF	C	s	q	p	P	IA	NF	CP	C	NC
1960	Jacquard [2]	.					2
1961	Tempelaar-Lutz [3]	.					2
1961	Lefkowitz <i>et al</i> [4]	.					n
1961	Duvaut [5]	.					n
1961	Pobesier and Seguers [6]	.					2
1961	Pottier [7]	.					2
1962	Polubarinova-Kocina [8]	.					n
1962	Russell and Prats [9]	.	.				2
1962	Russell and Prats [10]	.					2
1962	Katz and Tek [11]	.			.		2
1962	Pendergrass and Berry [12]	.			.		n
1969	Kazemi and Seth [13]	.			.		n
1970	Kazemi [14]	.			.		n	.	.		.				Δ
1970	Woods [15]	.			.		n
1972	Cobb <i>et al</i> [16]	.			.		2
1974	Earlougher <i>et al</i> [17]	.			.		n
1974	Raghavan <i>et al</i> [18]	.			.		2
1979	Tariq and Ramay [19]	.			.		n
1981	Chu and Raghavan [20]	.			.		n
1981	Larsen [21]	.			.		n
1981	Satman [22]	.			.		n
1982	Bennett <i>et al</i> [23]	.			.		n
1982	Larsen [24]	.			.		n
1983	Prats [25]	.	.		.		2
1983	Nike [26]	.			.		2
1983	Geo [27]	.			.		2
1983	Javandel and Witherspoon [28]	.	.		.		2
1984	Geo [29]	.			.		n	.	.		.				Δ
1984	Streltsova [30]	.			.		2
1984	Lee <i>et al</i> [31]	.			.		3
1985	Bourdet [32]	.			.		2
1985	Bramer <i>et al</i> [33]	.			.		2
1985	Prabhakar <i>et al</i> [34]	.			.		2
1985	Satman and Odeh [35]	.			.		2
1986	Ehlig-Economides and Ayoub [36]	.			.		2
1986	Kucuk <i>et al</i> [37]	.			.		2
1986	Ehlig-Economides and Joseph [1]	.			.		n
1986	Kucuk <i>et al</i> [38]	.			.		n
1986	Mavor and Whetup [39]	.			.		n
1986	Joseph <i>et al</i> [40]	.			.		2
1987	Chen [41]	.			.		n
1987	Geo [42]	.			.		n
1987	Ehlig-Economides and Joseph [43]	.			.		n
1987	Morris [44]	.			.		3
1987	Hatzignatiou <i>et al</i> [45]	.			.		2
1988	Geo and Deans [46]	.			.		n
1988	Larsen [47]	.			.		n
1988	Larsen [48]	.			.		n
1988	Park and Hame [49]	.			.		n
1988	Chen and Lee [50]	.			.		2	.	.		.				Δ
1988	Chen and Lee [51]	.			.		2
1988	Raghavan [52]	.			.		2
1988	Yeh and Reynolds [53]	.			.		n	.	.		.				Δ
1988	Yeh and Reynolds [54]	.			.		n	.	.		.				Δ
1988	Arbabi <i>et al</i> [55]	.			.		2	.	.		.				Δ
1988	Chen and Lee [56]	.			.		2
1988	Milnes and Ramay [57]	.			.		n
1988	Speth <i>et al</i> [58]	.			.		n
1988	Nieme [59]	.			.		n

^a L = Laplace transform; H = Hankel transform; F = Fourier transform; FD = finite difference; O = other.

^b NOCF = no formation crossflow; T = transient crossflow; PSS = pseudo-steady-state crossflow.

^c FWB = finite wellbore; LS = line source; VF = vertical fracture; C = wellbore storage; s = skin; Δ = partial penetration skin.

^d q = constant rate; p = constant pressure; P = pulse rate.

^e IA = infinite acting; NF = no flow; CP = constant pressure.

^f C = composite; NC = noncomposite.

layers. As a result, depending on the total number of discontinuity boundaries and their locations, an n -layer reservoir may have m number of regions in each layer. Therefore, the reservoir is divided into $n \times m$ zones and each zone may be identified by (i, j) , in which i and j denote the region and the layer, respectively. Each zone may have different rock and/or fluid properties, and can have variable length in the radial direction depending on the discontinuity boundary locations. In an actual reservoir, we may not need $n \times m$ zones of different rock and/or fluid properties. In Figure 2, the shaded and non-shaded areas represent two different fluid and/or rock types. Each layer has only two different rock and/or fluid types separated by a discontinuity boundary. In each layer, the discontinuity boundary is placed at a different location to simulate a tilted-front discontinuity boundary for the reservoir and for this particular situation, $m = n + 1$. Layers are assumed to be of constant thicknesses throughout the reservoir.

The crossflow between layers within the reservoir is modelled as in the semi-permeable wall model proposed by Gao [29]. Thus, crossflow resistance is assumed to be confined to the interlayer boundary and flow in each layer is horizontal. It is also assumed that the upper boundary of the top layer and the lower boundary of the bottom layer are closed. Other assumptions for the development of the mathematical model are as follows:

1. Reservoir fluids are slightly compressible and have constant compressibility.
2. The effects of gravity and capillary forces are negligible.
3. The flow in the formation can be described by Darcy's law.
4. When a fluid crosses the boundary of its zone, it behaves as the fluid in the downstream side.

The flow equation for zone i, j can be written as:

$$(1) \left(\frac{k h}{\mu} \right)_{i,j} \left(\frac{\partial^2 p_{i,j}}{\partial r^2} + \frac{1}{r} \frac{\partial p_{i,j}}{\partial r} \right) = (\phi c_t h)_{i,j} \frac{\partial p_{i,j}}{\partial t} + X_{A,i,j} (p_{i,j} - p_{i,j+1}) + X_{B,i,j} (p_{i,j} - p_{i,j-1})$$

where $X_{A,i,j}$ and $X_{B,i,j}$ are defined as follows:

$$(2) X_{A,i,j} = \frac{2}{\left(\frac{h \mu}{k_v} \right)_{i,j} + \left(\frac{h \mu}{k_v} \right)_{i,j+1}}$$

$$(3) X_{B,i,j} = \frac{2}{\left(\frac{h \mu}{k_v} \right)_{i,j} + \left(\frac{h \mu}{k_v} \right)_{i,j-1}}$$

$$(4) X_{B,i,1} = 0 \quad \text{for } i = 1, \dots, m$$

$$(5) X_{A,i,n} = 0 \quad \text{for } i = 1, \dots, m$$

Initial condition: We assume that initially all zones are at initial pressure and thus,

$$(6) p_{i,j}(r, 0) = p_{in} \quad \text{for all } i \text{ and } j$$

Inner boundary condition:

$$(7) p_{wf} = p_{1,j}(r_{wf}) - s_j \left(r \frac{\partial p_{1,j}}{\partial r} \right)_{r=r_{wf}} \quad \text{for } j = 1, \dots, n$$

$$(8) q = -C \frac{\partial p_{wf}}{\partial t} + 2\pi r_w \sum_{j=1}^n \left(\frac{k h}{\mu} \right)_{1,j} \left(\frac{\partial p_{1,j}}{\partial r} \right)_{r=r_{wf}} \quad \text{for } j = 1, \dots, n$$

Outer boundary conditions:

Infinitely large system:

$$(9) p_{m,j} = p_{in} \quad \text{for } r \rightarrow \infty \text{ and } j = 1, \dots, n$$

Finite system with a constant pressure at the outer boundary:

$$(10) p_{m,j} = p_{in} \quad \text{for } r = r_{ej} \text{ and } j = 1, \dots, n$$

Finite system with a closed outer boundary:

$$(11) \frac{\partial p_{m,j}}{\partial r} = 0 \quad \text{for } r = r_{ej} \text{ and } j = 1, \dots, n$$

The flow equations for different zones in the same layer are coupled using the following interface conditions defining pressure and flow rate continuity between these zones:

$$(12) p_{i,j} = p_{i+1,j} \quad \text{for } r = r_{ij} \text{ and } i = 1, \dots, m-1 \text{ and } j = 1, \dots, n$$

$$(13) \frac{dp_{i,j}}{dr} = M_{i,j} \frac{dp_{i+1,j}}{dr} \quad \text{for } r = r_w \text{ and } i = 1, \dots, m \\ \text{and } j = 1, \dots, n$$

where,

$$(14) M_{i,j} = \frac{\left(\frac{k\bar{h}}{\mu}\right)_{i+1,j}}{\left(\frac{k\bar{h}}{\mu}\right)_{i,j}}$$

Let us introduce the following dimensionless variables:

$$(15) r_D = \frac{r}{r_w}$$

$$(16) p_{Dh,j} = \frac{2\pi}{q} \left(\frac{k\bar{h}}{\mu}\right) (p_{in} - p_{i,j})$$

$$(17) p_{wD} = \frac{2\pi}{q} \left(\frac{k\bar{h}}{\mu}\right) (p_{in} - p_{wD})$$

$$(18) b_D = \frac{t}{r_w^2} \left(\frac{k\bar{h}}{\phi c_t h}\right),$$

where,

$$(19) \left(\frac{k\bar{h}}{\mu}\right) = \sum_{j=1}^n \left(\frac{k\bar{h}}{\mu}\right)_{1,j}$$

$$(20) (\phi c_t h) = \sum_{j=1}^n (\phi c_t h)_{1,j}$$

Expressing the flow equation and the boundary conditions in terms of dimensionless variables, we can write:

$$(21) \kappa_{i,j} \left(\frac{\partial^2 p_{Di,j}}{\partial r_D^2} + \frac{1}{r_D} \frac{\partial p_{Di,j}}{\partial r_D} \right) = \omega_{i,j} \frac{\partial p_{Di,j}}{\partial b_D} \\ + \lambda_{Ai,j} (p_{Di,j} - p_{Di,j+1}) + \lambda_{Bi,j} (p_{Di,j} - p_{Di,j-1}).$$

where,

$$(22) \kappa_{i,j} = \frac{\left(\frac{k\bar{h}}{\mu}\right)_{i,j}}{\left(\frac{k\bar{h}}{\mu}\right)}$$

$$(23) \omega_{i,j} = \frac{(\phi c_t h)_{i,j}}{(\phi c_t h)}$$

$$(24) \lambda_{Ai,j} = \frac{r_w^2}{\left(\frac{k\bar{h}}{\mu}\right)} X_{Ai,j}$$

$$(25) \lambda_{Bi,j} = \frac{r_w^2}{\left(\frac{k\bar{h}}{\mu}\right)} X_{Bi,j}$$

Initial condition:

$$(26) p_{Di,j}(r_D, 0) = 0, \quad \text{for all } i \text{ and } j$$

Inner boundary condition:

$$(27) p_{wD} = p_{Di,j}(1, b_D) - s_j \left(\frac{\partial p_{Di,j}}{\partial r_D} \right), \quad \text{for } j = 1, \dots, n$$

$$(28) 1 = C_D \frac{\partial p_{wD}}{\partial b_D} - \sum_{j=1}^n \kappa_{1,j} \left(\frac{\partial p_{Di,j}}{\partial r_D} \right).$$

Outer boundary conditions:

Infinitely large system:

$$(29) p_{Di,j} = 0, \quad \text{for } r_D \rightarrow \infty \text{ and } j = 1, \dots, n$$

Finite system with a constant pressure at the outer boundary:

$$(30) p_{Di,j} = 0, \quad \text{for } r_D = r_{Dw} \text{ and } j = 1, \dots, n$$

Finite system with a closed outer boundary:

$$(31) \frac{\partial p_{Di,j}}{\partial r_D} = 0, \quad \text{for } r_D = r_{Dw} \text{ and } j = 1, \dots, n$$

Interface conditions defining pressure and flow rate continuity between the zones of a layer:

$$(32) \quad p_{Di,j} = p_{Di+1,j} \quad \text{for } r_D = r_{Di} \text{ and } i = 1, \dots, m-1 \\ \text{and } j = 1, \dots, n$$

$$(33) \quad \frac{\partial p_{Di,j}}{\partial r_D} = M_{i,j} \frac{\partial p_{Di+1,j}}{\partial r_D} \quad \text{for } r_D = r_{Di} \\ \text{and } i = 1, \dots, m-1 \\ \text{and } j = 1, \dots, n$$

The Laplace transformation of Eqs. (21), and (27) through (33), yields:

$$(34) \quad \kappa_{i,j} \left(\frac{d^2 \bar{p}_{Di,j}}{dr_D^2} + \frac{1}{r_D} \frac{d\bar{p}_{Di,j}}{dr_D} \right) = \omega_{i,j} p_{Di,j} l \\ + \lambda_{Ai,j} (\bar{p}_{Di,j} - \bar{p}_{Di,j+1}) + \lambda_{Bi,j} (\bar{p}_{Di,j} - \bar{p}_{Di,j-1}).$$

Inner boundary condition:

$$(35) \quad \bar{p}_{wD} = \bar{p}_{Di,j}(1, l) - s_j \left(\frac{d\bar{p}_{Di,j}}{dr_D} \right), \quad \text{for } j = 1, \dots, n$$

$$(36) \quad \frac{1}{l} = C_D \bar{p}_{wD} l - \sum_{j=1}^n \kappa_{1,j} \left(\frac{d\bar{p}_{Di,j}}{dr_D} \right).$$

Outer boundary conditions:

Infinitely large system:

$$(37) \quad \bar{p}_{Di,m,j} = 0, \quad \text{for } r_D \rightarrow \infty \text{ and } j = 1, \dots, n$$

Finite system with a constant pressure at the outer boundary:

$$(38) \quad \bar{p}_{Di,m,j} = 0, \quad \text{for } r_D = r_{De} \text{ and } j = 1, \dots, n$$

Finite system with a closed outer boundary:

$$(39) \quad \frac{d\bar{p}_{Di,m,j}}{dr_D} = 0, \quad \text{for } r_D = r_{De} \text{ and } j = 1, \dots, n$$

Interface conditions defining pressure and flow rate continuity between the zones of a layer:

$$(40) \quad \bar{p}_{Di,j} = \bar{p}_{Di+1,j} \quad \text{for } r_D = r_{Di} \text{ and } i = 1, \dots, m-1 \\ \text{and } j = 1, \dots, n$$

$$(41) \quad \frac{d\bar{p}_{Di,j}}{dr_D} = M_{i,j} \frac{d\bar{p}_{Di+1,j}}{dr_D}, \quad \text{for } r_D = r_{Di} \\ \text{and } i = 1, \dots, m-1 \\ \text{and } j = 1, \dots, n$$

Eq. (34) has the form of a modified Bessel's equation. Let us assume a solution of the following form for Eq. (34):

$$(42) \quad \bar{p}_{Di,j} = A_{i,j} K_0(\sigma r_D) + B_{i,j} I_0(\sigma r_D)$$

Introducing Eq. (42) into the left-hand side of Eq. (34), we get:

$$(43) \quad \kappa_{i,j} \left(\frac{d^2 \bar{p}_{Di,j}}{dr_D^2} + \frac{1}{r_D} \frac{d\bar{p}_{Di,j}}{dr_D} \right) = \kappa_{i,j} \sigma^2 p_{Di,j}.$$

Substituting Eq. (43) into Eq. (34) results in the following general equation:

$$(44) \quad \lambda_{Ai,j} \bar{p}_{Di,j+1} + (\sigma^2 \kappa_{i,j} - \omega_{i,j} l - \lambda_{Ai,j} - \lambda_{Bi,j}) \bar{p}_{Di,j} \\ + \lambda_{Bi,j} \bar{p}_{Di,j-1} = 0$$

Eq. (44) has the form of a generalized eigenvalue system. As pointed out by Ehlig-Economides and Joseph [1], Eq. (44) has a non-trivial solution (i.e., $p_{Di,j} \neq 0$) if and only if its coefficient matrix is singular. Thus, the determinant of the coefficient matrix has to be zero. The coefficient matrix is an $n \times m$ by $n \times m$ tridiagonal matrix. The coefficient matrix can be divided into m smaller real-symmetric, positive-definitive tridiagonal matrices, where the σ^2 act as the eigenvalues, and these eigenvalues are always positive. The determinant of each of these matrices is an n th order polynomial in σ^2 ; and, from each determinant, n eigenvalues can be obtained. Now, a general solution for each zone can be written as:

$$(45) \quad \bar{p}_{Di,j} = \sum_{k=1}^n \left[A_{i,j}^k K_0(\sigma_i^k r_D) + B_{i,j}^k I_0(\sigma_i^k r_D) \right].$$

Constants $A_{i,j}^k$ and $B_{i,j}^k$ can be split into two parts as follows:

$$(46) A_{i,j}^k = E_{i,j}^k A_i^k$$

$$(47) B_{i,j}^k = E_{i,j}^k B_i^k$$

where $E_{i,j}^k$ is the eigenvector for region i , and this eigenvector can be calculated from Eq. (44). Constants A_i^k and B_i^k are to be determined from the boundary conditions. Now, a general solution for region i and layer j becomes:

$$(48) p_{i,j} = \sum_{k=1}^n \left[A_i^k E_{i,j}^k K_0(\sigma_i^k r_D) + B_i^k E_{i,j}^k I_0(\sigma_i^k r_D) \right]$$

Eq. (48) contains $2n \times m$ constants to be evaluated from the boundary conditions. For the inner boundary condition, without considering wellbore storage, we can write:

$$(49) \bar{p}_{wD} = \sum_{k=1}^n \left[\left(A_1^k E_{1,j}^k K_0(\sigma_1^k) + B_1^k E_{1,j}^k I_0(\sigma_1^k) \right) + s_j \sigma_1^k \left(A_1^k E_{1,j}^k K_1(\sigma_1^k) - B_1^k E_{1,j}^k I_1(\sigma_1^k) \right) \right] \quad \text{for } j = 1, \dots, n$$

$$(50) \frac{1}{l} = \sum_{j=1}^n \kappa_{1,j} \sum_{k=1}^n \sigma_1^k \left[A_1^k E_{1,j}^k K_1(\sigma_1^k) - B_1^k E_{1,j}^k I_1(\sigma_1^k) \right] \quad \text{for } j = 1, \dots, n$$

For an infinite outer boundary condition, we can write:

$$(51) \sum_{k=1}^n \left[A_m^k E_{m,j}^k K_0(\sigma_m^k r_D) + B_m^k E_{m,j}^k I_0(\sigma_m^k r_D) \right] = 0 \quad \text{for } r_D \rightarrow \infty \text{ and } j = 1, \dots, n$$

In order that the pressure be bounded, we can write:

$$(52) \sum_{k=1}^n B_m^k = 0 \quad \text{for } j = 1, \dots, n$$

A constant pressure outer boundary condition yields:

$$(53) \sum_{k=1}^n \left[A_m^k E_{m,j}^k K_0(\sigma_m^k r_{Dej}) + B_m^k E_{m,j}^k I_0(\sigma_m^k r_{Dej}) \right] = 0 \quad \text{for } j = 1, \dots, n$$

A no flow outer boundary condition yields:

$$(54) \sum_{k=1}^n \left[A_m^k E_{m,j}^k K_1(\sigma_m^k r_{Dej}) + B_m^k E_{m,j}^k I_1(\sigma_m^k r_{Dej}) \right] = 0 \quad \text{for } j = 1, \dots, n$$

The interface conditions defining pressure and flow rate continuity yield:

$$(55) \sum_{k=1}^n \left[A_i^k E_{i,j}^k K_0(\sigma_i^k r_{Dwi}) + B_i^k E_{i,j}^k I_0(\sigma_i^k r_{Dwi}) \right] = \sum_{k=1}^n \left[A_{i+1}^k E_{i+1,j}^k K_0(\sigma_{i+1}^k r_{Dwi}) + B_{i+1}^k E_{i+1,j}^k I_0(\sigma_{i+1}^k r_{Dwi}) \right] \quad \text{for } j = 1, \dots, n \text{ and } i = 1, \dots, m-1$$

$$(56) \sum_{k=1}^n \left[A_i^k E_{i,j}^k K_1(\sigma_i^k r_{Dwi}) - B_i^k E_{i,j}^k I_1(\sigma_i^k r_{Dwi}) \right] = \sum_{k=1}^n \left[A_{i+1}^k E_{i+1,j}^k K_1(\sigma_{i+1}^k r_{Dwi}) - B_{i+1}^k E_{i+1,j}^k I_1(\sigma_{i+1}^k r_{Dwi}) \right] \quad \text{for } j = 1, \dots, n \text{ and } i = 1, \dots, m-1$$

Eqs. (47) through (56) give a total of $2n \times m$ simultaneous equations which can be solved to find $2n \times m$ values of the coefficients A_i^k and B_i^k .

Thus, the preceding solution models transient fluid flow in an n -layer, composite reservoir with pseudo-steady-state crossflow. This new solution uses the eigenvalues and eigenvectors of the system and is computationally more efficient than other methods proposed in the literature. For example, for a 5-layer,

composite reservoir ($m = 6$), this new solution requires the solution of only 60 simultaneous equations, whereas the method proposed by Anbarci *et al.* [55] requires the solution of 300 simultaneous equations to solve the same problem. By assigning a constant-pressure boundary at the top or at the bottom, this new solution can include a gas cap or a bottom-water drive, respectively. This new solution is also capable of treating any irregularly shaped fluid front by dividing the reservoir into a number of mathematical layers.

To include a bottom-water drive, the lower boundary of the bottom layer is considered as a constant-pressure boundary. Mathematically, the vertical permeability of the bottom-water zone is considered infinite and Eq. (4) is modified as follows:

$$(4a) X_{Bi,1} = \frac{2}{\left(\frac{h\mu}{k_v}\right)_{i,1}} \quad \text{for } i = 1, \dots, m$$

Also, in the diffusivity equation for layer $j = 1$, $p_{i,j-1}$ is replaced by the initial pressure, p_{in} . Similarly, to include a gas-cap drive, the upper boundary of the top layer is considered as a constant-pressure boundary, and the vertical permeability of the gas-cap zone is considered infinite. Therefore, Eq. (5) is modified as follows:

$$(5a) X_{Ai,n} = \frac{2}{\left(\frac{h\mu}{k_v}\right)_{i,n}} \quad \text{for } i = 1, \dots, m$$

Also, in the diffusivity equation for layer $j = n$, $p_{i,j+1}$ is replaced by the initial pressure, p_{in} .

For a partially penetrating well, the inner boundary condition needs some modification. Both Eqs. (7) and (8) are considered to apply only for layers penetrated by the well. For layers that are not open to flow to the wellbore, the inner boundary condition can be written as:

$$(8a) \frac{\partial p_{1,j}}{\partial r} = 0, \quad \text{for } r = r_w \text{ and } j = \text{layers not open to flow to the wellbore}$$

For a partially penetrating well, Eqs. (7), (8) and (8a) together describe the inner boundary condition.

SOLUTION METHODOLOGY

The following steps were utilized to solve Eq. (48) at any region i and layer j :

1. From Eq. (44), eigenvalues and eigenvectors were calculated using an appropriate subroutine from the IMSL Math/Library [60].
2. From the boundary conditions, $2n \times m$ simultaneous equations were set up and then solved using Gauss' elimination routine from the IMSL Math/Library [60] for the constants A_i^A and B_i^A .
3. Dimensionless pressure in Laplace space is calculated using Eq. (48) and then numerically inverted using the Stehfest algorithm [61].
4. The wellbore storage effect is included using the following well known relationship:

$$(57) \bar{p}_{wD} = \frac{1}{C_D I^2 + \frac{1}{(\bar{p}_{wD})_{C_D=0}}}$$

The computation process involves repeated calculation of Bessel's functions. Very small and large arguments of Bessel's functions create an overflow problem during the computational process. This problem is overcome by using a dimensionless radius, r_D , based on the minimum front radius, r_{a1} , instead of the wellbore radius, and by calculating Bessel's functions in exponentiated form.

MODEL VALIDATION

The new analytical solution was validated by generating some well-known pressure transient responses for various cases of homogeneous, composite, and layered reservoirs, which are subsets of the general solution developed. Figure 3 shows a comparison of results generated by the new analytical solution with an Agarwal *et al.* [62] type-curve for homogeneous reservoirs. Homogeneous reservoir responses were generated by setting identical reservoir properties for each of the layers of a two-layer reservoir and by setting very high crossflow parameters. The responses were generated for different wellbore storage and skin effects. Figure 3 shows a successful match between the two solutions. Figure 4 shows a comparison of the responses of this study with Tariq and Ramay's solution [19] for a two-layer, commingled reservoir with a closed outer boundary. Commingled layered reservoir responses

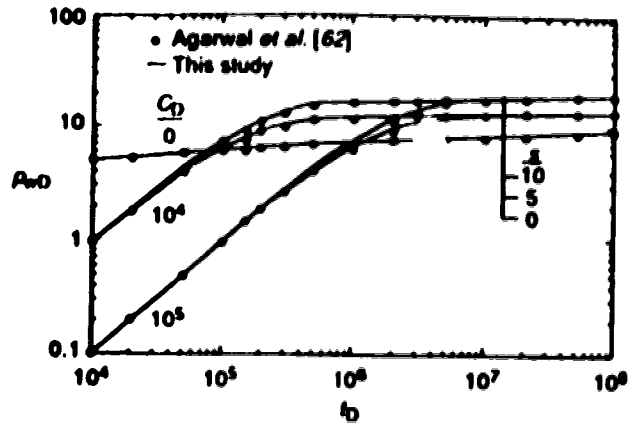


Figure 3. Comparison of this study with Agarwal *et al.*'s [62] solution for a homogeneous reservoir.

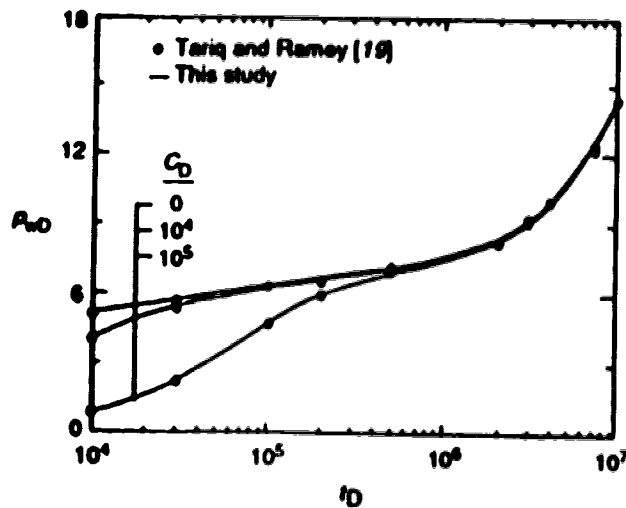


Figure 4. Comparison of this study with Tariq and Ramey's [19] solution for a two-layer reservoir with closed outer boundary.

were generated by setting different layer properties for each layer and assigning very small crossflow parameters. Figure 4 shows a very good match between the two results for different wellbore storage effects. Figure 5 shows a comparison of responses of this study with the Eggenschwiler *et al.* [63] solution for a single-layer, two-region composite reservoir. In the model, a single-layer, composite reservoir is obtained by dividing a two-layer reservoir into two regions and setting different properties for them. In each region, the layers are assigned identical fluid and rock properties and a very high crossflow parameter. The responses were

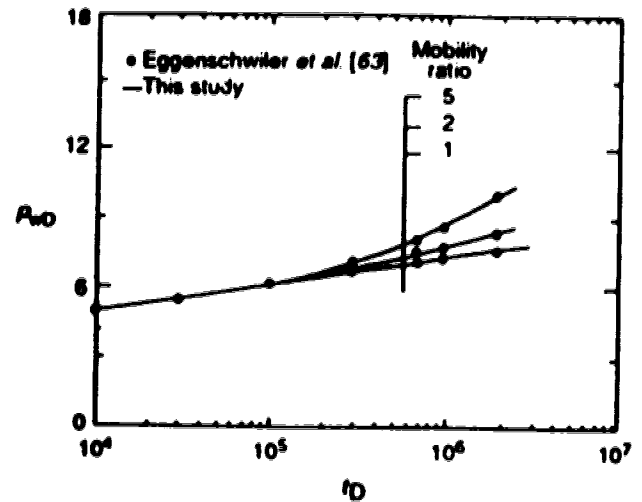


Figure 5. Comparison of this study with Eggenschwiler *et al.*'s [63] solution for a two-region composite reservoir.

generated for different mobility ratios and Figure 5 shows a good match between the two solutions. Figure 6 shows a comparison of the results of this study with Ambastha and Ramey's [64] pressure derivative solution for a single-layer, two-region, composite reservoir. Again, Figure 6 shows a good match between the two solutions. One important aspect of the new solution is its versatility. Figure 7 shows a comparison of this study with Ambastha and Ramey's solution [65] for a three-region composite reservoir. The three-region composite reservoir response was generated by dividing a two-

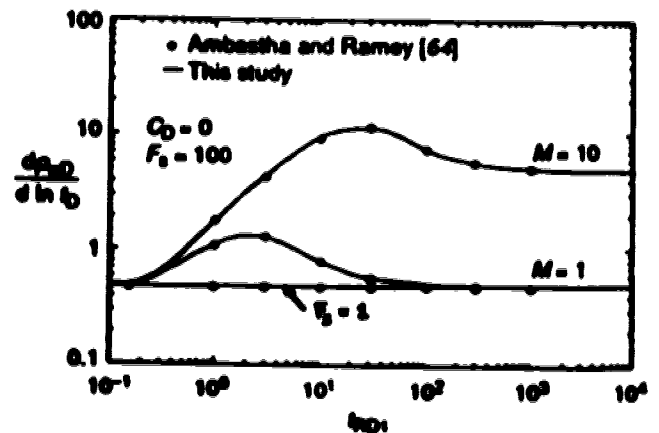


Figure 6. Comparison of this study with Ambastha and Ramey's [64] study for a two-region, composite reservoir.

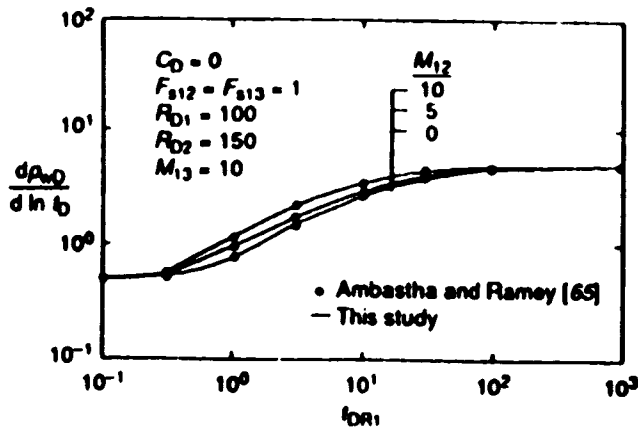


Figure 7. Comparison of this study with Ambastha and Ramey's [65] study for an infinitely large, three-region, composite reservoir.

layer reservoir into three regions and setting different fluid properties for each region. The layers were assigned identical fluid and rock properties in each region and very high crossflow parameters. Figure 7 shows pressure derivative responses for different mobility ratios between zones one and two, and the responses show a good match between the two solutions.

Figure 8 shows the effect of crossflow on pressure transient responses for a two-layer reservoir. The upper and the lower straight lines represent commingled and homogeneous reservoir responses, respectively. Initially, the reservoir behaves like a commingled reservoir. Then, depending on the crossflow parameter λ , there is a transition period during which the crossflow effect becomes important and the responses change from

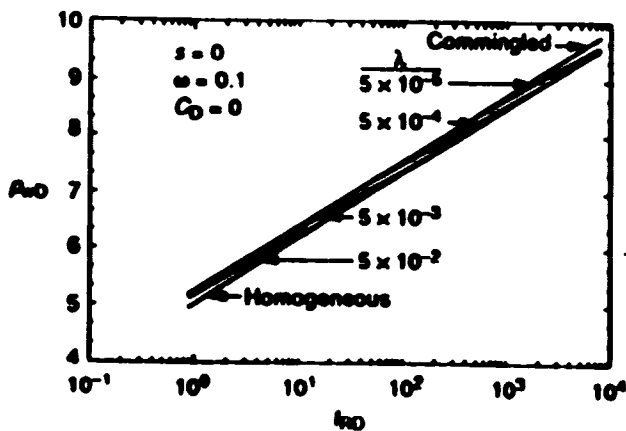


Figure 8. Effect of crossflow on wellbore pressure for a two-layer reservoir.

those for a commingled reservoir to those for a homogeneous reservoir. At late time, the reservoir behaves like an equivalent homogeneous system. The transition from commingled reservoir behaviour to homogeneous reservoir behaviour depends on the crossflow parameter. The higher the crossflow parameter, the earlier the transition occurs. The above observation is consistent with layered reservoir behaviour reported in the literature.

Figure 9 shows the pressure drawdown responses of a partially penetrating well in a two-layer reservoir subject to bottom-water drive. The upper layer is open to flow and the lower layer is closed. For a penetration ratio of 0.5, the two curves show the responses for two different crossflow parameters. Both curves show radial flow characteristics until the effect of the constant-pressure boundary becomes dominant. Similar observations have been made by Streltsova-Adams [66] and Buhidma and Raghavan [67]. For a lower crossflow parameter, it takes a longer time for the constant pressure boundary to have a dominant effect on the pressure drawdown responses.

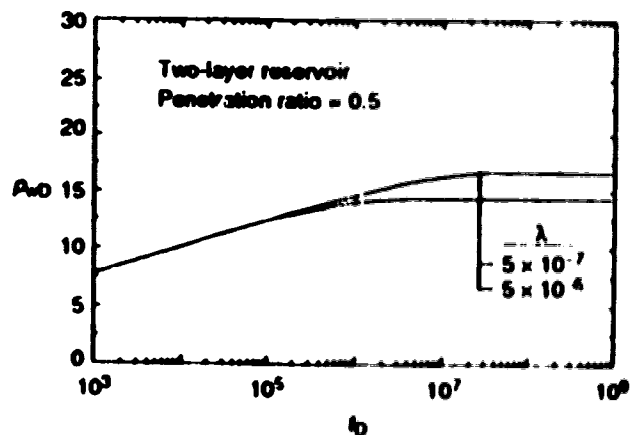


Figure 9. Pressure drawdown response of a partially penetrating well in a two-layer reservoir subject to bottom-water drive.

FUTURE POSSIBILITIES

In this study, a general analytical solution for an n -layer composite reservoir with pseudosteady-state interlayer crossflow has been developed and validated. Formation crossflow has been modelled as pseudosteady-state interlayer crossflow. This method is very general and computationally efficient. This method has

certain advantages over the finite-difference method in that this method does not have a numerical dispersion problem and rounding off error like the finite-difference method.

A reservoir undergoing a thermal recovery process has been idealized as a single-layer, composite reservoir for a long time [63,64,68-71]. This new model can be used to analyze more general scenarios of heterogeneous reservoirs undergoing thermal recovery processes. Effects of gravity override or underdrive, viscous fingering, *etc.*, on a discontinuity boundary can be treated as a tilted or any other irregularly shaped front and its effects on pressure transient responses can be studied. Pressure transient analysis of both drawdown and buildup tests can be studied with this model.

This new model can also accommodate the situation where each layer has a different outer boundary distance, r_{ej} . This can be done by vertically extending the outer boundary of each layer, the same way as has been done for the discontinuity boundaries. This will create some mathematical zones (which do not exist) which will be taken care of by assigning very small horizontal and vertical permeabilities to them.

Another possibility is to use automated type-curve matching to analyze rate and pressure measurements from different layers of layered, composite reservoirs. The effect of a gas cap or bottom-water has been included by properly specifying pressure and semi-permeabilities at the appropriate boundary to yield a constant-pressure boundary at the top or bottom, respectively. Transient pressure responses of a partially penetrating well in a layered reservoir subject to the effects of a bottom-water and/or a gas cap can be investigated with this model. The proposed analytical solution may also lead to new and/or improved methods for analyzing well test data from multi-layered, composite reservoirs with formation crossflow. Efforts are underway to develop some simplified type-curves for the system under study.

CONCLUSIONS

1. A general analytical solution for pressure transient responses for an n -layer, composite reservoir with pseudosteady-state interlayer crossflow has been developed and validated.
2. The new analytical solution developed in this study is a more efficient and versatile solution than presently available solutions in the literature.
3. The new analytical solution of this study offers new

possibilities to analyze more complicated well-testing scenarios than the possibilities offered by presently available solutions.

ACKNOWLEDGMENTS

E. Gomes acknowledges the financial support from the CIDA/BUET scholarship program. Computer facilities were provided by the Department of Mining, Metallurgical and Petroleum Engineering at the University of Alberta. This paper was originally presented as SPE 26049 at the 1993 SPE Western Regional Meeting, held in Anchorage, AK, May 26-28, 1993.

NOMENCLATURE

A_i^k	= Constant in Eq. (46)
B_i^k	= Constant in Eq. (47)
C	= Wellbore storage coefficient, m^3/Pa
C_D	= Dimensionless wellbore storage
c_t	= Total system compressibility, Pa^{-1}
E_{ij}^k	= Eigenvector for the region i
F_s	= Storativity ratio, $(\phi c)_1/(\phi c)_2$
F_{s12}	= Storativity ratio between region 1 and 2 for a 3-region reservoir, $(\phi c)_1/(\phi c)_2$
F_{s13}	= Storativity ratio between region 1 and 3 for a 3-region reservoir, $(\phi c)_1/(\phi c)_3$
h	= Formation thickness, m
k	= Permeability, m^2
l	= Laplace variable
M	= Mobility ratio, $(k/\mu)_1/(k/\mu)_2$
M_{12}	= Mobility ratio between region 1 and 2 for a 3-region reservoir, $(k/\mu)_1/(k/\mu)_2$
M_{13}	= Mobility ratio between region 1 and 3 for a 3-region reservoir, $(k/\mu)_1/(k/\mu)_3$
M_{ij}	= Mobility ratio between zone ij and $i+1j$
p	= Pressure, Pa
p_{in}	= Initial pressure, Pa
p_{wf}	= wellbore flowing pressure, Pa
p_D	= Dimensionless pressure
p_{wD}	= Dimensionless wellbore pressure
q	= Flow rate, $m^3 s^{-1}$
r	= Radial distance, m
r_D	= Dimensionless radial distance
r_s	= Radial from distance, m
r_{s1}	= Minimum radial from distance, m
r_{si}	= Radial from distance located between regions i and $i+1, m$
r_{ej}	= Outer boundary distance of layer j, m

- R_{D1} = Dimensionless front radius for region 1 for a 3-region reservoir, r_{a1}/r_w
 R_{D2} = Dimensionless front radius for region 2 for a 3-region reservoir, r_{a2}/r_w
 s = Wellbore skin effect
 s_j = Wellbore skin effect for layer j
 t = Time, sec
 t_D = Dimensionless time
 t_{RD} = Dimensionless time based on radial front distance, $r_a \cdot k(h)_1 / r_w^2 (\mu \phi c_r h)_1$
 t_{RD1} = Dimensionless time based on radial front distance, $r_{a1} \cdot k(h)_1 / r_{a1}^2 (\mu \phi c_r h)_1$
 X_{Aij} = Semi-permeability of the zone ij between layer j and $j+1$
 X_{Bij} = Semi-permeability of the zone ij between layer j and $j-1$

GREEK SYMBOLS

- σ_i^k = Eigenvalues for the region i
 κ_{ij} = Defined by Eq. (22)
 θ = Front angle, degrees
 ∂ = Partial
 λ = Crossflow parameter for a two-layered reservoir,

$$\frac{2r_w^2}{\left[\left(\frac{h\mu}{k_v} \right)_1 + \left(\frac{h\mu}{k_v} \right)_2 \right] \left(\frac{k_h}{\mu} \right)}$$

- λ_{Aij} = Defined by Eq. (24)
 λ_{Bij} = Defined by Eq. (25)
 μ = Viscosity
 ω = Relative storativity, $(\phi c_r h)_1 / (\phi c_r h)_2$
 ω_{ij} = Defined by Eq. (23)
 ϕ = Porosity

REFERENCES

1. C.A. Ehlig-Economides and J.A. Joseph, A New Test for Determination of Individual Layer Properties in a Multilayered Reservoir, *SPE Formation Evaluation* (Sept. 1987) 261.
2. P. Jacquard., Etude Mathematique du Drainage d'un Reservoir Heterogene, *Rev. Inst. Fr. Petrole*, 15 (1960) 1384.
3. W. Tempelaar-Lietz, Effect of the Rate of Oil Production Upon the Performance of Wells Producing from more than One Horizon, *SPE J.* (March 1961) 26.
4. H.C. Lefkovits, P. Hazebroek, E.E. Allen and C.S. Matthews, A Study of the Behavior of Bounded Reservoirs Composed of Stratified Layers, *SPE J.* (March 1961) 43.
5. G. Duvaut, Drainage des systemes heterogenes, *Rev. Inst. Fr. Petrole*, 16 (1961) 1164.
6. F. Pelissier and P. Seguiers, Analyse numerique des equations des bicouches, *Rev. Inst. Fr. Petrole*, 16 (1961) 1182.
7. J. Pottier, Modeles heterogenes avec communications, *Rev. Inst. Fr. Petrole*, 16 (1961) 1127.
8. P.Ya. Polubarinova-Kocina, Theory of Groundwater Movement, Translated from Russian by J.M. Roger de Weist, Princeton U. Press, Princeton, NJ (1962) p. 381.
9. D.G. Russell and M. Prats, Performance of Layered Reservoirs with Crossflow: Single-Compressible-Fluid Case, *J. Petrol. Technol.*, 14 (1962) 53.
10. D.G. Russell and M. Prats, The Practical Aspects of Interlayer Crossflow, *J. Petrol. Technol.*, 14 (1962) 589.
11. M.L. Katz and M.R. Tek, A Theoretical Study of Pressure Distribution and Fluid Flux in Bounded Stratified Porous Systems With Crossflow, *SPE J.* (March 1962) 68.
12. J.D. Pendergrass and V.J. Berry, Pressure Transient Performance of a Multilayered Reservoir with Crossflow, *SPE J.* (Dec. 1962) 347.
13. H. Kazemi and M.S. Seth, Effect of Anisotropy and Stratification on Pressure Transient Analysis of Wells with Restricted Flow Entry, *J. Petrol. Technol.*, 21 (1969) 639.
14. H. Kazemi, Pressure Buildup in Reservoir Limit Testing of Stratified Systems, *J. Petrol. Technol.*, 22 (1970) 943.
15. E.G. Woods, Pulse-Test Response of a Two-Zone Reservoir, *SPE J.* (Sept. 1970) 245.
16. W.M. Cobb, H.J. Ramey, Jr. and F.G. Miller, Well-Test Analysis for Wells Producing Commingled Zones, *J. Petrol. Technol.*, 24 (1972) 77.
17. R.C. Earlougher, Jr., K.M. Kersch and W.J. Kunzman, Some Characteristics of Pressure Buildup Behavior in Bounded Multiple-Layered Reservoirs without Crossflow, *J. Petrol. Technol.*, 26 (1974) 1178.
18. R. Raghavan, H.N. Topaloglu, W.M. Cobb and H.J. Ramey, Jr., Well-Test Analysis for Wells Producing From Two Commingled Zones of Unequal Thickness, *J. Petrol. Technol.*, 26 (1974) 1035.

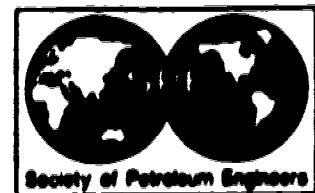
19. S.M. Tariq and H.J. Ramey, Jr., Drawdown Behavior of a Well with Storage and Skin Effect Communicating With Layers of Different Radii and Other Characteristics, paper SPE 7453 presented at the SPE Annual Technical Conference and Exhibition, Houston, TX, Oct. 1-3, 1978.
20. W.C. Chu and R. Raghavan, The Effect of Non-communicating Layers on Interference Test Data, *J. Petrol. Technol.*, 33 (1981) 370.
21. L. Larsen, Wells Producing Commingled Zones with Unequal Initial Pressures and Reservoir Properties, paper SPE 10325 presented at the SPE Annual Technical Conference and Exhibition, San Antonio, TX, Oct. 5-7, 1981.
22. A. Satman, An Analytical Study of Transient Flow in Stratified Systems with Fluid Banks, paper SPE 10264 presented at the 56th Annual Technical Conference and Exhibition, San Antonio, TX, Oct. 5-7, 1981.
23. C.O. Bennett, A.C. Reynolds and R. Raghavan, Analysis of Finite Conductivity Fractures Intercepting Multilayer Reservoirs, *SPE Formation Evaluation* (June 1982) 259.
24. L. Larsen, Determination of Skin Factor and Flow Capacities of Individual Layers in Two-Layered Reservoir, paper SPE 11138 presented at the Annual Tech. Conference and Exhibition of SPE, New Orleans, Sept. 26-29, 1982.
25. M. Prats, Interpretation of Pulse Tests in Reservoirs with Crossflow Between Contiguous Layers, *SPE Formation Evaluation* (Oct. 1983) 511.
26. H. Niko, Well Test Interpretation of Heterogeneous Reservoirs With Skin and Afterflow: Some New Theoretical Solutions and General Field Experience, paper SPE 11964 presented at the Annual Tech. Conference and Exhibition of SPE, San Francisco, CA, Oct. 5-8, 1983.
27. C. Gao, Crossflow Behaviour in a Partially Penetrated Two-Layer Reservoir: the Evaluation of Reservoir Parameters by Transient Well Tests, paper SPE 11875 presented at the Annual Tech. Conference and Exhibition of SPE, San Francisco, CA, Oct. 5-8, 1983.
28. I. Javandel and P.A. Witherspoon, Analytical Solution of Partial Penetration in a Two-Layer Aquifer, *Water Resource Res.*, 19 (1983) 567.
29. C. Gao, Single-Phase Fluid Flow in a Stratified Porous Medium with Crossflow, *SPE J.* (Feb. 1984) 97.
30. T.D. Streltsova-Adams, Buildup Analysis for Interference Tests in Stratified Formations, *J. Petrol. Technol.*, 36 (1984) 301.
31. S.T. Lee, M.C.H. Chien and W.E. Culham, Vertical Single-Well Pulse Testing of a Three-Layer Stratified Reservoir, paper SPE 13249 presented at the Annual Technical Conf. and Exhibition, Houston, TX, Sept. 16-19, 1984.
32. D. Bourdet, Pressure Behaviour of Layered Reservoirs with Crossflow, paper SPE 13628 presented at the California Reg. Mtg., CA, March 27-29, 1985.
33. R.E. Bremer, H. Winston and S. Vela, Analysis Model for Vertical Interference Tests Across Low-Permeability Zones, *SPE J.* (June 1985) 407.
34. R. Prijambodo, R. Raghavan and A.C. Reynolds, Well Test Analysis for Well Producing Layered Reservoir with Crossflow, *SPE J.* (June 1985) 380.
35. A. Satman and M.M. Oskay, Effect of a Tilted Front on Well Test Analysis, paper SPE 14701, available from SPE (1985).
36. C.A. Ehlig-Economides and J. Ayoub, Vertical Interference Testing Across a Low Permeability Zone, *SPE Formation Evaluation* (Oct. 1986) 497.
37. F. Kucuk, M. Karakas and L. Ayestaran, Well Test Analysis Techniques for Layered Reservoirs, *SPE Formation Evaluation* (Aug. 1986) 342.
38. C.A. Ehlig-Economides and J. Joseph, Evaluation of Single Layer Transients in a Multilayer System, paper SPE presented at the European Petrol. Conference, London, U.K., Oct. 20-22, 1986.
39. F. Kucuk, M. Karakas and L. Ayestaran, Well Test Analysis of Commingled Zones Without Crossflow, paper SPE 15419 presented at the Annual Meeting, New Orleans, Oct. 5-8, 1986.
40. M.J. Mavor and G.W. Walkup, Jr., Application of Parallel Resistance Concept to Well Test Analysis of Multilayered Reservoirs, paper SPE 15117 presented at the California Regional Meeting, Oakland, CA, April 2-4, 1986.
41. J. Joseph, A. Boccock, F. Nai-Fu and L.T. Owi, A Study of Pressure Transient Behavior in Bounded Two-Layered Reservoirs: Shengli Field, China, paper SPE 15418 presented at the Annual Meeting, New Orleans, LA, Oct. 5-8, 1986.
42. T. Chen, Pressure Drawdown in a Layered Reservoir with Linear Boundaries, paper SPE 16767 presented at the Annual Meeting, Dallas, TX, Sept 27-30, 1987.

43. C. Gao, Determination of Parameters for Individual Layer Properties in a Multilayer Reservoir, SPE Formation Evaluation (Sept. 1987) 43.
44. C. Morris, Case Study of a Gulf Coast Layered Reservoir Using Multirate Transient Testing, paper SPE 16762 presented at the Annual Meeting, Dallas, TX, Sept. 27-30, 1987.
45. D.G. Hatzignatiou, D.O. Ogbe, K. Dehghani and M.J. Economides, Interference Behaviour in Multilayered Composite Reservoirs, paper SPE 16766 presented at the 62nd Annual Technical Conference and Exhibition, Dallas, TX, Sept. 27-30, 1987.
46. C. Gao and H.A. Deans, Pressure Transients and Crossflow Caused by Diffusivities in Multilayer Reservoirs, SPE Formation Evaluation (June 1988) 438.
47. L. Larsen, Similarities and Differences in Methods Currently used to Analyze Pressure-Transient Data From Layered Reservoirs, paper SPE 18122 presented at the Annual Meeting, Houston, TX, Oct. 2-5, 1988.
48. L. Larsen, Boundary Effects in Pressure-Transient Data From Layered Reservoirs, paper SPE 19797 presented at the 64th Annual Technical Conference and Exhibition of the SPE, San Antonio, TX, Oct. 8-11, 1989.
49. H. Park and R.N. Horne, Well Testing Analysis of a Multilayered Reservoir With Formation Crossflow, paper SPE 19800 presented at the 64th Annual Technical Conference and Exhibition of the SPE, San Antonio, TX, Oct. 8-11, 1989.
50. J.S. Olarewaju and W.J. Lee, Pressure Buildup Behavior of Partially Completed Wells in Layered Reservoirs, paper SPE 18876 presented at the SPE Production Operation Symposium, Oklahoma City, OK, Marc 13-14, 1989.
51. J.S. Olarewaju and W.J. Lee, Pressure Behavior of Layered and Dual-Porosity Reservoirs in the Presence of Wellbore Effects, SPE Formation Evaluation (Sept. 1989) 397.
52. R. Raghavan, Behavior of Wells Completed in Multiple Producing Zones, SPE Formation Evaluation (June 1989) 219.
53. N. Yeh and A.C. Reynolds, Analysis of Pressure Data From a Restricted Entry Well in a Multilayer Reservoir, SPE Formation Evaluation (March 1989) 81.
54. N. Yeh and A.C. Reynolds, Computation of the Pseudoskin Factor Caused by a Restricted-Entry Well Completed in a Multilayer Reservoir, SPE Formation Evaluation (June 1989) 253.
55. K. Anbarci, A.S. Grader and T. Erickin, Determination of Front Locations in Multilayer Composite Reservoir, Paper SPE 19799 presented at the 64th Annual Tech. Conference and Exhibition of the SPE, San Antonio, TX, Oct. 8-11, 1989.
56. J.S. Olarewaju and W.J. Lee, Rate Performance of a Layered Reservoir with Unsteady-state Interlayer Crossflow, SPE Formation Evaluation (March 1990) 46.
57. S. Mishra and H.J. Ramey, Jr., A Comparison of Pressure-Transient and Tracer-Concentration/Time Data for Layered Reservoirs Under Injection, SPE Formation Evaluation (March 1990) 60.
58. J.D. Spath, B. Ozkan and R. Raghavan, An Efficient Algorithm for Computation of Well Responses in a Commingled Reservoir, paper CIM/SPE 90-1 presented at the International Tech. Meeting, Calgary, AB, June 10-13, 1990.
59. I. Kiome, Pressure Transient Behaviour for a Well in a Multi-Layered Composite Reservoir with an Inclined Front, M.Sc. Thesis, University of Alberta, Edmonton, AB, 1991.
60. User's Manual, IMSL Math/Library, version 1.0 (April 1987) pp. 13 and 329.
61. H. Stehfest, Algorithm 368, Numerical Inversion of Laplace Transforms, D-5, Comm. of ACM, 13, No.1 (Jan. 1970) 49.
62. R.G. Agarwal, R. Al-Hussainy and H.J. Ramey, Jr., An Investigation of Wellbore Storage and Skin effect in Unsteady Liquid Flow, SPE J. (September 1970) 279.
63. M. Eggenchwyler, H.J. Ramey, Jr., A. Sattman and H. Cinco-Ley, Interpretation of Injection Well Pressure Transient Data in Thermal Oil Recovery, paper SPE 8908 presented at the California Reg. Mtg. of SPE of AIME, Los Angeles, CA, April 9-11, 1980.
64. A.K. Ambastha and H.J. Ramey, Jr., Thermal Recovery Well Test Design and Interpretation, SPE Formation Evaluation (June 1989) 173.
65. A.K. Ambastha and H.J. Ramey, Jr., Pressure Transient Analysis for a Three-Region Composite Reservoir, paper SPE 24378 presented at the SPE Rocky Mountain Reg. Mtg., Wyoming, May 18-21, 1992.
66. T.D. Strelkova-Adams, Pressure Drawdown in a Well with Limited Flow Entry, J. Petrol. Technol., 29 (1977) 1469.
67. I.M. Buhidma and R. Raghavan, Transient Pressure Behavior of Partially Penetrating Wells Subject to Bottomwater Drive, J. Petrol. Technol., 32 (1988) 1251.

-
68. J.W. Walsh, H.J. Ramey, Jr. and W.E. Brigham, Thermal Injection Well Falloff Testing, paper SPE 10227 presented at the 56th Annual Technical Conference and Exhibition of SPE of AIME, San Antonio, TX, Oct. 5-7, 1981.
 69. G. Da Prat, A. Bockh and L. Prado, Use of Pressure Falloff Tests to Locate the Burning Front in the Miga Field, Eastern Venezuela, paper SPE 13667 presented at the California Reg. Mtg. Bakersfield, CA, March 27-29, 1985.
 70. J.F. Stanislav, C.V. Easwaran and S.L. Kokal, Interpretation of Thermal Injection Well Testing, SPE Formation Evaluation (June 1989) 181.
 71. M.R. Fassihi, Evaluation of An Analytical Technique for Estimating Swept Volume from Thermal Pressure Falloff Tests in Heterogeneous Systems, SPE Formation Evaluation (June 1988) 449.

Appendix H: Presented Paper From Chapter 4

This appendix shows the paper SPE 26484 presented at the 1993 SPE Annual Meeting, held in Houston, TX, October 3-6, 1993.



SPE 26484

Analytical Expressions for Pseudoskin for Partially Penetrating Wells Under Various Reservoir Conditions

Edmond Gomes and A.K. Ambastha, U. of Alberta

SPE Members

Ω

Copyright 1993 Society of Petroleum Engineers Inc.

This paper was prepared for presentation at the 68th Annual Technical Conference and Exhibition of the Society of Petroleum Engineers held in Houston, Texas, 3-6 October 1993.

This paper was selected for presentation by an SPE Program Committee following review of information contained in an abstract submitted by the author(s). Contents of the paper as presented have not been reviewed by the Society of Petroleum Engineers and are subject to correction by the author(s). The material, as presented, does not necessarily reflect any position of the Society of Petroleum Engineers, its officers, or members. Papers presented at SPE meetings are subject to publication review by Editorial Committees of the Society of Petroleum Engineers. Permission to copy is restricted to an abstract of not more than 300 words. Illustrations may not be copied. The abstract should contain conspicuous acknowledgment of where and by whom the paper is presented. Write Librarian, SPE, P.O. Box 833889, Richardson, TX 75083-3889, U.S.A. Telex: 163245 SPEUT.

Abstract

Many times, oil reservoirs are accompanied by bottom-water zones and/or gas caps, and these reservoirs are produced using partially-penetrating wells. An extra pressure drop occurs around such wells during production because of partial penetration. Several correlations have been presented in the literature to estimate pseudoskin for a partially-penetrating well located in either a homogeneous or a layered reservoir with closed top and bottom boundaries. This study aims to develop new analytical expressions for pseudoskin for partially-penetrating wells in multi-layered reservoirs with both closed top and bottom boundaries, and with bottom water zones and/or gas caps. A pseudosteady-state interlayer crossflow has been assumed in this study.

These new analytical expressions are simple and easy to use. Evaluation of pseudoskin using these expressions requires a knowledge of two parameters when the top and the bottom boundaries are closed, and three parameters in the presence of a bottom-water zone or a gas cap, regardless of the number of layers. The estimated pseudoskin is very close to the actual pseudoskin obtained from the complete analytical solution. These new analytical expressions are also applicable to the corresponding homogeneous and single-layered cases. The estimated pseudoskin values have been compared with those estimated by other researchers. Effects of the open interval location, the presence of bottom-water zone and/or gas cap, and the layer refinement on pseudoskin have also been studied.

Introduction

Reservoir deposition occurs over geologic period of time and, because of this, many reservoirs are layered instead of homogeneous. (Oil reservoirs are often accompanied by a bottom-water zone and/or a gas cap. In such situations, wells are completed over a fraction of the productive zone to delay water and/or gas coning. These wells are known as partially-penetrating wells. Because of partial penetration, pressure transient responses show additional pressure drop in comparison to the pressure drop for a fully-penetrating well. This additional pressure drop is referred to as pseudoskin. Partially-penetrating wells have their own characteristic responses which, if not properly evaluated, may lead to errors in the interpretation of well-test data. The purpose of this paper is to study the pressure transient responses and pseudoskin factor in a partially-penetrated, multi-layered reservoir with or without a bottom-water zone or a gas cap.

Muskat¹ studied partially-penetrating wells in single-layered reservoirs under steadystate conditions using the method of images and estimated productivity loss because of partial penetration. Nisio² presented buildup pressure transient responses for a partially-penetrating well in a single-layered homogeneous reservoir. He considered a partially-penetrating well in an infinite slab and used the method of images to solve the problem. He observed two different straight lines for early and late time pressure buildup responses and used ratio of the slopes of these two straight lines to estimate penetration ratio. Beens and Marting³ observed three sequences in pressure transient responses of a partially-penetrating well in a single-layered isotropic reservoir: a radial flow period with a slope corresponding to open interval thickness, a transition period, and a pseudoradial flow period with a slope corresponding to total formation thickness. They presented an empirical expression for pseudoskin factor, s_p . But they did not consider the variation in the horizontal and the

References and illustrations at end of paper

vertical permeabilities when defining dimensionless wellbore thickness and their pseudoskin factor had to be numerically evaluated.

Bilhariz and Ramey⁴ used a 2-D finite-difference model to study wellbore storage and skin effects in a single-layered, partially-penetrated reservoir. They concluded that radial flow period and transition to pseudoradial flow period may be masked in the presence of significant wellbore storage. They extended Bruns and Marting³ pseudoskin expression for anisotropic reservoirs and discussed methods to estimate horizontal and vertical permeabilities.

Strelisova-Adams⁵ used Laplace and Hankel transformations to solve partial-penetration problem in a single-layered reservoir and derived an expression for pseudoskin factor in terms of infinite sine and cosine series. She considered the presence of a gas cap as a constant-pressure boundary in her solution. She investigated the effect of open interval (penetrated portion) location on pseudoskin factor and concluded that pseudoskin factor is minimum for centrally-located open intervals, other parameters remaining unchanged. She also observed that for a reservoir with a gas cap, the pseudoskin factor is lower than that for a reservoir with no gas cap, when the open interval is adjacent to the constant-pressure boundary. Buhidma and Raghavan⁶ studied drawdown and buildup behaviour of a partially-penetrating well in a square reservoir subject to bottom-water drive. Using Green's function for solution, they concluded that under bottom-water drive, pseudoradial flow does not exist and pseudoskin factor can not be calculated by the methods presented by Bruns and Marting³ and other researchers. Although pseudoradial flow period does not exist under bottom-water or gas-cap drive, the expression for pseudoskin developed in this study can be used to estimate the pseudoskin factor under these reservoir conditions.

Using a 2-D finite-difference simulator, Reynolds et al.⁷ graphically presented the pressure transient responses of a partially-penetrated, two-layered reservoir. Analyzing the steady-state analytical solution, they identified the correlating parameters and then obtained a correlation for pseudoskin factor by regression analysis. They also concluded that using different layers for different fluid regions, a multi-phase flow system can be approximated by a layered, single-phase flow system.

Papatzacos⁸ used the method of images to solve partial-penetration problem for a single-layered, homogeneous reservoir and derived an expression for pseudoskin factor in terms of dimensionless open interval, its location and dimensionless wellbore radius.

Olarowaju and Lee⁹ studied buildup pressure behaviour of a partially-penetrating well in a two-layered reservoir with closed top and bottom boundaries. Of the two layers they considered, one layer is open to flow and the other layer is closed. In the closed layer, they considered flow only in the vertical direction, neglecting the radial component of the flow, which may limit the applicability of their model. Olarowaju and Lee⁹ considered crossflow as a time-dependent source term for the open layer based on the vertical flow component for the closed layer. By regression analysis, they developed a series of expressions correlating the pseudoskin factor with the penetration ratio for various k_1/k_2 values.

Using a numerical simulator, Yeh and Reynolds¹⁰ presented some type-curves for partially-penetrated, multi-layered reservoirs with transient crossflow. Using the same numerical model, Yeh and Reynolds¹¹ graphically presented pseudoskin factors for a partially-penetrated, multi-layered reservoir. Using regression analysis, they obtained an expression for pseudoskin factor.

Vrbik¹² derived a simplified approximate expression for a single-layered, homogeneous reservoir in terms of three correlating parameters which are related to dimensionless open interval length, its location and dimensionless wellbore radius. Ding and Reynolds¹³ extended Papatzacos⁸ expression for pseudoskin for a single-layered reservoir to that for a multi-layered reservoir and reported good match with simulated results.

Shah and Thambynayagam¹⁴ presented an analytical solution for a two-layered, partially-penetrated reservoir by successive application of Laplace and Hankel transformations. They considered transient crossflow between the two layers and the presence of a gas-cap drive. They presented some pressure transient responses for fully- and partially-penetrating wells and did not study the pseudoskin factor because of the partial penetration.

Table 1 summarizes most of the studies¹⁻¹⁹ conducted on partially-penetrated reservoirs and pseudoskin factor. Table 1 shows that most of the studies considered single-layered reservoirs and only a limited number of studies have focused on partially-penetrating, multi-layered reservoirs. Partially-penetrated, multi-layered reservoir problem has been studied either by using a numerical simulator with graphical presentation of pressure transient responses and pseudoskin values (Yeh and Reynolds^{10,11}), or by extending the single-layered expression of pseudoskin to multi-layered case by redefining some parameters (Ding and Reynolds¹³). Table 1 also shows that very few studies have been conducted for a partially-penetrated reservoir subject to a bottom-water or a gas-cap drive.

This study attempts to give some new insights in understanding partially-penetrated, multi-layered reservoirs and covers both pressure transient responses and pseudoskin factors in situations when the top and bottom boundaries are closed and when one of the boundaries is at a constant pressure because of a bottom-water or a gas-cap drive.

Pseudoskin Factor Correlation for a Partially-Penetrated Reservoir with Closed Top and Bottom Boundaries

Figure 1 schematically shows a two-layered, partially-penetrated reservoir. In this study, the layers are numbered from bottom to top. Thus, layer 1 is always the bottom-most layer. In Figure 1, layer 1 is penetrated and layer 2 is closed at the wellbore. The upper boundary of the layer 2 and the lower boundary of the layer 1 are considered as closed boundaries. Pseudosteady-state crossflow is considered between the two layers. Appendix A shows a detailed derivation of the pressure transient solution and late-time limiting solution for this case. From the late-time limiting solution, we obtain the expression for pseudoskin as:

$$s_b = \frac{(1-\kappa)}{\kappa} \frac{K\left(\sqrt{\frac{\lambda_A}{\kappa(1-\kappa)}}\right)}{\sqrt{\frac{\lambda_A}{\kappa(1-\kappa)}} K\left(\sqrt{\frac{\lambda_A}{\kappa(1-\kappa)}}\right)} \quad (1)$$

where s_b denotes the pseudoskin, and λ_A and κ denote dimensionless crossflow parameter and mobility-thickness ratio of the open interval, respectively. Equation (1) can be extended for a multi-layered reservoir by appropriately defining λ_A and κ as:

$$s_b = \frac{(1-\bar{\kappa})}{\bar{\kappa}} \frac{K\left(\sqrt{\frac{\bar{\lambda}_A}{\bar{\kappa}(1-\bar{\kappa})}}\right)}{\sqrt{\frac{\bar{\lambda}_A}{\bar{\kappa}(1-\bar{\kappa})}} K\left(\sqrt{\frac{\bar{\lambda}_A}{\bar{\kappa}(1-\bar{\kappa})}}\right)} \quad (2)$$

where, $\bar{\kappa}$ = total mobility-thickness ratio of the open interval
 $\bar{\lambda}_A$ = average crossflow parameter

Equation (2) is applicable for a multi-layered reservoir having any arbitrary number of layers consisting the open interval and any arbitrary location of the open interval. In equation (2), $\bar{\kappa}$ and $\bar{\lambda}_A$ are calculated by adding the individual layer mobility-thickness ratio of the open interval, and by adding the bottom and the top boundary crossflow parameters of the open interval, respectively. For multi-layered reservoirs, instead of considering crossflow parameters of each and every layer, only top and bottom boundary crossflow parameters of the open interval are considered in defining the average crossflow parameter. This was done because equation (2) gives better results with an average crossflow parameter defined in this manner, rather than with an average crossflow parameter, which considers the crossflow parameters of each and every layer. Similar observation is made by Ding and Reynolds¹³ in defining the average vertical permeability. Irrespective of the number of layers in the reservoir, only two parameters (i.e., $\bar{\kappa}$ and $\bar{\lambda}_A$) are required to estimate the pseudoskin using equation (2).

For a single-layered, anisotropic reservoir, the mobility-thickness ratio, κ , and the crossflow parameter, λ_A , reduce to the penetration ratio (b) and $2b^2/h_D^2$, respectively. With these simplifications, equation (1) reduces to:

$$s_b = \frac{1}{\sqrt{2}} \left(\frac{1-b}{b} \right) \frac{K\left(\sqrt{\frac{2b}{b^2(1-b)}}\right)}{K\left(\sqrt{\frac{2b}{b^2(1-b)}}\right)} \quad (3)$$

$$\text{where, } b = \frac{h}{h_D} \sqrt{\frac{k}{k_v}} \quad (4)$$

Equation (3) estimates pseudoskin factor for a single-layered, anisotropic reservoir with closed top and bottom boundaries.

Equation (3) is also applicable for homogeneous reservoirs with an appropriate change (i.e., $k = k_v$) in the definition of h_D .

Pseudoskin Factor Expression for a Partially-Penetrated Reservoir Subject to a Gas-Cap or a Bottom-Water Drive

Figure 2 schematically shows a two-layered, partially-penetrated reservoir subject to a gas-cap drive. Layer 1 is penetrated and layer 2 is closed at the wellbore. The upper boundary of the layer 2 is considered as a constant-pressure boundary because of the gas cap, whereas the lower boundary of the layer 1 is considered as a closed boundary. Pseudosteady-state crossflow is considered between the two layers. Appendix B shows a detailed derivation of the pressure transient solution and late-time limiting solution. From late-time limiting solution, we obtain the pseudoskin expression as:

$$s_b = \frac{s_{b1} K_1(G_1)}{(s_{b1} - s_{b2}) K_1(G_1)} - \frac{s_{b2} K_2(G_2)}{(s_{b1} - s_{b2}) K_1(G_1)} - \frac{(s_{b1} - s_{b2}) K_2(G_2) K_1(G_1)}{b_1} \quad (5)$$

where s_b denotes the pseudoskin factor, and G_1 , G_2 , s_{b1} , and b_1 are late-time limiting values defined by the equations (B.22) through (B.26) and (B.30) in Appendix B. The variable, λ_C , in the equations (B.22) through (B.26), is the crossflow parameter between the reservoir and the gas cap and this parameter is required to calculate the late-time limiting values in equation (5). Equation (5) estimates the pseudoskin in a two-layered, partially-penetrated reservoir subject to a gas-cap or a bottom-water drive. Equation (5) is also applicable for a multi-layered reservoir having any arbitrary number of layers representing the open interval and any arbitrary location of the open interval, provided κ and λ_A are calculated by adding the individual layer mobility-thickness ratio of the open interval, and by adding the top and the bottom boundary crossflow parameters of the open interval, respectively. Irrespective of the number of layers in the reservoir, only three parameters (i.e., $\bar{\kappa}$, $\bar{\lambda}_A$ and λ_C) are required to estimate the pseudoskin. An effort was made to simplify equation (5) for a single-layered reservoir without much success.

Accuracy of Pseudoskin Factor Expressions

For multilayered reservoirs, Table 2 compares the estimated pseudoskins using the simplified expressions of equations (2) and (5), with those calculated using the actual analytical solutions. Layered reservoirs of 2, 3 and 5 layers are considered. Various cases of reservoir configuration in Table 2 are explained in Table 3. In Table 2, for a particular reservoir, s_{bC} denotes the actual or 'correct' pseudoskin from the analytical solution of Gomes and Amratha²⁰, which is the late-time dimensionless pressure difference between the response of the partially-penetrating well and that of the fully-penetrating well at a particular time, whereas s_{bGA} denotes the estimated pseudoskin using the simplified expressions of equations (2) and (5). For different values of open

interval mobility-thickness ratio ($\bar{\kappa}$) and crossflow parameter ($\bar{\lambda}_A$) and for different open interval locations, pseudoskin factors are estimated for layered reservoirs having different number of layers. For both the closed top and bottom boundaries and the bottom-water zone, Table 2 shows excellent match between the estimated and the actual pseudoskins for all different cases considered.

Comparison with Reference 3

Figure 3 compares the pseudoskin factors estimated from equation (3) of this study with those from Figure 2 of Brons and Martin³ study for a single-layered, homogeneous reservoir. Figure 3 shows that, except for small penetration ratios ($b < 0.3$), the pseudoskin factors estimated from equation (3) are very close to those estimated from Brons and Martin³ study. The difference between the two pseudoskin values increases with the decrease in penetration ratios. Also, pseudoskin factors calculated from equation (3) are consistently higher than those of Brons and Martin³ study. The reason for the differences in pseudoskin values may be the difference in crossflow modelling in the two studies.

Comparison with References 11 and 13

Table 4 compares the pseudoskin factors estimated from this study with those estimated from Yeh and Reynolds¹¹ and Ding and Reynolds¹³ studies. Various cases in Table 4 refer to different data sets. Cases in Table 4 are not related to cases in Table 3. Table 4 shows data for a three-layered reservoir with closed top and bottom boundaries and with layer 3 open to flow. These data are taken from Ding and Reynolds¹³ study. In Table 4, s_{DYN} and s_{DNR} denote the pseudoskin obtained from Yeh and Reynolds¹¹ study and Ding and Reynolds¹³ study, respectively. Table 4 shows consistently close comparison of the pseudoskins of this study with those of Ding and Reynolds¹³ study, and of Yeh and Reynolds¹¹ study. Ding and Reynolds¹³ reported good match between their pseudoskin and that obtained from the numerical simulator. In most cases, pseudoskin factors obtained from the analytical solution as well as from the simplified expression developed in this study are observed to be greater than those obtained from Ding and Reynolds¹³ study, and from Yeh and Reynolds¹¹ study. This is probably because of the pseudosteady state crossflow assumption in the development of the analytical model of this study. Significance of this assumption is that the resistance to vertical flow is assumed to be limited in the interlayer area instead of uniformly dispersed in the vertical direction. This pseudosteady state crossflow assumption is more applicable when shale streaks are present in the interlayer areas.

Development of New Time Criteria and Comparison with Reference 4

Figure 4 shows the effect of crossflow parameter, λ_A , on pressure derivative responses of a two-layered reservoir with different open interval mobility-thickness ratio, κ . The crossflow parameter (λ_A) has been varied between 0.5×10^{-5} and 0.5×10^{-7} , and the

mobility-thickness ratio (κ) has been varied between 0.25 and 0.75. For all values of the crossflow parameter and the mobility-thickness ratio, the early time responses show radial flow behaviour with a constant semi-log slope of $0.5/\kappa$. At very early time, the semi-log slopes are slightly lower than their constant value because of the numerical errors introduced in solving the system of equations. After some time, the responses show a transition from the radial flow behaviour, and the time at which the transition occurs is a strong function of the crossflow parameter and the mobility-thickness ratio. At late time, all responses show pseudoradial flow behaviour with a semi-log slope of 0.5. Again, the time to the beginning of the pseudoradial flow is a function of the crossflow parameter and the mobility-thickness ratio. The higher the crossflow parameters are, the sooner the radial flow period ends and the sooner the pseudoradial flow period begins. The lower the mobility-thickness ratio is, the earlier the radial flow period ends and the later the pseudoradial flow period begins. Analysis of the pressure derivative responses shown in Figure 4 results in the following criteria for the end of the radial flow period and the beginning of the pseudoradial (second radial) flow period as:

$$t_{01} = 0.0196 \kappa^2 / \lambda_A \quad (6)$$

$$t_{02} = 0.658 / (\lambda_A \sqrt{\kappa}) \quad (7)$$

Equations (6) and (7) describe the times by which the semi-log pressure derivatives are within 5% of the correct slope values. Equations (6) and (7) have been extended for reservoirs having more than two layers by replacing λ_A and κ by $\bar{\lambda}_A$ and $\bar{\kappa}$, respectively, and have been tested to be applicable for three layered and five-layered reservoirs.

Bilharz and Ramsey⁴ used a 2-D finite-difference model to study the pressure transient responses of a partially-penetrating well with wellbore storage and skin effects. Based on an analysis of pressure responses, they developed the time criteria for the end of radial flow and the beginning of the pseudoradial flow periods as follow:

$$t_{01} = 0.02 h_D^2 \quad (8)$$

$$t_{02} = h_D^2 \left(\frac{h}{h_w} \right)^2 \left[\ln \left(\frac{2 \sin \left(\frac{\pi h_x}{h} \right) \cos \left(\frac{\pi h_x}{2h} \right) \cos \left(\frac{3\pi h_x}{4h} \right)}{2} \right) \right] \cdot \ln (0.02) \quad (9)$$

where, h_D is defined by equation (4).

For a single-layered reservoir, equations (6) and (7) degenerate to the following form:

$$t_{01} = 0.0098 h_D^2 \quad (10)$$

$$t_{02} = 0.329 \frac{h_D}{\sqrt{\kappa}} \quad (11)$$

The time for the end of the first radial flow period given by equation (10) is about half of that given by equation (8). Thus, the first radial flow period ends earlier as predicted by equation (10) than by equation (8). For a single-layered reservoir, equation (11) estimates the time for the beginning of the second radial flow period, $t_{D2} = 837,500$ with a crossflow parameter $\lambda_A = 1.11 \times 10^{-6}$ and a penetration ratio of 0.5. For the same data, equation (9) estimates $t_{D2} = 196,500$. Analysis with some more values of crossflow parameter and penetration ratio showed that the time for the beginning of the second radial flow period estimated from equation (11) is approximately 2 to 4 times greater than those estimated from equation (9). Thus, according to the time criteria obtained in this study, the first radial flow period ends earlier and the second radial flow period begins later than the times predicted by Bilhartz and Ramey's⁴ correlations. Some of the differences in these time criteria may be attributed to different ways of modelling the crossflow in these two studies. However, a smaller t_{D1} and a larger t_{D2} based on pressure derivative responses (equations (10) and (11)) than those based on pressure responses (equations (8) and (9)) are consistent with the general observations regarding time criteria based on pressure and pressure derivative responses presented by Ambastha²¹.

Figure 5 compares the correlations for the time to the beginning of the second radial flow period from this study (equation 11) and that from Bilhartz and Ramey's⁴ study (equation 9) for a single-layered reservoir. Equation (9) is not applicable for all penetration ratios. Equation (9) becomes meaningless for $b \geq 2/3$ because $\cos(3\pi b/4b)$ becomes zero or negative. However, computationally, equation (9) is applicable for $b < 0.64$, because beyond this penetration ratio, t_{D2} becomes negative. To the best of our knowledge, this limitation of equation (9) has not been pointed out in the literature. But equation (11) has been derived for $0.1 \leq b \leq 0.8$ and for t_{D2} between 100 and 10,000. Although there is no mathematical or computational limitation to equation (11), t_{D2} value calculated at $b = 1$ becomes physically meaningless. When $b = 1$, all t_{D2} values should coincide with the time to the beginning of radial flow period for a fully-penetrated, single-layered reservoir, which does not happen with equation (11).

Figure 6 compares the pressure transient responses from this study with those from Figure 3 of Bilhartz and Ramey's⁴ study. Figure 6 graphs dimensionless wellbore pressure against dimensionless time for penetration ratios of 0.25 and 0.5. Initially, the responses show a straight line corresponding to the first radial flow period with a semi-log slope of 0.5/b. After the first radial flow period, there is a transition period after which, the responses again show straight lines corresponding to the second radial (pseudoradial) flow period with a slope of 0.5. Since pseudoskin factors obtained from this study are slightly higher than those obtained from Bilhartz and Ramey's⁴ study, pressure responses for the second radial flow period are slightly higher than those of Bilhartz and Ramey's⁴. For the penetration ratios of 0.25 and 0.5, pseudoskin factors obtained from this study are 19.6 and 3.98, respectively, whereas those obtained from Bilhartz and Ramey's⁴ study are 17.83 and 3.47, respectively. Thus, the pseudoskin factors obtained from the two studies are very close.

Effects of Gas-Cap (or Bottom-Water) Drive on Pseudoskin and Comparison with Reference 5

Table 5 shows the effects of gas cap on pseudoskin factor for a three-layered reservoir with $k_1 = k_2 = k_3 = 4.9346 \times 10^{-14} \text{ m}^2$ and with $h = 200 \text{ m}$. The various cases of reservoir configuration in Table 5 are explained in Table 3. Cases 1 and 2 show pseudoskins when there is no gas cap and cases 3 and 4 show pseudoskins when the reservoir is subject to a gas-cap drive. In the absence of the gas cap, pseudoskin is lower when the open interval is away from the top or the bottom boundary than when the open interval is located adjacent to the top or the bottom boundary. This happens because the crossflow parameter, λ_A , is higher when the open interval is away from the top or bottom boundary. But case 3 shows that when the gas cap is present, pseudoskin is smaller when the open interval is adjacent to the constant-pressure boundary than when the open interval is away from the constant-pressure boundary. This happens because when the open interval is adjacent to the constant-pressure boundary, the wellbore pressure stabilizes faster than when the open interval is away from the constant-pressure boundary. Similar observations were also made by Streletska-Adams⁵. The above observations are also valid for the corresponding cases when the reservoir is accompanied by a bottom-water zone.

Figure 7 compares the pseudoskin factors from this study with those from Streletska-Adams⁵ study for a partially-penetrating well in a reservoir subject to a gas-cap drive. Gas-oil contact has been modelled as a constant pressure boundary in both studies. Figure 7 compares pseudoskin factors with those from Figure 9 of Streletska-Adams⁵ study. The solid lines in Figure 7 show the pseudoskin factors estimated from equation (5) of this study for various penetration ratios and under gas-cap condition. Streletska-Adams⁵ estimated the pseudoskin by taking the difference between the late-time pressure responses of a partially-penetrating well and a fully-penetrating well in a particular reservoir. Figure 7 shows very close comparison of the pseudoskin factors estimated from this study with those from Streletska-Adams⁵ study, except for very small penetration ratios ($b < 0.3$). Pseudoskin factors estimated from this study are slightly higher than those obtained from Streletska-Adams⁵ study. This is likely due to the different ways of modelling the crossflow in the two studies.

Comparison with Reference 2

Figure 8 shows a comparison of the pseudoskin factors obtained from equation (1) of this study with those obtained from Figure 8 of Olorowaju and Lee's² study. Figure 8 graphs the pseudoskin factors against various penetration ratios for a two-layered reservoir with layer two open to flow and layer one closed. Figure 8 shows that the pseudoskin factors obtained from this study are significantly higher (more than double) than those obtained from Olorowaju and Lee's² study. The reason for this may be the assumption that Olorowaju and Lee² made in developing their model. They assumed that there is no radial flow component in the closed layer (i.e., layer one). Because of this assumption, fluid particles travel shorter distances and only vertically to move from the closed layer to the open layer (layer two). If there were radial

flow component in the closed layer, fluid particles would have travelled longer distances to move from the closed layer to the open layer and this would have caused higher pressure drops, i.e., higher pseudoskin factors. Thus, neglecting the radial flow component in the closed layer may not be a satisfactory assumption while studying pressure transient responses for partially-penetrating wells.

Effect of Layer Refinement on Pseudoskin Factor

Table 6 shows the effects of layer refinement on pseudoskin factor. For a particular reservoir thickness and open interval, the reservoir is divided into a number of mathematical layers to study the effects of layer refinement on pseudoskin factor. In Table 6, cases 1 through 3 represent a reservoir height of 30 m with an open interval thickness of 10 m, and cases 4 through 6 represent a reservoir thickness of 100 m with an open interval thickness of 20 m, respectively. For both reservoir thicknesses of 30 m and 100 m, the open interval is considered as a single layer, and the closed interval of the reservoir is divided into 1, 2 and 4 layers. The results in Table 6 show a small decrease in pseudoskin factor as the number of mathematical layers increases and this decrease in pseudoskin factor is greater when the reservoir thickness is larger. But the value of pseudoskin factor stabilizes as the number of mathematical layers is further increased. This layer refinement effect occurs because of the pseudosteady-state crossflow assumption. The layer refinement effect has also been observed by Larsen²².

Conclusions

1. Pressure transient responses and pseudoskin factors for a partially-penetrated, multi-layered reservoir can be analytically studied by a pseudosteady-state crossflow model.
2. Simplified expressions for pseudoskin factor have been derived for a partially-penetrated, multi-layered reservoir with or without a bottom-water or a gas-cap drive and pseudoskin factors can be estimated from these expressions with reasonable accuracy.
3. Times for the end of the radial flow period and the beginning of the pseudoradial flow period depend on the crossflow parameter and the mobility-thickness ratio of the open interval. Simplified expressions have been derived for these time criteria.
4. Pseudoskin factors obtained from this study have been compared with those obtained from other studies in the literature and these comparisons have shown good matches with most of the studies.

Nomenclature

A	=	Constant in equation (A.25)
A ₁ , A ₂	=	Constants in equations (A.36) and (A.37)
B	=	Constant in equation (A.26)
B ₁ , B ₂	=	Constants in equations (A.36) and (A.37)
a ₁ , a ₂	=	Constants in equations (A.36) and (A.37)
a _{1L} , a _{2L}	=	Limiting values of a ₁ and a ₂ as $t \rightarrow \infty$
b	=	Penetration ratio = h_w/h
b _L	=	Constant defined by equation (B.30)
c	=	Total system compressibility, Pa ⁻¹
h	=	Formation thickness, m
h _w	=	Open interval thickness, m
h _D	=	Dimensionless wellbore thickness, see equation (4)
k	=	Horizontal permeability, m ²
k _v	=	Vertical permeability, m ²
l	=	Laplace parameter
P	=	Pressure, Pa
p _i	=	Initial pressure, Pa
P _D	=	Dimensionless pressure
P _{wD}	=	Dimensionless wellbore pressure
P _{wDPI}	=	Late time dimensionless pressure presented in equation (B.28)
P _{wDPI}	=	Late time dimensionless pressure presented in equation (B.29)
q	=	Flow rate, m ³ /s
r	=	Radial distance, m
s _b	=	Pseudoskin factor because of partial penetration
s _{bC}	=	Pseudoskin factor from the analytical solution
s _{bGA}	=	Pseudoskin factor from the simplified expressions
s _{bDR}	=	Pseudoskin factor from Ding and Reynolds ¹³ study
s _{bYR}	=	Pseudoskin factor from Yeh and Reynolds ¹¹ study
t	=	Time, sec
t _D	=	Dimensionless time
t _{D1}	=	Dimensionless time for the end of first radial flow period
t _{D2}	=	Dimensionless time for the beginning of second radial flow period
X _A	=	Semi-permeability between layer 1 and 2 = $2A[(h\mu/k_v)_1 + (h\mu/k_v)_2]$
X _C	=	Semi-permeability between layer 2 and gas cap region = $2B(h\mu/k_v)_2$

Subscripts

- 1, 2 = Layer number
 D = Dimensionless
 w = Wellbore
 L = Limiting value as $t_D \rightarrow \infty$
 Open = Layers representing perforated interval

Greek Symbols

- $\sigma, \sigma_1, \sigma_2$ = Eigenvalues
 κ = Mobility-thickness ratio = $(kh/\mu)_{\text{open}} / (\overline{kh/\mu})$
 $\bar{\kappa}$ = Total mobility-thickness ratio for a multi-layered reservoir
 ∂ = Partial
 λ_A = Crossflow parameter for a two-layered reservoir
 $\quad = r_1^2 X_A / (\overline{kh/\mu})$
 $\bar{\lambda}_A$ = Crossflow parameter for a multi-layered reservoir
 λ_C = Crossflow parameter between the reservoir and the gas cap = $r_1^2 X_C / (\overline{kh/\mu})$
 μ = Viscosity, Pa.sec
 ω = Storage ratio = $(\partial c/\partial p)_{\text{form}} / (\partial c/\partial p)$
 ϕ = Porosity
 ∇ = Differential operator
 Δ = Expression defined by Equation (A.35)

References

1. Muskat, M.: *Physical Principles of Oil Production*, McGraw-Hill Book Co. Inc., New York City (1949) 259-70.
2. Niels, R. G.: "The Effect of Partial Penetration on Pressure Build-Up in Oil Wells," *Trans., AIME* (1958), Vol. 213, 85-90.
3. Brown, F. and Martin, V. E.: "The Effect of Restricted Flow Entry on Well Productivity," *JPT* (Feb. 1961) 172-74.
4. Dikhera, H. L. and Ramey, H. J., Jr.: "The Combined Effect of Storage, Skin, and Partial Penetration on Well Test Analysis," paper SPE 6753 presented at the 1977 Annual Meeting, Denver, Colorado, Oct. 9-12.
5. Steinhilber-Adams, T. D.: "Pressure Drawdown in a Well with Limited Flow Entry," *JPT* (Nov. 1976) 1409-76.
6. Dehghan, I. M. and Raghavan, R.: "Transient Pressure Behavior of Partially Penetrating Wells Subject to Bottomwater Drive," *JPT* (July 1980) 1231-41.
7. Reynolds, A. C., Chen, J. C. and Raghavan, R.: "Pseudoskin Factor Caused by Partial Penetration," *JPT* (Dec. 1984) 2197-2210.
8. Papatzacos, P.: "Approximate Partial-Penetration Pseudoskin for Infinite-Conductivity Wells," *SPEE* (May 1987) 227-34.
9. Olatuwaju, J.S. and Lee, W.J.: "Pressure Buildup Behavior of Partially Completed Wells in Layered Reservoirs," paper SPE 18876 presented at the 1989 Production Operations Symposium, Oklahoma, March 13-14.
10. Yeh, N.S. and Reynolds, A. C.: "Analysis of Pressure Data From a Restricted-Entry Well in a Multilayer Reservoir," *SPEE* (March 1989) 81-89.
11. Yeh, N.S. and Reynolds, A. C.: "Computation of Pseudoskin Factor Caused by a Restricted-Entry Well Completed in a Multilayer Reservoir," *SPEE* (June 1989) 253-63.
12. Vrblík, J.: "A Simple Approximation to the Pseudoskin Factor Resulting from Restricted Entry," *SPEE* (Dec. 1991) 444-46.
13. Ding, W. and Reynolds, A. C.: "Computation of the Pseudoskin Factor for a Restricted-Entry Well," paper SPE 21705 presented at the 1991 Production Operation Symposium, Oklahoma, April 7-9.
14. Shah, P. C. and Thambynayagam, R. K. M.: "Transient Pressure Response of a Well with Partial Completion in a Two-Layer Crossflowing Reservoir," paper SPE 24681 presented at the 1992 Annual Meeting, Washington, DC, Oct. 4-7.
15. Odoh, A. S.: "Steady-State Flow Capacity of Wells with Limited Entry to Flow," *SPEJ* (March 1966) 43-51.
16. Seth, M. S.: "Unsteady-State Pressure Distribution in a Finite Reservoir with Partial Well-Bore Opening," *JPT* (Oct. 1968) 153-63.
17. Kazemi, H. and Seth, M. S.: "Effect of Anisotropy and Stratification on Pressure Transient Analysis of Wells with Restricted Flow Entry," *JPT* (May 1969) 639-47.
18. Gringarten, A. C. and Ramey, H. J., Jr.: "An Approximate Infinite Conductivity Solution for a Partially Penetrating Line-Source Well," *SPEJ* (April 1975) 140-48.
19. Vrblík, J.: "Calculating the Pseudo-skin Factor due to Partial Well Completion," *JPT* (Sept.-Oct. 1986) 57-61.

20. Gomes, E. and Ambastha, A.K.: "An Analytical Pressure-Transient Model for Multilayered, Composite Reservoirs with Pseudosteady-State Formation Crossflow," paper SPE 26049 presented at the 1993 Western Regional Meeting, Alaska, May 26-28; also accepted for publication in the *AOSTRA Journal of Research* (Nov. 13, 1992).
21. Ambastha, A.K.: "Pressure Transient Analysis in Composite Systems," Ph.D. Thesis, Stanford University (Oct. 1988) 193 pp.
22. Larsen, L.: "Boundary Effects in Pressure-Transient Data From Layered Reservoirs," paper SPE 19797 presented at the 1989 Annual Meeting, San Antonio, TX, Oct. 8-11.
23. Bourdet, D.: "Pressure Behavior of Layered Reservoirs With Crossflow," paper SPE 13628 presented at the 1985 Regional Meeting, California, March 27-29.
24. Stehfest, H.: "Algorithm 368, Numerical Inversion of Laplace Transformations, D-5," *Comm. of ACM*, 13, No.1 (Jan. 1970) 47-49.

Appendix A

Late Time Behaviour of a Partially Penetrating Well in a Two-layered Reservoir with Pseudosteady-State Crossflow.

Figure 1 schematically shows a two-layered, partially-penetrated reservoir. Layer 1 is penetrated and layer 2 is closed at the wellbore. The upper boundary of the layer 2 and the lower boundary of the layer 1 are considered as closed boundaries. Pseudosteady-state crossflow is considered between the two layers. The problem is solved following the steps taken by Bourdet²³. The diffusivity equations for the two layers are:

$$\left(\frac{kh}{\mu}\right) \left(\frac{\partial^2 p_1}{\partial r^2} + \frac{1}{r} \frac{\partial p_1}{\partial r}\right) = (\phi c h) \frac{\partial p_1}{\partial t} + \chi_d(p_1 - p_2) \quad (A.1)$$

$$\left(\frac{kh}{\mu}\right) \left(\frac{\partial^2 p_2}{\partial r^2} + \frac{1}{r} \frac{\partial p_2}{\partial r}\right) = (\phi c h) \frac{\partial p_2}{\partial t} + \chi_d(p_2 - p_1) \quad (A.2)$$

$$\text{Initial condition: } p_1 = p_2 = p_{in} \quad (A.3)$$

$$\text{Outer boundary condition: } \lim_{r \rightarrow \infty} p_1 = \lim_{r \rightarrow \infty} p_2 = p_o \quad (A.4)$$

Inner boundary condition: Assuming layer 1 is penetrated and layer 2 is closed, and neglecting wellbore storage and skin, we can write:

$$p_1 = p_o \quad \text{for } r = r_w \quad (A.5)$$

$$\left(\frac{\partial p_2}{\partial r}\right)_{r=r_w} = 0 \quad (A.6)$$

$$q = 2\pi \left(\frac{kh}{\mu}\right) \left(r \frac{\partial p_1}{\partial r}\right)_{r=r_w} \quad (A.7)$$

We define the following dimensionless variables:

$$p_{D1,2} = \frac{2\pi \left(\frac{kh}{\mu}\right)}{q} (p_o - p_{1,2}) \quad (A.8)$$

$$r_D = \frac{\left(\frac{kh}{\mu}\right)}{(\phi c h)} \frac{1}{r_L} \quad (A.9)$$

$$\text{where, } \left(\frac{kh}{\mu}\right) = \left(\frac{kh}{\mu}\right)_1 + \left(\frac{kh}{\mu}\right)_2, \text{ and} \quad (A.10)$$

$$(\phi c h) = (\phi c h)_1 + (\phi c h)_2 \quad (A.11)$$

All other dimensionless parameters are defined in the Nomenclature

The differential equations and the boundary conditions can be written in a dimensionless form as:

$$\kappa \nabla^2 p_{D1} = \omega \frac{\partial p_{D1}}{\partial t_D} + \lambda_d(p_{D1} - p_{D2}) \quad (A.12)$$

$$(1 - \kappa) \nabla^2 p_{D2} = (1 - \omega) \frac{\partial p_{D2}}{\partial t_D} + \lambda_d(p_{D2} - p_{D1}) \quad (A.13)$$

$$\text{Initial condition: } p_{D1}(r_{D0}, 0) = p_{D2}(r_{D0}, 0) = 0 \quad (A.14)$$

$$\text{Outer boundary condition: } \lim_{r_D \rightarrow \infty} p_{D1} = \lim_{r_D \rightarrow \infty} p_{D2} = 0 \quad (A.15)$$

$$\text{Inner boundary condition: } p_{D1}(1, t_D) = p_{wD} \quad (A.16)$$

$$\left(\frac{\partial p_{D2}}{\partial r_D}\right)_{r_D=1} = 0 \quad (A.17)$$

$$1 = \kappa \left(\frac{\partial p_{D1}}{\partial r_D}\right)_{r_D=1} \quad (A.18)$$

Taking Laplace transformation of equations (A.12) through (A.18) yields:

$$\kappa \nabla^2 \bar{p}_{D1} = \omega / \bar{p}_{D1} + \lambda_d(\bar{p}_{D1} - \bar{p}_{D2}) \quad (A.19)$$

$$(1 - \kappa) \nabla^2 \bar{p}_{D2} = (1 - \omega) \bar{p}_{D2} + \lambda_d(\bar{p}_{D2} - \bar{p}_{D1}) \quad (A.20)$$

$$\text{Outer boundary condition: } \lim_{r_D \rightarrow \infty} \bar{p}_{D1} = \lim_{r_D \rightarrow \infty} \bar{p}_{D2} = 0 \quad (\text{A.21})$$

$$\text{Inner boundary condition: } \bar{p}_{D1}(1, t) = \bar{p}_{D2} \quad (\text{A.22})$$

$$\left(\frac{\partial \bar{p}_{D2}}{\partial r_D} \right)_{r_D=1} = 0 \quad (\text{A.23})$$

$$\frac{1}{l} = -\kappa \left(\frac{\partial \bar{p}_{D1}}{\partial r_D} \right)_{r_D=1} \quad (\text{A.24})$$

Solutions of equations (A.19) and (A.20) are modified Bessel's functions, $I_0(\sigma r_D)$ and $K_0(\sigma r_D)$, where σ is the eigenvalue of the system. For an infinite system, only $K_0(\sigma r_D)$ function applies. Therefore,

$$\bar{p}_{D1} = AK_0(\sigma r_D) \quad (\text{A.25})$$

$$\bar{p}_{D2} = BK_0(\sigma r_D) \quad (\text{A.26})$$

Equations (A.19) and (A.20) together with equations (A.25) and (A.26) yield:

$$\omega \sigma^2 AK_0(\sigma r_D) = \omega l AK_0(\sigma r_D) + \lambda_A [AK_0(\sigma r_D) \cdot BK_0(\sigma r_D)] \quad (\text{A.27})$$

$$(1 - \kappa) \sigma^2 BK_0(\sigma r_D) = (1 - \omega) l BK_0(\sigma r_D) + \lambda_A [BK_0(\sigma r_D) \cdot AK_0(\sigma r_D)] \quad (\text{A.28})$$

Equations (A.27) and (A.28) reduce to:

$$[\omega \sigma^2 - \omega l - \lambda_A] A + \lambda_A B = 0 \quad (\text{A.29})$$

$$\lambda_A A + [(1 - \kappa) \sigma^2 - (1 - \omega) l - \lambda_A] B = 0 \quad (\text{A.30})$$

Non-trivial solutions are possible, if the determinant is zero, i.e.,

$$(\omega \sigma^2 - \omega l - \lambda_A) [(1 - \kappa) \sigma^2 - (1 - \omega) l - \lambda_A] - \lambda_A^2 = 0 \quad (\text{A.31})$$

Equation (A.31) can be reorganized as:

$$\sigma^4 - \left[\frac{(1 - \omega) l + \lambda_A}{1 - \kappa} + \frac{\omega l + \lambda_A}{\kappa} \right] \sigma^2 + \frac{\omega l (1 - \omega) + \lambda_A l}{\kappa (1 - \kappa)} = 0 \quad (\text{A.32})$$

This polynomial has two positive roots and they are:

$$\sigma_1^2 = \frac{1}{2} \left[\left(\frac{(1 - \omega) l + \lambda_A}{1 - \kappa} + \frac{\omega l + \lambda_A}{\kappa} \right) + \Delta \right] \quad (\text{A.33})$$

$$\sigma_2^2 = \frac{1}{2} \left[\left(\frac{(1 - \omega) l + \lambda_A}{1 - \kappa} + \frac{\omega l + \lambda_A}{\kappa} \right) - \Delta \right] \quad (\text{A.34})$$

$$\text{where, } \Delta = \left[\left(\frac{(1 - \omega) l + \lambda_A}{1 - \kappa} + \frac{\omega l + \lambda_A}{\kappa} \right)^2 + \frac{4 \lambda_A^2}{\kappa (1 - \kappa)} \right]^{1/2} \quad (\text{A.35})$$

Putting σ_1^2 and σ_2^2 from equations (A.33) and (A.34), respectively, in equation (A.30) and rearranging, we can write:

$$a_1 = \frac{A_1}{B_1} = 1 + \frac{1}{\lambda_A} [(1 - \omega) l - (1 - \kappa) \sigma_1^2] \quad (\text{A.36})$$

$$a_2 = \frac{A_2}{B_2} = 1 + \frac{1}{\lambda_A} [(1 - \omega) l - (1 - \kappa) \sigma_2^2] \quad (\text{A.37})$$

Putting $A_1 = a_1 B_1$ and $A_2 = a_2 B_2$ in equations (A.25) and (A.26) yield:

$$\bar{p}_{D1} = a_1 B_1 K_0(\sigma_1 r_D) + a_2 B_2 K_0(\sigma_2 r_D) \quad (\text{A.38})$$

$$\bar{p}_{D2} = B_1 K_0(\sigma_1 r_D) + B_2 K_0(\sigma_2 r_D) \quad (\text{A.39})$$

Equations (A.38) and (A.39) together with equations (A.22) and (A.23) yield:

$$B_1 = - \frac{B_2 \sigma_2 K_1(\sigma_2)}{\sigma_1 K_1(\sigma_1)} \quad (\text{A.40})$$

Equations (A.38) and (A.39) together with equation (A.24) yield:

$$\frac{1}{\kappa l} = a_1 B_1 \sigma_1 K_1(\sigma_1) + a_2 B_2 \sigma_2 K_1(\sigma_2) \quad (\text{A.41})$$

From equations (A.40) and (A.41), we get:

$$B_1 = - \frac{1}{(a_2 - a_1) \kappa l \sigma_1 K_1(\sigma_1)} \quad (\text{A.42})$$

$$B_2 = \frac{1}{(a_2 - a_1) \kappa l \sigma_2 K_1(\sigma_2)} \quad (\text{A.43})$$

Now, equation (A.38) becomes:

$$\bar{p}_{D1} = - \frac{a_1 K_0(\sigma_1)}{(a_2 - a_1) \kappa l \sigma_1 K_1(\sigma_1)} + \frac{a_2 K_0(\sigma_2)}{(a_2 - a_1) \kappa l \sigma_2 K_1(\sigma_2)} \quad (\text{A.44})$$

Equation (A.44) represents pressure transient responses of a partially-penetrating well in a two-layered reservoir in Laplace space and these responses are numerically inverted to real space using the Duhamel algorithm²⁴.

Late Time Behaviour for a Partially-penetrating Well with No Bottom-Water Zone or Gas Cap

At late time $t_D \rightarrow \infty$ and $I \rightarrow 0$, and equations (A.33) through (A.37) become:

$$\lim_{t \rightarrow 0} \Delta = \lim_{t \rightarrow 0} \left[\left(\frac{\lambda_A}{1-\kappa} + \frac{\lambda_A}{\kappa} \right)^2 + I[\dots] + I^2[\dots] \right]^{1/2} = \frac{\lambda_A}{\kappa(1-\kappa)} \quad (\text{A.45})$$

$$\lim_{t \rightarrow 0} \sigma_1^2 = \lim_{t \rightarrow 0} \left[\frac{\lambda_A}{1-\kappa} + \frac{\lambda_A}{\kappa} + I[\dots] + I^2[\dots] \right] = \frac{\lambda_A}{\kappa(1-\kappa)} \quad (\text{A.46})$$

$$\lim_{t \rightarrow 0} \sigma_2^2 = \lim_{t \rightarrow 0} \frac{1}{2} \left[\frac{1-\omega}{1-\kappa} + \frac{\omega}{\kappa} \cdot \frac{1-\omega}{1-\kappa} + \frac{\omega}{\kappa} \right] = I \quad (\text{A.47})$$

Appendix C shows the simplification proposed in equation (A.47) in detail.

$$\lim_{t \rightarrow 0} a_1 = \lim_{t \rightarrow 0} \left[1 + \frac{(1-\omega)I - (1-\kappa)\sigma_1^2}{\lambda_A} \right] = \frac{\kappa-1}{\kappa} \quad (\text{A.48})$$

$$\lim_{t \rightarrow 0} a_2 = \lim_{t \rightarrow 0} \left[1 + \frac{(1-\omega)I - (1-\kappa)\sigma_2^2}{\lambda_A} \right] = 1 \quad (\text{A.49})$$

Using the late-time limits shown in equations (A.45) through (A.49), equation (A.44) may be written as:

$$\bar{p}_{wD} = \frac{(1-\kappa)}{\kappa I} \frac{K \left(\sqrt{\frac{\lambda_A}{\kappa(1-\kappa)}} \right)}{\sqrt{\frac{\lambda_A}{\kappa(1-\kappa)}} K \left(\sqrt{\frac{\lambda_A}{\kappa(1-\kappa)}} \right)} + \frac{K(\sqrt{I})}{I\sqrt{I} K(\sqrt{I})} \quad (\text{A.50})$$

The first term in equation (A.50) is a constant and it represents the additional pressure drop because of partial penetration, which is usually known as pseudoskin. The second term in equation (A.50) represents the equivalent infinite, homogeneous reservoir

response for the whole reservoir. So, for a two layered reservoir, the expression for pseudoskin is:

$$s_0 = \frac{(1-\kappa)}{\kappa} \frac{K \left(\sqrt{\frac{\lambda_A}{\kappa(1-\kappa)}} \right)}{\sqrt{\frac{\lambda_A}{\kappa(1-\kappa)}} K \left(\sqrt{\frac{\lambda_A}{\kappa(1-\kappa)}} \right)} \quad (\text{A.51})$$

Equation (A.51) can be extended for a multi layered reservoir by appropriately defining κ and λ_A :

$$s_0 = \frac{(1-\bar{\kappa})}{\bar{\kappa}} \frac{K \left(\sqrt{\frac{\bar{\lambda}_A}{\bar{\kappa}(1-\bar{\kappa})}} \right)}{\sqrt{\frac{\bar{\lambda}_A}{\bar{\kappa}(1-\bar{\kappa})}} K \left(\sqrt{\frac{\bar{\lambda}_A}{\bar{\kappa}(1-\bar{\kappa})}} \right)} \quad (\text{A.52})$$

where, $\bar{\kappa}$ = total mobility-thickness ratio of the open interval

$\bar{\lambda}_A$ = total crossflow parameter

Equation (A.52) is applicable for a multi-layered reservoir having any arbitrary number of layers consisting the open interval and any arbitrary location of the open interval. In equation (A.52), $\bar{\kappa}$ and $\bar{\lambda}_A$ are calculated by adding the individual layer mobility-thickness ratio of the open interval and by adding the lower and the upper boundary crossflow parameters, respectively. Irrespective of the number of layers in the reservoir, only two parameters are required to estimate the pseudoskin. A similar treatment for a reservoir subject to a gas-cap drive (or a bottom-water drive) is shown in Appendix B.

Appendix B**Late Time Behaviour of a Partially-Penetrated Well in a Two-layered Reservoir Subject to a Gas-Cap Drive**

Figure 2 schematically shows a two-layered, partially-penetrated reservoir subject to a gas-cap drive. Layer 1 is penetrated and layer 2 is closed at the wellbore. The upper boundary of the layer 2 is considered as a constant-pressure boundary because of gas cap, whereas the lower boundary of the layer 1 is considered as a closed boundary. Pseudosteady-state crossflow is considered between the two layers. The diffusivity equations for the two layers are:

$$\left(\frac{kh}{\mu} \right) \left(\frac{\partial^2 p_1}{\partial r^2} + \frac{1}{r} \frac{\partial p_1}{\partial r} \right) = (\phi c h) \frac{\partial p_1}{\partial t} + K_d(p_1 - p_2) \quad (\text{B.1})$$

$$\left(\frac{kh}{\mu} \right) \left(\frac{\partial^2 p_2}{\partial r^2} + \frac{1}{r} \frac{\partial p_2}{\partial r} \right) = (\phi c h) \frac{\partial p_2}{\partial t} + K_d(p_2 - p_1) + K_d(p_2 - p_w) \quad (\text{B.2})$$

Inner and outer boundary conditions, and initial condition are the same as in Appendix A. In dimensionless form, the differential equations and the boundary conditions can be written as:

$$\kappa \nabla^2 p_{D1} = \omega \frac{\partial p_{D1}}{\partial t_D} + \lambda_A (p_{D1} - p_{D2}) \quad (\text{B.3})$$

$$(1 - \kappa) \nabla^2 p_{D2} = (1 - \omega) \frac{\partial p_{D2}}{\partial t_D} + \lambda_A (p_{D2} - p_{D1}) + \lambda_C p_{D2} \quad (\text{B.4})$$

$$\text{Initial condition: } p_{D1}(r_D, 0) = p_{D2}(r_D, 0) = 0 \quad (\text{B.5})$$

$$\text{Outer boundary condition: } \lim_{r_D \rightarrow \infty} p_{D1} = \lim_{r_D \rightarrow \infty} p_{D2} = 0 \quad (\text{B.6})$$

$$\text{Inner boundary condition: } p_{D1}(1, t_D) = p_{wD} \quad (\text{B.7})$$

$$\left(\frac{\partial p_{D2}}{\partial r_D} \right)_{r_D=1} = 0 \quad (\text{B.8})$$

$$1 = -\kappa \left(\frac{\partial p_{D1}}{\partial r_D} \right)_{r_D=1} \quad (\text{B.9})$$

Following the same steps as in Appendix A, we can obtain:

$$[\omega \sigma^2 - \omega \lambda_A + \lambda_C] A + \lambda_A B = 0 \quad (\text{B.10})$$

$$\lambda_A A + [(1 - \kappa) \sigma^2 - (1 - \omega) \lambda_A - \lambda_C] B = 0 \quad (\text{B.11})$$

Non-trivial solutions are possible, if the determinant is zero, i.e.,

$$(\omega \sigma^2 - \omega \lambda_A) [(1 - \kappa) \sigma^2 - (1 - \omega) \lambda_A - \lambda_C] - \lambda_A^2 = 0 \quad (\text{B.12})$$

Equation (B.12) can be reorganized as:

$$\sigma^4 - \left[\frac{(1 - \omega) \lambda_A + \lambda_C}{1 - \kappa} + \frac{\omega \lambda_A + \lambda_A}{\kappa} \right] \sigma^2 + \frac{(\omega \lambda_A + \lambda_A) [(1 - \omega) \lambda_A + \lambda_A + \lambda_C] - \lambda_A^2}{\kappa(1 - \kappa)} = 0 \quad (\text{B.13})$$

This polynomial has two positive roots and these are:

$$\sigma_1^2 = \frac{1}{2} \left[\left(\frac{(1 - \omega) \lambda_A + \lambda_C}{1 - \kappa} + \frac{\omega \lambda_A + \lambda_A}{\kappa} \right) + \Delta \right] \quad (\text{B.14})$$

$$\sigma_2^2 = \frac{1}{2} \left[\left(\frac{(1 - \omega) \lambda_A + \lambda_C}{1 - \kappa} + \frac{\omega \lambda_A + \lambda_A}{\kappa} \right) - \Delta \right] \quad (\text{B.15})$$

where, $\Delta =$

$$\left[\left(\frac{(1 - \omega) \lambda_A + \lambda_C}{1 - \kappa} + \frac{\omega \lambda_A + \lambda_A}{\kappa} \right)^2 - \frac{4(\omega \lambda_A + \lambda_A) [(1 - \omega) \lambda_A + \lambda_A + \lambda_C] - \lambda_A^2}{\kappa(1 - \kappa)} \right]^{1/2} \quad (\text{B.16})$$

Putting σ_1^2 and σ_2^2 from equations (B.14) and (B.15), respectively, in equation (B.11) and rearranging, we can write:

$$a_1 = \frac{A_1}{B_1} = 1 + \frac{\lambda_C}{\lambda_A} + \frac{1}{\lambda_A} [(1 - \omega) \lambda_A - (1 - \kappa) \sigma_1^2] \quad (\text{B.17})$$

$$a_2 = \frac{A_2}{B_2} = 1 + \frac{\lambda_C}{\lambda_A} + \frac{1}{\lambda_A} [(1 - \omega) \lambda_A - (1 - \kappa) \sigma_2^2] \quad (\text{B.18})$$

As in Appendix A, putting $A_1 = a_1 B_1$ and $A_2 = a_2 B_2$ in the solution yields:

$$\bar{p}_{D1} = a_1 B_1 K_0(\sigma_1 r_D) + a_2 B_2 K_0(\sigma_2 r_D) \quad (\text{B.19})$$

$$\bar{p}_{D2} = B_1 K_0(\sigma_1 r_D) + B_2 K_0(\sigma_2 r_D) \quad (\text{B.20})$$

Again, following the same steps as in Appendix A, we obtain the expression for the wellbore pressure as:

$$\bar{p}_{wD} = - \frac{a_1 K_0(\sigma_1)}{(a_2 - a_1) \omega \sigma_1 K_1(\sigma_1)} + \frac{a_2 K_0(\sigma_2)}{(a_2 - a_1) \omega \sigma_2 K_1(\sigma_2)} \quad (\text{B.21})$$

Equation (B.21) represents pressure transient responses in Laplace space of a partially-penetrating well in a two-layered reservoir subject to a gas-cap drive and these responses are numerically inverted to real space using the Stehfest Algorithm²⁶.

Late Time Behaviour for a Partially-penetrating Well Under a Gas-cap Drive

At late time $t_D \rightarrow \infty$ and $r \rightarrow 0$, and equations (B.14) through (B.18) become:

$$\lim_{t_D \rightarrow \infty} \sigma_1^2 = \sigma_1^2 = \frac{1}{2} \left[\frac{\lambda_A + \lambda_C}{1 - \kappa} + \frac{\lambda_A}{\kappa} + \left(\left(\frac{\lambda_A + \lambda_C}{1 - \kappa} + \frac{\lambda_A}{\kappa} \right)^2 - \frac{4\lambda_A \lambda_C}{(1 - \kappa)\kappa} \right)^{1/2} \right] \quad (\text{B.22})$$

$$\lim_{t_D \rightarrow \infty} \sigma_2^2 = \sigma_2^2 = \frac{1}{2} \left[\frac{\lambda_A + \lambda_C}{1 - \kappa} + \frac{\lambda_A}{\kappa} - \left(\left(\frac{\lambda_A + \lambda_C}{1 - \kappa} + \frac{\lambda_A}{\kappa} \right)^2 - \frac{4\lambda_A \lambda_C}{(1 - \kappa)\kappa} \right)^{1/2} \right] \quad (\text{B.23})$$

$$\lim_{t \rightarrow 0} \Delta = \left[\left(\frac{\lambda_A + \lambda_C}{1 - \kappa} + \frac{\lambda_A}{\kappa} \right)^2 \cdot \frac{4\lambda_A \lambda_C}{(1 - \kappa)\kappa} \right]^{\frac{1}{2}} \quad (\text{B.24})$$

$$\lim_{t \rightarrow 0} a_1 = a_{1L} = 1 + \frac{\lambda_C}{\lambda_A} \cdot \frac{(1 - \kappa) \left[\frac{\lambda_A + \lambda_C}{1 - \kappa} + \frac{\lambda_A}{\kappa} \right] \left[\left(\frac{\lambda_A + \lambda_C}{1 - \kappa} + \frac{\lambda_A}{\kappa} \right)^2 \cdot \frac{4\lambda_A \lambda_C}{(1 - \kappa)\kappa} \right]^{\frac{1}{2}}}{2\lambda_A} \quad (\text{B.25})$$

$$\lim_{t \rightarrow 0} a_2 = a_{2L} = 1 + \frac{\lambda_C}{\lambda_A} \cdot \frac{(1 - \kappa) \left[\frac{\lambda_A + \lambda_C}{1 - \kappa} + \frac{\lambda_A}{\kappa} \right] \left[\left(\frac{\lambda_A + \lambda_C}{1 - \kappa} + \frac{\lambda_A}{\kappa} \right)^2 \cdot \frac{4\lambda_A \lambda_C}{(1 - \kappa)\kappa} \right]^{\frac{1}{2}}}{2\lambda_A} \quad (\text{B.26})$$

Using the late-time limits shown in equations (B.22) through (B.26), equation (B.21) may be written as:

$$\bar{p}_{\text{well}} = - \frac{a_{1L} K_d(\sigma_{1L})}{(a_{2L} - a_{1L})\kappa \sigma_{1L} K_1(\sigma_{1L})} + \frac{a_{2L} K_d(\sigma_{2L})}{(a_{2L} - a_{1L})\kappa \sigma_{2L} K_1(\sigma_{2L})} \quad (\text{B.27})$$

Equation (B.27) denotes the limiting pressure drop in Laplace space for a partially-penetrating well subject to a gas-cap drive. Taking inverse Laplace transformation of equation (B.27), we obtain the corresponding pressure drop in the real space as:

$$p_{\text{well}} = - \frac{a_{1L} K_d(\sigma_{1L})}{(a_{2L} - a_{1L})\kappa \sigma_{1L} K_1(\sigma_{1L})} + \frac{a_{2L} K_d(\sigma_{2L})}{(a_{2L} - a_{1L})\kappa \sigma_{2L} K_1(\sigma_{2L})} \quad (\text{B.28})$$

Performing the same treatment for a fully-penetrating well in a two-layered reservoir subject to a gas-cap drive, we obtain:

$$p_{\text{well}} = \frac{(a_{2L} - a_{1L}) K_d(\sigma_{2L}) K_d(\sigma_{1L})}{b_L} \quad (\text{B.29})$$

where,

$$b_L = (1 - a_{1L})(\kappa a_{2L} + 1 - \kappa) \sigma_{2L} K_d(\sigma_{1L}) K_1(\sigma_{2L}) - (1 - a_{2L})(\kappa a_{1L} + 1 - \kappa) \sigma_{1L} K_d(\sigma_{2L}) K_1(\sigma_{1L}) \quad (\text{B.30})$$

Difference between equations (B.28) and (B.29) is the additional pressure drop because of the partial penetration of a two-layered reservoir subject to a gas-cap drive. Therefore, the expression for pseudoskin for this case is:

$$s_k = \frac{a_{2L} K_d(\sigma_{2L})}{(a_{2L} - a_{1L})\kappa \sigma_{2L} K_1(\sigma_{2L})} - \frac{a_{1L} K_d(\sigma_{1L})}{(a_{2L} - a_{1L})\kappa \sigma_{1L} K_1(\sigma_{1L})} - \frac{(a_{2L} - a_{1L}) K_d(\sigma_{2L}) K_d(\sigma_{1L})}{b_L} \quad (\text{B.31})$$

Equation (B.31) estimates the pseudoskin in a two-layered, partially-penetrated reservoir subject to a gas-cap or a bottom water drive. Equation (B.31) is also applicable for a multi-layered reservoir having any arbitrary number of layers consisting the open interval and any arbitrary location of the open interval, provided κ and λ_A are calculated by adding the individual layer mobility-thickness ratio of the open interval and by adding the lower and the upper boundary crossflow parameters of the open interval, respectively. Parameter, λ_C , is the crossflow parameter between the reservoir and the gas cap or the bottom water zone. Irrespective of the number of layers in the reservoir, only three parameters (κ , λ_A , λ_C) are required to estimate the pseudoskin factor.

Appendix C

Late Time Approximation of σ_1^2

From Appendix A,

$$\sigma_1^2 = \frac{1}{2} \left[\left(\frac{\lambda_A}{1 - \kappa} + \frac{\lambda_A}{\kappa} + \left(\frac{1 - \omega}{1 - \kappa} + \frac{\omega}{\kappa} \right) \right) \Delta \right] \quad (\text{C.1})$$

$$\text{and, } \lim_{t \rightarrow \infty} \Delta = \lim_{t \rightarrow \infty} \left[\left(\frac{(1 - \omega)\Delta + \lambda_A}{1 - \kappa} - \frac{\omega\Delta + \lambda_A}{\kappa} \right)^2 \cdot \frac{4\lambda_A^2}{\kappa(1 - \kappa)} \right]^{\frac{1}{2}} \quad (\text{C.2})$$

Equation (C.2) can be written as

$$\lim_{t \rightarrow \infty} \Delta = \lim_{t \rightarrow \infty} \left[\left(\frac{\lambda_A}{1 - \kappa} + \frac{\lambda_A}{\kappa} \right)^2 \left\{ 1 + 2 \frac{1 - \omega}{1 - \kappa} \frac{\omega}{\kappa} + \left(\frac{1 - \omega}{1 - \kappa} + \frac{\omega}{\kappa} \right)^2 \right\} + \frac{4\lambda_A^2}{\kappa(1 - \kappa)} \right]^{\frac{1}{2}} \quad (\text{C.3})$$

Neglecting the term containing t^2 and rearranging equation (C.3) yields:

$$\lim_{t \rightarrow \infty} \Delta = \lim_{t \rightarrow \infty} \left(\frac{\lambda_A}{1 - \kappa} + \frac{\lambda_A}{\kappa} \right) \left[1 + \frac{\left(\frac{1 - \omega}{1 - \kappa} + \frac{\omega}{\kappa} \right) \left(\frac{\lambda_A}{1 - \kappa} + \frac{\lambda_A}{\kappa} \right)}{\left(\frac{\lambda_A}{1 - \kappa} + \frac{\lambda_A}{\kappa} \right)^2} \right]^{\frac{1}{2}} \quad (\text{C.4})$$

Expanding equation (C.4) using the binomial theorem yields:

$$\lim_{t \rightarrow \infty} \left(\frac{\lambda_A}{1 - \kappa} + \frac{\lambda_A}{\kappa} \right) \left[1 + \frac{\left(\frac{1 - \omega}{1 - \kappa} + \frac{\omega}{\kappa} \right) \left(\frac{\lambda_A}{1 - \kappa} + \frac{\lambda_A}{\kappa} \right)}{\left(\frac{\lambda_A}{1 - \kappa} + \frac{\lambda_A}{\kappa} \right)^2} \right]^{\frac{1}{2}} \cdot \left(1 + \frac{1}{2} \left(\frac{\lambda_A}{1 - \kappa} + \frac{\lambda_A}{\kappa} \right)^{-2} \cdot \left(\frac{1 - \omega}{1 - \kappa} + \frac{\omega}{\kappa} \right) \left(\frac{\lambda_A}{1 - \kappa} + \frac{\lambda_A}{\kappa} \right) \right) \quad (\text{C.5})$$

Neglecting the higher order terms in l in equation (C.5) yields

$$\Lambda \left[\frac{\lambda_A}{k}, \frac{\lambda_A}{k}, \left(\frac{1}{k} \frac{\omega}{k} \right) (2k-1) \right] \quad (C.6)$$

At late time, the reservoir behaves like a fully-penetrated, equivalent homogeneous system with a pseudoskin. Thus, at late time, $k = \omega = 1$, and equation (C.6) becomes

$$\Lambda \left[\frac{\lambda_A}{k}, \frac{\lambda_A}{k}, \left(\frac{1}{k} \frac{\omega}{k} \right) \right] \quad (C.7)$$

Now, equation (C.1) becomes

$$\sigma_i \frac{\omega_i}{k} = l \quad (C.8)$$

Table 1: Summary of Studies on Partially-Penetrating Wells																		
Year	Author(s)	Ref. no.	Solution Method(s)							Number of Layers	Gas Cap or Bottom Water(h)			Pseudoskin Estimation(c)				
			I	F	L	H	G	S	N		C	B	G	G	R	E	A	
1949	Muskat	1	.							1	.			.				
1958	Nisik	2	.							1	.			.				
1961	Brons and Marting	3	.							1	.			.				
1968	Odch	15		.						1	.			.				
1968	Seth	16		.	.					1	.			.				
1969	Kazemi and Seth	17						.		1	.			.				
1975	Gringarten and Ramey	18					.			1	.			.				
1977	Wilhartz and Ramey	4						.		1	.			.				
1979	Streltsova-Adams	5					.			1	.			.				.
1980	Buhidma and Raghavan	6					.			1		.		.				
1984	Reynolds et. al	7						.		2	.			.				
1986	Vrbik	19						.		1	.			.				.
1987	Papatzacos	8	.							1	.			.				.
1989	Olarowicz and Lee	9			.					2	.			.				
1989	Yeh and Reynolds	10						.		n	.			.				
1989	Yeh and Reynolds	11						.		n	.			.				
1991	Vrbik	12						.		1	.			.				.
1991	Ding and Reynolds	13		.						n	.			.				.
1992	Shah and Thambynayagam	14				.	.			2
1993	This study					.	.			n

a
I-Included of images
F-Factor uniform
L-Laplace uniform
H-Hybrid uniform
G-Gauss function
S-Substitution of variables
N-Numerical method

b
C-Coil seam
G-Gas cap
B-Bottom water

c
G-Gringarten
R-Ramey
E-Equivalent
A-Analytical

Table 2: Comparison of pseudoskin factors estimated from the simplified expression and that from the actual analytical solution.

Reservoir Configuration Case (see Table 3)	$\bar{\kappa}$	$\bar{\lambda}_A \times 10^7$	Closed top and bottom boundaries		$\bar{\lambda}_C \times 10^7$	Bottom Water	
			%GA	%C		%GA	%C
1	0.702	4.18	3.321	3.323	5.97	3.680	3.679
2	0.429	0.37	10.577	10.650	4.74	10.977	11.150
3	0.333	6.52	15.273	15.280	4.74	15.555	15.470
4	0.763	0.28	2.476	2.492	4.74	2.830	2.860
5	0.640	0.65	4.310	4.380	0.22	4.490	4.620
6	0.480	1.29	7.966	7.980	0.22	8.086	8.110

Table 3: Reservoir configurations considered in Tables 2 and 5.

Case	No. of layer	Penetrated layer
1	2	2
2	3	1
3	3	2
4	3	2 & 3
5	5	4 & 5
6	5	1 & 4

Table 4: Comparison of pseudoskin factors estimated from this study with those estimated from other studies for a three-layered reservoir with closed top and bottom boundaries and with layer 3 open to flow ($h = 200$ m and $k_1 = 4.9346 \times 10^{-15}$ m²).

Case	1	2	3	4	5
h_1/h	0.50	0.10	0.10	0.49	0.10
h_2/h	0.40	0.10	0.10	0.02	0.60
k_1/k_2	100	0.25	0.25	0.41	0.857
k_1/k_3	0.10	1.60	1.60	0.26	1.5
k_1/k_{s1}	10.0	1.0	1.0	1.04	4.0
k_2/k_{s2}	1.0	0.16	0.16	625.0	0.544
k_3/k_{s3}	100.0	0.39	39.06	1.58	177.78
k_1/k_w	400.0	20.0	20.0	20.0	20.0
%C	16.31	33.89	26.00	20.28	41.20
%GA	15.68	32.90	32.90	19.15	40.30
%YR	13.38	26.36	26.36	20.03	34.44
%BR	13.47	26.33	26.33	20.03	34.41

Table 5: Effect of gas cap (bottom-water) on pseudoskin factor
(three layered reservoir, $h = 200$ m, $k_1 = k_2 = k_3 = 4.9346 \times 10^{-14}$ m²)

Case	Reservoir Configuration Case (see Table 3)	\bar{k}	$\bar{\lambda}_D \times 10^3$	Gas cap	$\bar{\lambda}_C \times 10^3$	Pseudo-skin s_D
1	2	0.333	0.47	No	.	15.26
2	3	0.333	1.50	No	.	14.44
3	2	0.333	0.47	Yes	1.50	13.51
4	1	0.333	1.50	Yes	1.50	14.66

Table 6: Effect of layer refinement on pseudoskin factor
($k = 2.9477 \times 10^{-14}$ m², $k_v = 2.9477 \times 10^{-15}$ m²)

Case	Total reservoir thickness m	Open interval thickness m	Number of Layers	Pseudo-skin Factor, s_D
1	30	10	2	11.74
2	30	10	3	11.47
3	30	10	5	11.39
4	100	20	2	27.65
5	100	20	3	26.89
6	100	20	5	26.55

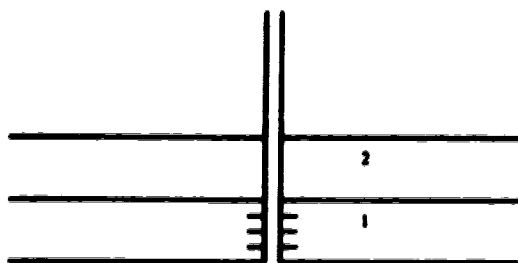


Figure 1: Schematic diagram of a two-layered, partially-penetrated reservoir with closed top and bottom boundaries.

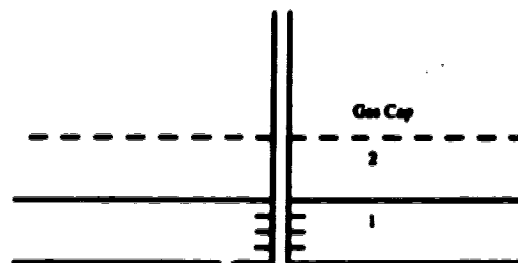


Figure 2: Schematic diagram of a two-layered, partially-penetrated reservoir with a gas cap.

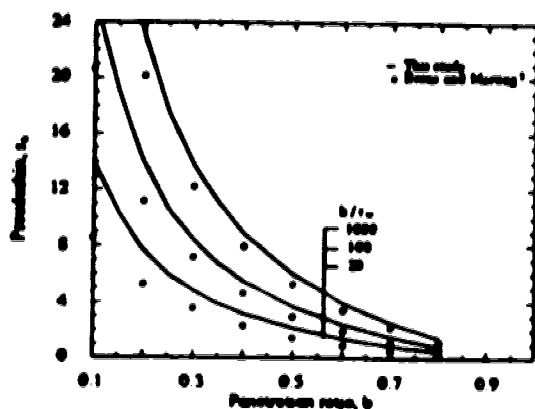


Figure 3: Comparison of pseudoskin factor from this study with that from Breits and Morley's

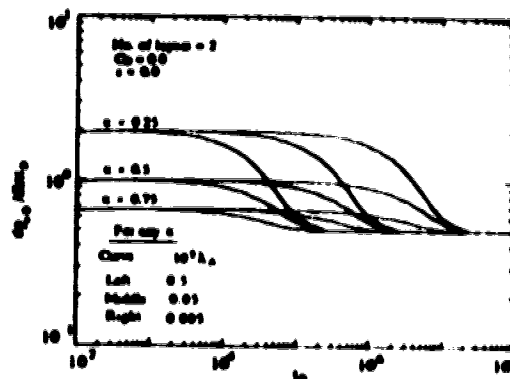


Figure 4: Effect of crossflow parameter and mobility thickness ratio on pressure derivative responses

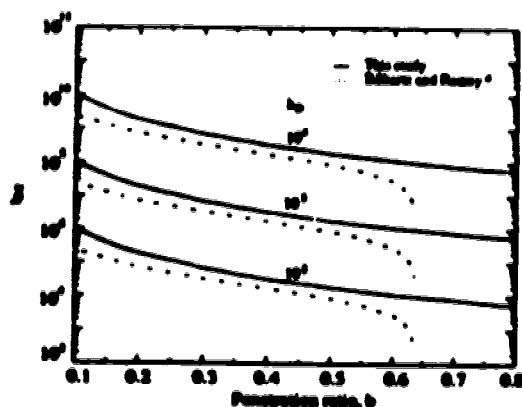


Figure 5: Comparison of the correlation for the time to the beginning of the second radial flow from this study and Reference 4.

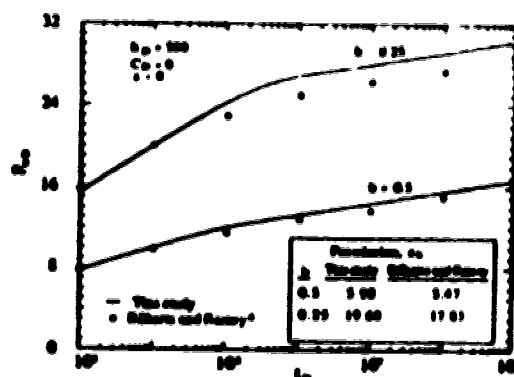


Figure 6: Comparison of pseudoskin and dimensionless pressure from this study with those from Breits and Morley's study.

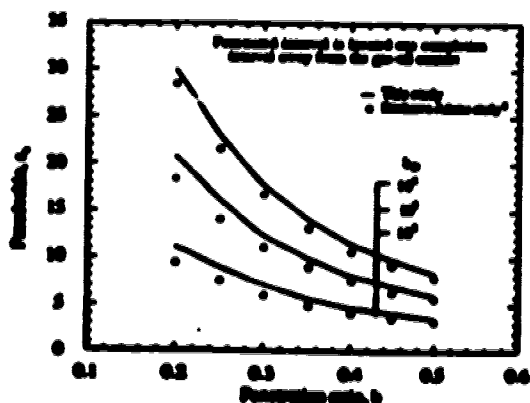


Figure 7: Comparison of pseudoskin factor from this study with that from Reference 4's study for a constant wellbore radius.

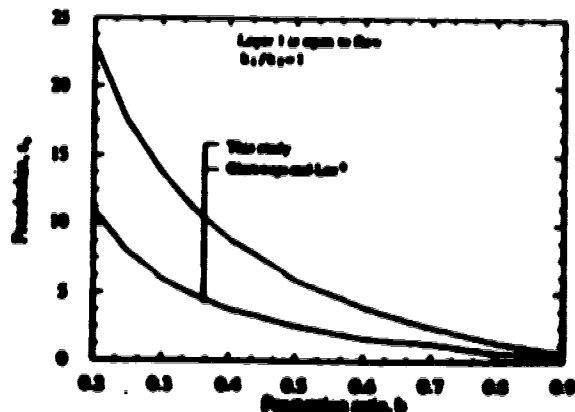


Figure 8: Comparison of pseudoskin factor from this study with that from Chappuis and Lee's study.

END

2 8 1 0 8 1 9 6

FIN